

MAGNETOM Flash

The Magazine of MR

Issue Number 2/2011
Pediatric Imaging

SIEMENS

How I do it

Techniques in
Pediatric MRI
Page 6

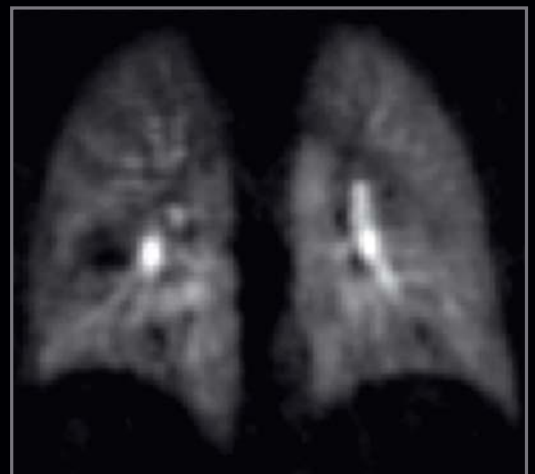
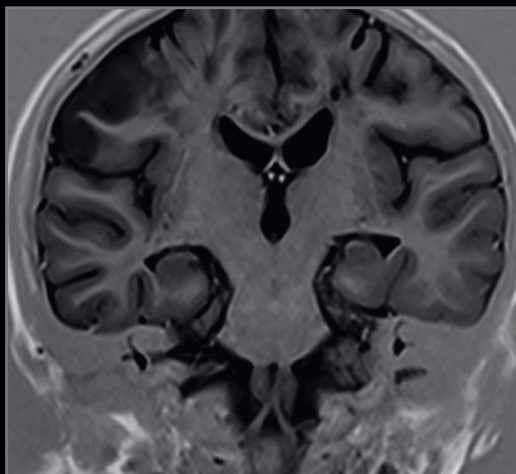
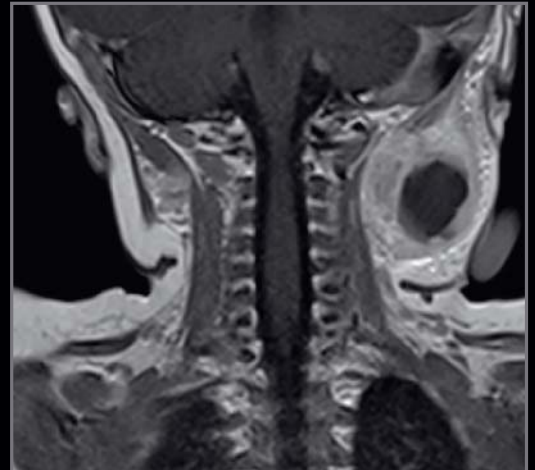
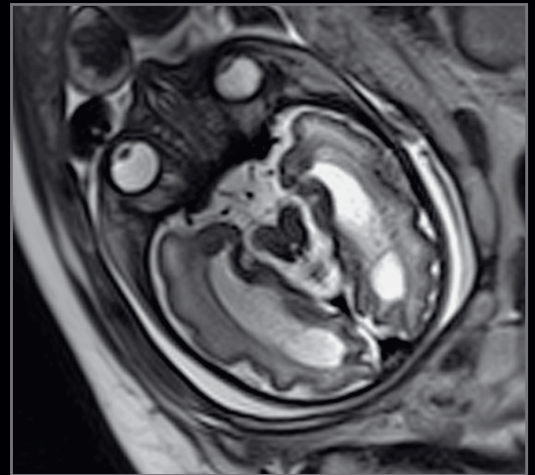
Fetal Imaging
Page 95

Clinical

MR Urography
Page 31

Neuro-Infections
in Childhood –
MR Imaging Patterns
Page 60

MRI of the Lung
Page 74



47

Matthias Lichy, MD
Editor-in-Chief



Dear MAGNETOM user,

This special issue of the MAGNETOM Flash magazine is devoted to pediatric* MRI. But why this clear focus on our youngest patients? Because we all know that children are not small adults – they suffer from different types of disease than adults, they are much more sensitive to radiation effects (a deciding factor in strengthening the role of MRI in pediatric radiology) and also demonstrate a different physiology as well as behavior. This has a direct impact on the way we image them and on the way we care for them during an examination.

Nevertheless, the numerous debates about all the various and complex aspects of pediatric MRI mean that this issue of MAGNETOM Flash cannot aim to provide a complete overview of even one specialized field-of-interest in pediatric radiology. What you will find within these pages, however, is a wide range of highly interesting clinical cases, practical tips and tricks for your routine work, and an insight into developments in clinical applications. It is clear that pediatric MRI is more than just imaging in smaller dimensions.

From a purely MR technology point of view, it is important to note that innovations espe-

cially within the last ten years, together with the overall quality of current MR technology applied to the imaging of adults, also benefit the pediatric radiologist: his use of MRI has become more efficient and new clinical applications have opened up in his daily work. Of course, MR applications have to be adopted to meet the demands of children, but what is perhaps the most important parallel to general radiology is that only by working together, industry and clinical experts, can we bring MR technology successfully into daily clinical usage. And we do this because we are convinced that the applications of MRI have already had, and will continue to have, an increasingly important impact on the care of your youngest patients.

I hope you will find the articles in this special issue not only interesting, but also inspiring, and that they provide you with new ideas on the usage of MRI in pediatric radiology.

Matthias Lichy, MD

*MR scanning has not been established as safe for imaging fetuses and infants under two years of age. The responsible physician must evaluate the benefit of the MRI examination in comparison to other imaging procedures.

Editorial Board

We appreciate your comments.

Please contact us at magnetomworld.med@siemens.com



Antje Hellwich
Associate Editor



Wellesley Were
MR Business Development
Manager Australia and New
Zealand



Dr. Sunil Kumar S.L.
Senior Manager Applications,
Canada



Christiane Bernhardt
Head Outbound Marketing
Erlangen, Germany



Milind Dhamankar, M.D.
Sr. Director, MR Product
Marketing, Malvern, PA, USA



Michelle Kessler
US Installed Base Manager
Malvern, PA, USA



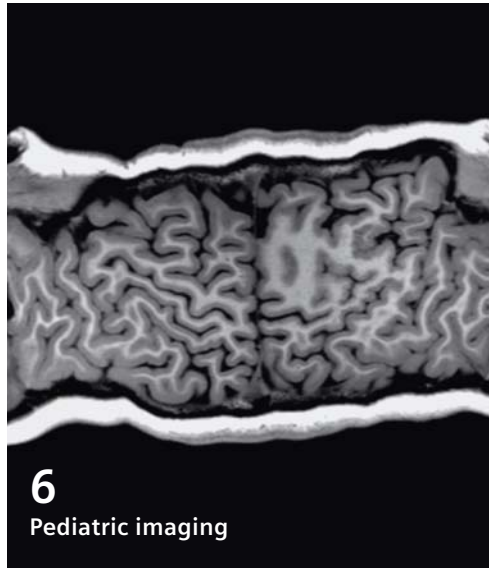
Gary R. McNeal, MS (BME)
Advanced Application Specialist,
Cardiovascular MR Imaging
Hoffman Estates, IL, USA



Peter Kreisler, PhD
Collaborations & Applications,
Erlangen, Germany

Review Board

Okan **Ekinci**, MD, Center of Clinical Competence – Cardiology
 Jens-Christoph **Georgi**, PhD, Global Marketing Manager Biograph mMR
 Christian **Geppert**, PhD, Application Development Breast Applications
 Wilhelm **Horger**, Application Development Oncology
 Jürgen **Kampmeier**, PhD, MR/PET
 Berthold **Kiefer**, PhD, Oncological and Interventional Applications
 Lars **Lauer**, PhD, Orthopedic Applications
 Heiko **Meyer**, PhD, Neuro Applications
 Edgar **Müller**, Cardiovascular Applications
 Silke **Quick**, Global Marketing Manager Women's Health
 Ignacio **Vallines**, PhD, Global Marketing Manager Neurology and Orthopedics
 Heike **Weh**, Clinical Data Manager



Further clinical information



Visit the MAGNETOM World Internet pages at www.siemens.com/magnetom-world for further clinical information and talks by international experts.

How I do it

- 6 Techniques in Pediatric MRI – Tips for Imaging Children
Glenn Cahoon

Clinical Oncology

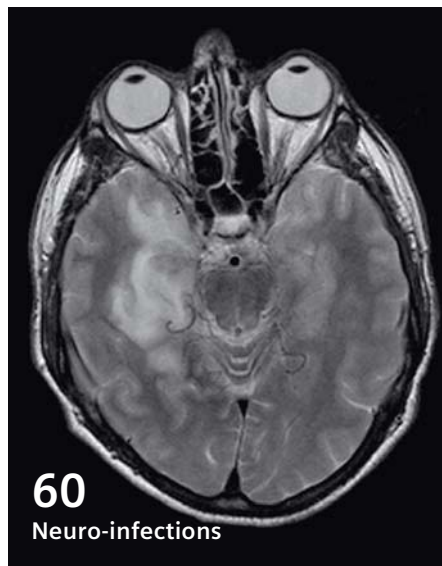
- 18 MRI: New Developments in Bone Tumor Imaging
Markus Uhl, et al.

Clinical Orthopedic Imaging

- 22 Case Report: Transient Patellar Dislocation
Claudia C. Cotes, et al.

Clinical Abdominal Imaging

- 26 Case Series: Body Trunk Imaging of Inflammatory Disease in Childhood and Adolescence
G. Schneider, A. Bücke
- 31 Pediatric MR Urography
Richard A. Jones, et al.
- 39 Pediatric MR Urography
G. Hadjidekov, et al.



- 44** Case Report: Ectopic Ureter:
Magnetic Resonance Urography
Sally Harman, Padma Rao

Image Gallery

- 46** Pediatric Imaging in Daily
Routine with MAGNETOM ESSENZA –
a Pictorial Essay
Han Yan Qiao

Clinical Neurology

- 60** Neuro-Infections in Childhood –
MR Imaging Patterns
Birgit Ertl-Wagner
- 66** Case Report: Chiari II Malformation
Raghuram K. Rao, et al.

How I do it

- 68** Optimized Examination Technique
Reduces Examination Time for Chil-
dren with Retinoblastoma by Half
Anton S. Quinsten, et al.

Clinical Thorax

- 74** Case Report: MRI of the Lung
in a Young Child with Abscess
Pneumonia Caused by H1N1
Infection
Monika Eichinger, et al.

- 80** Case Report: Virtual MR
Bronchoscopy in the Fetus
Heron Werner, et al.

Clinical Cardiology

- 84** Pediatric Congenital Heart MR
Imaging at 3T and 1.5T Systems
Pamela K. Woodard, et al.
- 92** Case Report: ASD (Ostium
Secundum Defect)
Harnoor Singh, et al.

How I do it

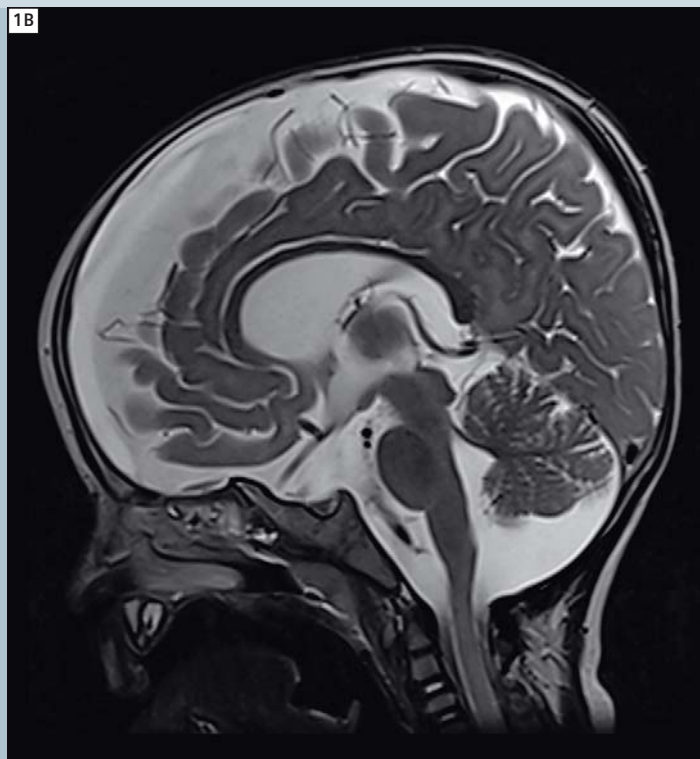
- 95** Fetal Imaging: How I do it
Aaron J. Flammang

Clinical Fetal Imaging

- 100** Case Series: Fetal MR Imaging
of the Brain at 3T
Jacques F. Schneider
- 104** Case Report: Intracranial Lipoma
Confidently Diagnosed Antenatally
using the Dixon Technique
Sally Agnew, A. Michelle Fink
- 106** Case Series: Fetal MRI of Triplets
for Evaluation of the Urinary Tract
A. Zahiri, et al.
- 108** Case Series: MR Imaging of the
Fetus in Vietnam
Nguyen Thi Thu Trang, et al.

The information presented in MAGNETOM Flash is for illustration only and is not intended to be relied upon by the reader for instruction as to the practice of medicine. Any health care practitioner reading this information is reminded that they must use their own learning, training and expertise in dealing with their individual patients. This material does not substitute for that duty and is not intended by Siemens Medical Solutions to be used for any purpose in that regard. The treating physician bears the sole responsibility for the diagnosis and treatment of patients, including drugs and doses prescribed in connection with such use. The Operating Instructions must always be strictly followed when operating the MR System. The source for the technical data is the corresponding data sheets.

MR scanning has not been established as safe for imaging fetuses and infants under two years of age. The responsible physician must evaluate the benefit of the MRI examination in comparison to other imaging procedures.



1 Longer TR and TE times are generally required when imaging very young children. The high water content in neonatal brains, coupled with the lack of fatty myelin results in a reduction in contrast-to-noise ratio (CNR) and grey/white matter differentiation. Restore pulses on T2w imaging can improve CSF contrast and allow shorter TR times to reduce scan time.

Techniques in Pediatric MRI – Tips for Imaging Children

Glenn Cahoon

Royal Children's Hospital, Melbourne, Australia

Magnetic resonance imaging (MRI) examinations of children require a particular set of skills and expertise in order to successfully obtain diagnostic images with minimal distress to the patients and their family. There have been many developments in MRI in recent years, which have led to a dramatic increase in the number and types of referrals we are now seeing for pediatric MR examinations. This paper provides an overview of the challenges that pediatric patients raise

in the MR setting, and some of the different techniques that may be employed to overcome these difficulties. While some technical modifications are described, the focus is on practical recommendations that can assist young children to comply with the MR procedure, and minimize the use of anesthesia with this vulnerable population. Pediatric MR imaging can be considered a series of subspecialties. Each area, neurology, cardiac, MSK, oncology, all

have their own subtle nuances that alter as patients mature. In our facility we routinely scan patients from the early fetal* stages right through to young (and not so young) adults with complex congenital conditions. Each of these fields, and stages of development requires their own specialized skills, knowledge, and equipment to be performed appropriately, however, there is a number of common challenges and techniques that apply to imaging pediatric patients.

Challenges of scanning children

Safety

MRI of children poses a number of specific safety issues with patient heating being the primary concern. Neonates and infants in particular have immature thermoregulation mechanisms, and higher core body temperatures making them particularly sensitive to RF heating effects [1]. These mechanisms are further affected by sedation and anesthesia common in pediatric imaging [2], or when babies are swaddled for imaging [1]. Children also have a greater surface area to weight ratio than adults. This means for a given weight we often need to expose a greater surface area of the patients to the RF field. This can lead to increased heating in children, and decrease their ability to dissipate this heat. There is intrinsic uncertainty in current specific absorption rate (SAR) predictions based on extrapolated data from phantom models [3] particularly due to factors such as body shape, size, composition, and position within the MR scanner. While definitive data on safety risks are not yet available, close monitoring of children, particularly critically ill or compromised infants, is desirable when using higher field strengths and high SAR scan techniques [1].

Anesthesia is an important safety consideration in pediatric MRI. While serious complications such as death are rare, there are significantly higher rates of morbidity, particularly amongst neonates, when compared to adult anesthesia [2]. Aside from adverse events there are a number of common side effects including nausea, vomiting, drowsiness and agitation upon awakening, which affect about one third of pediatric patients [2]. The challenge of monitoring patients in the MR environment coupled with the reduced ability for the patient to communicate adverse events creates significant additional risks [4]. If sedation is required, the associated risks need to be taken into account when deciding to image young children.

Anatomy

Normal structures in children are smaller than in the average adult. This creates a challenge both in terms of the available signal, and the limits of our scan resolution. Anatomy is further complicated by congenital anomalies and malformations as well as developmental changes [5]. At birth we are about 75% water and we dry out as we age to about 55–65% water for an average adult. This is best appreciated in the neonatal brain. The high water content, and lack of fatty myelin, requires an increase in TE on T2-weighted imaging to around 150–160 ms to improve contrast. With so much of the available hydrogen in loosely bound water, there often is not much to influence relaxation. The use of fast recovery (restore) pulses at the end of the echo train improves the signal-to-noise ratio (SNR) while allowing for shorter TRs to be used (Fig. 1).

T1 contrast can be particularly flat requiring an increase in TR to around 1,200 ms at 1.5 Tesla. The use of inversion recovery techniques, and magnetization prepared 3D imaging such as MPRAGE, are evident at many institutions, particularly at higher field strengths [5].

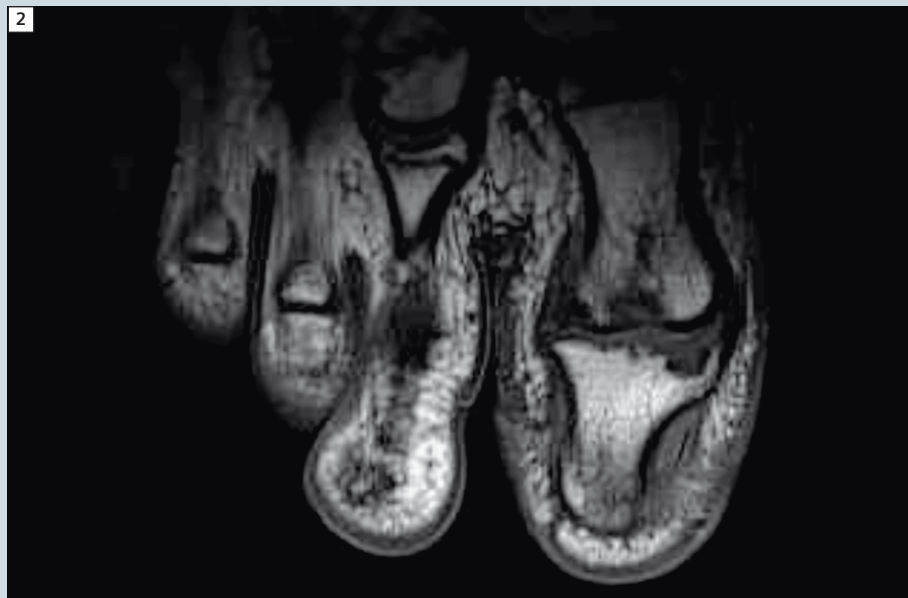
Pathology

Children are notoriously poor reporters of symptomatology, and their often vague and non-specific symptoms can belie the seriousness of their condition. Clinical examination is often very difficult, so MRI requests are seldom specific. There are many transient appearances on MR images that can be considered normal at some stages of development and abnormal at others. Recognizing the appearance of normal from abnormal development on MR images and determining the optimal sequences and factors to best display them presents a challenge to technologists with little pediatric experience.

An awareness of the conditions that are commonly found in the pediatric population is necessary to tailor scans appropriately.

Physiology

Pulse rate, blood flow, and respiration rates are considerably faster in children, with normal heart rates that can be in excess of 140 bpm and respiratory rates of 40/min [5]. Children typically find it difficult to satisfactorily hold their breath, creating significant challenges in cardiac,



2 Coronal PD-weighted image of an osteo-chondral defect (OCD) of the distal phalanx of the right toe.

chest and abdominal imaging. Increased flow rates lead to artifacts from blood vessels and cerebrospinal fluid (CSF) pulsations, creating difficulties with spine and Time-of-Flight (TOF) vessel imaging [5]. Differences and evolution in pediatric physiology may also lead to changes in the mechanism of injury, or the types of injuries that occur in children, such as growth plate injuries and osteo-chondral defects (OCD) [6].

Behavioral

Sedation or anesthetic is commonly required for younger children or those with significant behavioral problems. Factors such as temperament, stress, pain, and illness play an important role in patient compliance, creating difficulties in establishing definitive age limits for identifying which children will require these procedures [7]. Encouraging children to co-operate for an MRI examination and identifying those who cannot are arguably the most significant challenges in pediatric MRI.

Techniques in scanning children without sedation

Preparation

At our institution we begin scanning without sedation from about five years of age, although some positive outcomes have been obtained with patients as young as three years. Adequate preparation of children for the MRI procedure has been vital in achieving these results. Our facility employs the services of educational play therapists who use a range of resources to assist children to comply with the procedure, such as brochures, MRI toys and storybooks, discussions with parents, and, most importantly, the 'mock MRI' procedure.

Simulation

The 'mock MRI' procedure involves children undergoing a simulated scan with the assistance of a play therapist prior to the actual diagnostic scan. It acts as both a screening tool, to assist in identifying children who are likely to be able

to comply with the MRI procedure, and also helps to prepare these children, by familiarizing them with the environment, sounds, and equipment, while teaching them skills (such as breathing, relaxation, or distraction) to cope with the actual procedure (Fig. 2). Use of the 'mock' magnet has led to a marked reduction in the numbers of patients who have required anesthetic [7] and reduced the time required for the diagnostic scan [8]. Several pediatric facilities in various countries have introduced a mock procedure in their facilities in recent years [9].

Communication

Specialist staff and equipment are clearly helpful in assisting children to comply with an MR scan. However, for technologists, an awareness of how to talk to children and adolescents at different stages of development and the use of psychological techniques, such as distraction and relaxation, can be the critical factor determining whether a young person is willing, or able, to carry out the procedure. Many children are withdrawn or uncommunicative when nervous about a medical procedure, and taking the time to help the child to feel safe and secure in the environment is important. Compliance with preschool children may be facilitated by engaging in pretend play, where the child can be encouraged to frame the experience in familiar and non-threatening ways [10]. Nonverbal communication comprises a significant proportion of a child's interaction with the world at this stage, and young children can pick up on their parents' anxiety or the technologist's impatience through nonverbal clues. They may not understand these feelings and can interpret them as anger or fear of the examination. Professionals who work with children typically take steps to ensure that both their verbal communication and body



3 Mock MRI simulator – this procedure identifies patients that are able to comply with the requirements of an MRI examination, as well as prepare them for the clinical scan, saving unnecessary appointments and valuable scanner time.

Table 1: Communicating with children

Engage with the child	Get down on their level	Use simple language	Maintain eye contact
Frame the experience	Help them verbalize their experience	Involve the child's past experiences / play	Smile
Empower the child	Offer limited choices	Praise good behavior	Be positive "I know you can do this"

language are reassuring and convey calmness and confidence (Table 1). Positive reinforcement, where the child is praised for their efforts at each step, can be very helpful.

School age children are able to engage more actively in the procedure, and may respond well to efforts to increase their perceived control. Medical examinations often take the locus of control away from the patient, and this is particularly true in pediatrics where someone else usually makes the decisions for the patient. Empowering children by offering some choice in how they can have the scan can be helpful. This is particularly important during adolescence; a period of rapid social and physical changes [10], when increased autonomy is important, yet can be hampered by serious illness. Adolescents are less likely than children or adults to blindly follow instructions, and may be reluctant to accept or comply with the scan in the absence of a flexible approach, where the technologist is sensitive to their concerns.

Distraction and relaxation

Distraction can be a powerful tool for reducing anxiety and increasing patient compliance. Distraction techniques can be either active or passive. Passive techniques such as audiovisual aids are useful during the scan when patients are required to lie still in the bore. Having a point of interest (such as a parent or

video screen) is helpful in maintaining the patient in one position. Active techniques which require patient participation such as relaxation breathing, guided imagery, or complex puzzle tasks, are useful in relaxing children before MRI or performing interventions such as intravenous cannulation and general anesthetic (GA) inductions.

Successful use of intravenous (IV) contrast

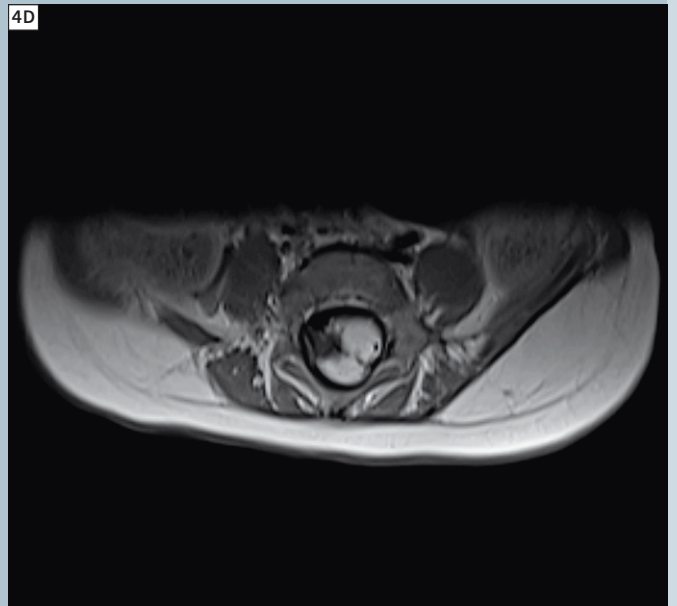
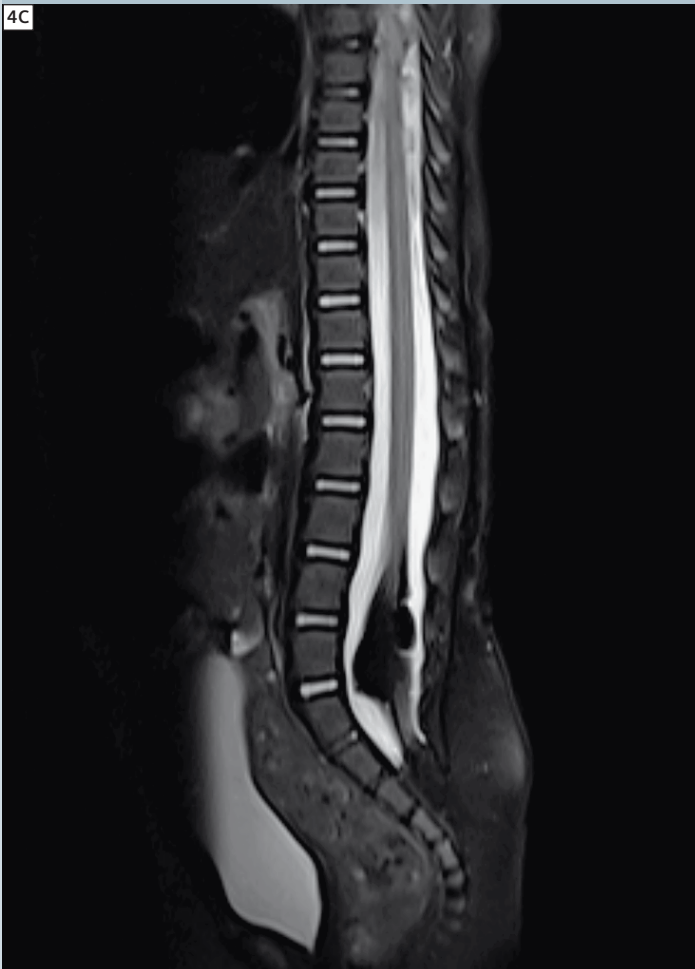
IV cannulation is a major cause of anxiety in young patients presenting for MRI examination. Limiting the use of IV contrast in pediatric examinations can often mean the difference between a successful awake scan and a rebook for sedation. This requires the support of the radiologists to make decisions regarding whether the benefits of contrast are worth the potential distress to the patient. Where contrast is necessary, it is often helpful to separate the procedures of IV placement and the MR exam by either placing the cannula before the examination or offering a break between the pre and post contrast scans. Many children respond well to being able to

choose an IV site. Active distraction techniques can be helpful, and there are several aids available to assist with the pain, such as local anesthetic creams, ice, or nitrous oxide.

Protocols and sequences

Protocol based scanning can be difficult in presenting pediatric patients, as the required sequences differ dramatically depending upon pathology, patient age, compliance, and the clinical questions being asked. It is often necessary for the technologist or radiologist to screen the examination as it progresses and tailor the sequences for the patient and pathology. A wide field-of-view scan can be helpful to obtain an overview to screen for other pathologies, particularly in children who are difficult to examine clinically. Children can be unpredictable in how long they will remain still, so it is important to prioritize sequences with the highest diagnostic yield such as T2, FLAIR, and diffusion. Scanning in multiple planes or using 3D sequences can help delineate disorders as well as minimize the chance of pathology being missed through partial voluming or interslice gap.

Often it is necessary to modify a protocol or sequence when imaging children of different sizes or capabilities. It is important to strike a balance between optimum image resolution and scan time.



4 Images of a 3-month-old child with a lipomatous tether of the spinal cord. The patient was scanned awake in a bean bag restraint (4A) using the 4-channel flex array (4B) positioned flat beneath. The high SNR afforded by this coil allowed high resolution thin slice imaging and the addition of iPAT to reduce scan time. Siemens Tim architecture allows flexibility to use coils in a number of orientations, or in combination with other coils, vital for imaging pediatric anatomy.

When modifying pulse sequences, the following suggestions may be helpful:

- Select pulse sequences that closely match the FOV required and the coil being used. The less changes you need to make to a sequence, the less chance for error.
- Concentrate on maintaining voxel size and signal-to-noise when changing field-of-view or matrix size, and consider using interpolation to maintain signal and resolution. The day optimizing throughput (Dot) engines on the newer Siemens scanners can be used to automate many of these decisions.
- Utilize recovery pulses, where available, to achieve reduction in TR times and to collect the images in multiple concatenations. When combined with interleaving this dramatically reduces the chance of crosstalk when using minimal slice gaps.
- Use the shortest TE that will maintain image contrast to boost signal and reduce image blur.

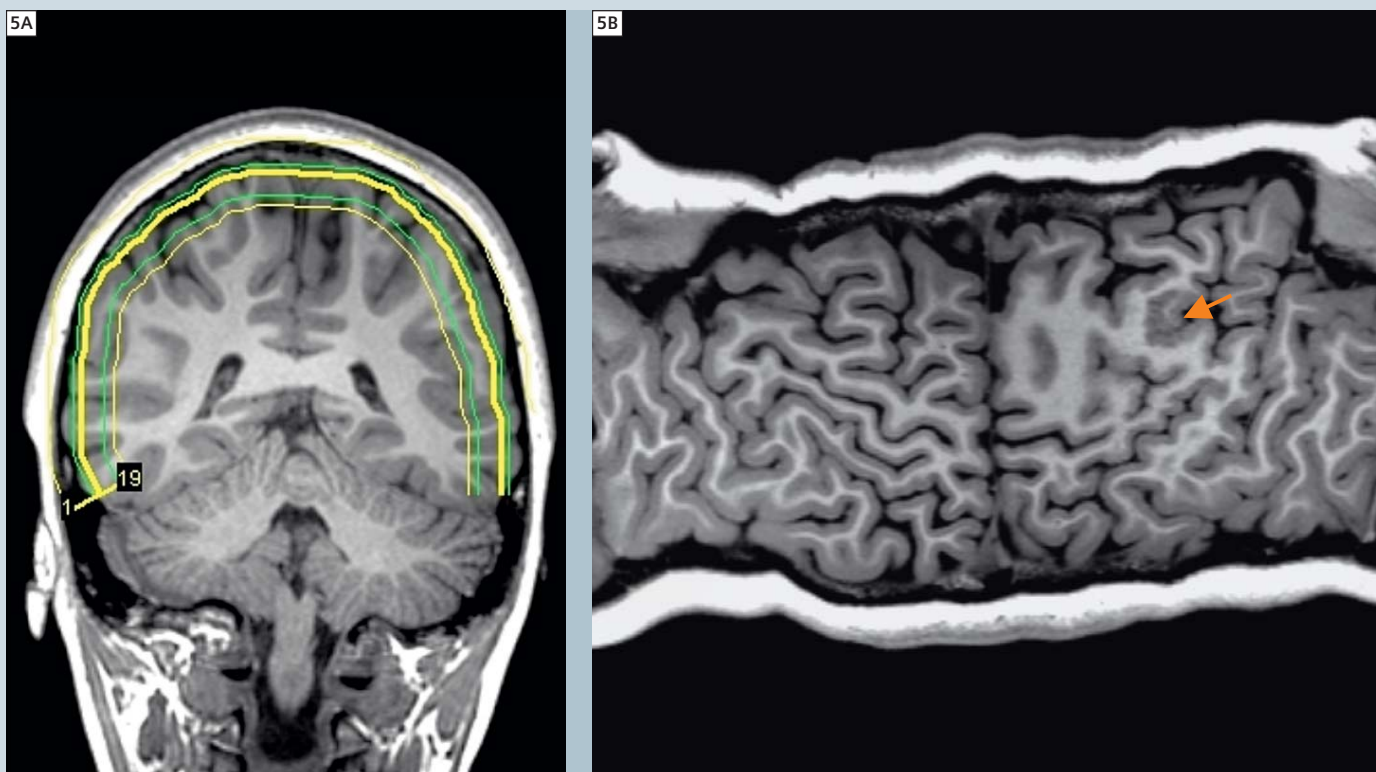
Scanning techniques

Coil selection

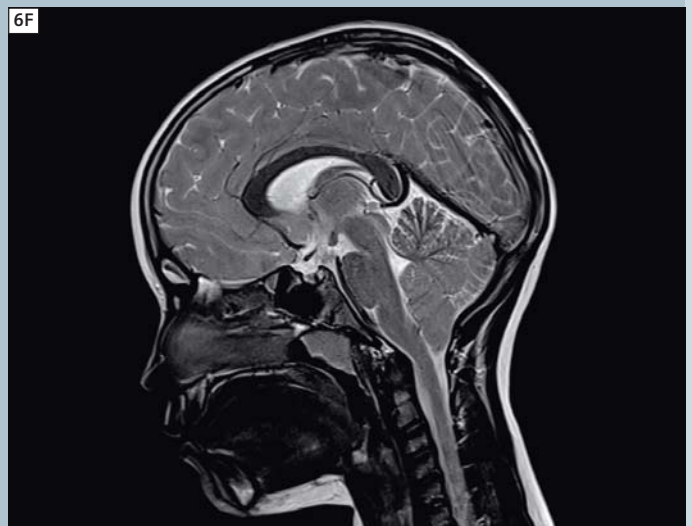
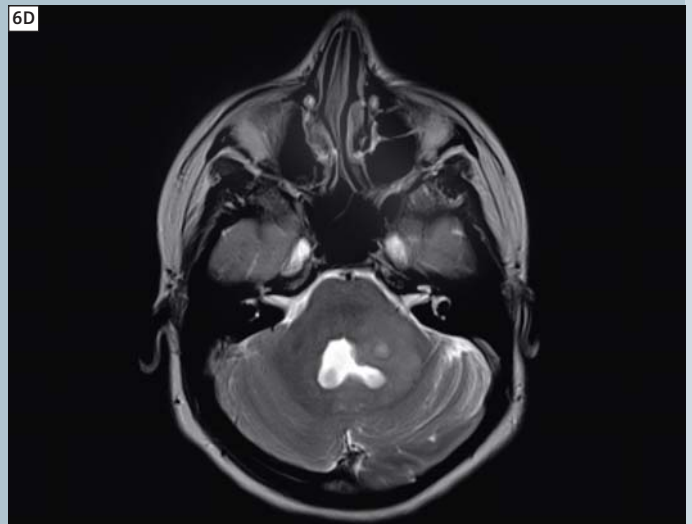
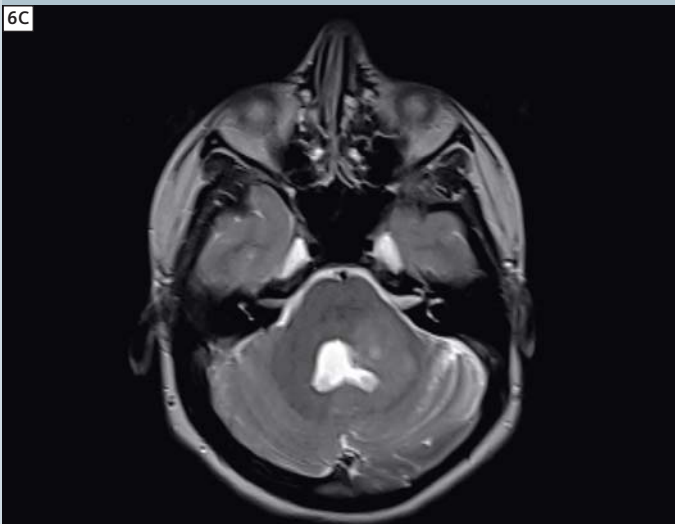
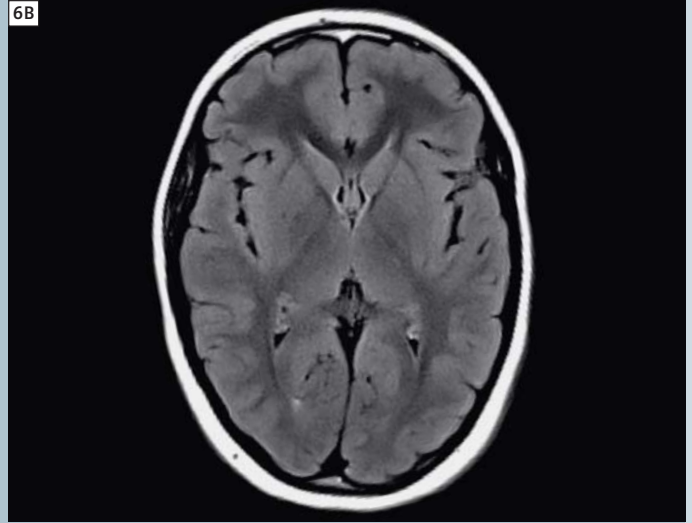
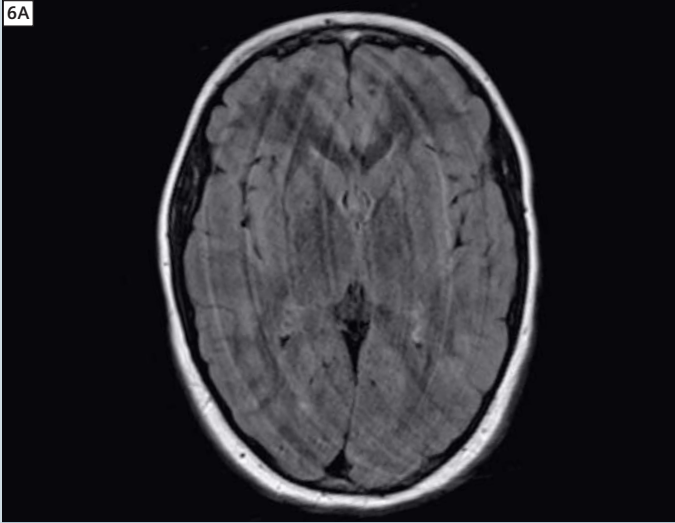
Novel uses of MR coils are possible and often necessary in pediatric imaging. Choosing a coil that closely matches the FOV you are imaging is important in extracting the maximum signal from your patients. Use of multichannel arrays is desirable when available to take advantage of parallel imaging techniques (Fig. 4).

Volume imaging

3D imaging can be utilized in all areas of the body. The use of 3D sequences permits reformatting, which can be helpful



5 Volume imaging: Reformatting of 3D imaging is useful in the investigation of complex congenital conditions. The curved reformat of the T1-weighted MPRAGE sequence allows appreciation of the disorganised left cerebral cortex, and helped in identification of a region of polymicrogyria which was the seizure focus in this 12-year-old girl.



6 Motion correction – *syngo* BLADE can be used to provide a limited study in uncooperative patients (6A, 6B), but is particularly useful in imaging posterior fossa lesions in pediatric patients where complex and high flow from CSF and vascular structures cause artifacts that may obscure some lesions (6C, 6D). High parallel imaging factors can also be utilised with multiple excitations to average out motion artifacts (6E None, 6F PAT3).

in reviewing and diagnosing complex congenital conditions, and may reduce the number of 2D sequences performed. It allows for high resolution, no gap imaging which can be used to accurately measure lesion size, and monitor changes in follow up imaging (Fig. 5).

BLADE

Rotating k-space techniques are utilised in pediatric MR imaging to reduce artifacts from physiological motion in the brain, as well as other body areas such as the shoulder, chest, abdomen, and pelvis. It is particularly useful with younger patients scanned at 3T where complex and turbulent flow artifacts can mask pathology [11]. Recent studies show improvement in lesion conspicuity in the posterior fossa through reduction in pulsation artifacts [12]. Disadvantages of BLADE include increased scan time, altered image contrast, increased SAR, and reduction in sensitivity to some pathology, particularly haemorrhage [13]. Motion reduction with propeller sequences can be utilized to obtain limited diagnostic information in moving patients; however, their limitations restrict widespread use for correcting voluntary patient motion in pediatric patients (Fig. 6).

Parallel imaging

The advent of parallel imaging techniques and multiple element, phased array coils has transformed pediatric imaging in recent years, providing a boost in either signal or speed. Parallel imaging techniques combine signals from several coil elements to produce an image with increased SNR, or allow partial sampling to reduce scan time. The use of parallel image acceleration and multiple acquisitions can be used to average motion artifacts in pediatric imaging. Parallel imaging techniques can also be exploited to reduce the duration of breathhold imaging, allowing dynamic capture of fast moving pediatric anatomy. Parallel imaging also reduces inhomogeneity artifacts such as seen in diffusion-weighted imaging [14].

Time resolved angiography

When imaging arterio-venous malformations and vascular shunts it is important for treatment and management to identify feeder vessels as well as the direction of blood flow. Rapid heart rates and high flow rates in children often make imaging of complex vasculature difficult with traditional MR angiography techniques. Time resolved contrast-enhanced MR angiography (MRA) techniques can provide anatomical as well as functional assessment of these vascular conditions [14].

High field strength imaging (3T)

Higher field strengths offer the opportunity to address many of the difficulties encountered with pediatric MR imaging. The increased SNR allows for smaller voxels and increased resolution, or reduced averages for increased speed. Parallel imaging factors can be increased further reducing scan time. Prolonged T1 times facilitate better background suppression for MRA and improved visualization of paramagnetic contrast agents [5]. The advantages offered by higher field strengths have led to the viability of several new techniques in pediatric MRI. Unfortunately, higher field strengths can also present a number of challenges. The increased field strength leads to greater RF deposition, resulting in increased heating (SAR), which can cause sequence limitation in pediatric imaging. B₁-field inhomogeneities, chemical shift, motion artifacts and susceptibility artifacts are more pronounced at higher field strengths. However, there are a number of new techniques, which offer potential to mitigate against these difficulties. Prolonged T1 relaxation at higher field strengths creates challenges in image contrast, particularly in the neonatal brain [5].

Emerging techniques in pediatric MRI

SWI

Susceptibility-weighted imaging is being increasingly utilized in pediatric patients for imaging trauma, vascular disease such as haemorrhage, telangiectasia, and cavernous and venous angiomas, tumors and epilepsy imaging, as well as investigating metabolic disorders (Figs. 7, 8). The use of the phase images can be used to differentiate calcification from haemorrhage in lesions [15].

Parallel transmit technology

The use of multiple coil elements to transmit part of the RF pulse results in shorter pulse durations, reductions in SAR, and corrections of patient-related inhomogeneities [16]. This addresses some major challenges of pediatric MRI, particularly at higher field strengths.

Diffusion Tensor Imaging

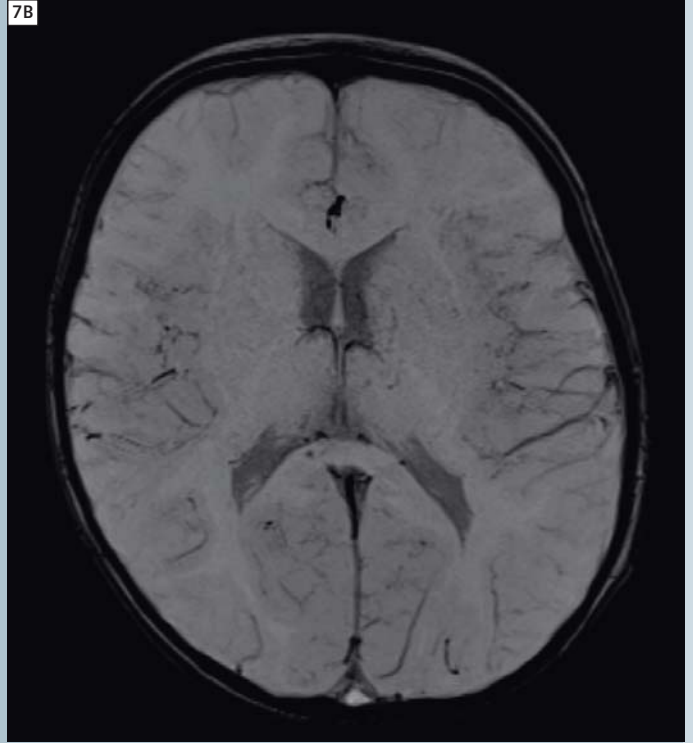
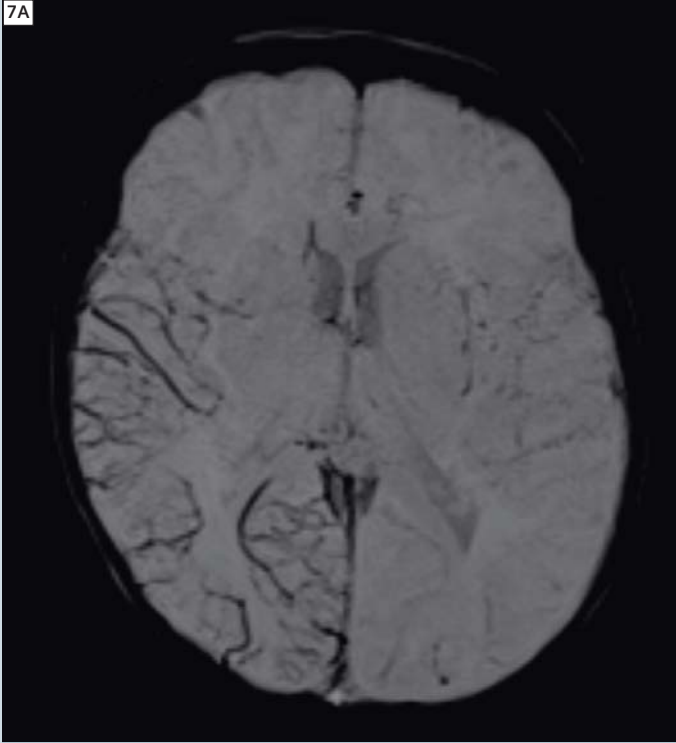
DTI has provided insights into connectivity and plasticity in the developing brain. It is now entering the clinical realm in the assessment of traumatic brain injury, epilepsy and white matter disease [14].

Arterial Spin Labeling

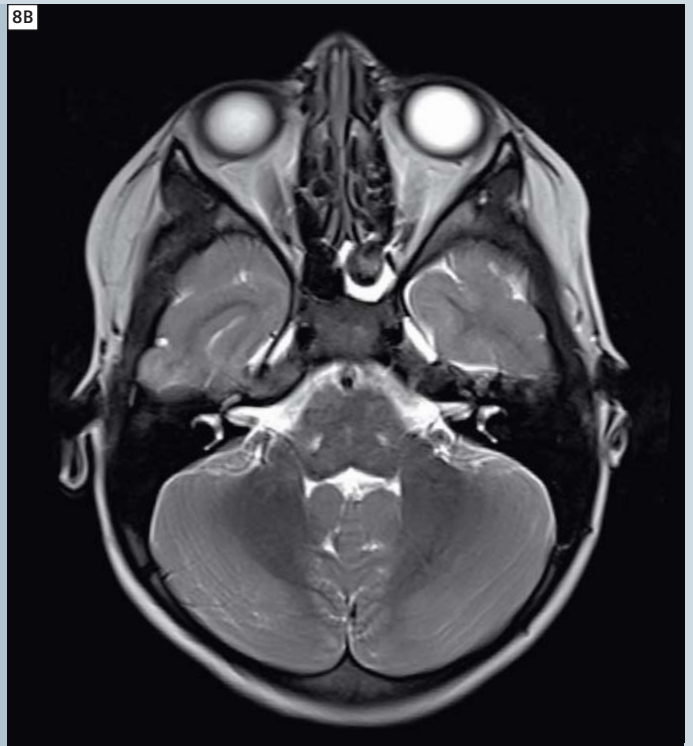
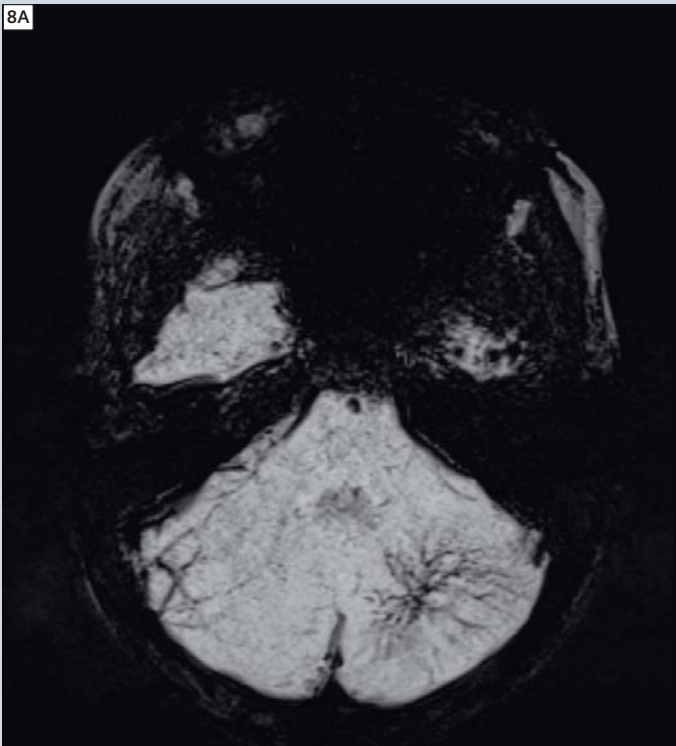
ASL provides functional information of blood perfusion by magnetically tagging inflowing blood upstream from the region of interest. Persistence of the 'tag' limits its use in adults; however, this is of less concern in pediatric patients, due to fast flows and relatively short perfusion distances [5]. This technique offers the potential to investigate regions of hypo- and hyper-perfusion, in conditions such as stroke or tumors, without the use of intravenous contrast media; however, further validation is required to demonstrate the clinical utility of this technique in pediatric patients [17].

MR urography

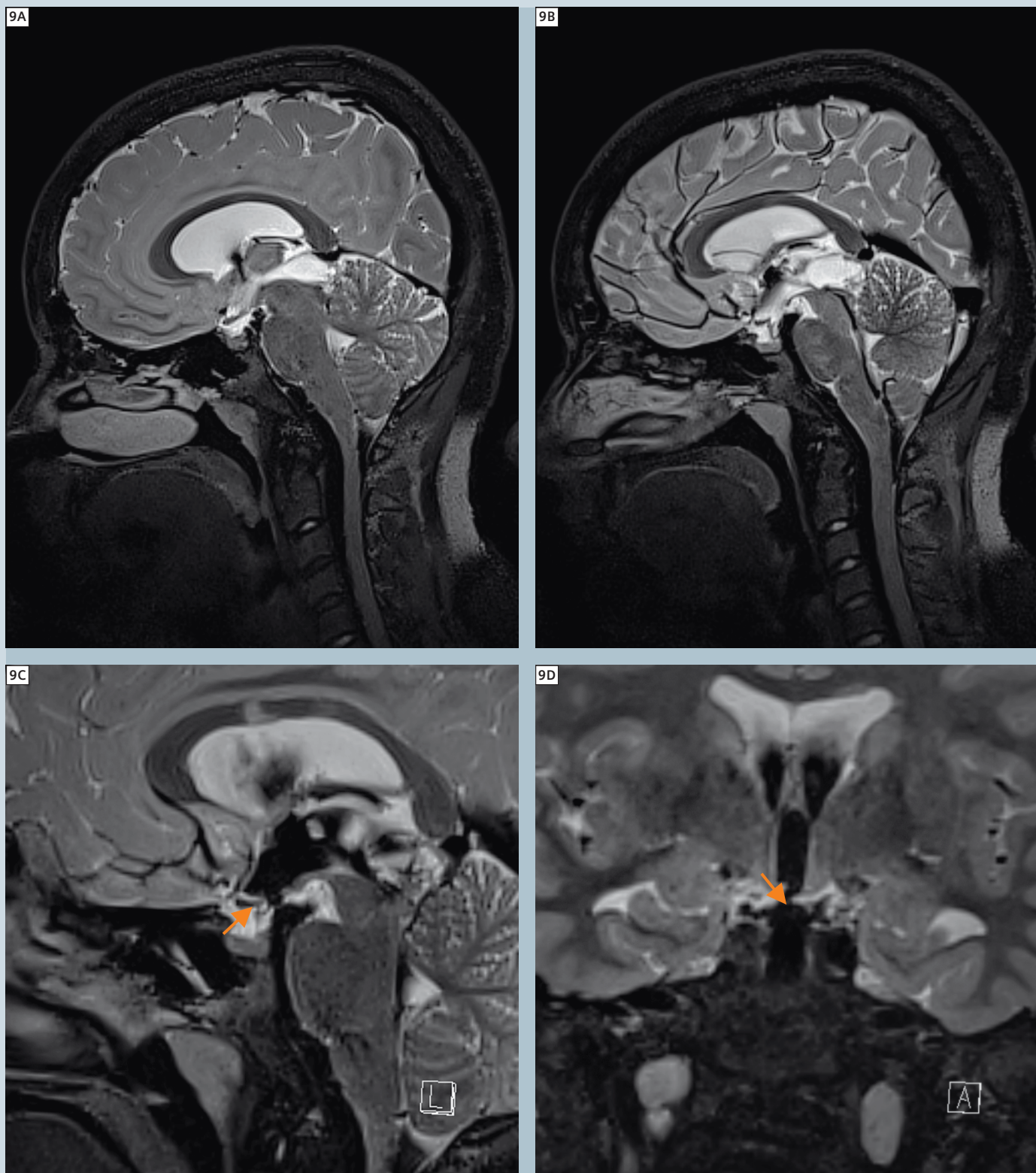
Magnetic resonance urography provides both anatomical and functional assessment of the kidneys and urinary collecting system. The multi-planar capabilities



7 Images of a 1-month-old who presented with acute seizures. T2w, T1w and diffusion-weighted imaging were unremarkable. Susceptibility-weighted imaging (**7A**) shows increased venous drainage in the right temporal-parietal region. (**7B**) The same patient imaged 48 hours later after seizure control with phenobarbital showing normalization of the cerebral flow. The sensitivity of *syngo* SWI is being increasingly utilized in the pediatric population.



8 Venous angioma as imaged on *syngo* SWI (**8A**) and T2w sequences (**8B**). The ability to obtain this level of detail has allowed us to reduce our reliance on intravenous contrast agents to delineate these lesions.



9 These images are of a patient with a pineal cyst causing obstruction of the cerebral aqueduct with associated enlargement of the lateral and third ventricles. The sensitivity to flow of the T2w SPACE sequence can be used to demonstrate the obstruction in the pre surgical images (**9A**) as well as the increased retrograde flow through the foramen of Monro. The post surgical image (**9B**) shows the reduction in the size of the cyst as well as the restored flow to the cerebral aqueduct. The 3D sequence can be easily reformatted to show the site of the fenestration of the third ventricle (**9C**, **9D** arrows). Third ventriculotomies have been traditionally difficult to demonstrate with standard 2D and phase contrast imaging, however, with a single 3D acquisition we can now easily answer all of the questions of the neurosurgeon.

of MRI are ideal for displaying complex congenital anomalies of the genitourinary tract. This information can be used to predict outcome and select patients that are most likely to benefit from surgical intervention [18].

MR enterography

Crohn's disease is a serious and lifelong condition affecting the digestive system. It affects primarily the ileum and colon causing inflammation, ulceration and can lead to abscess formation or fistulae to other organs. Approximately 30% of patients with Crohn's disease will present before the age of 20. MRI provides the ability to diagnose and monitor this condition as well as complications such as peri-anal fistulae without exposing the patient to radiation [19].

Conclusion

Magnetic resonance imaging referrals for children continue to rise. The lack of ionizing radiation coupled with the high level of detail afforded by MR imaging has made it the examination of choice for a growing number of pediatric presentations. Most children who require magnetic resonance imaging will be examined in specialist pediatric centers or hospitals; however, heightened pressure on specialist centers has led to many children being scanned in non-specialist facilities where technologists may have little experience in pediatric imaging. These referrals need to be treated differently to standard adult imaging requests in order to ensure diagnostic imaging with minimal distress and intervention to the patient. There is no 'one size fits all' approach to imaging children and pediatric MRI requires dedicated specialist knowledge, flexibility, and expert input from the technologist. An awareness of the challenges in pediatric MRI and experience in pediatric imaging techniques is vital to successful exami-

nation in this population. MRI in children can be extremely challenging physically, mentally, and emotionally, even for a seasoned pediatric technologist; however, these very challenges are also what make pediatric imaging such an interesting and rewarding field for MR technologists.

Acknowledgments

I would like to thank the patients and staff of the Royal Children's Hospital, Melbourne, for their inspiration, advice, and support in compiling this paper.

References

- Machata AM, Willshke H, Kaban B, Prayer D, Marhofer P (2009) "Effect of Brain MRI on Body Core Temperature in Sedated Infants and Children" *British Journal of Anaesthesia* 102(3):385-9.
- Cohen MM, Cameron Cal B, Duncan PG (1990) "Pediatric Anesthesia Morbidity and Mortality in the Perioperative Period" *Anesthesia and Analgesia* 70:160-7.
- Homman H, Bornert P, Eggers H, Nehrke K, Dossel O, Graesslin I (2011) "Toward individualised SAR models and in vivo validation" *Magnetic resonance in Medicine* doi: 10.1002/mrm.22948.
- Serafini G, Ongaro C, Mori A, Rossi C, Cavalloro F, Tagliaferri C, Mencherini S, Braschi A (2005) "Anesthesia for MRI in the Pediatric Patient" *Minerva Anesthesiology* Jun 71(6) 361-6.
- Dagia C, Ditchfield M. (2008) "3T MRI in paediatrics: Challenges and clinical applications" *European Journal of Radiology* doi:10.1016/j.ejrad.2008.05.019.
- Hussain HM, Barnes CE (2007) "Pediatric skeletal trauma- Plain film to MRI" *Applied Radiology* 36(8):24-33.
- Carter AJ, Greer ML, Gray SE, Ware, RS (2010) "Mock MRI: reducing the need for anaesthesia in children" *Pediatric Radiology* Aug;40(8):1368-74.
- de Amorim e Silva, C.T.J., Mackenzie, A., Hallowell, L.M., Stewart, S.E., Ditchfield, M.R. (2006) "Practice MRI: Reducing the need for sedation and general anaesthesia in children undergoing MRI" *Australasian Radiology* 50(4),319-323.
- Hallowell, L.M., Stewart, S.E., de Amorim e Silva, C.T., Ditchfield, M.R. (2008) "Reviewing the process of preparing children for MRI" *Pediatric Radiology* 38(3), 271-279.
- Gable S (2010) "Communicating effectively with children" University of Missouri, Columbia, Outreach and Extension information sheet.
- Vertinsky AT, et al. (2009) "Performance of PROPELLER relative to standard FSE T2-weighted imaging in pediatric brain MRI" *Pediatric Radiology*. Oct;39(10):1038-47.
- Von Kalle T, et al. (2010) "Diagnostic Relevant Reduction of Motion Artifacts in the Posterior Fossa by syngo BLADE Imaging" *MAGNETOM Flash* 43(1/2010):6-11.
- Forbes KP, et al. (2003) "Brain Imaging in the Unsedated Pediatric Patient: Comparison of Periodically Rotated Overlapping Parallel Lines with Enhanced Reconstruction and Single-Shot Fast Spin-Echo Sequences" *American Journal of Neuroradiology* 24:794-798.
- Shenoy-Bangle A, Nimkin K, Gee MS (2010) "Pediatric Imaging: Current and Emergent Trends" *Journal of Postgrad Medicine* 56:98-102.
- Zhen Wu, Sandeep Mittal, Karl Kish, Yingjian Yu, J. Hu, Mark Haake (2009) "Identification of Calcification with Magnetic Resonance Imaging Using Susceptibility-Weighted Imaging: A Case Study" *Journal of Magnetic Resonance Imaging* 29(1): 177-182.
- Wald LL, Adalsteinsson E (2009) "Parallel Transmit Technology for High Field MRI" *MAGNETOM Flash* 40(1/2009):124-135.
- Chen J, et al. (2009) "Arterial Spin Labelling Perfusion MRI in Pediatric Arterial Ischemic Stroke- Initial Experiences" *Journal of Magnetic Resonance Imaging* February; 29(2) 282-290.
- Grattan-Smith JD, Jones R (2008) "Magnetic resonance urography in Children" *Magnetic Resonance Imaging Clinics of North America* 16 515-531.
- Sinha R (2009) "Role of MRI in Chron's disease" *Clinical Radiology* 64 (4):341-352.

Contact

Glenn Cahoon
Royal Children's Hospital
Melbourne
Australia
Glenn.Cahoon@rch.org.au

*MR scanning has not been established as safe for imaging fetuses and infants under two years of age. The responsible physician must evaluate the benefit of the MRI examination in comparison to other imaging procedures.

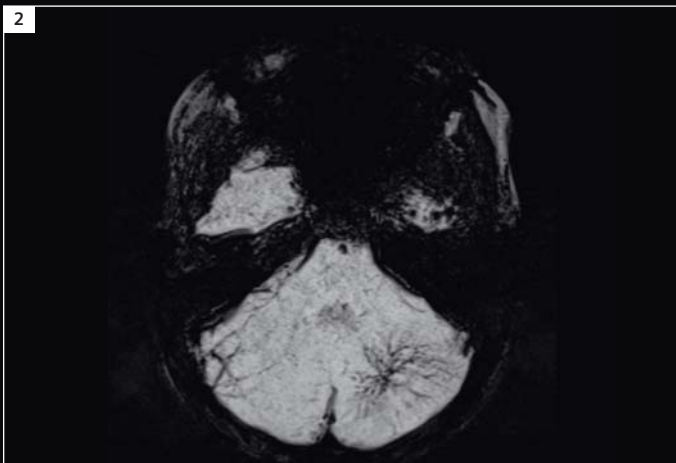
Try them on your system

Trial licenses for most of the applications featured in this issue of MAGNETOM Flash are available free of charge for a period of 90 days: Please contact your local Siemens representative for system requirements and ordering details or

visit us online* at www.siemens.com/discoverMR for further details, product overviews, image galleries, step-by-step videos, case studies and general requirement information.



1 Motion correction with *syngo* BLADE (page 12)



2 Venous angioma imaged on susceptibility-weighted imaging, *syngo* SWI (page 14).



3 MIP of a time resolved *syngo* TWIST acquisition (page 89).

*Direct link for US customers:
www.siemens.com/WebShop

Direct link for UK customers:
www.siemens.co.uk/mrwebshop

MRI: New Developments in Bone Tumor Imaging

Markus Uhl, MD¹; W. Reichardt², Udo Kontny, MD³

¹RKK, Dept. of Diagnostic Radiology, Freiburg, Germany

²University Hospital Freiburg, Dept. Med. Physics (Head: Prof. Dr. J. Hennig), Freiburg, Germany

³University Children Hospital, Dept. of Oncology (Head: Prof. Dr. C. Niemeyer), Freiburg, Germany

MR imaging has evolved as the most important diagnostic method for local staging of primary bone tumors and for detecting postoperative tumor relapse. It allows accurate preoperative staging of local tumor extent and helps to obtain

adequate safety margins: prerequisites for successful limb-salvage surgery. Assessment of the effectiveness of cancer therapy traditionally relies on the comparison of tumor images acquired before and after therapeutic interven-

tion by inspection of cross-section images to evaluate changes in tumor size. In osteosarcoma there exists a specific problem: During successful chemotherapy, the tumor size does not diminish significantly because the therapy has



1 Typical osteosarcoma of the metaphysis of the tibia. The sarcoma breaks through the bony cortex and invades the adjacent soft tissue (1A). The diffusion-weighted EPI-sequence (1B) reveals the restricted proton diffusion in this high-cellular malignant tumor (original b-value image shown at $b = 700 \text{ s/mm}^2$). In the center of the tumor, a tumor necrosis displays a less hyperintense signal, however, to avoid potential misinterpretation caused by T2-shine-through effects, evaluation of tumour necrosis and cell density should incorporate quantification of diffusion restriction – especially when evaluating therapy response.

only low impact on the mineralized matrix of the osteogenic sarcoma. However, neo-adjuvant chemotherapy here does have a significant favorable impact on event-free survival. It is essential to monitor the response to chemotherapy to determine whether the prescribed treatment regime is effective. Treatment response is considered successful if more than 90% of the tumor cells histologically show necrosis. However, histological assessment of tumor necrosis during the course of chemotherapy would require repeated biopsy [1].

Diffusion-weighted imaging

The use of water diffusion as a surrogate marker to probe tumor necrosis is compelling because the parameter is strongly affected by membrane permeability between intra- and extracellular compartments, active transport and directionality of cellular structures that impede water mobility. Therefore, diffusion-weighted imaging (DWI) could be used to characterize highly cellular regions of tumors versus regions which change their cellularity (quantifiable by calculating the apparent diffusion coefficient (ADC)) within the tumor over time (acellular and necrotic regions). It could also detect treatment response, which manifests itself as a change in cellularity within the tumor over time [1]. Subtle changes in the degree of restriction of diffusion by, for example, an alteration in cell membrane integrity or permeability to water, are reflected in changes in the diffusion-weighted MR signal. Therefore, we expect a signal change in diffusion-weighted images in necrotic tumour in compari-

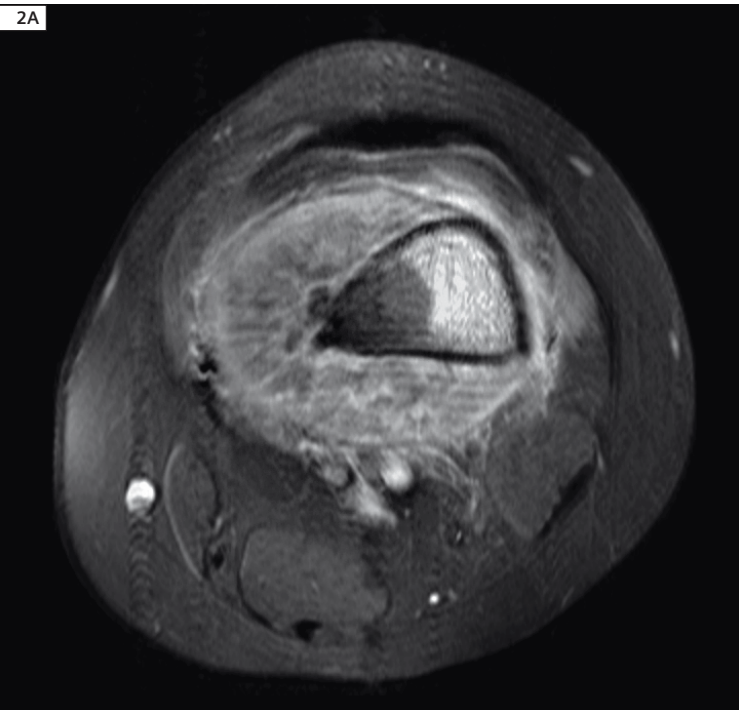
son to viable tumor tissue. We postulated that the water mobility within a tumor would increase over time after treatment and that the magnitude of change would be related to the effectiveness of therapy which results in membrane damage and subsequent reduction in cell density. Based on a clinical feasibility study in eight patients [1], we found a correlation between the increase of signal in ADC maps and the amount of necrotic tumor-cells in treated human osteogenic sarcomas, indicated by the histological Salzer-Kuntschik-index. Chemotherapy is considered satisfactory if more than 90% of tumor volume becomes necrotic (Salzer-Kuntschik grades 1, 2 or 3). In these cases, the increase in ADC value was more than 0.33×10^{-3} mm²/sec despite steady tumor volumes during chemotherapy. Calculation of ADC was based on a three scan-trace DWI EPI MR sequence with b-values up to 700 s/mm²; a linear decay of the signal was assumed. These preliminary results reveal that the calculation of an ADC value seems a promising quantitative and sensitive substitute for monitoring the response to chemotherapy in osteosarcoma. The value of DWI for determining therapy response in case of osteosarcoma could also be shown in animal studies e.g. we observed a significant relationship between dosages of treosulfan applied in a Ewing sarcoma mice model, and effect on ADC as well as delayed tumor volume response [4]. Since the cellularity of osteosarcomas is heterogeneous, especially post-chemotherapy, the variations in the ADC values are large. For this reason, Kiyoshi [2] considered that the average ADC did not necessarily reflect the higher cellularity

component in osteosarcomas. He presumed that the areas with the highest cellularity within heterogeneous tumors best reflect the characteristics of the tumors. According to Kiyoshi, we are now using the minimum ADC in the solid tumor components. A significant difference can be demonstrated between the patients with a good response to chemotherapy and those with a poor response. We can therefore assume that the minimum ADC, which reflects a higher cellular component in the tumor, provides more valuable information for patients with osteosarcoma.

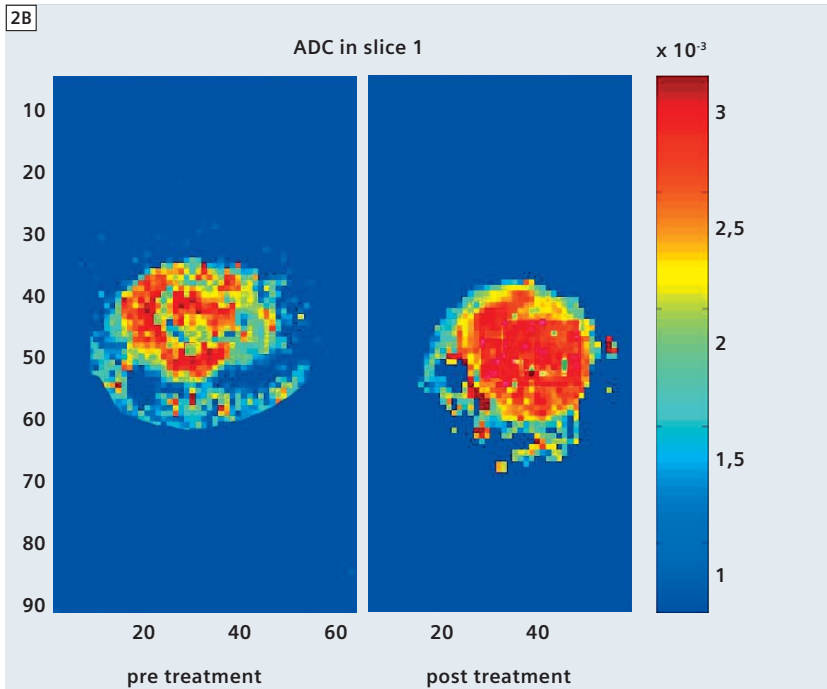
DWI as a prognostic tool

Based on the results of Kiyoshi's study, the use of the minimum ADC for evaluating the histological response to chemotherapy in osteosarcoma is considered preferable to the use of the average ADC. Calculating the ADC ratios ($(ADC_{\text{post}} - ADC_{\text{pre}}) / ADC_{\text{pre}}$) using the minimum ADC, patients with a good response had a significantly higher minimum ADC ratio than those with a poor response (1.01 ± 0.22 and 0.55 ± 0.29 respectively, $p < 0.05$).

Since the high tumor necrosis rate after chemotherapy is an important prognostic factor, the minimum ADC ratio might be the most useful prognostic factor in imaging for patients with osteosarcoma [3]. The COSS-study group (European Cooperative Osteosarkoma study group) is currently prospectively testing this fascinating new method. Final results showing the significance of DWI-monitoring of osteosarcomas are expected in 2014.



2A Osteosarcoma of the distal femur before chemotherapy (T1-weighted fat-saturated Spin Echo sequence after intravenous contrast medium application). Notice the large soft-tissue part of the bone tumor. (Note: slight motion artifacts present in this MR image; DWI is in general acquired before administration of contrast media, also EPI based DWI is less error-prone as a consequence of motion as compared to conventional morphologic MR sequences.)



2B The ADC map displays the proton-diffusion within the tumor. In comparison, after 4 cycles of chemotherapy the tumor ‘becomes more red’ as a consequence of increased ADC values, or in other words, more necrotic. In histology, more than 90% of tumor cells were necrotic (good result of chemotherapy). Please note different degrees of necrosis within the tumor tissue, as shown by local variances of degree of increase of ADC values. ADC calculation and further analysis was performed in this case by a self-written evaluation tool (MATLAB®, The MathWorks Inc.), however, ADC values can easily be derived in clinical routine from ADC maps which are automatically calculated by an Inline tool, available for all DWI capable scanners.

References

1 Uhl M, Saueressig U, Koehler G, Kontny U, Niemeyer C, Reichardt W, Ilyasof K, Bley T, Langer M. Evaluation of tumour necrosis during chemotherapy with diffusion-weighted MR imaging: preliminary results in osteosarcomas. *Pediatr Radiol.* 2006 Dec; 36(12):1306–11.

2 Kiyoshi Oka, Toshitake Yakushiji, Hiro Sato et al. The value of diffusion-weighted imaging for monitoring the chemotherapeutic response of osteosarcoma: a comparison between average apparent diffusion coefficient and minimum

apparent diffusion coefficient. *Skeletal Radiol* (2010) 39:141–146.

3 Bley TA, Wieben O, Uhl M. Diffusion-weighted MR imaging in musculoskeletal radiology: applications in trauma, tumors, and inflammation. *Magn Reson Imaging Clin N Am.* 2009 May; 17(2):263–75.

4 Reichardt W, Juettner E, Uhl M, Elverfeldt DV, Kontny U. Diffusion-weighted imaging as predictor of therapy response in an animal model of Ewing sarcoma. *Invest Radiol.* 2009 May; 44(5):298–303.

Contact

Prof. Dr. Markus Uhl
 RKK
 Diagnostic and Interventional Radiology
 Pediatric Radiology
 Sautierstr. 1
 79104 Freiburg
 Germany
 Phone: +49 761-270-3940
 markus.uhl@rkk-sjk.de

Musculoskeletal Advisory Board Provides Protocols for 1.5 and 3T MAGNETOM systems

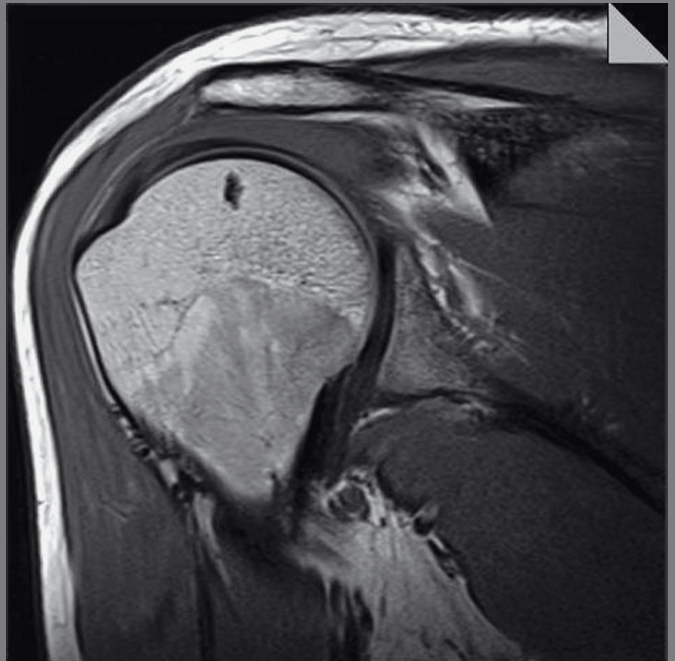
We have launched the MSK Advisory Board website, providing proven MSK protocols (.edx files) for download. To support Technologists there are also coil positioning videos and tips & tricks.

Board members are:

- Christian Glaser, LMU Grosshadern, Germany
- Jürg Hodler, Balgrist University Hospital, Switzerland
- Young-Jo Kim, Harvard Medical School, Children's Hospital Boston, USA
- Tallal Charles Mamisch, Bern University, Switzerland
- Michael Recht, New York University, USA
- Siegfried Trattnig, AKH Wien, Austria
- Lawrence M. White, University of Toronto, Canada

Visit us at

www.siemens.com/magnetom-world



Case Report:

Transient Patellar Dislocation

Claudia C. Cotes, MD; Raghuram K. Rao, MD, MPH; Harnoor Singh, MD

University of Texas-Medical Branch, Galveston, TX, USA

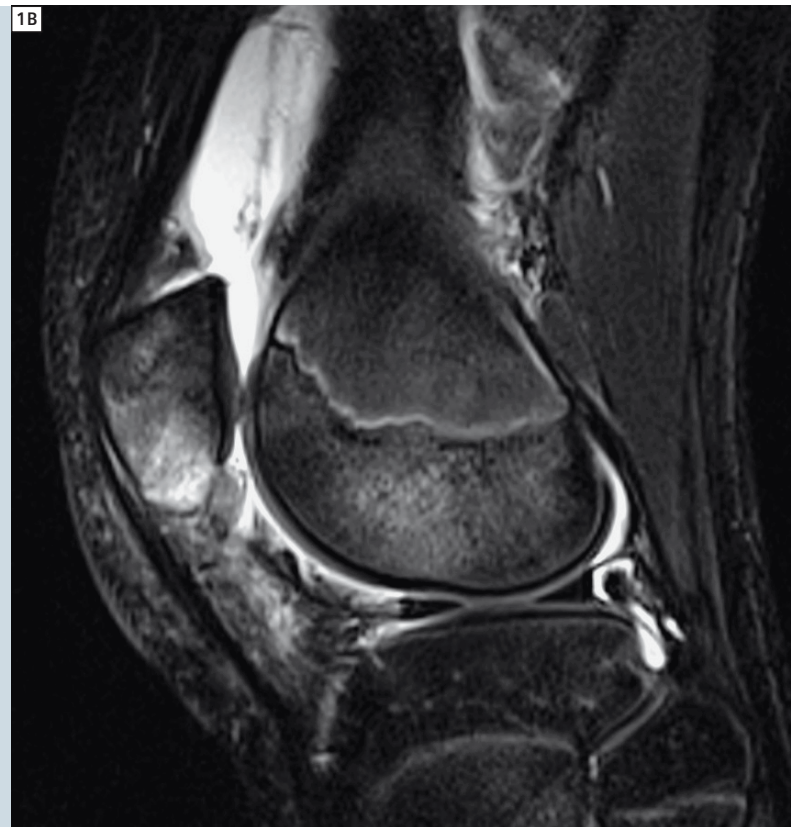
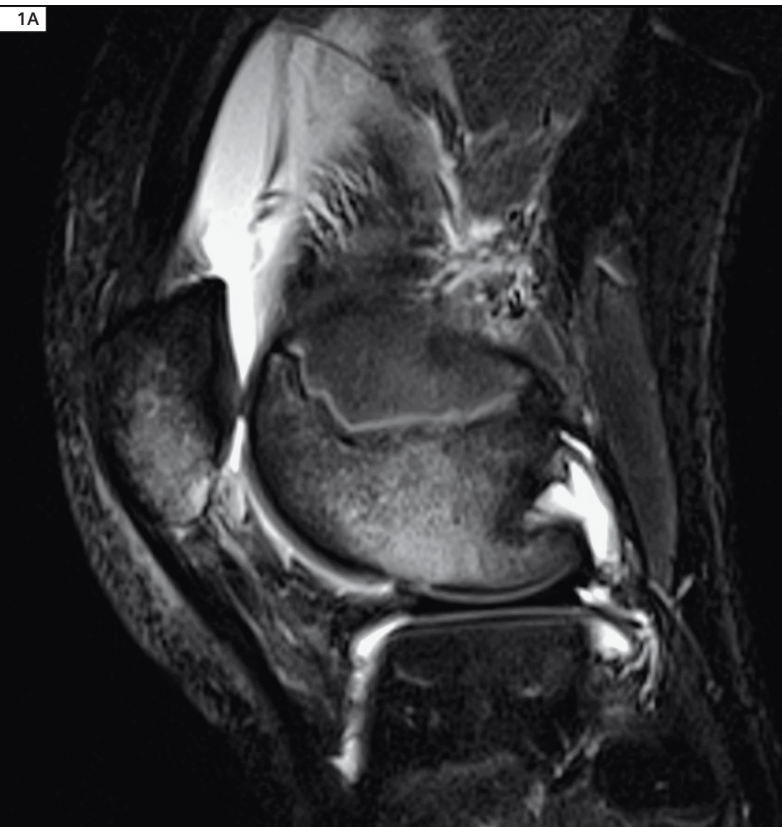
Patient history

A 13-year-old active boy with no past medical history arrived to the Emergency Room complaining of pain in the medial aspect of his left knee. He had a non-contact injury during athletics at school, and he is unsure of the position of the knee during the injury. The patient ambulates with difficulty using a single

crutch. Physical exam demonstrated mild pain during flexion with intact extension, tenderness to palpation over the medial retinaculum, and stable Lachman test and no drawer sign. A radiograph of the left knee revealed no fractures and a small suprapatellar joint effusion. The patient underwent an MRI for further evaluation.

Sequence details

Images were obtained utilizing a 3T Siemens MAGNETOM Verio scanner utilizing an 8-channel knee coil. The sequence parameters used were: Figures 1A–C: Sagittal STIR (TR/TE 5580/34 ms, scan time 2:12 min, slice thickness 3 mm). Figures 2A–B: Coronal T1 TurboIR with



1A–C Sagittal STIR images show moderate bone contusions.

Magnitude Display (TIRM) using iPAT with a factor of 2 (TR/TE/TI 5250/34/220 ms, scan time 2:12 min, slice thickness 3 mm).

Figure 3: Axial T2-weighted image (TR/TE 833/23 ms, scan time 3:45 min, slice thickness 3 mm).

Figure 4: Sagittal T2-weighted Turbo Spin Echo (TSE) using iPAT with a factor

of 2 with a base resolution of 384 (TR/TE 4880/70 ms, scan time 3:41 min, slice thickness 3 mm).

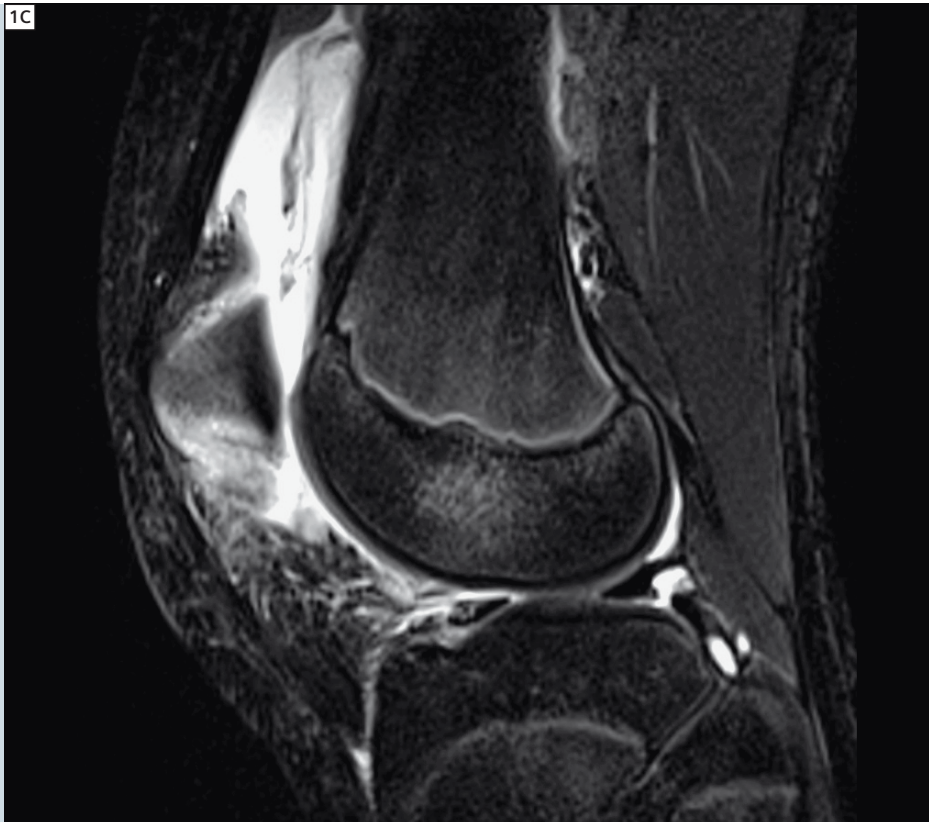
Imaging findings

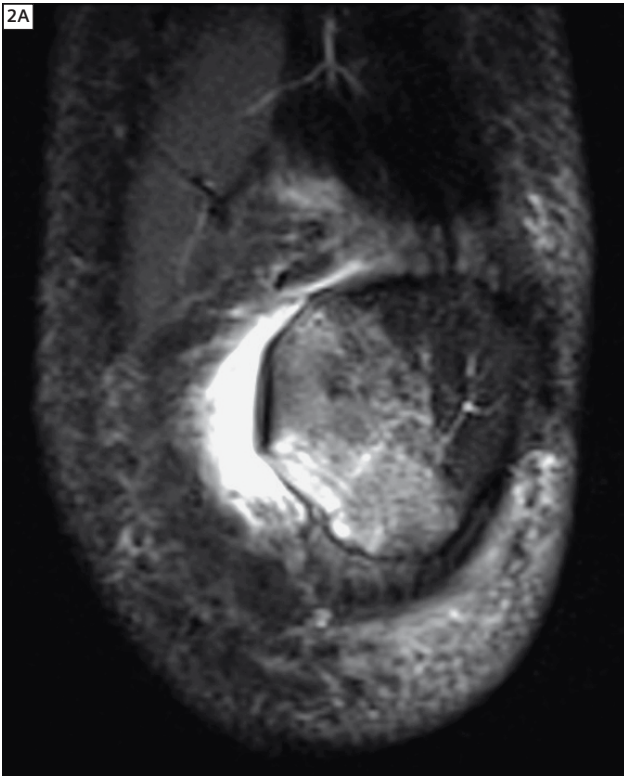
MRI of the left knee shows a partial tear of the medial patellar retinaculum at its patellar insertion (Fig. 3) and moderate bone contusions in the anterolateral

femoral condyle and medial aspect of the patella (Figs. 1A, B, and 2B). A nondisplaced fracture is present in the inferomedial pole of the patella, which extends to the articular margin (Figs. 1C and 2A). A large lipohemarthrosis is present (Fig. 4).

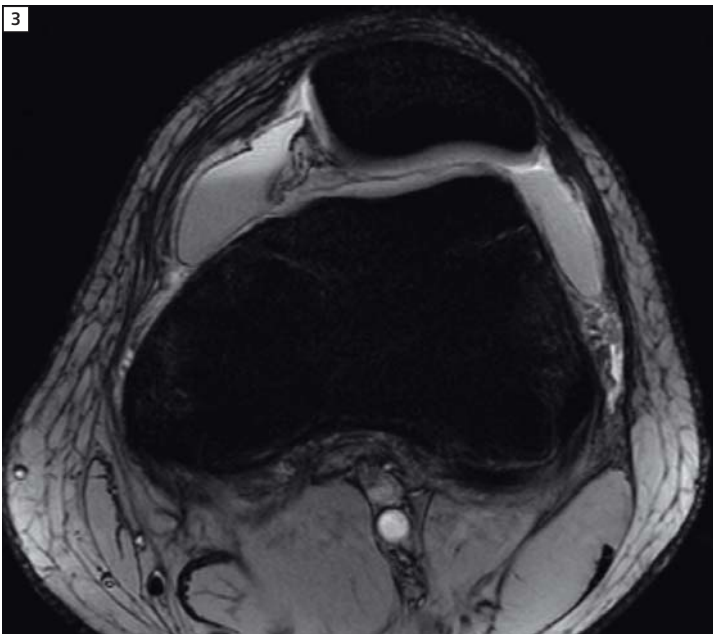
Discussion

Patellar dislocation most commonly occurs in young athletic patients. It results from rotational motions of the knee with rupture of the medial patellofemoral ligament and medial patellar retinaculum, the main stabilizers of the patella. The dislocation is usually transient, and the patella returns to its normal location immediately after the injury. When it occurs in women in the second decade of life, risk factors such as patella alta and trochlear dysplasia play an important role. MRI is the modality of choice in patellar dislocation. It clearly depicts the typical findings including medial patellofemoral ligament and medial patellar retinaculum injury, bone contusion, and joint effusion, as well as the previously mentioned risk factors (if present), all of which determine patient treatment.





2 Coronal TIRM images.



3 Axial T2-weighted image shows partial tear of the medial patellar retinaculum.



4 Sagittal T2-weighted Turbo Spin Echo (TSE) shows a large lipohemarthrosis.

Contact
Claudia C. Cotes, MD
University of Texas-Medical Branch

Galveston, TX
USA
cccotes@utmb.edu

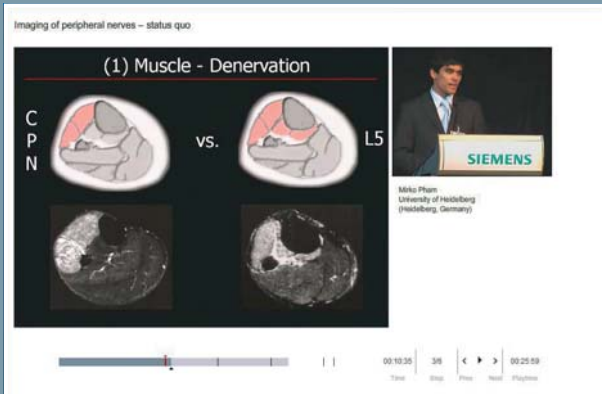
Relevant clinical information at your fingertips

From technology to clinical applications, you will find all the latest news on Siemens MR at

www.siemens.com/magnetom-world

Imaging of peripheral nerves – status quo

(1) Muscle - Denervation



Mikko Pfann
University of Heidelberg
(Heidelberg, Germany)

Don't miss the talks of international experts on Magnetic Resonance Imaging.

Go to
Education > e-trainings & Presentations

Case Report:
Traumatic Lesion of the Left Brachial Plexus

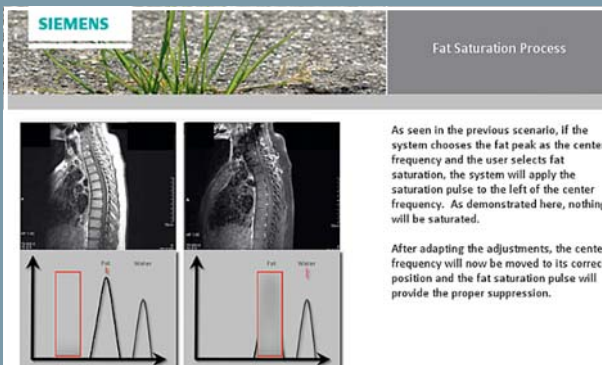


The centerpiece of the MAGNETOM World Internet platform consists of our users' clinical results. Here you will find case reports and clinical methods.

Go to
Clinical Corner > Case Studies

SIEMENS

Fat Saturation Process



As seen in the previous scenario, if the system chooses the fat peak as the center frequency and the user selects fat saturation, the system will apply the saturation pulse to the left of the center frequency. As demonstrated here, nothing will be saturated.

After adapting the adjustments, the center frequency will now be moved to its correct position and the fat saturation pulse will provide the proper suppression.

Just a mouse click away you will find application videos and useful tips allowing you to optimize your daily MR examinations.

Go to
Clinical Corner > Application Tips

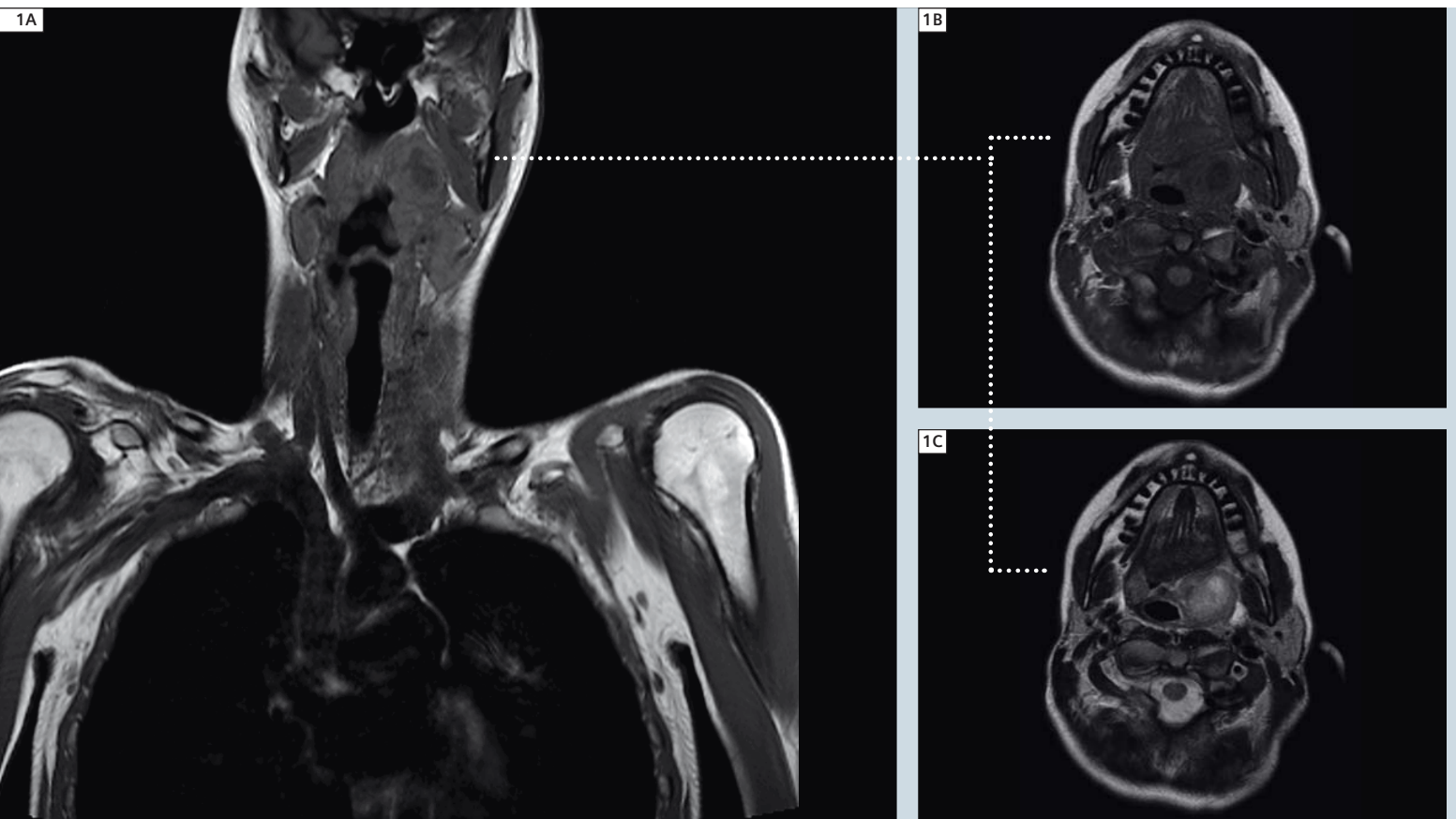
For the whole range of clinical MR information visit us at

www.siemens.com/magnetom-world

Case Series: Body Trunk Imaging of Inflammatory Disease in Childhood and Adolescence

G. Schneider, MD, PhD; A. Bücken, MD

Saarland University Hospital, Dept. of Diagnostic and Interventional Radiology, Homburg / Saar, Germany



1 Coronal T1w TSE (1A) and corresponding transversal native T1w SE (1B) and T2w TSE (1C).

Case 1

Patient history

A 6-year-old girl presented at our MR department with the clinical suspicion of a peritonsillar abscess; the request was not to prove the peritonsillitis but to provide reliable information about the presence / absence of an abscess. The

imaging protocol included unenhanced coronal TIRM and T1w TSE images as well as transversal T1w SE and T2w TSE sequences; after injection of Gd-DTPA, axial and coronal T1w TSE with fat saturation (Dixon technique) were acquired.

Imaging findings

The space occupying lesions of the left hypopharynx proved to be inhomogenous on T2w and partially hypointense on T1w images with peripheral contrast-media enhancement. With a maximum diameter of 3.5 x 3 x 5.7 cm, the structure reaches

Background

In our daily clinical practice, children presenting with signs of infection and inflammation either spontaneously or after any type of intervention undergo a thorough clinical examination including blood tests as the first and most important evaluation step.

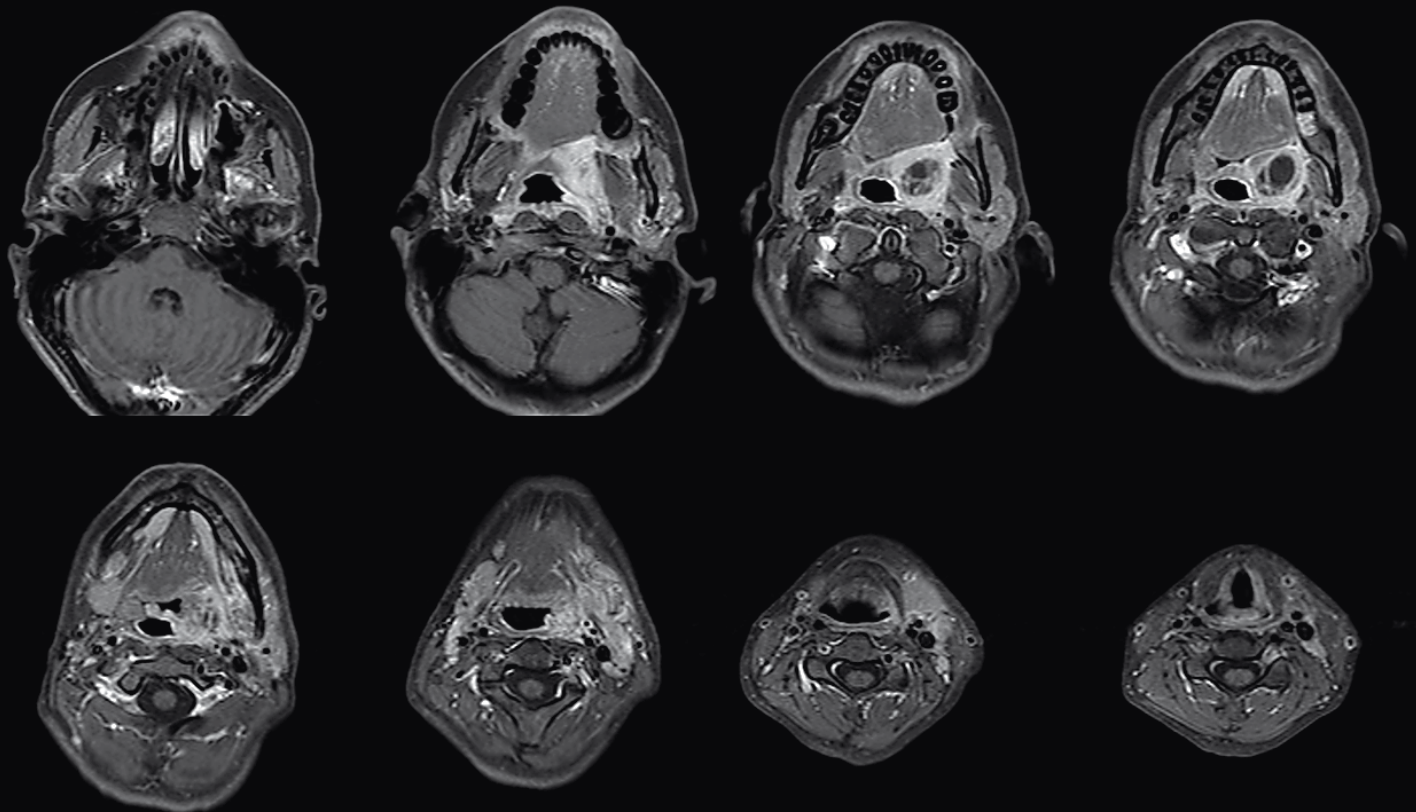
Nowadays, clinical examination of these children includes ultrasound as imaging modality of first choice. It allows to answer most of the clinical questions

e.g. appendicitis, nephritis, enteritis – to name a few. Thereby, it usually supports the clinician in narrowing the differential diagnoses sufficiently to make a therapeutic decision. However, if the therapeutic decision points towards surgery consequently imaging prompts for very accurate diagnosis. Abscess formations, necrosis or perforations have to be depicted fast and accurately in order to be able

to adequately choose therapy. One example is surgery in case of perforated appendicitis, which might not be diagnosed by clinical examination, laboratory tests and even ultrasound with sufficient accuracy. There are many reasons for this, but incomplete visualization of all relevant anatomical structures because of bowel air is one of the most common practical problems for ultrasound. However, ultrasound demonstrates

Continued on page 30

1D



1D Post-contrast T1w TSE with fat saturation (Dixon) demonstrating the extent of the abscess.

from dorsal of the left nuchal nerve / vessel street up to the left mandible. A mass effect towards the pharynx can be seen. But, so far, no relevant narrowing of the pharynx has occurred. Lymph nodes are seen but none of these are significantly

enlarged. The examination reveals regular pneumatisation of the mastoids and sinuses. No suspicious finding in the upper mediastinum and apical lung was found.

The unambiguous diagnosis of an abscess of the left palatine tonsil accompanied by mass effect towards the pharynx prompted immediate surgery followed by an uneventful recovery of this young girl.

Case 2

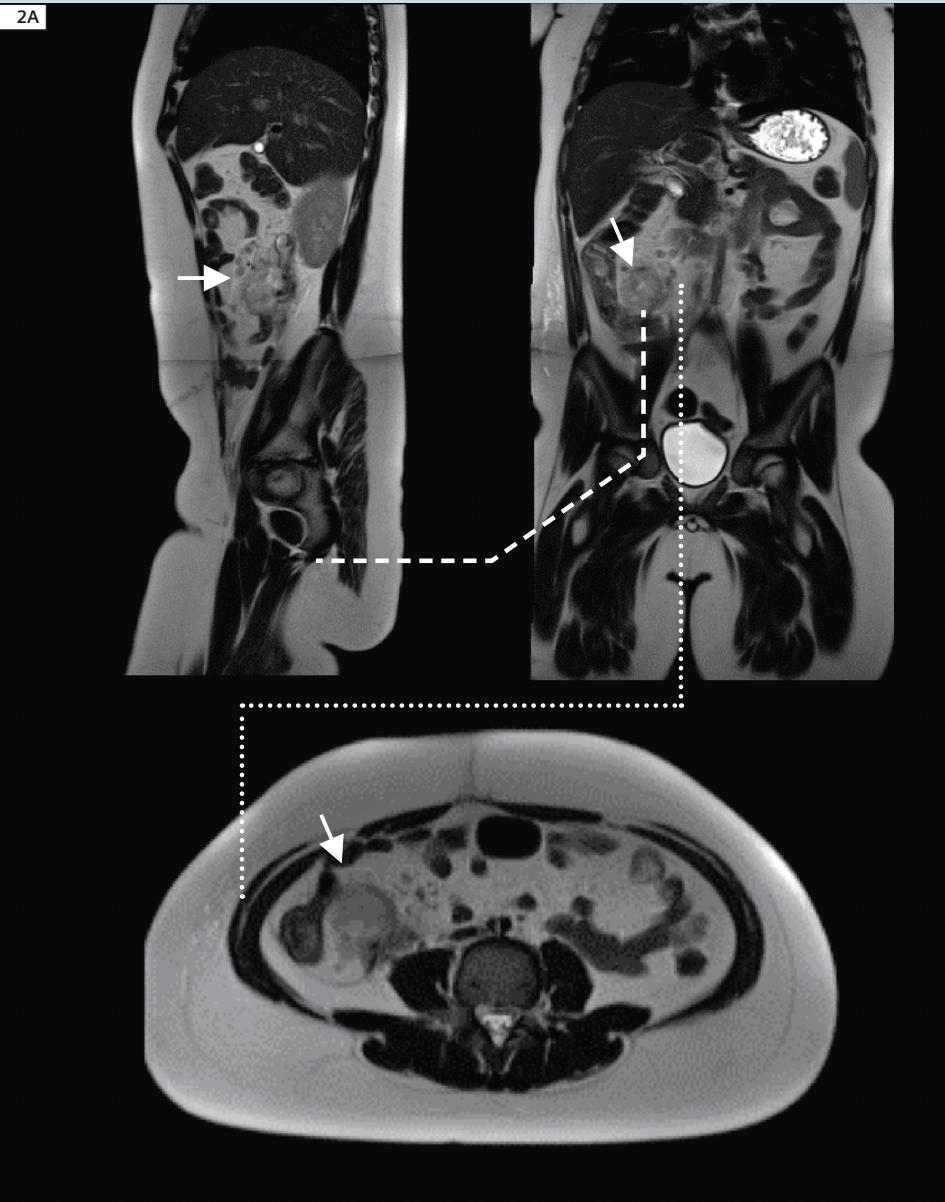
Patient history

A 3-year-old boy underwent laparoscopic appendectomy because of the diagnoses of a perforated appendicitis. After initial good recovery, the boy presented with signs of infection and abdominal pain. Two weeks after surgery, he was referred to our MR unit for further evaluation.

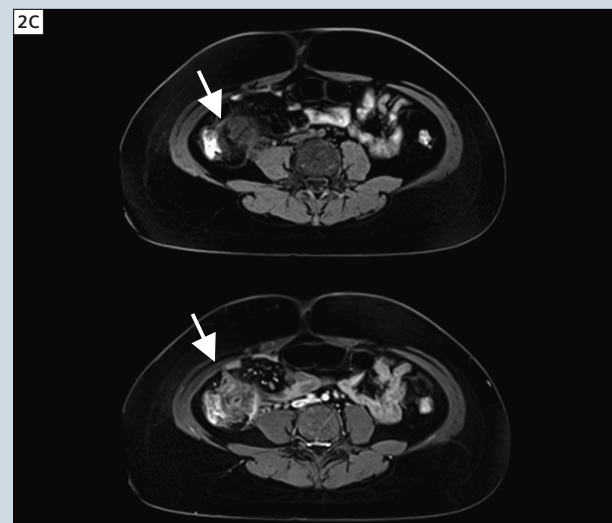
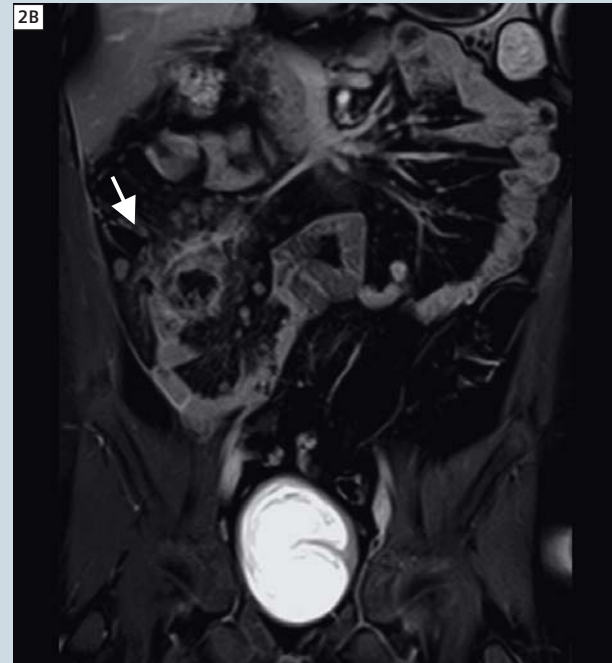
Imaging protocol included HASTE (coronal, transversal and sagittal), axial T1w 2D FLASH and T2w TSE as well as DWI (including ADC mapping). After injection of 0.05 mmol/kg bodyweight Gd-BOPTA, transversal and coronal T1w 2D FLASH with fat saturation were acquired.

Imaging findings

In the area of the former appendix, a contrast-media enhancing, central necrotic appearing mass with a diameter of approximately 4 cm can be seen. The perifocal fatty tissue shows signs of diffuse oedemateous reaction as well as contrast-media uptake. Multiple lymph



2A Sagittal, coronal and transversal HASTE demonstrating a mass at the location of the resected appendix.

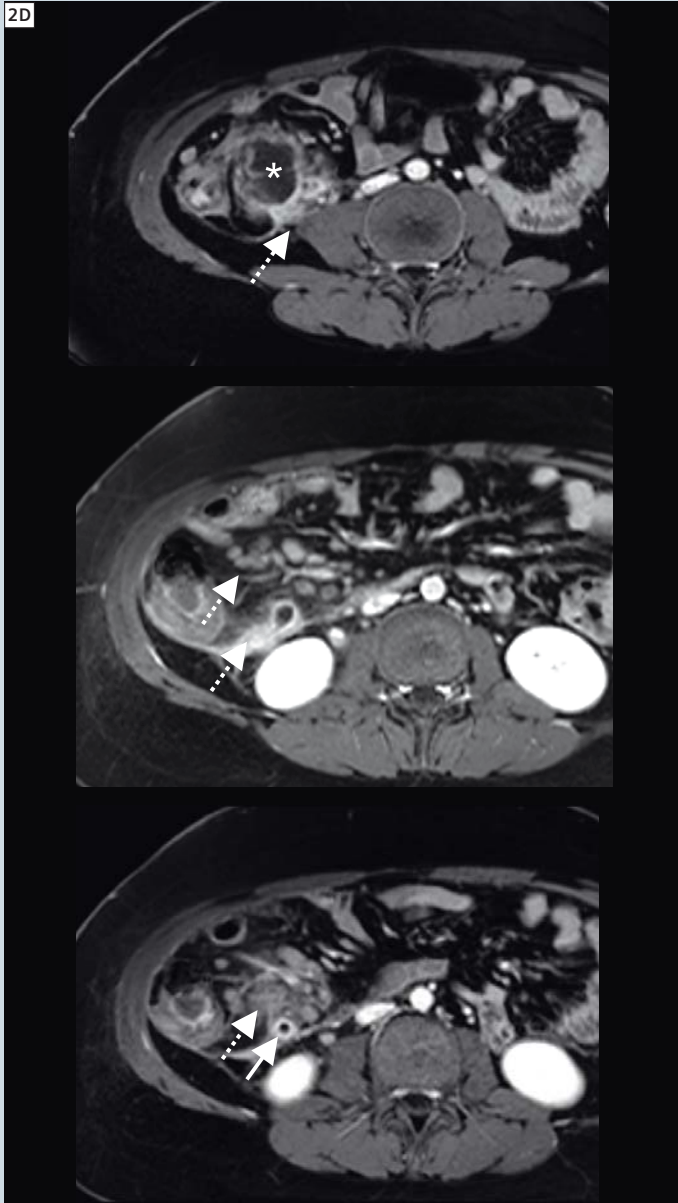


2B, C Coronal (2B) and transversal (2C) T1w 2D FLASH with fat saturation after contrast media injection showing the abscess formation.

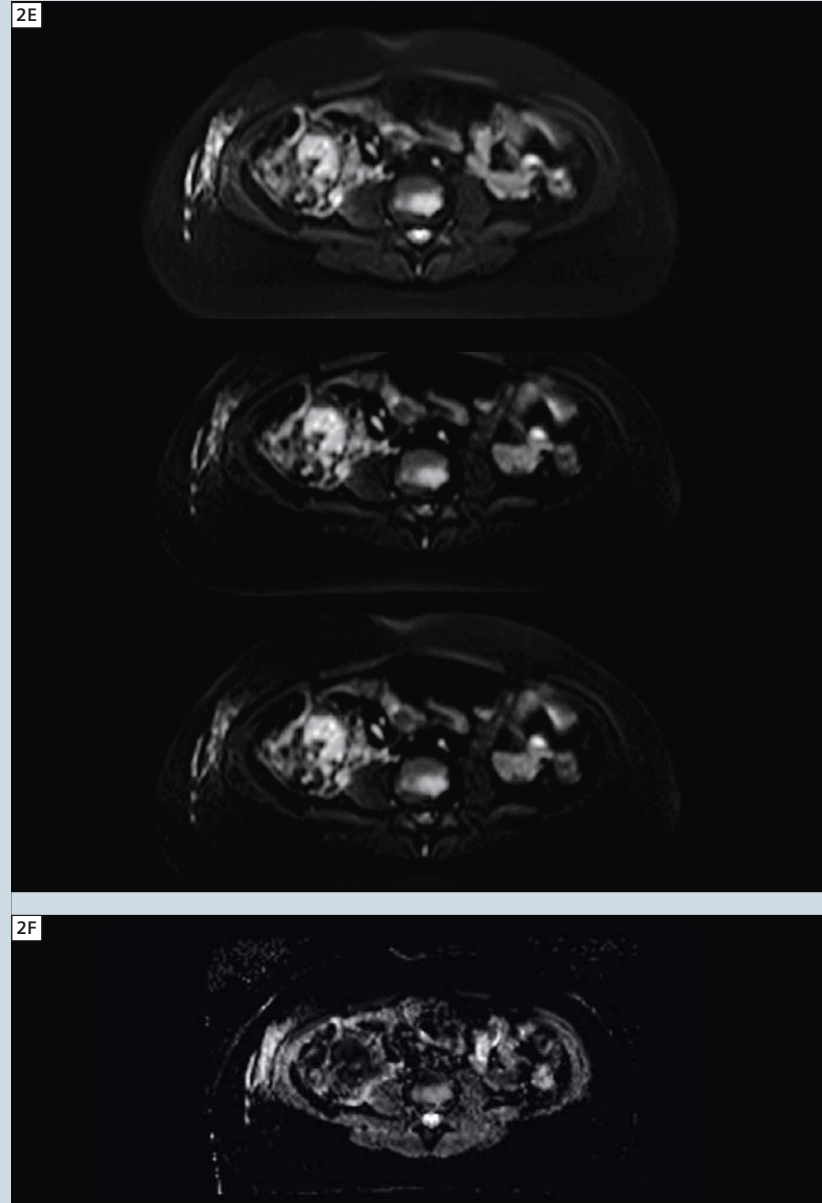
nodes are shown in this area, too. In addition, further signs of inflammation and smaller necrotic areas ventral to the right kidney and broad contact to Gerota's fascia is seen. There are no signs of free fluid within the abdomen or pelvis. The other parenchymal

organs show no pathologies. Based on the imaging findings, the diagnosis of an abscess formation after laparoscopic appendectomy was given. Treatment decision was open surgery. The abscess was removed and a drain was inserted. The boy recovered fast and

could leave the hospital 5 days post treatment.



2D Magnified transversal images after contrast-media injection showing in detail the abscess (*), surrounding inflammation reaction (dotted arrows) and further abscess suspicious formation (arrow) with direct contact to the ventral border of the Gerota fascia.



2E, F Original b-value images of the DWI scan (b = 50, 400, 800 s/mm²) and corresponding ADC map (2F).

a higher clinical efficiency in small children and adolescents compared to adults. This is mainly due to the reduced depth to be imaged allowing higher frequency probes and better spatial resolution in pediatric ultrasound examinations compared to its application in older and especially obese patients. Furthermore, manoeuvres to displace disturbing air and alternative approaches to image relevant structures e.g. assessment of the appendix via a dorsolateral subrenal view instead of the left fronto-lateral window, are more often successful in younger patients.

But what if ultrasound fails or because of the invasiveness of the therapeutic decision further imaging is required to strengthen the diagnostic confidence and therapy planning?

In most of these cases, computed tomography (CT) is used as a robust, fast and nowadays 24/7 available imaging modality. But despite all attempts to reduce radiation exposure, the utilization of imaging modalities like x-ray, fluoroscopy and CT [1], still use ionizing radiation with potentially harmful effects. This is especially true for children, who are more susceptible to ionizing radiation as compared to adults [NRPB (1999). "Guidelines on patient dose to promote the optimization of protection for diagnostic medical exposure." Radiological Protection Board 10(1).].

In this clinical scenario, MRI offers two advantages as compared with CT: First a superior soft tissue contrast and second a complete lack of ionizing radiation. Consequently, MRI is very often used in clinical settings, when inflammation is considered a differential diagnosis, e.g. juvenile dermatomyositis, juvenile idiopathic arthritis, meningitis and encephalitis [2-5] are clinical questions where CT cannot provide the required information offered by MRI. In addition,

MRI often is also able to differentiate the origin of soft tissue masses [6]. Regarding availability of MRI, at least in maximum-care centres, MRI is available on an emergency basis. In addition, by applying sequences such as HASTE or using motion artifacts reducing k-space acquisition schemes like BLADE, MRI can provide a high and robust image quality even in less compliant patients, where conventional MR techniques might fail. We present two cases from our daily routine that probably would not have undergone MRI ten years ago. These cases clearly demonstrate that MRI can play an important role in imaging of inflammatory complications and infection outside the brain in pediatric patients. These new possibilities using today's state of the art imaging techniques in MRI are asking for a re-evaluation of a daily practise, where CT is often considered the one and only emergency imaging modality beyond ultrasound imaging.

General remarks on applied imaging protocols

All images shown were acquired at 1.5 Tesla (MAGNETOM Aera); for the body trunk (pelvis / abdomen to the upper mediastinum), a combination of the 18-channel body coil(s) with the integrated 32-channel spine coil was used; for imaging of the neck and skull base, the standard 20-channel head / neck coil was added. Administration of contrast media is in our view essential in cases of inflammation and its potential complications. We also apply routinely diffusion-weighted imaging (DWI) for abdominal scans. According to our experience DWI allows excellent visualization of inflamed tissue. However, its relevance for differentiating inflammation versus tumor or therapy response to anti-inflammatory drugs, is still subject of clinical research.

References

- 1 image gentlySM – The Alliance for Radiation Safety in Pediatric Imaging <http://www.pedrad.org/associations/5364/ig/>
- 2 Damasio MB, Malattia C, Martini A, Tomà P. Synovial and inflammatory diseases in childhood: role of new imaging modalities in the assessment of patients with juvenile idiopathic arthritis. *Pediatr Radiol.* 2010 Jun;40(6):985-98. Epub 2010 Apr 30. Review.
- 3 Tzaribachev N, Well C, Schedel J, Horger M. Whole-body MRI: a helpful diagnostic tool for juvenile dermatomyositis case report and review of the literature. *Rheumatol Int.* 2009 Oct;29(12):1511-4. Epub 2009 Mar 20. Review.
- 4 Bonthius DJ, Karacay B., Meningitis and encephalitis in children. An update. *Neurol Clin.* 2002 Nov;20(4):1013-38, vi-vii. Review.
- 3 Faingold R, Oudjhane K, Armstrong DC, Albuquerque PA. Magnetic resonance imaging of congenital, inflammatory, and infectious soft-tissue lesions in children. *Top Magn Reson Imaging.* 2002 Aug;13(4):241-61. Review.
6. Turkington JR, Paterson A, Sweeney LE, Thornbury GD. Neck masses in children. *Br J Radiol.* 2005 Jan;78(925):75-85. Review.

Contact

PD Dr. Dr. Günther Schneider
Dept. of Diagnostic and Interventional
Radiology
Saarland University Hospital
Kirrberger Strasse
66421 Homburg/Saar
Germany
dr.guenther.schneider@uks.eu

Pediatric* MR Urography

Richard A. Jones; Stephen Little; J. Damien Grattan-Smith

Children's Healthcare of Atlanta, Department of Radiology, Atlanta, GA, USA

MR urography represents the next stage in the evolution of urology because it fuses superb anatomic and functional imaging in a single test that does not use ionizing radiation. It has the potential to revolutionize the imaging approach to renal disease in children. MR urography has advantages over other modalities in that it generates tissue contrast from a variety of sources. In addition to spin echo T1 and T2-weighted images, dynamic imaging is performed in conjunction with the injection of a Gadolinium based contrast agent (GBCA) in order to assess the concentrating and excretory functions of the kidney. The evaluation of the dynamic contrast-enhanced images is similar to renal scintigraphy but with the important distinction that the signals originating from the renal parenchyma can be separated from those originating from the collecting system. The primary indication for MR urography is in the evaluation of hydronephrosis. Other evolving indications for MR urography include evaluation of renal scarring and dysplasia, identification of ectopic ureters in children with urinary incontinence and characterization of renal masses.

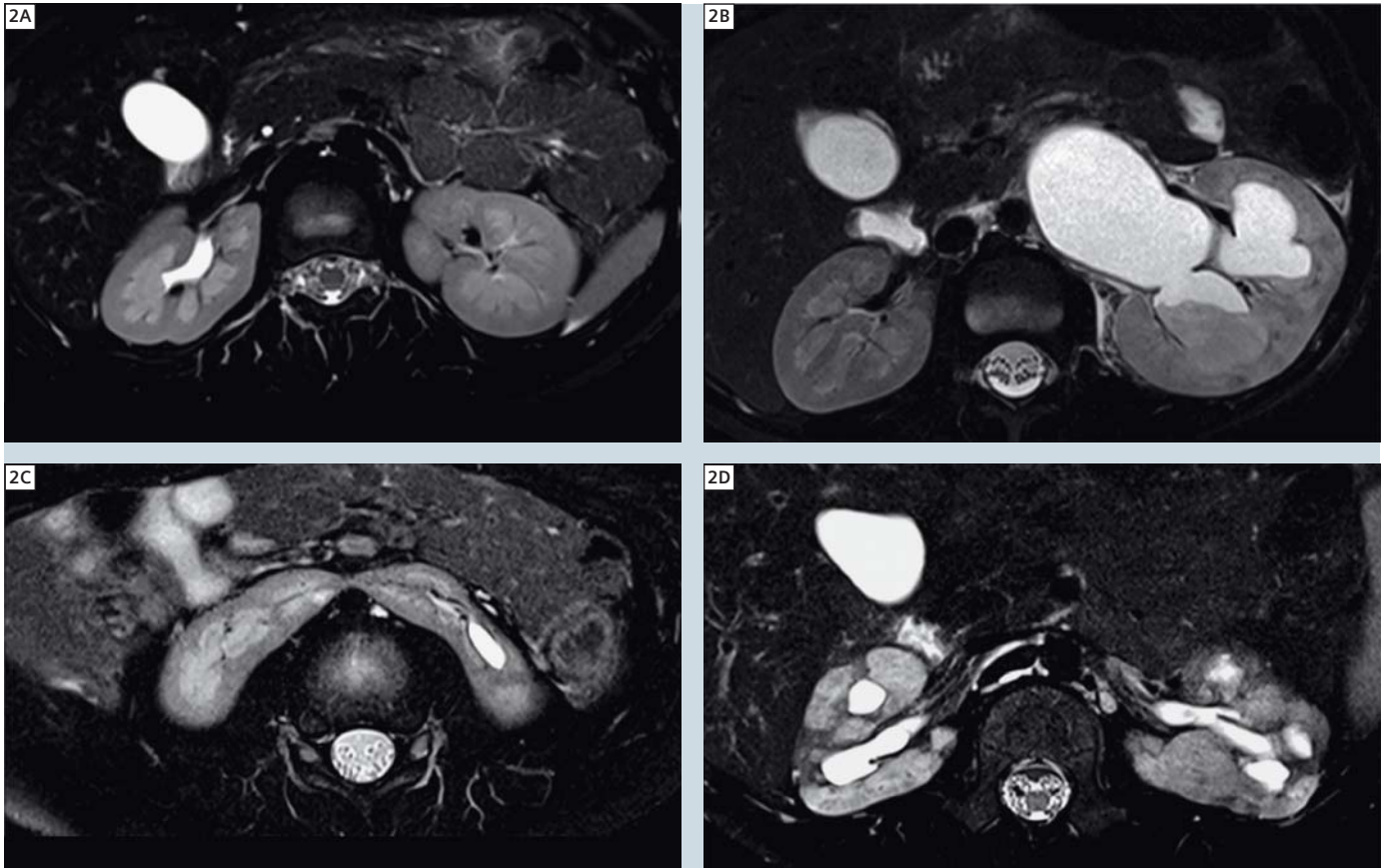
Patient preparation of MR urography is of crucial importance. For a patient where the indications are hydronephrosis, renal scarring and dysplasia the patient preparation consists of hydration, injection of a diuretic agent, bladder catheterization and, in younger children, sedation. When the indication is a renal mass the diuretic and the bladder catheter can be omitted. Because a fluid challenge is integral to a high quality study, and because we want to limit the concentration of the GBCA in the kidney, the patient has to be hydrated prior to the start of the study and the hydration regime needs to be as reproducible as



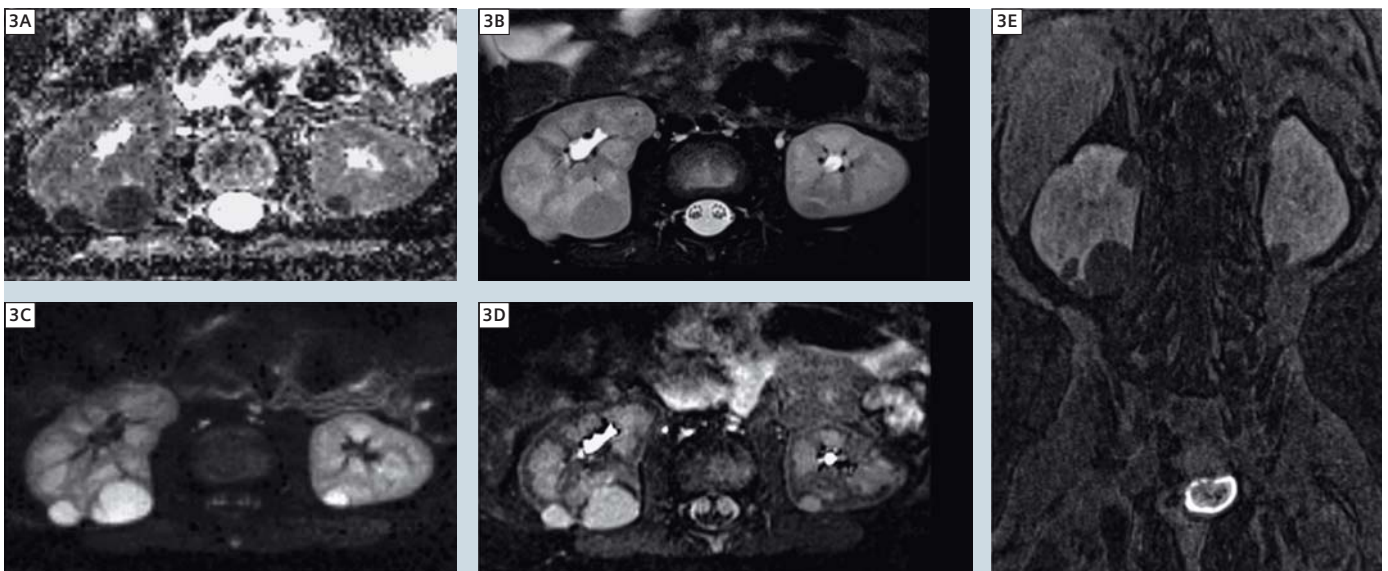
1 Two oblique views of a MIP created from the heavily T2-weighted volumetric sequence for a patient with an ectopic insertion of the ureters from the upper pole of a duplex kidney.

possible. For this reason we use standardized intravenous hydration regime. If children are to be sedated, we correct their nil per os (NPO) deficit using Ringer's solution according to the following formula:
4 ccl/kg/hour for first 10 kg of patient's weight
2 ccl/kg/hour for next 10 kg of patient's weight
4 ccl/kg/hour for each kg above 20 kg patient's weight
 If the child is not going to be sedated we

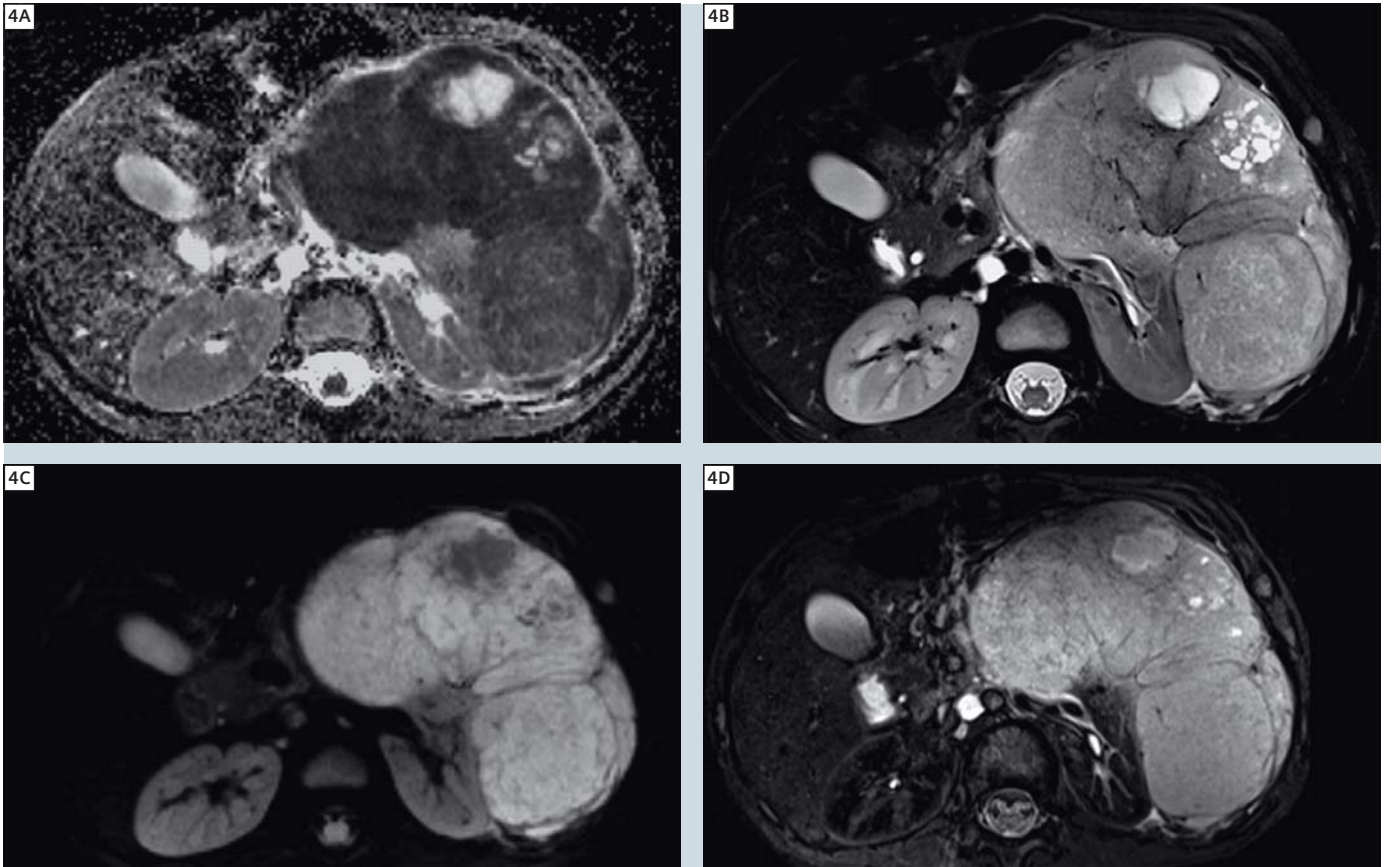
hydrate with Ringer's solution at a dose of 10 cc/kg and given intravenously over 30–40 minutes. The second element of the fluid challenge is an injection of a loop diuretic (Furosemide). We use a standard dose of 1 mg/kg, up to a maximum dose of 20 mg, injected 15 minutes prior to the injection of the GBCA. In addition to being an integral part of the fluid challenge the early administration of the furosemide distends the urinary tract and minimizes the duration of the study. By administering the GBCA after



2 T2-weighted axial images from 4 patients. Fig. **2A** is from a relatively normal subject and shows good cortico-medullary differentiation. Fig. **2B** is from a patient with pyelonephritis, poor cortico-medullary differentiation is seen in the left kidney along with a fluid level in the collecting system. Fig. **2C** is through the isthmus of a patient with a horseshoe kidney. Fig. **2D** is from a patient with severe renal dysplasia and shows cortical scarring and poor cortico-medullary differentiation.



3 Shows images from a child with nephroblastomatosis. Figs. **3A** and **3C** are the ADC and isotropic diffusion-weighted images respectively. Figs. **3B**, **3D** and **3E** are pre-contrast T2-weighted, post-contrast STIR and post-contrast T1-weighted (delayed volume) images respectively. There are multiple small peripheral masses that are homogeneous in appearance on all imaging sequences as well as demonstrating restricted diffusion when compared with normal kidney.



4 Shown images from a 3-year-old girl with Wilms tumors. Figs. **4A** and **4C** are the ADC and isotropic diffusion-weighted images respectively. Figs. **4B** and **4D** are pre-contrast T2-weighted and post-contrast STIR respectively. Wilms tumors are large and heterogeneous in signal characteristics containing both solid and cystic areas. There is restricted diffusion within the mass, but it is not as homogeneous as in areas of nephroblastomatosis.

the fluid challenge and during the time of maximal diuresis, pathophysiological changes in the kidney that occur in response to this stressed state can be visualized. A bladder catheter is placed whenever possible. The main reason for placing a catheter is that children become uncomfortable and tend to wake from sedation if the bladder is full. There are additional imaging benefits from using a bladder catheter in that interpretation of the images is easier as confounding issues such as vesico-ureteric reflux and transmitted bladder pressure are eliminated. If there is a question of a bladder abnormality, the catheter can be clamped and images of the distended urinary bladder obtained. Almost all children under 7 years of age will need to be sedated. Optimal solutions include general anesthesia or dedicated sedation physicians who are able to

titrate the depth of sedation for the individual patient. Many of our patients are referred for the evaluation of antenatal hydronephrosis. In this population our sedation physicians usually like to wait until the patient is at least 3 months of age before scheduling the MR urogram. Older children who are not sedated are asked to either breathe quietly or if they are able to co-operate, breathhold imaging is performed for most sequences.

Pre-contrast imaging

One of the strengths of MR urography is the ability to combine both contrast-enhanced imaging with T2-weighted images so that both static and dynamic evaluation of the urinary tract is obtained. This is particularly helpful in cases of marked hydronephrosis or poorly functioning systems. We obtain a 3D heavily T2w urogram which is used to generate

maximum intensity projections (MIPs) and volume rendered images of the pelvic/lyceal system and ureters (Fig. 1). Volume rendered images are very helpful in analyzing duplex systems or complicated anatomical variants. We also perform an axial T2w TSE through the bladder to identify abnormalities of the bladder base including ureteroceles and ectopic ureteric insertion. Additionally we have come to rely on axial high resolution T2-weighted images in the assessment of the renal parenchyma (Fig. 2). These are typically performed immediately after the HASTE scouts and are obtained prior to the Furosemide injection so that we have a baseline evaluation of the degree of hydronephrosis to which we can compare the delayed images. In the case of a renal mass we have found diffusion-weighted imaging to be helpful in the characterization of

the mass and we acquire high resolution diffusion images using either RESOLVE** (readout-segmented EPI) or zoomed-EPI**. The former splits the EPI readout into segments thus reducing the length of the individual EPI echo trains resulting in reducing distortion and allowing higher resolution images with little distortion to be obtained. The latter uses a two dimensional RF pulse to limit the field-of-view in the phase direction in order to achieve the same goals. Because of the limited amount of respiratory related motion in younger patients high quality diffusion images can be obtained using these techniques, leading to reduced partial volume effects and higher image quality (Figs. 3 and 4).

Contrast-enhanced imaging

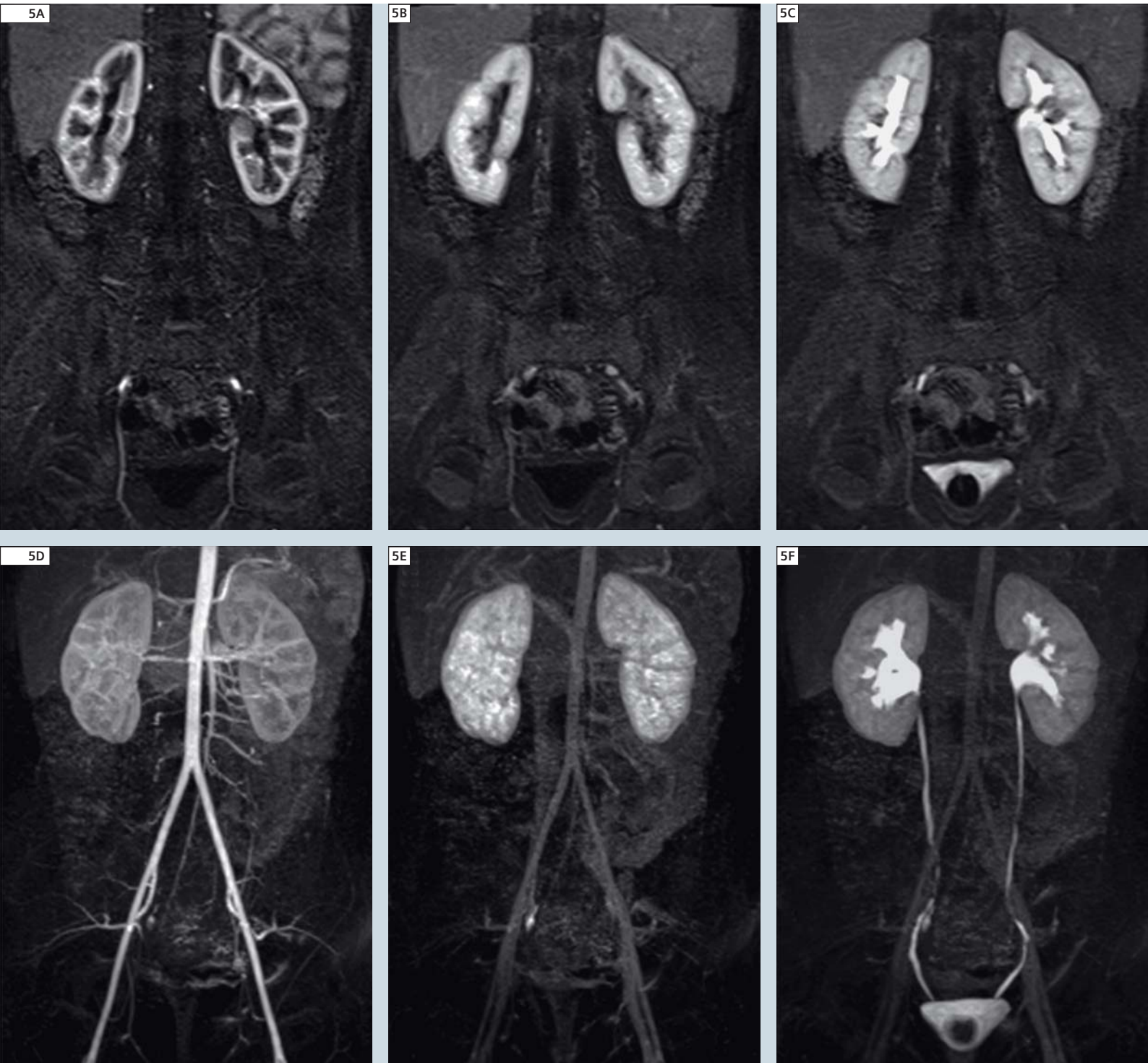
The change in T1 induced by a GBCA is directly related to the concentration and relaxivity of the GBCA. Thus if the T1 relaxation time can be measured, and we assume the relaxivity is the same as that measured ex-vivo, we can calculate the contrast agent concentration. However, a dynamic measurement of T1 is not straightforward, so in clinical practice one tends to use the change in signal, with respect to the pre-contrast images, in order to estimate the concentration of the GBCA. At low concentrations T1 effects predominate and the relationship between signal change and GBCA concentration is relatively linear, however, as the concentration increases T2* effects become increasingly important, leading to signal dephasing and an increasingly non-linear relationship between the change in signal and the concentration of the GBCA. If the signal change is to be used to estimate the concentration of the GBCA then it is important to keep the concentration of the GBCA low enough to ensure it is within the linear range. We use a standard dose (0.1 mmol/kg) of a GBCA (Magnevist) and have found that the standard dose provides excellent enhancement of the kidneys and allows evaluation of the MR nephrogram by differentiating the enhancing parenchyma from the background. Others have

used smaller doses of contrast but we have found that using a lower dose is particularly challenging when trying to segment poorly functioning kidneys. Because of the risks associated with using a GBCA on patients in renal failure a serum creatinine test is used to estimate the glomerular filtration rate (GFR) on all patients. If the total estimated GFR, as measured with serum creatinine, is below 60 ml/min we change the GBCA to an agent with a cyclic structure and no net charge (Gadoteridol). Children with estimated GFR below 30 ml/min are not typically referred for an MR urogram. For the dynamic, contrast-enhanced, sequences some groups have used one, or a limited number of slices in conjunction with higher temporal resolution. We have preferred to use a 3D acquisition covering the entirety of both kidneys with a more modest temporal resolution. The 3D approach has several advantages, it ensures that small areas of interest, such as renal scarring are included in the acquired volume, it means an ideal rectangular slice profile can be assumed (in 2D approaches imperfections in the slice profile must be corrected for) and it allows measures which are representative of the whole kidney to be derived. Because of the lower temporal resolution (typically 8 seconds on a scanner with a standard gradient system) and the desire to keep the arterial concentration of the GBCA in the linear range we typically use a power injector to deliver a slow infusion of the GBCA at a rate between 0.1 and 0.25 ml/sec, depending on the patients weight, resulting in an injection duration of between 20 and 60 seconds. The dynamic sequence is started prior to the commencement of the injection and due to the slow rate of infusion we have at least 5 pre-contrast dynamics which can be used to obtain a robust estimate of the pre-contrast signal. The dynamic sequence is a 3 dimensional, T1-weighted, fat saturated, gradient echo sequence acquired in an oblique coronal plane. The flip angle is set at 30° in order to improve the linearity of the signal intensity and a high bandwidth is used to minimize the echo time. The slice thickness is typically 2 mm. In most

cases 50 volume acquisitions are acquired in the first 10 minutes after contrast injection. Volumetric data is acquired continuously for the first five minutes of scanning and then delays of increasing duration are inserted between the subsequent dynamic acquisitions since high temporal resolution is not required for the washout phase. A MIP image of each dynamic series is automatically generated which facilitates rapid review of the data sets (Fig. 5). This MIP image of each volumetric data set is termed a concatenated MIP. Following the dynamic sequence high resolution STIR and a high resolution 3D, T1-weighted volumetric data set are acquired. The post-contrast STIR sequence provides an excellent depiction of the renal morphology and in particular renal scarring (Fig. 6). In younger children the volumetric 3D, T1-weighted sequence is acquired with isotropic resolution and requires around 2 minutes of imaging. The resulting images, and associated MIPs, provide a good overview of the functioning renal tissue and the excreted contrast (Fig. 7). In older children three orientations are acquired with thicker slices, with each orientation being acquired in a breath-hold. We typically acquire our MR urograms on 1.5T scanners, using a 3T scanner improves the T2 volumetric and other non-contrast images but the SAR limits typically require that the dynamic sequence is run either without fat saturation or with a lower flip angle. The former complicates the visual inspection of the images and in particular the concatenated MIPs, while the latter reduces the linear range for the relationship between the change in signal and the contrast agent concentration.

Post-Processing

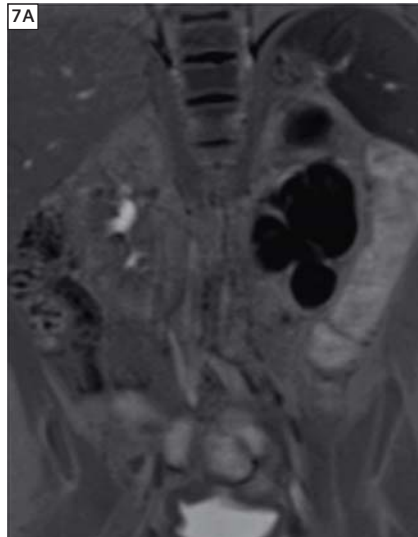
The basic steps in the post-processing of the dynamic series are the segmentation of the kidneys, the derivation of arterial and parenchymal curves and the fitting of these to an appropriate model in order to derive indices of renal function. The segmentation provides both an estimate of the renal volume which is required when calculating the GFR for the whole kidney and provides a mask



5 Shows images from a single slice (top row) and the corresponding MIPs (lower row) through the entire volume for three different time points corresponding to the vascular (5A, 5D), parenchymal (5B, 5E) and excretory (5C, 5F) phases. In the individual slices in the vascular phase the renal cortex is well seen due to its high vascularity while the MIP of this phase provides a good overview of the vasculature and allows features such as crossing vessels to be detected. In the parenchymal phase the cortex and medulla are iso-intense, while in the excretory phase high signal intensity is seen in the collecting system, ureters and bladder. The dark area in the bladder is the balloon for the bladder catheter.



6 Post-contrast STIR image from a patient with a small, poorly functioning, left kidney and bilateral scarring.



7 Post-contrast STIR (**7A**) and delayed, high resolution, T1-weighted (**7B**) images from the patient with horseshoe kidney shown in figure 2. While the right kidney has contrast in the collecting system and ureter and has drained contrast into the bladder the left kidney shows minimal contrast in the collecting system indicating very delayed filtration/concentration of the GBCA.

which determines the pixels that contribute to the average time course for the kidney. We currently use either in-house software or a beta version of a processing tool that has been developed by Siemens to perform the segmentation. In both cases the user performs an initial segmentation which is then reviewed and refined as necessary until an acceptable segmentation is obtained.

Arterial input function (AIF)

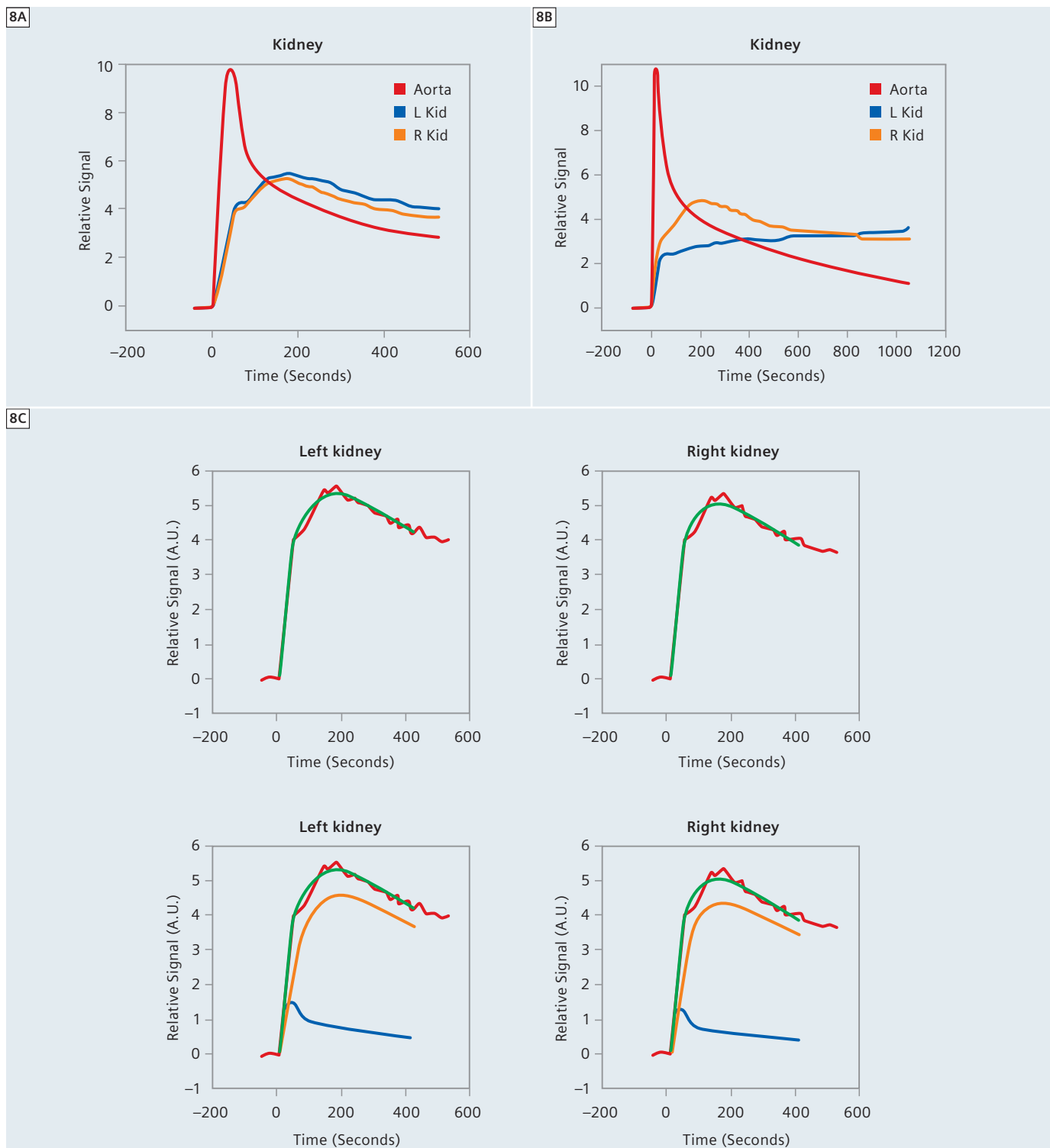
In order to model renal function an estimate of the time course of the vascular concentration of the GBCA is required and this is generally referred to as the arterial input function (AIF). The AIF is required since the vascular concentration affects the rate of filtration of the GBCA by the kidneys and even with a standardized dose and injection protocol there will be idiosyncratic variations in the AIF caused by physiological differences. For pediatric renal studies the arterial signal is usually measured in a region-of-interest (ROI) in the descending aorta, the renal arteries being typically too small for reliable measurements in children. The aorta is viewed in both coronal and sagittal planes in order to minimize partial volume effects by excluding, if possible,

regions where the aorta cuts through the imaging plane. The ROI consists of an arbitrary number of points – the points typically being positioned at or below the level of the renal arteries in order to minimize in-flow effects. Even with careful selection of the location of the ROI pulsatility effects can still be present and it is not always possible to eliminate partial volume and inflow effects. In order to reduce the noise in the AIF we routinely fit the measured AIF signal to a model, however, even after fitting the imprecision in the AIF still limits the accuracy of GFR quantification with MR urography. For methods based on the differential function then the imperfections in the AIF are common to both kidneys and hence cancel out.

Concentration versus time curves

Deriving the mean signal from the segmented volumes and converting the signal values to concentrations allows concentration versus time-curves to be derived. Although the contrast dynamics can be assessed visually, the curves can provide extra information that is not always apparent from a visual inspection. Figures 8A and 8B show whole kidney

curves for the patients shown in figures 5 and 7 respectively. The curves enable an assessment of perfusion, concentration and excretion for each kidney and are analogous to the time activity curves of renal scintigraphy. These curves reflect only the changes occurring in the renal parenchyma, rather than in the parenchyma and collecting systems as is the case with renal scintigraphy. The initial sharp increase in signal predominantly reflects the perfusion phase, with the renal cortex enhancing more than the medulla due to its higher blood volume. The subsequent slower increase in signal intensity reflects the accumulation of contrast agent in the renal parenchyma as it passes through the nephrons. Peak parenchymal enhancement typically occurs at approximately 150 seconds after the initial perfusion phase. After this peak there is a general decline in signal intensity due to the excretion of contrast into the urine and the on-going decline in the plasma concentration of the GBCA. The late parenchymal curves tend to parallel the aortic signal curve. As the post-processing becomes easier, segmental analysis will become more practical and provide greater insights into the anatomic and pathophysiologic



8 The curves are shown in terms of relative signal, which is defined as $(S(t)-S_0)/S_0$ where S_0 is the pre-contrast signal and is linearly related to the contrast agent concentration providing the contrast agent concentration is not too elevated. Figure **8A** shows the curves from the normal subject shown in figure 5 with relatively symmetrical curves from both kidneys and a peak relative signal approx. 3 minutes post-contrast. Figure **8B** are the curves from the subject with the obstructed horseshoe kidney shown in figures 2 and 7. The curve for the right kidney shows a similar pattern to that seen in figure 8A but the curve for the left kidney shows no peak, even though the dynamic imaging covers over 15 minutes after the injection of contrast. Figure **8C** shows the fits to the Annet model for the curves shown in figure 8A. The top row shows the overall fit for the model while the lower row shows the vascular and filtered components of the model.

changes occurring in the different compartments with various renal diseases. Similarly, fitting the models on a pixel by pixel basis to produce statistical parametric maps of the model parameters is currently too time consuming for routine clinical use but as increased computational power becomes available these will also become clinically feasible. The dynamic series can also be used to visualize the uptake of contrast in renal masses and hence help characterize the mass.

Modeling renal function

Several models of renal function have been developed. The Rutland-Patlak model, which is widely used in SPECT and CT, has also been applied to DCE MRI data. This model measures the GFR as the transfer of a GBCA from arterial blood to the renal tubules and the fact that the kidney includes both vascular and tubular components is taken into account. The amount of GBCA in any one kidney at a time point prior to the excretion of the GBCA can be expressed as the sum of the GBCA in the vascular space and nephrons respectively. Assuming that the plasma concentration of the GBCA in the vascular space is proportional to the plasma concentration in the aorta one can then define constants to represent the vascular volume within the kidney and the clearance of the GBCA from the vascular space and write an equation for the GFR in terms of the measured arterial and renal curves. This equation can be rewritten in the form of a linear equation and values for the vascular volume and the clearance of the GBCA can be derived from the plot of this equation. Typically one measures the average concentration of the GBCA within the kidney, thus the equation calculates the clearance per unit volume of tissue, which we refer to as the unit GFR. We believe this quantity is related to the single nephron GFR and have noted that this quantity is reduced in decompensated, as well as dysplastic and uropathic kidneys. An estimate of the single kidney GFR (SK-GFR) can be obtained by multiplying the unit GFR by the renal volume. The Patlak model breaks down after a

certain time because it fails to take account of the onward transport of the GBCA (i.e. the drop in signal seen at later time points in the parenchymal curves). Several more advanced models have been developed, the most widely used of these being the model developed by Annet et al. which includes an additional term which accounts for the onward transport of the GBCA and hence allows the whole time course to be modeled. Figure 8C shows the results of fitting the data from the subject shown in figures 5 and 8A to the Annet model. In the case of renal masses other models, such as the Tofts model, can be applied to the dynamic data to extract other parameters such as the tissue permeability or the size of the various tissue compartments.

The results from the renal modeling can then be reported as absolute values or in terms of the differential renal function. The differential renal function (DRF) is widely used in nuclear medicine and simply expresses the results of functional measurements for each kidney as a percentage of the total function (i.e. sum of both kidneys). Despite the obvious shortcomings, which include the assumption of a normal contra-lateral kidney as a reference and hence neglecting the effect of compensatory changes in the contra-lateral kidney, the DRF is very useful clinically since it removes the effect of the main source of error in the functional calculation, the AIF.

References

- 1 Rohrschneider WK, Haufe S, Wiesel M et al. Functional and morphologic evaluation of congenital urinary tract dilatation by using combined static-dynamic MR urography: findings in kidneys with a single collecting system. *Radiology*. 2002;224:683-694.
- 2 Grattan-Smith JD, Perez-Brayfield MR, Jones RA, Little S, Broecker B, Smith EA, Scherz, HC Kirsch AJ. Dynamic contrast enhanced magnetic resonance urography in the evaluation of hydronephrosis in children. *Pediatric Radiology* (2003). :33; 293-304.
- 3 Jones RA, Grattan-Smith JD, Little S. Pediatric magnetic resonance urography. *J Magn Reson Imaging*. 2011;33:510-526.
- 4 Patlak CS, Blasberg RG, Fenstermacher JD. Graphical evaluation of blood-to-brain transfer constants from multiple-time uptake data. *J Cereb Blood Flow Metab*. 1983;3:1-7.
- 5 Peters AM. Graphical analysis of dynamic data: the Patlak-Rutland plot. *Nucl Med Commun*. 1994;15:669-672.
- 6 Hackstein N, Heckrodt J, Rau WS. Measurement of single-kidney glomerular filtration rate using a contrast-enhanced dynamic gradient-echo sequence and the Rutland-Patlak plot technique. *J Magn Reson Imaging*. 2003;18:714-725.
- 7 Annet L, Hermoye L, Peeters F et al. Glomerular filtration rate: assessment with dynamic contrast-enhanced MRI and a cortical-compartment model in the rabbit kidney. *J Magn Reson Imaging*. 2004;20:843-849.
- 8 Sourbron, SP, Michaely HJ, Reiser MF, Schoenberg SO. MRI-Measurement of Perfusion and Glomerular Filtration in the Human Kidney with a Separable Compartment Model. *Invest. Radiol*. 2008;43:40-48.
- 9 Bokacheva L, Rusinek H, Zhang JL et al. Estimates of glomerular filtration rate from MR renography and tracer kinetic models. *J Magn Reson Imaging*. 2009;29:371-382.
- 10 Pedersen M, Shi Y, Anderson P et al. Quantitation of differential renal blood flow and renal function using dynamic contrast-enhanced MRI in rats. *Magn Reson Med*. 2004;51:510-517.
- 11 Mendichovszky I, Pedersen M, Frokiaer J et al. How accurate is dynamic contrast-enhanced MRI in the assessment of renal glomerular filtration rate? A critical appraisal. *J Magn Reson Imaging*. 2008;27:925-931.
- 12 Tofts, PS, Brix G, Buckley DL et al. Estimating kinetic parameters from dynamic contrast enhanced T1-weighted MRI of a diffusible tracer: standardized quantities and symbols. *J. Magn. Reson. Imag*. 1999;10:223-232.
- 13 Ries M, Jones RA, Basseau F, Moonen CTW and Grenier N (2001). Diffusion tensor imaging of the kidney. *JMRI* 14, 42-49.
- 14 Porter DA, Heidemann RM. High resolution diffusion weighted imaging using readout segmented echo planar imaging, parallel imaging and a two dimensional navigator based reacquisition. *Magn. Reson. Med* (2010): 62:468-475.

Contact

Richard A. Jones
Department of Radiology
Children's Healthcare of Atlanta
1001 Johnson Ferry Road
Atlanta, GA 30342
USA
Richard.Jones@choa.org

*MR scanning has not been established as safe for imaging fetuses and infants under two years of age. The responsible physician must evaluate the benefit of the MRI examination in comparison to other imaging procedures.

**The information about this product is preliminary. The product is under development and not commercially available in the U.S., and its future availability cannot be ensured.

Pediatric* MR Urography

G. Hadjidekov; G. Tonev; G. Georgieva

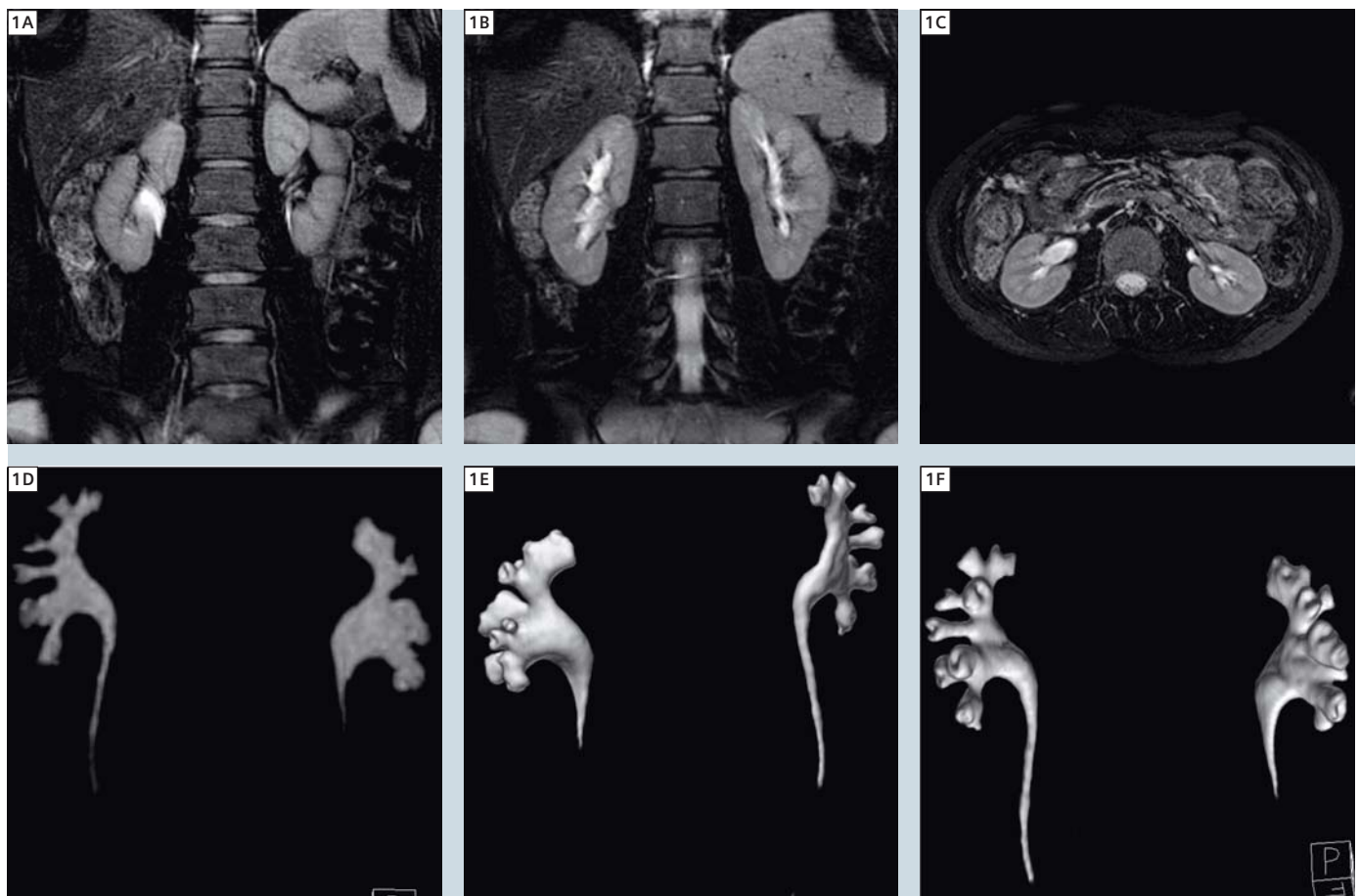
MC "Pro-Vita", Sofia, Bulgaria

Introduction

MR urography (MRU) – a modern imaging modality – was introduced to pediatric urology more than a decade ago and has evolved into an effective imaging tool for the assessment of various urologic abnormalities in children. MRU provides both morphological and functional information by means of different sequences with or without injection of

gadolinium. Combined static and dynamic contrast-enhanced MR urography is particularly advantageous in the pediatric population, offering high spatial resolution morphologic imaging of the urinary tract with reliable information about kidney function and urinary excretion in a single examination, without exposure to ionizing radiation. The

method is most commonly applied for the evaluation of hydronephrosis and provides valuable insight into a wide range of obstructive uropathies. It is also beneficial in tumor characterization, in preoperative planning and in the diagnosis of pyelonephritis and renal scarring where MRU has been shown to be superior to renal scintigraphy. Post-pro-



1 Static MR urography images of a 16-year-old patient with subtle hydronephrosis grade 1 of the right kidney. Coronal T2w syngo BLADE (1A, 1B) and axial T2w syngo BLADE (1C) images with fat saturation, 3D coronal T2w TSE maximum intensity projection (1D) and volume rendered images (1E, 1F).

Table 1: Sequence parameters – 1.5T MAGNETOM ESSENZA

	t2_tru- fi_loc	haste_ 16sl_sag	t2_blade_ tra_fs	t2_ blade_ cor_fs	t2_tse 3d_cor	t1_sin- gle_ vibe_ cor	t1_ vibe_ dyn_cor	t1_tse 3d_sag	vibe_ fs_cor_ bh	single_ cor_CE
TE	2.09	59	123	123	627	0.83	0.83	9	2.38	1.09
TR	4.17	700	2280	1800	1600	2.62	2.62	696	4.38	3.11
FA	50	160	150	150	150	10	10	150	8,0	25
BW	501	789	362	362	219	1090	1090	219	610	520
FOV	40	38	30	32	34	38	38	34	40	38,5
ST	8.0	8.0	5,0	5,0	1,5	5,0	3.35	1,5	4,0	1,5
TA	0:13	0:36	0:48	0:43	2:48	0:04	13:51	1:13	0:11	0:14
SpS	7	–	–	–	60	32	32	60	80	56

Legend: TA = time acquisition in sec., TE = echo time, TR = repetition time, FA = flip angle, FOV = field-of-view, ST = slice thickness, bh = breathhold, SpS = slices per slab, BW = bandwidth, VIBE = Volume Interpolated GRE

cessing algorithms permit the evaluation of the split renal function by generating time-intensity curves representative for the renal function, as well as many other parameters. The use of MRU for the assessment of urolithiasis, vesicoureteral reflux, renal trauma, and fetal urinary tract abnormalities is still partially limited and technical refinements are required. Judicious use of gadolinium-based (Gd) contrast agents in children at risk for nephrogenic systemic fibrosis (NSF) should be employed with attention so as to avoid new occurrences.

Purpose

The aim of our work is to promote the use of MRU in pediatrics trying to present a safe and reliable MRI protocol for anatomic imaging that is generally accepted. Defining imaging and procedural recommendations in pediatric uro-radiology is an important task, not only in standardization of pediatric uro-radiologic imaging protocols but also in reducing invasiveness and radiation

dose. The lack of standardization for quantitative renal functional evaluation and urinary excretion assessment requires new studies and extensive interdisciplinary consultations.

Patient preparation

The adequate preparation is a prerequisite for good image quality [1–2]. We do not routinely place a bladder catheter in order to reduce invasiveness of the procedure, although catheterization of small children is recommended in case of megaureter (with or without reflux). The intravenous hydration and administration of furosemide are crucial for reducing the concentration of Gd [1]. Diuretics are recommended in both static urography and dynamic urography 15 minutes before contrast administration. In this context, we adopted the F-15 protocol and we administered standardized hydration and diuretics prior to Gd, in order to reduce artifacts and shorten the examination time [3]. In children younger than six years of age

and those who are non-cooperative for breathhold techniques, sedation should be performed with ketamine (Ketalar) and midazolam (Dormicum) according to the department's standard sedation protocol [4–5]. Blood pressure, respiration, heart rate, and oxygen saturation are continuously monitored throughout MR imaging in all patients.

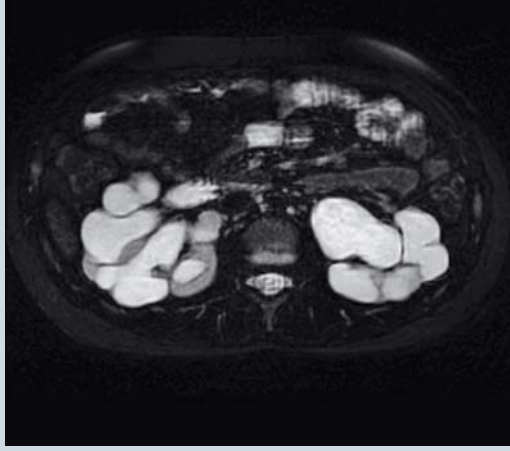
Imaging protocol

MRU examinations are performed on a 1.5T MAGNETOM ESSENZA, using a 4-channel Body Matrix coil. The MRU protocol should allow a correct evaluation of the renal parenchyma, upper urinary tract, bladder, renal vessels and surrounding structures. Such a comprehensive 'one-stop-shop' protocol must be able to provide the required morphological and functional information within 30–35 minutes. Our MRU protocol consists of a native MRI examination with T2w coronal, T1w and T2w axial sequences, administration of diuretic followed by a dynamic study with gado-

2A



2B



2C



2D



2E



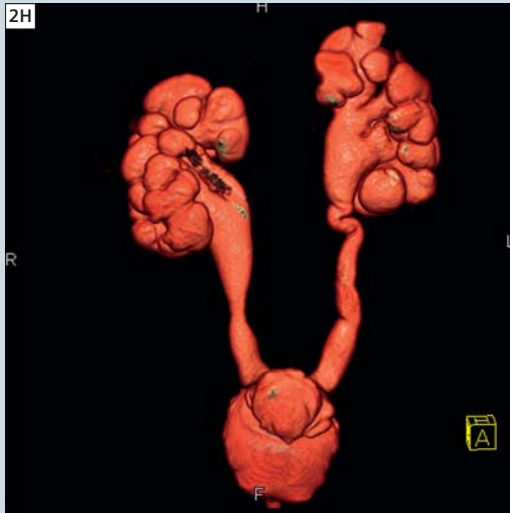
2F



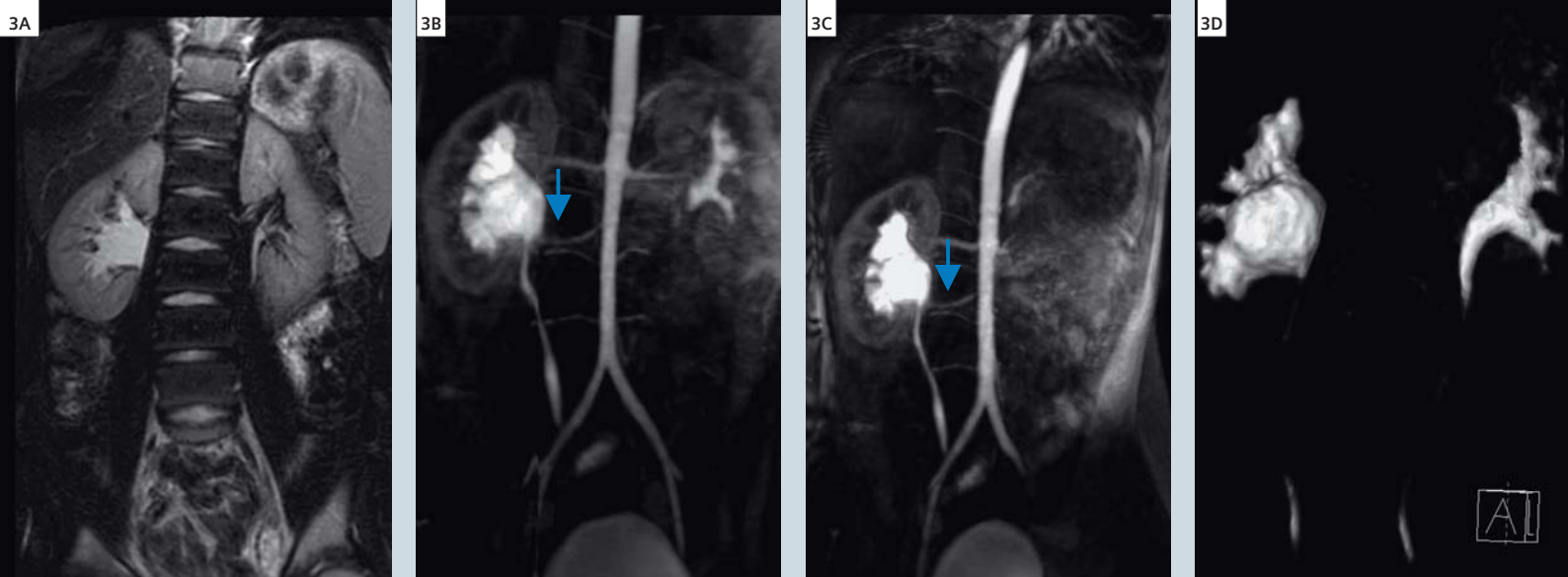
2G



2H



2 13-year-old boy with high grade bilateral hydronephrosis and megaureters. Persistent vesicoureteral reflux (VUR) following several ureterocystoneostomies (UCNS). Static MR urography axial T2w syngo BLADE images (**2A**, **2B**), coronal T2w syngo BLADE images (**2C**, **2D**), coronal 3D T2w TSE images (**2E**, **2F**), 3D coronal T2w TSE maximum intensity projection (MIP) (**2G**) and volume rendered image (**2H**).



3 Ureteropelvic junction (UPJ) obstruction leading to hydronephrosis with dilatation of the right pyelocalyceal system in a 9-year-old girl. Coronal T2w syngo BLADE image (**3A**). MR angiography following Gd administration (Single COR CE) demonstrates accessory right lower pole renal artery (arrows), compressing the ureteropelvic junction – Thin MIP images (**3B, 3C**). Right side hydronephrosis demonstrated on 3D coronal T2w TSE maximum intensity projection (**3D**). The girl was treated successfully by pyeloplasty.

linium (Gd) injection and 3D reconstructions. This MRU protocol allows the combination of the whole information, provided by conventional exams, ultrasound and scintigraphy in a single examination, with or without minimal drug toxicity – furosemid and Gd. We commence the MRU examination with a 3-plane localizer and we use a sagittal view to depict the kidneys and bladder in order to obtain an oblique coronal plan angled parallel to the long axis of the kidneys, including ureters and bladder. We select a large field-of-view (FOV) above both hemidiaphragms so as to avoid artifacts from aliasing or post-contrast signal intensity decline in the upper renal poles. Following the coronal T2w plane, we perform axial T2w and T1w sequences. Fat-suppression techniques are used in T1 and T2 hyper intense findings and in cases of suspicion of tumor formation – in and out of phase sequences for contour delineation. An important pre-contrast sequence is 3D T2w urogram with fat-suppression. T1-weighted gradient-echo sequence with fat-saturation (3D VIBE dynamic) is used for the post-contrast scan. The dynamic scan is repeated within 15 minutes, following Gd injection with increasing intervals between acquisitions, for the need of post-processing. We inject the standard dose of 0.1 mmol/kg of gadolinium. Regardless of the patient's size, placement of

the coils is crucial. In newborns and small children we use the smaller Flex coil. Otherwise we use the Body Matrix coil to scan older children. It is recommended to adjust the Body Matrix coil anteriorly to assure proper signal distribution throughout the volume. The technical parameters of our sequences are presented in Table 1.

Discussion

MR urography is a feasible method for evaluation of urinary tract pathology in neonates and infants [6]. It overcomes the limitations of the conventional imaging techniques and is a superior tool in many aspects, especially in the evaluation of parenchymal kidney diseases and poorly functioning systems, assessment of ureteral anatomy, renal vasculature and tumors. The method is particularly helpful for further therapeutic decisions, planning of surgical intervention and future diagnostic work-up. The most common MRU techniques, used to visualize the urinary tract, are the static (T2w) MRU and excretory (T1w) MRU [7–9]. Static MRU uses the long relaxation times of the liquids by T2w sequences (Fig. 1). Three-dimensional (3D) respiratory-triggered sequences are used to obtain thin-section data sets that can be further post-processed to create volume rendered (VR) or maximum intensity projection (MIP) images of the entire urinary tract

(Fig. 2) [10–11]. Excretory (T1w) MRU is similar to CT urography and intravenous urography and is performed after intravenous injection of Gd. The use of conventional dose – 0.1 mmol/kg and in some occasions low-dose Gd opacification – 0.01 mmol/kg allows to maintain the linearity between signal and Gd concentration, which is essential for quantitative measurements and analysis. Administration of diuretics improves the quality of MRU by increasing the quantity of the urine and therefore lead to better dilution and appropriate distribution of Gd in the urinary tract [12–13]. The most important sequence of excretory MRU is 3D gradient-echo. Fat-suppression is recommended for better demonstration of the ureters. MR angiography, in addition to excretory MR urography, demonstrates excellently the renal vasculature (Fig. 3). Modern MR units scan simultaneously in one volume the kidneys, the ureters and the bladder, using 3D gradient-echo sequences in one breathhold [14–15]. Sometimes segmental scanning of the kidneys or bladder separately is recommended for more detailed image visualization. An advantage of static MRU over dynamic, T1w MRU is the demonstration of the ureters and the ureterovesical junction in cases of obstruction or impaired renal function [6, 16]. There is a growing number of publications concerning the criteria for assess-

ment of the renal function in children by dynamic MRU, but the achievement of consensus requires more and deeper investigations. Functional criteria include renal transit time, differential renal function, and time–signal intensity curves. The technique is challenging and is best performed in specialized centers. However, this single MRI examination could avoid the use of multiple modalities (e.g. US, conventional urography, renal scintigraphy) that individually help assess various morphologic features, renal function and excretion and there is an expanding use of MRI. Current limitations for widespread distribution of the technique are understaffed pediatric radiologic departments and time-consuming post-processing. Alongside the advantages of MRU, mentioned above, it is necessary to note some limitations. Sometimes it requires a placement of bladder catheter, administration of furosemide and Gd, sedation and even anesthesia (for newborns and younger children), which is a complementary risk [16]. Breathhold techniques could not be applied in neonates and small infants. We use *syngo* BLADE to minimize motion artifacts. Patient preparation and the examination itself are time-consuming; post-processing and calculation of functional curves and differential renal function require an additional 30 minutes.

Until recently it was believed that the extracellular Gd-based contrast agents are safe. However, in 2006, it was demonstrated that some Gd-based contrast agents may provoke the development of NSF and/or a generalized fibrotic disorder in renal failure patients [17]. Gd-ions, released from Gd-based MR contrast agents, are the likely etiologic agent of NSF [18]. The guidelines of the European Society of Urogenital Radiology (ESUR) suggest a very careful administration of Gd in children with renal failure. Absolute contraindications are high levels of creatinine and a glomerular filtration under 30 ml/min/1.73 m² and in cases of glomerular filtration between 30 and 60 ml/min/1.73 m² discussions with pediatric nephrologists are mandatory. Written consent should be

obtained in spite of the fact that most cases of NSF occur in adults and the reported cases of NSF without Gd administration. In all patients at high risk of developing NSF and in the pediatric group, cyclic Gd-helators should be used due to their higher stability [19].

Conclusion

MRU has the potential to become the leading diagnostic modality in the near future of a wide range of pathological conditions affecting the urinary tract in newborns and children. It integrates exquisite anatomical information with a variety of functional data and avoids ionizing radiation. MRU is increasingly employed as a problem solver when conventional imaging studies remain inconclusive and its growing application will likely improve availability and reduce cost in the future. The introduction of parallel imaging, higher field strength systems, multielement coil technology, and gadolinium-based contrast agents with increased T1 relaxivity will further improve the overall signal-to-noise ratio (SNR) and spatial resolution of the images. The advances of molecular imaging techniques will provide new insights about the nature of hereditary diseases in pediatric nephrology and urology. Potential future applications include also virtual endoscopy and MRU-guided procedures.

*MR scanning has not been established as safe for imaging fetuses and infants under two years of age. The responsible physician must evaluate the benefit of the MRI examination in comparison to other imaging procedures.

References

- Grattan-Smith, J.D., S.B. Little, and R.A. Jones, MR urography in children: how we do it. *Pediatr Radiol*, 2008. 38 Suppl 1: p. S3-17.
- Leyendecker, J.R., C.E. Barnes, and R.J. Zagoria, MR urography: techniques and clinical applications. *Radiographics*, 2008. 28(1): p. 23-46; discussion 46-7.
- Grattan-Smith, J.D., et al., MR imaging of kidneys: functional evaluation using F-15 perfusion imaging. *Pediatr Radiol*, 2003. 33(5): p. 293-304.
- Cengiz, M., Z. Baysal, and S. Ganidagli, Oral sedation with midazolam and diphenhydramine compared with midazolam alone in children undergoing magnetic resonance imaging. *Paediatr Anaesth*, 2006. 16(6): p. 621-6.
- Lin, T.F., et al., Antiemetic and analgesic-sparing effects of diphenhydramine added to morphine intravenous patient-controlled analgesia. *Br J Anaesth*, 2005. 94(6): p. 835-9.
- Riccabona, M., et al., Feasibility of MR urography in neonates and infants with anomalies of the upper urinary tract. *Eur Radiol*, 2002. 12(6): p. 1442-50.
- Nolte-Ernsting, C.C., et al., MR urography today. *Abdom Imaging*, 2003. 28(2): p. 191-209.
- Garcia-Valtuille, R., et al., Magnetic resonance urography: a pictorial overview. *Br J Radiol*, 2006. 79(943): p. 614-26.
- Nolte-Ernsting, C.C., et al., Diuretic-enhanced gadolinium excretory MR urography: comparison of conventional gradient-echo sequences and echo-planar imaging. *Eur Radiol*, 2001. 11(1): p. 18-27.
- Roy, C., et al., MR urography in the evaluation of urinary tract obstruction. *Abdom Imaging*, 1998. 23(1): p. 27-34.
- O'Malley, M.E., et al., MR urography: evaluation of a three-dimensional fast spin-echo technique in patients with hydronephrosis. *AJR Am J Roentgenol*, 1997. 168(2): p. 387-92.
- Szopinski, K., et al., Magnetic resonance urography: initial experience of a low-dose Gd-DTPA-enhanced technique. *Eur Radiol*, 2000. 10(7): p. 1158-64.
- Hughes, J., et al., MR urography: evaluation of different techniques in non-dilated tracts. *Clin Radiol*, 2002. 57(11): p. 989-94.
- Nolte-Ernsting, C.C., G.B. Adam, and R.W. Gunther, MR urography: examination techniques and clinical applications. *Eur Radiol*, 2001. 11(3): p. 355-72.
- Sudah, M., et al., MR urography in evaluation of acute flank pain: T2-weighted sequences and gadolinium-enhanced three-dimensional FLASH compared with urography. *Fast low-angle shot. AJR Am J Roentgenol*, 2001. 176(1): p. 105-12.
- Riccabona, M., Pediatric MRU-its potential and its role in the diagnostic work-up of upper urinary tract dilatation in infants and children. *World J Urol*, 2004. 22(2): p. 79-87.
- Thomsen, H.S. and P. Marckmann, Extracellular Gd-CA: differences in prevalence of NSF. *Eur J Radiol*, 2008. 66(2): p. 180-3.
- Abraham, J.L., et al., Dermal inorganic gadolinium concentrations: evidence for in vivo transmetallation and long-term persistence in nephrogenic systemic fibrosis. *Br J Dermatol*, 2008. 158(2): p. 273-80.
- Martin, D.R., et al., Individual kidney blood flow measured with contrast-enhanced first-pass perfusion MR imaging. *Radiology*, 2008. 246(1): p. 241-8.

Contact

Georgi Hadjidekov, MD
MC "Pro-Vita"
Montevideo str. N66
Sofia 1632
Bulgaria
jordiman76@yahoo.com

Case Report

Ectopic Ureter: Magnetic Resonance Urography

Sally Harman; Padma Rao, MD

Children's MRI Centre, Royal Children's Hospital, Melbourne, Victoria, Australia

Patient history

A 4-year-old female presented with persistent urinary incontinence. Previous ultrasound findings queried bilateral duplex kidneys. A cystoscope was negative for ectopic ureter. Referring urologist requested a Magnetic Resonance Urogram (MRU) to be carried out.



1 Curved multi-planar reconstruction (MPR) of the right urinary tract based on T2w 3D TSE MR data (*syngo* SPACE) showing the ectopic ureter.

Sequence details

This protocol is carried out at our institution on a 3T Siemens MAGNETOM Tim Trio with software version *syngo* MR B17 using a 12-channel Body Matrix coil. T2w 2D transverse fat suppressed turbo spin echo.

T2w 2D coronal fat suppressed turbo spin echo.

T2w SPACE – 3D T2w respiratory triggered sequence.

3D coronal T1w gradient sequence with fat suppression (dynamic sequence). (Undertaken with 8 second breathholds over a 15 minute period with 54 passes). 3D T1w sagittal (delayed after contrast) fat suppressed.

Because of the age of the child this scan was carried out under a general anesthetic.

Imaging findings

Bilateral duplex kidneys. The upper moiety ureter of the right kidney was found to be dilated and ectopic. It bypassed the bladder and appeared to insert in the vagina.

Discussion

With the use of 3D T2w respiratory triggered sequence and the rapid T1w gradient sequence, effective MRUs are easily achievable. At our institution we have seen cases where pathology is seen on one of these sequences, but not the other. Used in conjunction, both are equally valuable. The 3D T2w respiratory triggered sequence is helpful for gaining, amongst

others, volume rendered images of the complete urinary system, clearly demonstrating anatomy.

The 3D coronal gradient sequence with fat suppression carried out as a dynamic sequence is of great benefit when looking at the functional anatomy of the urinary system. When utilized in conjunction with an appropriate dose of furosemide and a well hydrated patient, the function of the urinary system can be demonstrated.

Post-processing of the dynamic sequence can also be undertaken. At our institution, post processing is carried out using 'Image J' software (www.rsbweb.nih.gov/ij/) with the MRU plug-in (www.univ-rouen.fr/med/MRurography/acccueil.htm).

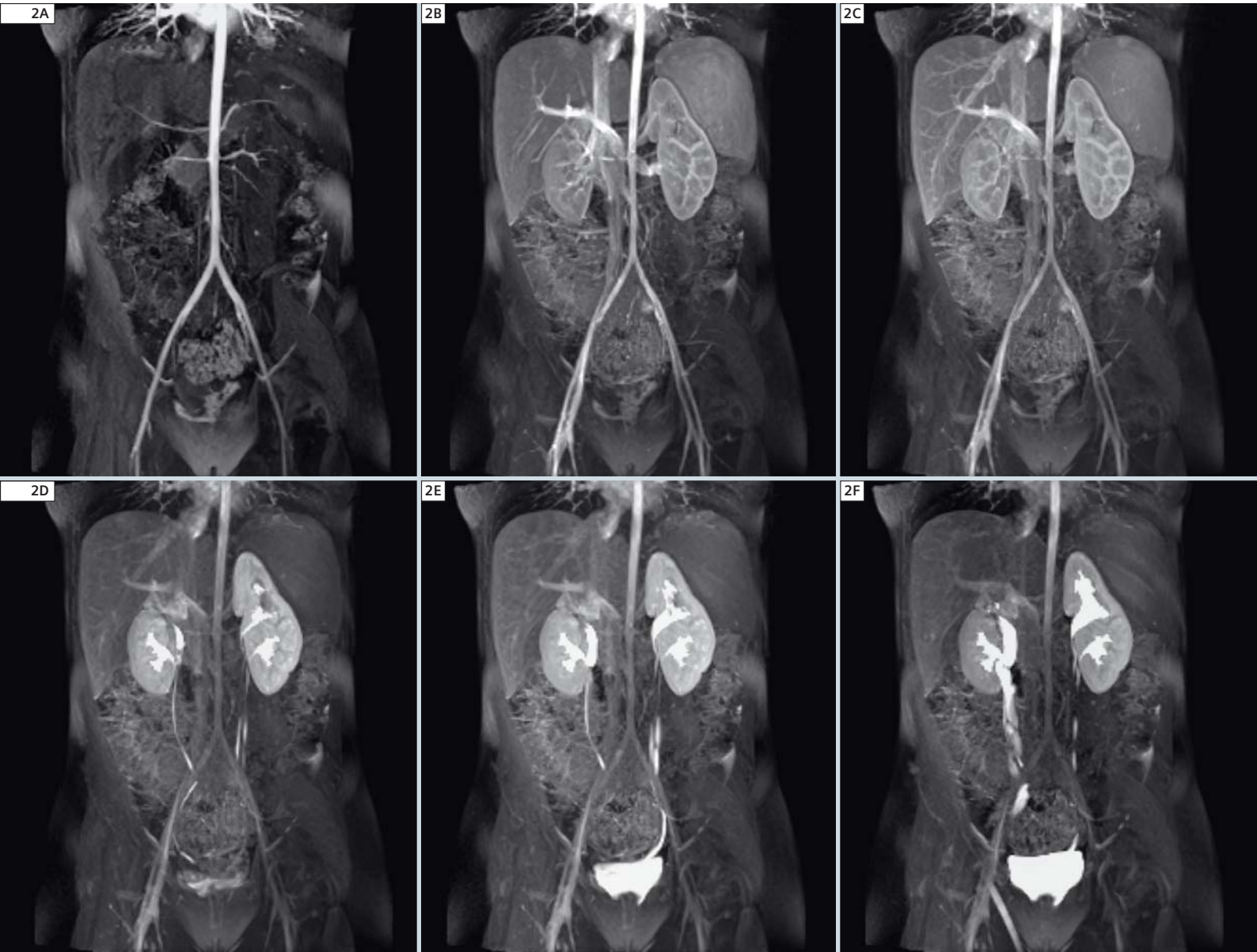
Acknowledgements

Chris Adamson – Developmental & Functional Brain Imaging – Murdoch Childrens Research Institute, Melbourne, Victoria, Australia.

Michael Kean & Amber Bristowe – Children's MRI Centre @ Royal Children's Hospital, Melbourne, Victoria, Australia.

Contact

Sally Harman
Children's MRI Centre
Royal Children's Hospital
Melbourne, Victoria
Australia
Phone +61 393454301
sally.harman@rch.org.au



2 Maximum intensity projection of the 4D data set (3D FLASH with fat saturation) which is used to assess the urinary tract including the kidneys (time sorting from **(2A)** as earliest to **(2F)** as latest time point).

Pediatric Imaging in Daily Routine with MAGNETOM ESSENZA – a Pictorial Essay

Han Yan Qiao, MD

Shanghai Children's Hospital, Department of Diagnostic Radiology, Shanghai, China

Introduction

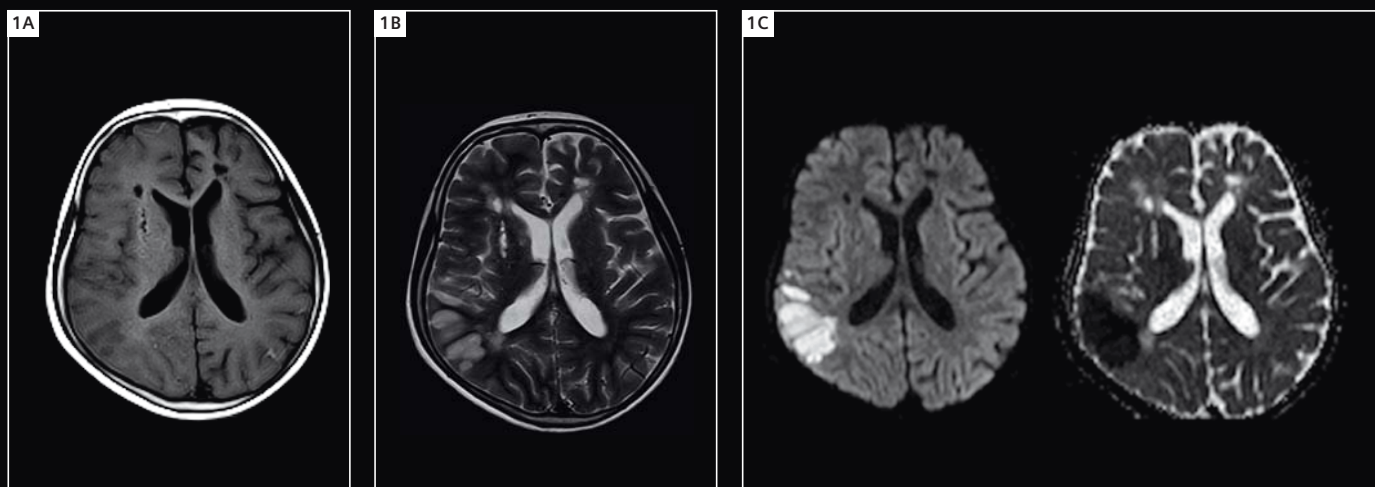
The Shanghai Children's Hospital is a maximum care centre, specialized solely in the needs of children. Founded in 1937, it was formerly known as the "Refugee Children Hospital of Shanghai". Among the founders of the hospital were the highly recognised Dr. Fu Wen Shou and Dr. Su Zu Fei. In 1953, the name was changed to "Shanghai Children's Hospital" and in 2003 it became affiliated to the Shanghai Jiaotong University. The Shanghai Children's Hospital provides all disciplines of pediatric

healthcare. Its staff care for more than 1 million outpatients and – equipped with 300 beds – approximately 18,000 inpatients per year.

Background

This high number of patients treated per year also reflects that the Shanghai Children's Hospital is recognised as one of the leading institutions for pediatric healthcare within the greater area of Shanghai, if not within China. But it also demonstrates the growing need for imaging capacities, including MR imaging (MRI), within the hospital to cover

all aspects of pediatric patient care. In 2009, the hospital decided therefore to expand its imaging department and add an MR unit. The requirements for this MR scanner are manifold; e.g. in the field of brain imaging, the availability of high quality diffusion-weighted imaging (DWI) as well as susceptibility-weighted imaging (SWI) for clinical routine is an important requirement. Flexible coil handling as well as high signal-to-noise ratio (SNR) and light-weight coil design are also important aspects, especially when imaging children. Such an MR system must also allow the scan of multiple



regions within one exam and without the need of coil repositioning e.g. to evaluate the whole central nervous system (CNS).

An ongoing debate concerns the right field strength for pediatric imaging. For many clinical questions, but also keeping in mind the dimensions of our smallest patients, resolution is one of the key elements for highest diagnostic confidence with MRI. However, increased resolution requires higher overall SNR and this can easily be achieved by simply increasing the B_0 magnetic field strength. On the other hand, SNR depends on the applied coils and SNR gains can be achieved without increasing the B_0 just by selecting the right coil technology. In addition, comparing 1.5 to 3 Tesla, this gain in SNR comes at the cost of higher energy deposition within the body and therefore sometimes a more complex sequence handling to comply with the specific absorption rate (SAR) limitations at 3T. Imaging where metallic implants or clips are present can be more challenging at 3T than at 1.5T. But the decision whether 3T or 1.5T represents the perfect system also

depends on many further and often individual aspects including cost. Lower field strengths than 1.5 Tesla have, generally speaking, failed to provide the required SNR in pediatric imaging, which is used either for high resolution or for fast scanning.

At our department we came to the conclusion that a 1.5 Tesla MR system would best answer our daily clinical and business demands. When defining the system requirements, a very flexible coil handling and its capacity for advanced applications such as SWI in clinical routine were prioritized. The decision was therefore to invest in a MAGNETOM ESSENZA which, thanks to Tim (Total Imaging Matrix) coil technology and advanced applications, addresses all the above requirements.

At this time point we scan approximately 20 children per day. Tim technology has fulfilled our initial expectations and the Tim coils enable us to scan all our patients, including neonates* and fetuses*. In total, we scanned approximately 8,000 children since the installation of the system in September 2009. Most requests concern neurological

problems including trauma and malformations. However, in areas where ultrasound is still the imaging modality of choice, we also see an increase in referrals for abdominal scans, especially for the evaluation of further differential diagnoses.

Purpose

The purpose of this pictorial essay is to share some of our interesting cases with readers of MAGNETOM Flash magazine and also to share our experience with the MAGNETOM ESSENZA MRI scanner for pediatric imaging.

Case 1

A 6-year-old boy with disability of the left arm for two days. MRI suspicious of Moyamoya disease and corresponding to the patients symptoms suspicious of cerebral infarction.

1A) Transversal FLAIR (DarkFluid) with motion correction (*syngo* BLADE).

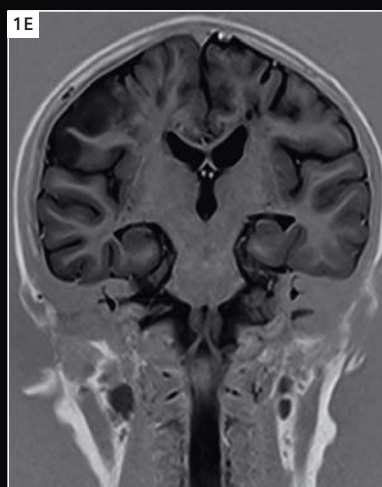
1B) Transversal T2w TSE.

1C) DWI ($b = 1000 \text{ s/mm}^2$ and ADC map)

1D) Time-of-flight MR angiography (MIP).

1E) Coronal inverted T2w TSE.

1F) Sagittal T2w TSE.



Case 2

A 4-year-old boy with more than one year of recurrent febrile convulsions. MRI demonstrated hydrocephalus, cerebral hypoplasia of the corpus callosum

and absent septum pellucidum as well as left frontal schizencephaly (open lip type). The boy received a left ventriculo-peritoneal shunt.

2A) Transversal T2w TSE.
2B) Transversal T1w TIRM with motion correction (*syngo* BLADE).
2C) Coronal inverted T2w TSE.
2D) Sagittal T2w TSE.



Case 3

An 8-year-old girl presented with early onset of breast development. MRI showed a cystic dilatation of the left ventricle at the temporal horn but could rule out abnormalities of the pituitary gland.

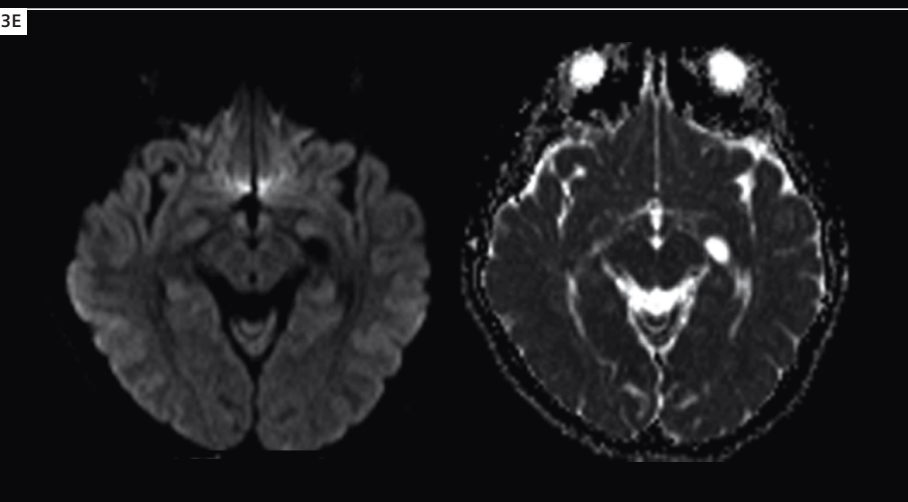
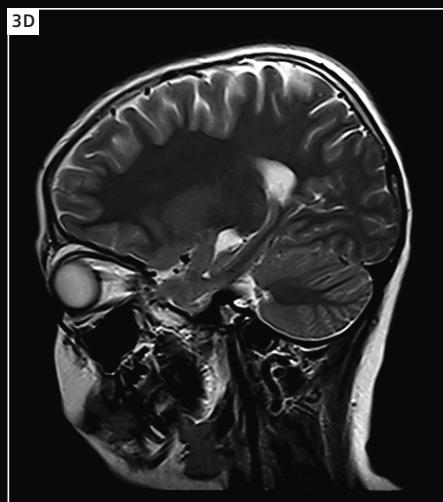
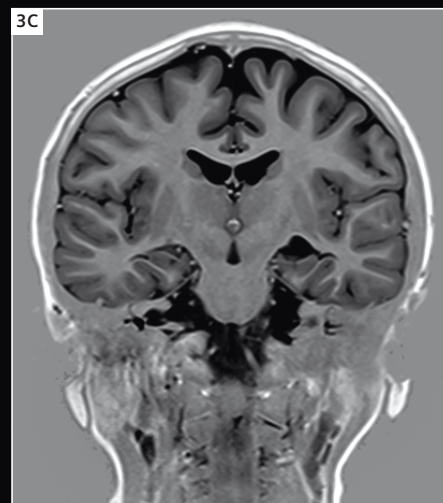
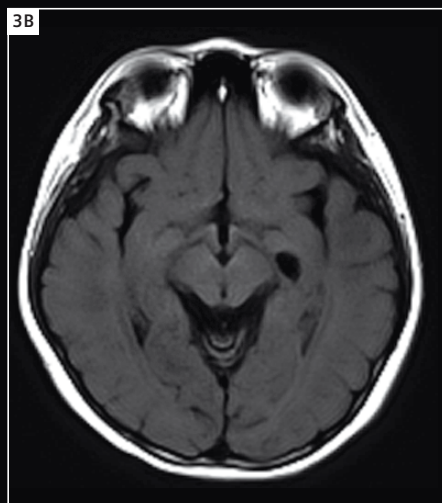
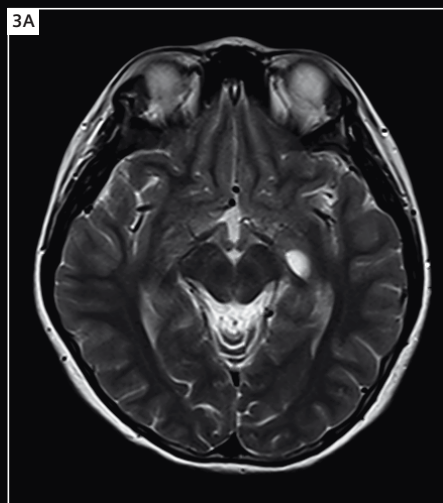
3A) Transversal T2w TSE.

3B) Transversal FLAIR (DarkFluid).

3C) Coronal inverted T2w TSE.

3D) Sagittal T2w TSE.

3E) DWI (b = 1000 s/mm² and ADC map).



Case 4

A 3-month-old girl* that fell into coma 45 days after birth. MRI shows bilateral temporo-occipital brain atrophy with cystic encephalomalacia.

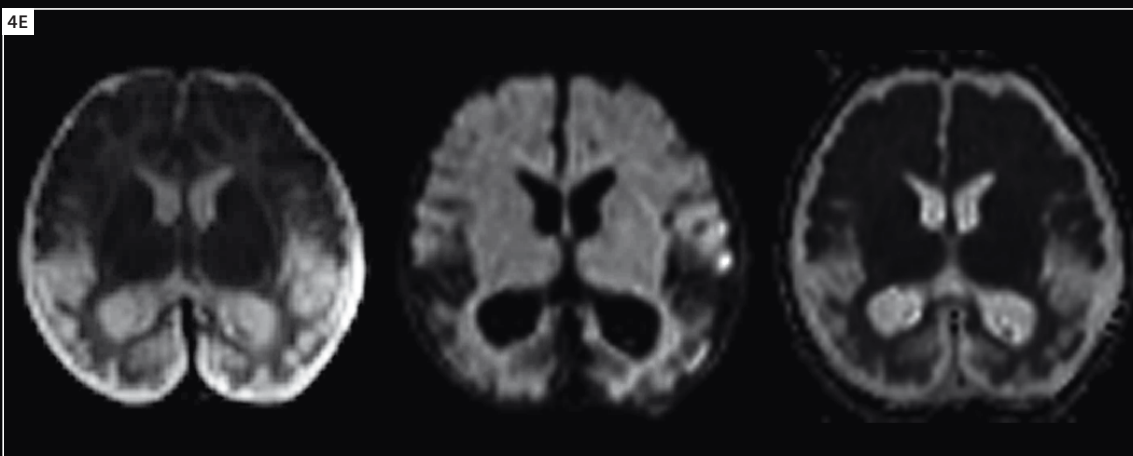
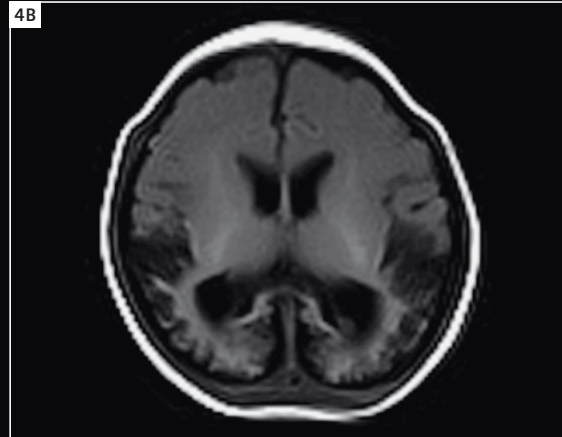
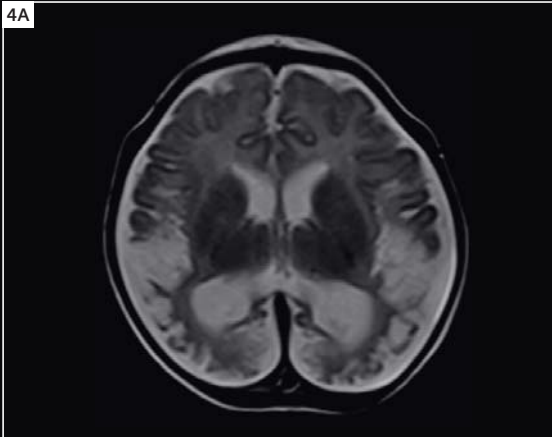
4A) Transversal T2w TSE.

4B) Transversal FLAIR (DarkFluid) with motion correction (*syngo* BLADE).

4C) Sagittal T2w TSE.

4D) Coronal T2w TSE.

4E) DWI (b = 0, 1000 s/mm² and ADC map).



Case 5

A 45-day-old boy* was rescued after asphyxia during birth. MRI follow-up exam of the subarachnoidal haemorrhage is shown. MRI demonstrates poly-

cystic encephalomalacia and bilateral subdural effusions.

5A) Transversal T2w TSE.

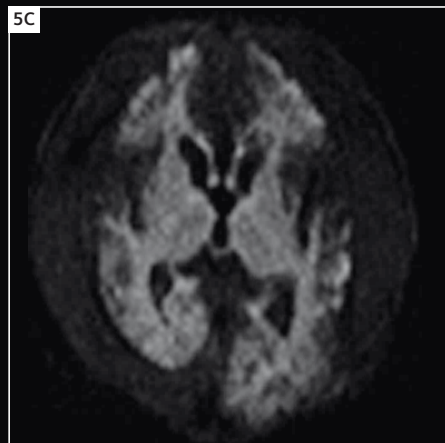
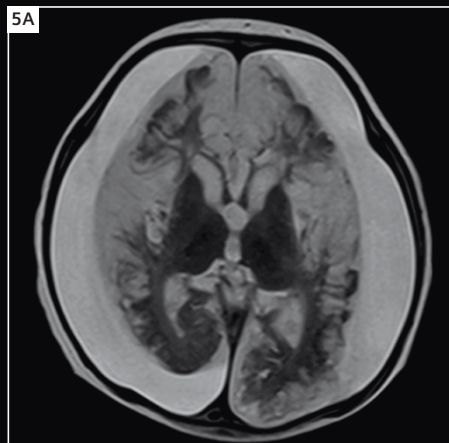
5B) Transversal FLAIR (DarkFluid) with

motion correction (*syngo* BLADE).

5C) DWI ($b = 1000 \text{ s/mm}^2$).

5D) Sagittal T2w TSE.

5E) Coronal inverted T2w TSE.

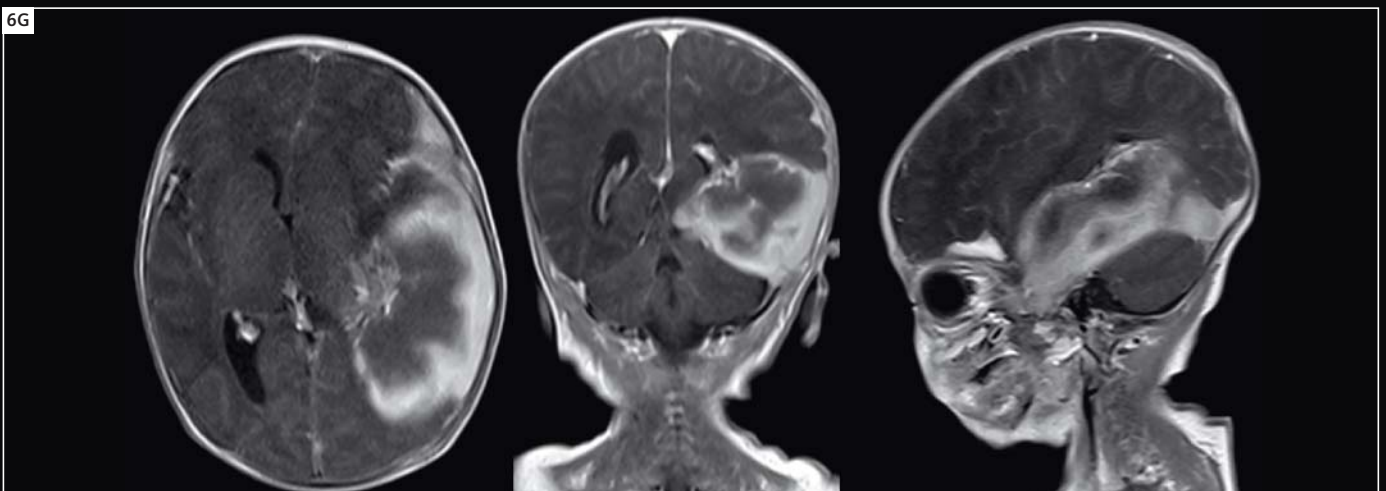
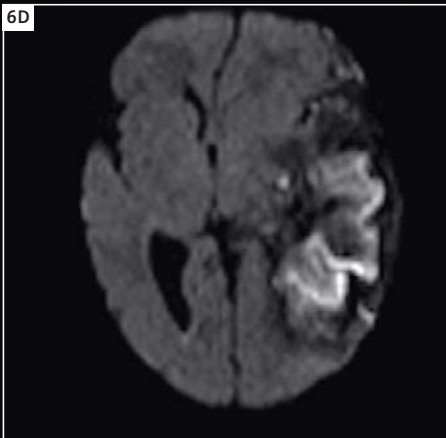
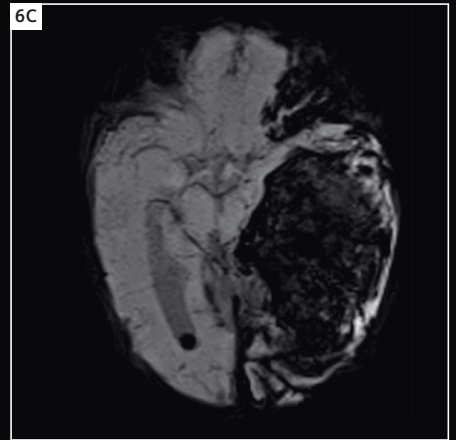
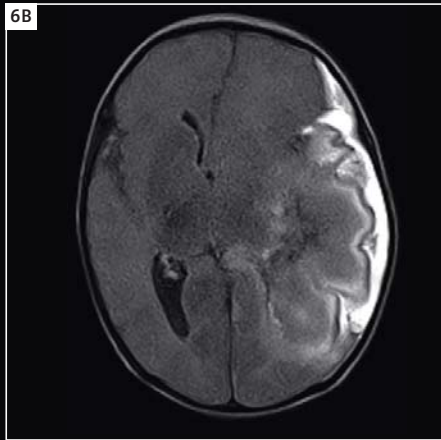


Case 6

An 11-day-old boy* with sub-acute intracranial haematoma left fronto-temporal of unknown origin.
6A) Transversal T2w TSE.
6B) Transversal FLAIR (DarkFluid) with

motion correction (*syngo* BLADE).
6C) SWI (thinslice MIP).
6D) DWI (b = 1000 s/mm²).
6E) Time-of-flight MR angiography (MIP).

6F) Sagittal T2w TSE.
6G) Transversal, coronal and sagittal T1w TSE after contrast media administration.

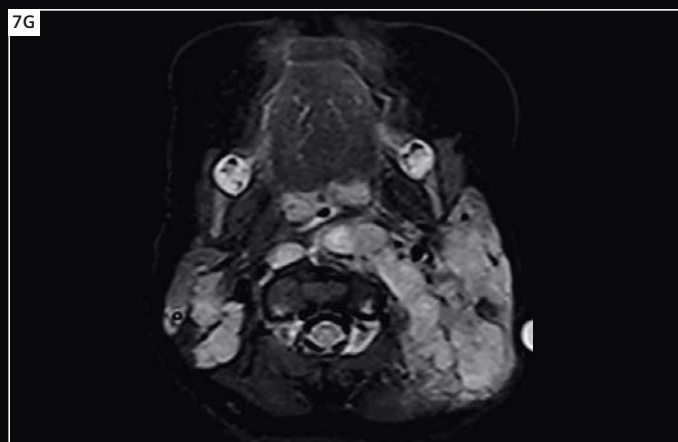
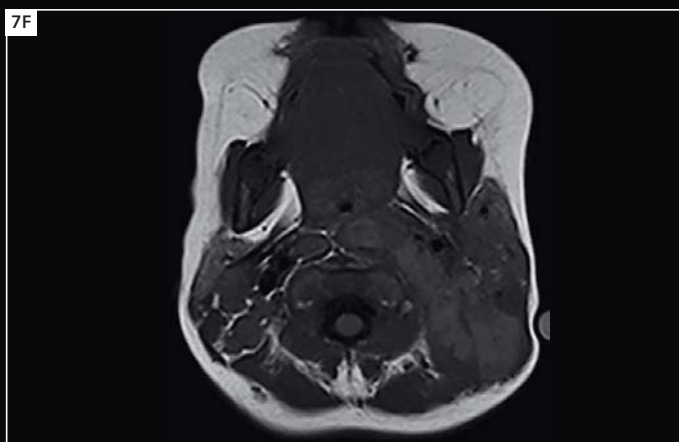
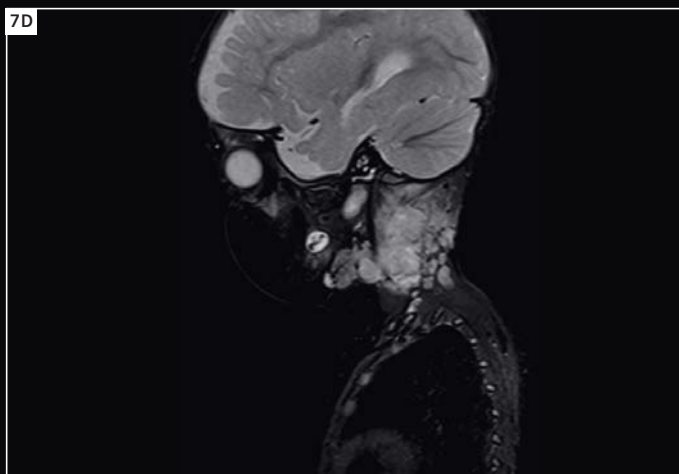


Case 7

An 8-month-old girl* presented with swelling of the neck since two weeks. MRI reveals a cervical lymphoma manifestation.

7A) Coronal T1w TSE.
7B) Coronal T2w TSE.
7C) Coronal T2w TIRM.
7D) Sagittal T2w TIRM.

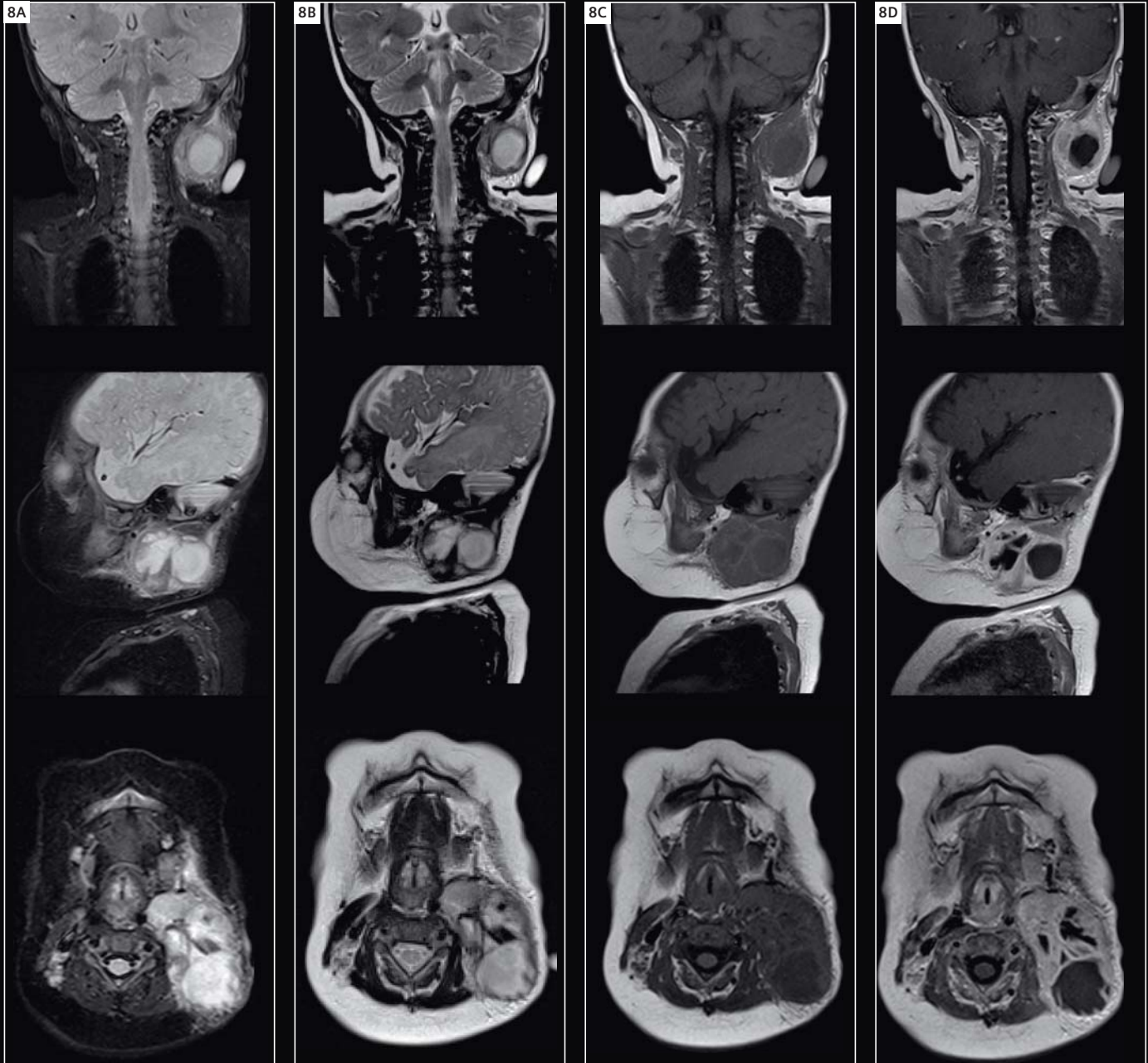
7E) Sagittal T1w TSE.
7F) Transversal T1w TSE.
7G) Transversal T2w TIRM.



Case 8

A 5-month-old boy* presented with swelling of the neck for six days but without fever. MRI shows clearly the abscess formation left cervical. From top to bottom coronal, sagittal, transversal.

- 8A) T2w TIRM.
- 8B) T2w TSE.
- 8C) Native T1w TSE.
- 8D) After contrast media administration.



Case 9

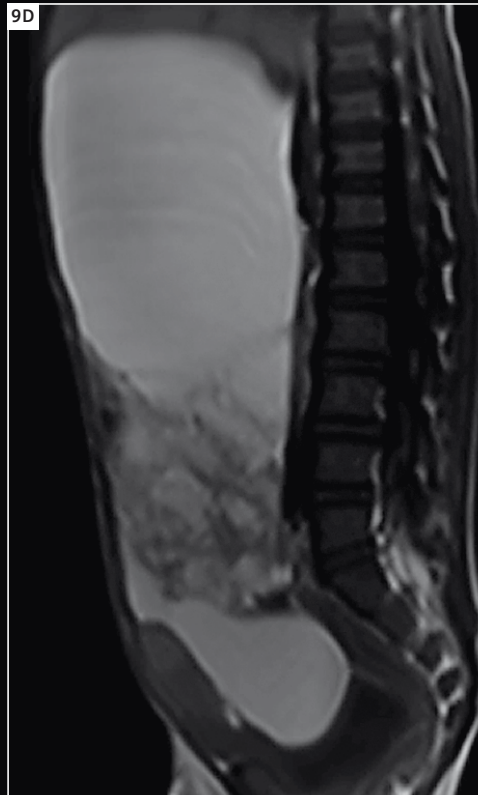
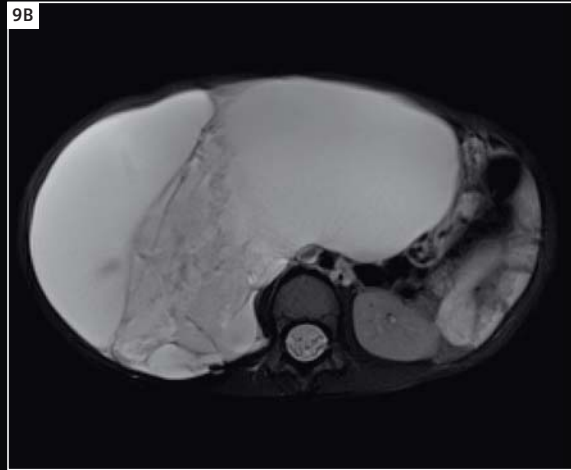
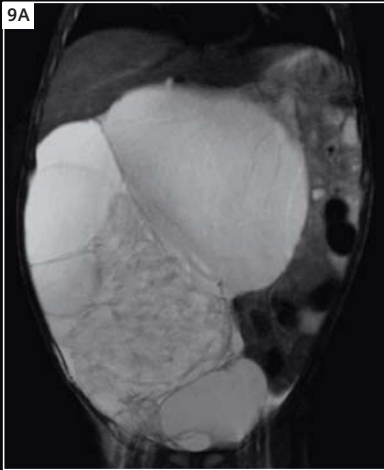
A 3-year-old boy with gigantic polylobulated cystic mass of the abdomen and pelvis with unknown origin.

9A) Coronal T2w TSE with fat saturation and triggering.

9B) Transversal T2w TSE with motion correction (*syngo* BLADE) and fat saturation.

9C) Sagittal T2w TSE.

9D) Sagittal T1w TSE.



Case 10

A 3-year-old girl was sent to MRI because of fever and weakness of both lower extremities for 10 days. MRI showed a large mass at Th 2–3. Pre (upper row) and images after surgery (resection of the intramedullar tumor) (lower row). Histopathology revealed a solitary bone plasmocytoma.

10A) Coronal T2w TSE.

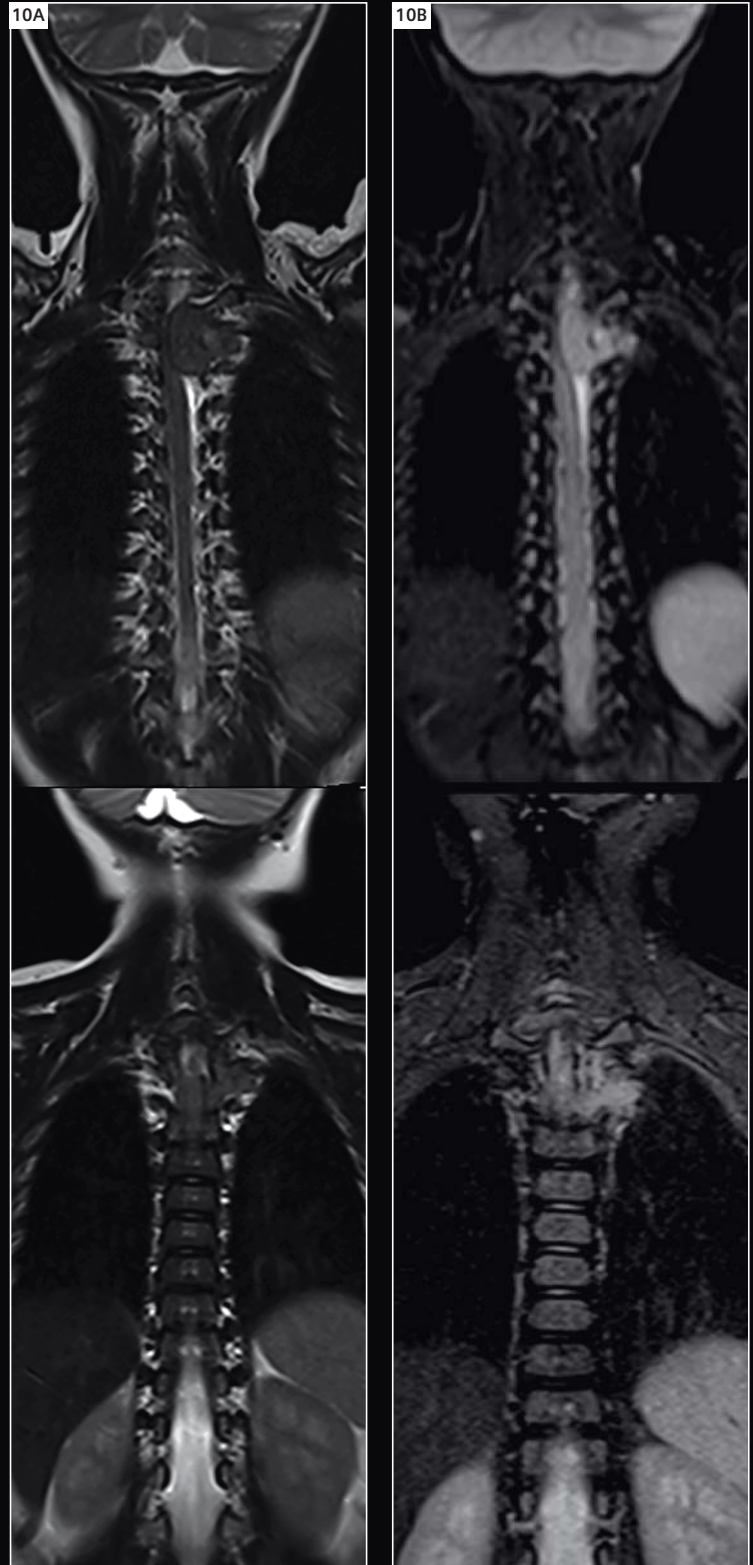
10B) Coronal T2w TIRM.

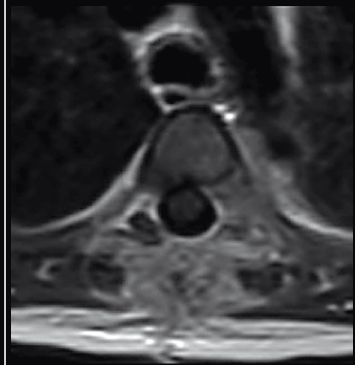
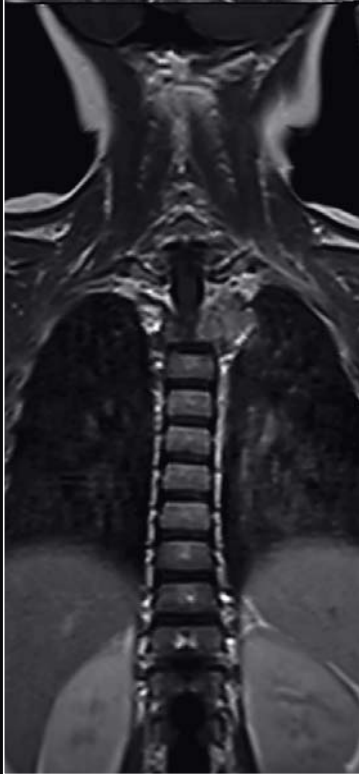
10C) Coronal T1w TSE.

10D) Transversal contrast-enhanced T1w TSE.

10E) Sagittal T2w TSE

10F) Sagittal contrast-enhanced T1w TSE.





Case 11

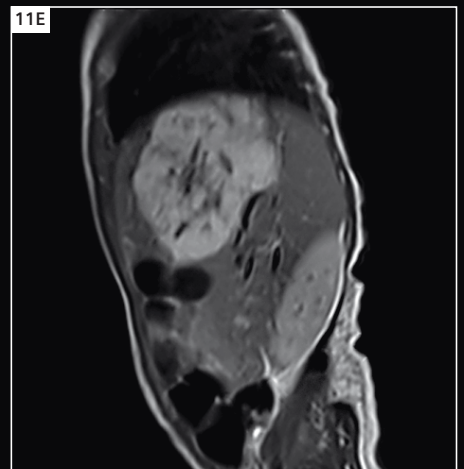
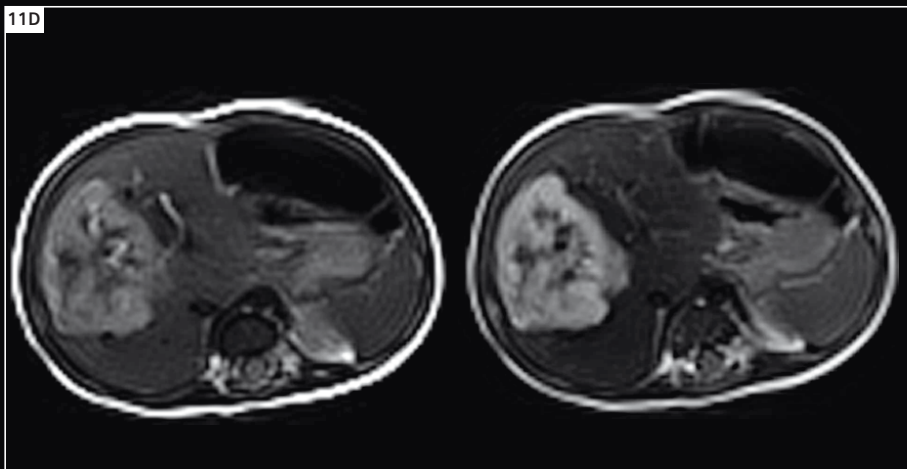
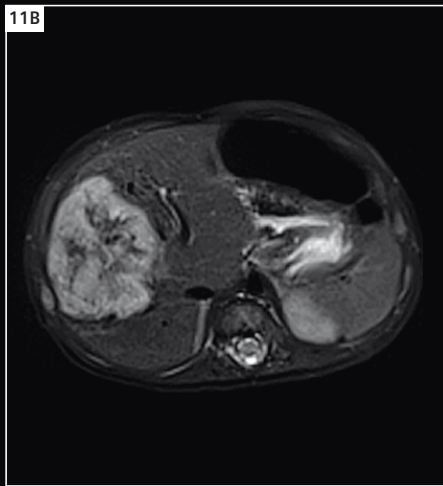
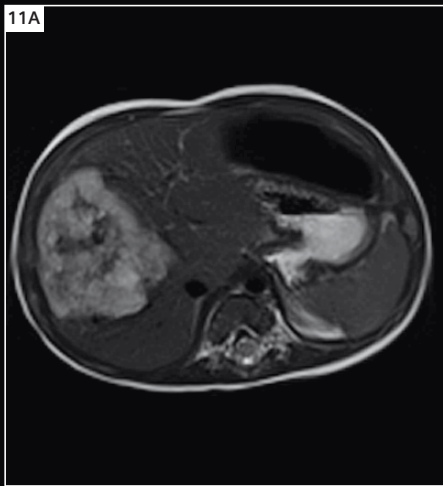
A 3-month-old girl* with coughing and short breath was found to have a large intra-hepatic tumor (ultrasound report). MRI shows a large cavernous haemangioma.

11A) Transversal T2w TSE without and
11B) with fat saturation.

11C) Sagittal T1w TSE.

11D) Early and late phase T1w TSE after contrast-administration.

11E) Sagittal T1w TSE after contrast-media administration.



Case 12

Fetal MRI* for further evaluation of right diaphragmal hernia and to evaluate residual lung volume and developmental status is shown. Coronal, sagittal and transversal T2w HASTE.



Contact

Han Yan Qiao, MD
Shanghai Children's Hospital
Department of Diagnostic Radiology
No.24, lane 1400 Beijing Xi Road
Shanghai 200040
China
Phone: +86 18917128338
yanqiaohan@163.com

*MR scanning has not been established as safe for imaging fetuses and infants under two years of age. The responsible physician must evaluate the benefit of the MRI examination in comparison to other imaging procedures.

Neuro-Infections in Childhood – MR Imaging Patterns

Birgit Ertl-Wagner

Institute of Clinical Radiology, University of Munich – Grosshadern Campus, Munich, Germany

Infectious diseases are among the most common disorders of the brain and spine in childhood. The manifestation of the disease and the MR imaging pattern vary widely depending on the time of infection in relation to the development of the brain. Cerebral infections cause different abnormalities of the brain during the following time periods:

- Fetal period: neuro-infections in the fetus are also called congenital infections; they occur in utero
- Perinatal period: neuro-infections occurring around the time of birth are also called neonatal infections
- Later childhood and adolescence

However, MR imaging patterns also depend on the infectious agent causing the disease. Neuro-infections can, for example, be classified as:

- Bacterial
- Viral
- Parasitic
- Fungal

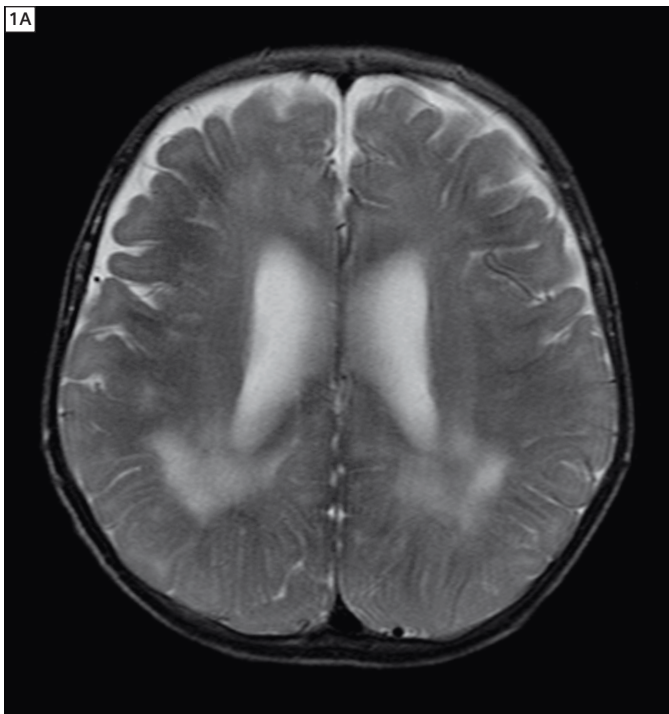
When investigating children with presumed infections of the brain, it is important to take into account the imaging patterns of the respective time of infection and of the various infectious agents.

Congenital infections

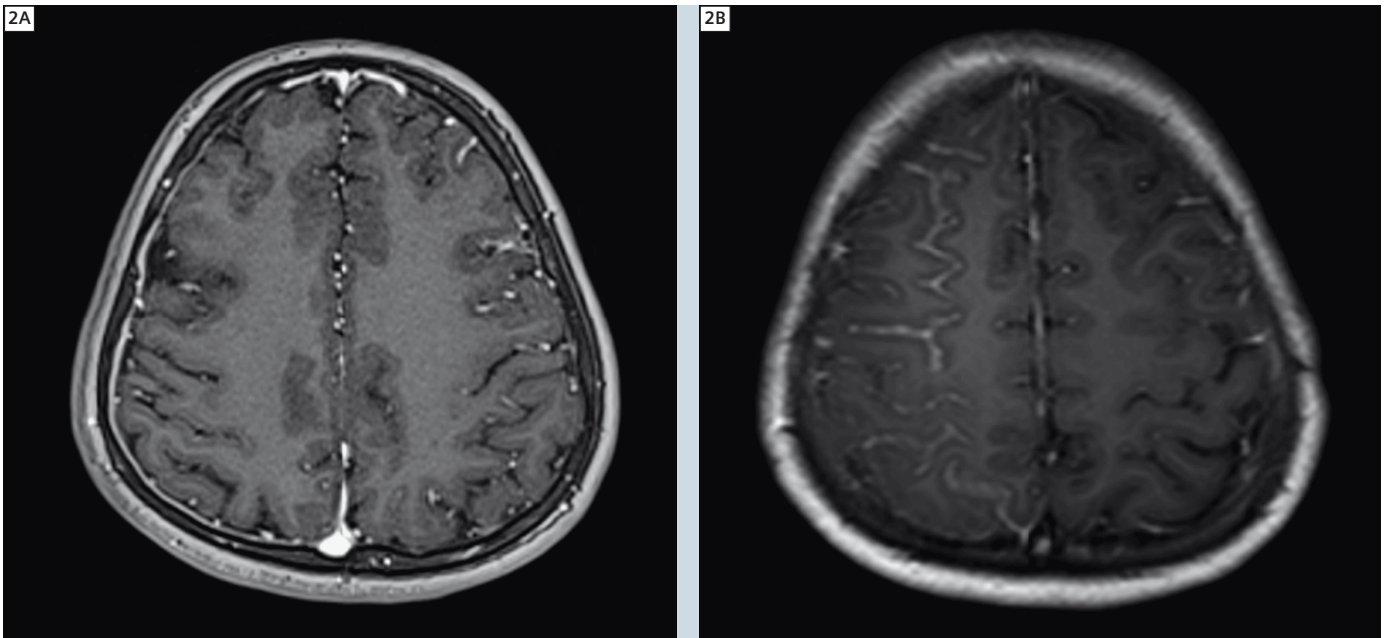
Congenital infections of the brain are commonly summarized under the acronym ToRCH. This acronym stands for several infectious agents causing congenital infections, i.e.:

- **T**oxoplasmosis gondii
- **R**ubella virus
- **C**ytomegalovirus (CMV)
- **H**erpes simplex virus (HSV)

Risk factors for a congenital **toxoplasmosis** are maternal contact with cat faeces and eating of raw or undercooked meat. It occurs in about 1:3,000 to 1:5,000 live births. Imaging often reveals calcifica-



1 Axial T2-weighted image (1A) and FLAIR image (1B) demonstrating patchy signal hyperintensities of the white matter in a 4-year-old girl with congenital CMV infection.



2 Contrast-enhanced axial T1-weighted images demonstrate an increased pachymeningeal and leptomenigeal enhancement in a 13-year-old girl with viral meningitis.

tions in the basal ganglia and in the periventricular region. The children may suffer from hydrocephalus, but also from microcephaly. In contrast to congenital CMV infection, disorders of cortical development do not usually occur [1]. Generally, the consequences tend to be less serious the later the infection occurs during gestation.

Due to widespread immunization campaigns, congenital **rubella infections** have become an exceedingly rare occurrence in the western world. The severity of the infections depends on the gestational age – infections have an especially severe course when they occur during the first trimester. The MR imaging appearance can resemble that of congenital toxoplasmosis. Microcephaly and calcifications are observed [2].

Cytomegalovirus (CMV) infections are by far the most common congenital infection in the western world. CMV infections during pregnancy are estimated to be ten times more common than congenital toxoplasma infections – occurring in up to 1% of live births. However, only 5 to 10% of congenital CMV infections affect the brain. A common presenting symptom in children is hearing loss. It is not

unusual for children to be referred for MR imaging prior to surgery for a cochlear implant to assess the morphology of the inner ear. The MR imaging appearance varies depending on the gestational age at the time of infection. CMV infections may lead to polymicrogyria and / or lissencephaly, especially if they occur during the second trimester of pregnancy. Very commonly, patchy white matter lesions with hyperintense signal on T2-weighted and FLAIR sequences are present (Fig. 1). These are often confluent and may occur in the absence of abnormalities of cortical development [3]. **Herpes simplex virus (HSV) infections** of the brain in the neonate are usually of type II and are acquired during vaginal birth. MR imaging usually demonstrates rapidly progressive signal alterations of the white matter eventually leading to cystic encephalomalacia with ensuing atrophy of the brain [4].

Other congenital infections include lymphocytic choriomeningitis (LCM) virus infection, syphilis, congenital HIV infection and congenital varicella zoster infection.

Generally, congenital infections should always be taken into consideration when

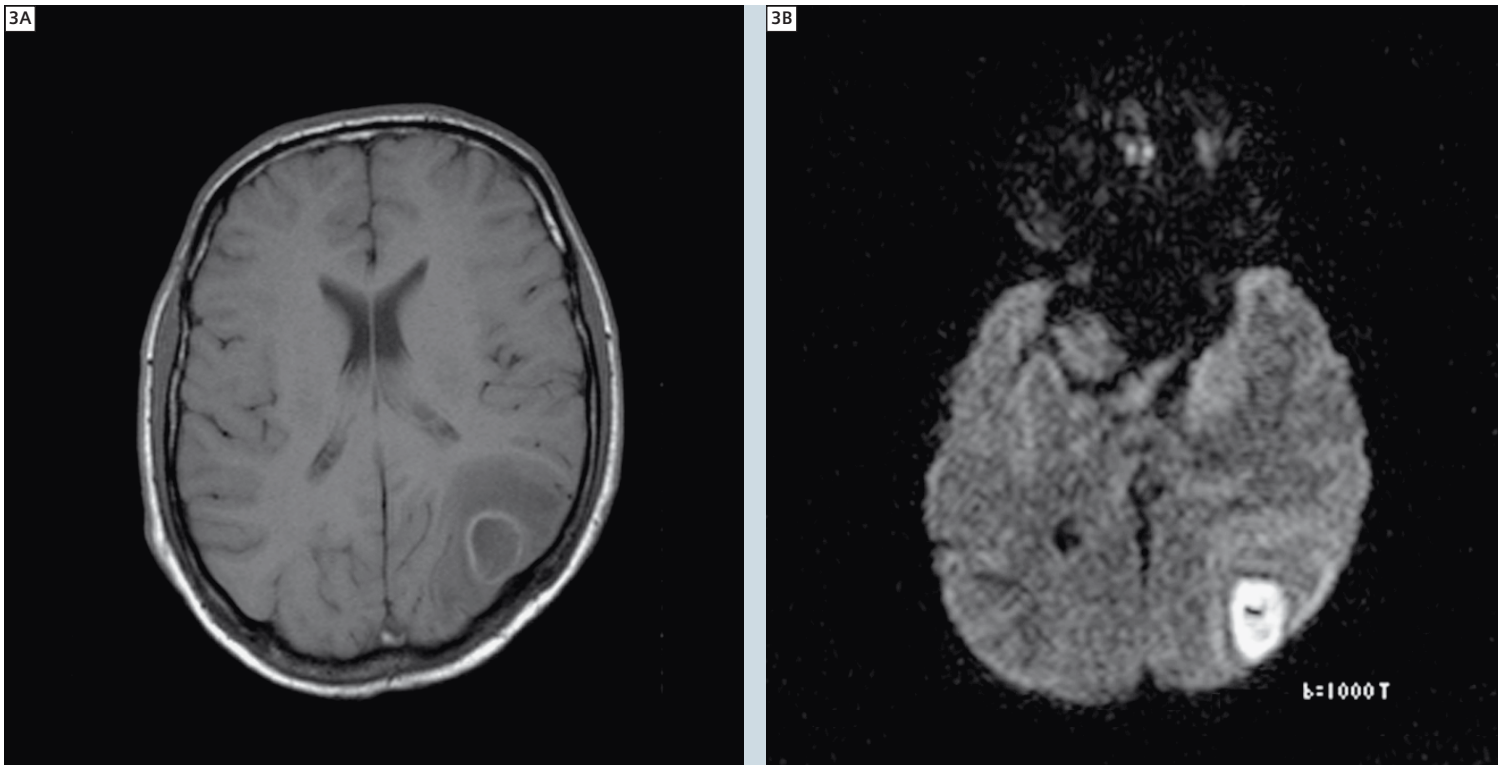
imaging a child with developmental delay and / or epilepsy. Children with congenital hearing loss usually undergo MR imaging prior to surgery for a cochlear implant. Congenital infections – especially congenital CMV infections – are a rather common cause for congenital hearing loss and the MR imaging should always be scrutinized for possible signs of congenital infections such as white matter lesions and / or disorders of cortical development.

Meningitis, cerebritis and abscess

Meningitis is the most common neuroinfection throughout childhood. The infectious agent may reach the meninges by different routes [5]:

- hematogeneously
- via an adjacent infection, e.g. mastoiditis
- through the choroid plexus
- via a penetrating injury
- by rupture of a cerebral abscess.

Most commonly, the infectious agent is viral. **Viral meningitis** is not a classic imaging diagnosis, but imaging may be performed to rule out complications and / or to rule out contraindications to perform a diagnostic lumbar puncture.



3 Contrast-enhanced axial T1-weighted images (3A), diffusion-weighted images (3B) and the concomitant ADC-map (3C) show an intracranial abscess with diffusion restriction.

MR imaging may show a thickening of the meninges with an increased enhancement after the administration of contrast agent – this can affect the leptomeninges and / or the pachymeninges (Fig. 2). However, the MR imaging appearance may also be completely normal in viral meningitis. A normal MR appearance generally does not rule out viral meningitis. Complications of viral meningitis include concomitant encephalitis, hydrocephalus and vasculitis.

Bacterial meningitis usually progresses more rapidly with a more severe clinical course than viral meningitis. Again, MR imaging is mostly performed to investigate complications and / or to rule out contraindications for lumbar puncture. The thickening of the meninges is usually more pronounced in bacterial meningitis compared to viral meningitis. Subdural empyemas are a potential complication of bacterial meningitis, the occurrence of which leads to a pronounced worsening of the prognosis [6]. *Hemophilus influenzae* may, however, lead to sterile sub-

dural fluid collections that need to be differentiated from empyema.

Other complications of bacterial meningitis include hydrocephalus, venous infarctions due to thromboses, and arterial infarctions due to arteritis / vasculitis. Moreover, bacterial meningitis may lead to cerebritis and abscess formation, as well as to ventriculitis.

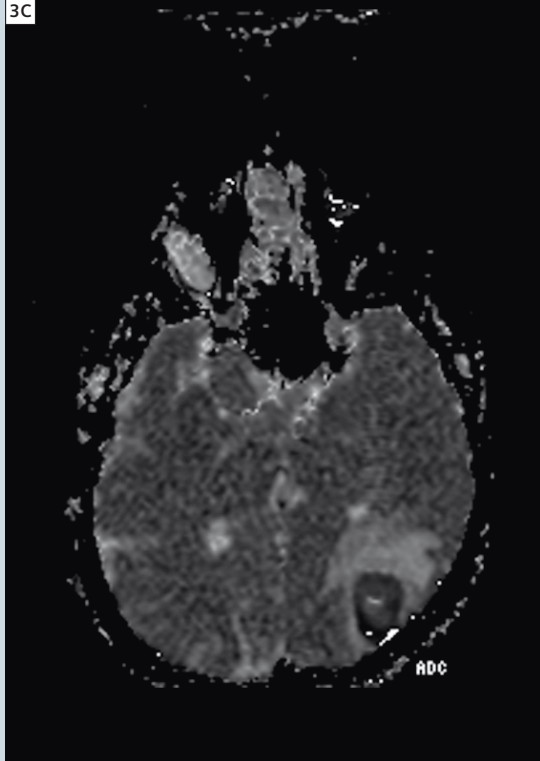
Tuberculous meningitis may occur in children or in adults. Tuberculosis preferentially affects the basal meninges, which show a marked thickening and enhancement on MR imaging. Focal tuberculomas may also be seen, which are often hypointense on T2-weighted MR imaging. Common complications include hydrocephalus and infarctions in the basal ganglia and thalami.

A focal infection of the brain is called **cerebritis**. At the stage of a cerebritis, the focal infection has not yet become centrally necrotic. MR imaging usually

reveals a contrast enhancement of the entire lesion with a perifocal edema.

At a later stage, cerebritis may become a cerebral **abscess**, especially if left untreated. Cerebral abscesses in children may be a result of a sinusitis or mastoiditis and are then commonly located in close proximity to either the paranasal sinuses or the petrous bones. MR imaging reveals one of the hallmark features of cerebral abscesses: a centrally restricted diffusion, which aids in differentiating cerebral abscess formation from primary brain tumors [7]. On conventional MR imaging, the central portion of a cerebral abscess is usually hyperintense on T2-weighted imaging and hypointense on T1-weighted imaging, while the rim of the lesion shows a pronounced enhancement after the administration of contrast agent (Fig. 3).

Especially in small children, **ventriculitis** frequently occurs as a complication of meningitis. This may lead to periventricular and intraventricular abscesses and the prognosis is rather unfavorable.



MR imaging typically shows a pronounced enhancement of the ventricular ependyma and dilatation of the ventricles. Later in the disease process, loculations with septae commonly ensue.

Viral encephalitis

Viral encephalitis is another important neuro-infectious differential diagnosis both in children and in adults. There is a plethora of viral infectious agents that may cause encephalitis. In the following, this report focuses on HSV I encephalitis, SSPE, tick-borne encephalitis and Rasmussen encephalitis.

HSV encephalitis is a crucial diagnosis not to be missed on MR imaging. The earlier treatment is initiated, the better the diagnosis is. About one third of HSV encephalitis occurs in children, most of which are HSV type I infections. Initial symptoms may be rather unspecific; therefore, the imaging diagnosis can be crucial for the patient's further prognosis. HSV preferentially involves the limbic system, and so an involvement of the

temporal lobes with a signal hyperintensity on T2-weighted and FLAIR sequences especially in the temporomesial portion is a common hallmark feature of the disorder (Fig. 4). The insular / peri-Sylvian regions are commonly involved as well. However, the MR imaging appearance can also be atypical. An asymmetrical involvement of the limbic structures is rather common. In addition, the pattern of involvement can also be unspecific and does not necessarily demonstrate a preferential involvement of the limbic system, especially in small children [8]. If in any doubt, the suspicion of HSV encephalitis should be raised and treatment should be swiftly initiated, until HSV infection is ruled out by cerebrospinal fluid (CSF) diagnostics.

Varicella-zoster-encephalitis is a rare complication of chicken pox. Affected children usually present with cerebellar signs such as ataxia or dysarthria. On MR imaging there is usually pronounced edema of the cerebellum. Supratentorial lesions may also be present, e.g. in the cortex or in the basal ganglia.

Subacute sclerosing panencephalitis (SSPE) is a devastating and eventually lethal disorder of the brain. It is considered a late complication of measles infection. Affected children suffer from a progressive neurodegeneration with dementia and pareses. MR imaging initially shows patchy signal alterations in the cortical and subcortical regions with hyperintensities on T2-weighted and FLAIR sequences. In the further course, pronounced atrophy ensues [9]. Other brain manifestations associated with measles infection include acute

postinfectious encephalitis, which is probably an autoimmune disorder in relation to the measles virus, and progressive infectious encephalitis, which is a persistent infection of the brain.

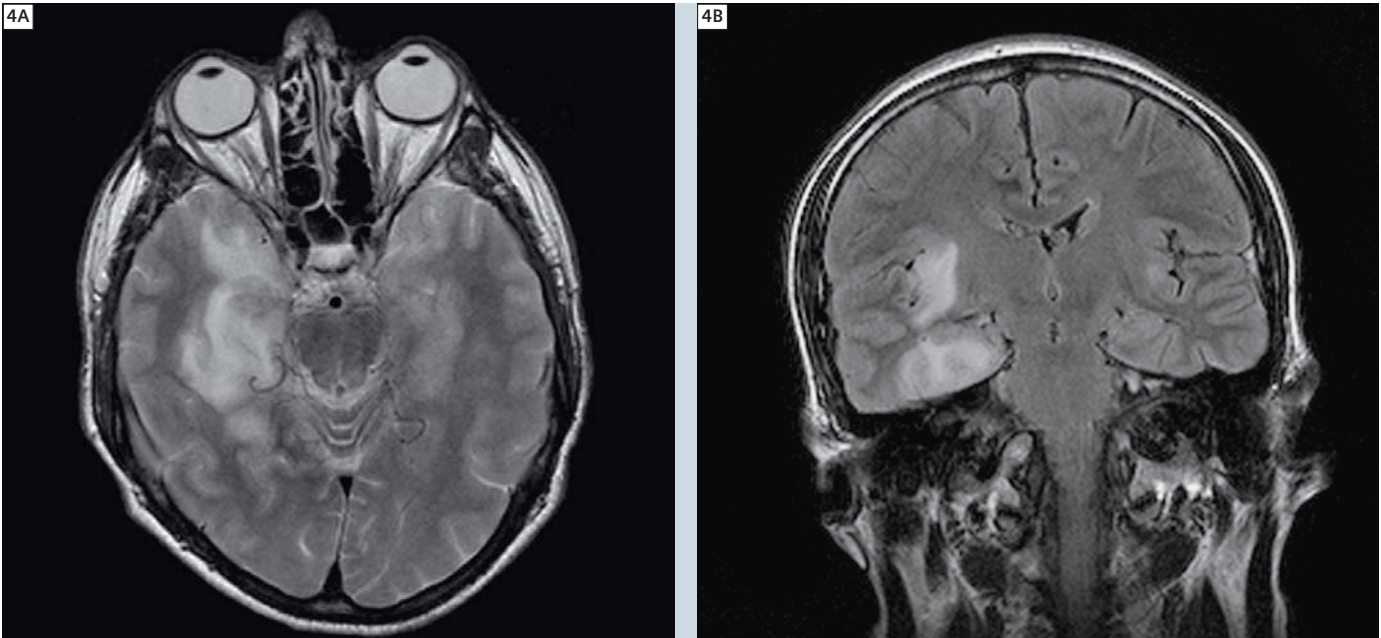
Tick-borne encephalites usually have a peak occurrence in early summer, when ticks are most prevalent. Depending on the region, the symptoms and imaging appearance may vary. Tick-borne encephalitis most commonly starts with flu-like symptoms, which may be followed by a cerebral and / or spinal affection. On MR imaging, edema of the basal ganglia and thalami with pronounced signal hyperintensities on T2-weighted and FLAIR sequences is the most common imaging pattern. However, both the cortical ribbon and the spinal cord may be involved as well.

Rasmussen encephalitis is a progressive disorder of the brain, the cause of which is still unknown. Both viral agents and autoimmune processes are discussed as potential causes. Affected children usually suffer from epilepsy and progressive hemiparesis with the epilepsy commonly being refractory to medical therapy. The disorder starts focally and subsequently spreads throughout the cerebral hemisphere. MR imaging shows cortical and subcortical edema and later progressive atrophy. It is important to remember that MR imaging can be completely normal in the early stages of the disease [10].

Parasitic infections

Parasites are among the most common infectious agents affecting the brain world-wide, even though they are rather rare in the western world.

Neurocysticercosis is caused by the tapeworm *taenia solium* [11]. Affected children commonly complain of head-



4 Axial T2-weighted (4A) and coronal FLAIR sequences (4B) demonstrate edema, predominantly in the right temporal lobe, in a 16-year-old boy with HSV type 1 encephalitis.

aches and epilepsy. Cysticerci can be found in a parenchymal, leptomeningeal or intraventricular location. Parenchymal cysticerci tend to be located in the grey matter, while leptomeningeal cysticerci are mostly found in the basal meninges. Intraventricular cysticerci can lead to an obstructive hydrocephalus depending on the location.

Echinococcal infections much more commonly affect the liver and the lung than the central nervous system. In rare instances, however, a cerebral echinococcosis can be the first sign of an echinococcal infection. As in cysticercosis, affected children may complain of headaches and / or epilepsy. On MR imaging, cystic lesions with a hyperintensity on T2-weighted sequences and a concomitant hypointensity on T1-weighted images can be found.

Conclusions

Neuroinfectious diseases in childhood can be very challenging to diagnose using MR imaging. When interpreting MR images of affected children, it is important to keep the respective imaging patterns in mind, as the imaging appearance varies in relation to the age

at infection and in relation to the infectious agent. In addition to establishing the diagnosis, it is especially important to scrutinize the MR images for potential signs of complications from the neuroinfection.

References

- 1 Diebler C, Dusser A, Dulac O. 1985. Congenital toxoplasmosis: clinical and neuroradiological evaluation of the cerebral lesions. *Neuroradiology*. 27:125-130.
- 2 Ishikawa A, Murayama T, Sakuma N. 1982. Computed cranial tomography in congenital rubella syndrome. *Arch Neurol* 39:420-422.
- 3 Van der Knaap MS, Vermeulen G, Barkhof F, et al. 2004. Pattern of white matter abnormalities at MR imaging: use of polymerase chain reaction testing of Guthrie cards to link pattern with congenital cytomegalovirus infection. *Radiology* 230:529-536.
- 4 Toth C, Harder S, Yager J. 2003. Neonatal herpes encephalitis: a case series and review of clinical presentation. *Can J Neurol Sci* 30:36-40.
- 5 Barkovich AJ. Infections of the Nervous System. In: Barkovich AK: *Pediatric Neuroimaging*. Lippincott Williams & Wilkins, Philadelphia, 2005.
- 6 Tsuchiya K, Osawa A, Katase S, et al. 2003. Diffusion-weighted MRI of subdural and epidural empyemas. *Neuroradiology*. 45:220-223.
- 7 Guzman R, Barth A, Lovblad K, et al. 2002. Use of diffusion-weighted magnetic resonance imaging in differentiating purulent brain processes from cystic brain tumors. *J Neurosurg* 97:1101-1107.
- 8 Leonard J, Moran C, Cross D, et al. 2000. MR imaging of herpes simplex type 1 encephalitis in infants and young children. *AJR Am J Roentgenol* 174:1651-1655.
- 9 Alkan A, Sarac K, Kutlu R, et al. 2003. Early and late-stage subacute sclerosing panencephalitis: chemical shift imaging and single-voxel MR spectroscopy. *AJNR Am J Neuroradiol* 24:501-506.
- 10 Geller E, Faerber EN, Legido A, et al. 1998. Rasmussen encephalitis: complementary role of multitechnique neuroimaging. *AJNR Am J Neuroradiol* 19:445-449.
- 11 Carpio A. 2002. Neurocysticercosis: an update. *Lancet Infect Dis* 22:751-762.

Contact

Prof. Dr. med. Birgit Ertl-Wagner
 Institute of Clinical Radiology
 University of Munich –
 Grosshadern Campus
 Marchioninstr. 15
 D-81377 München
 Germany
 Phone: +49-89-7095-3250
 Birgit.Ertl-Wagner@med.uni-muenchen.de

Siemens Healthcare Publications

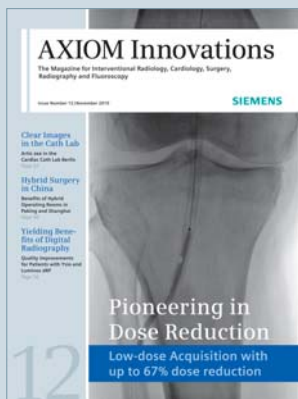
Our publications offer the latest information and background for every healthcare field. From the hospital director to the radiological assistant – here, you can quickly find information relevant to your needs.



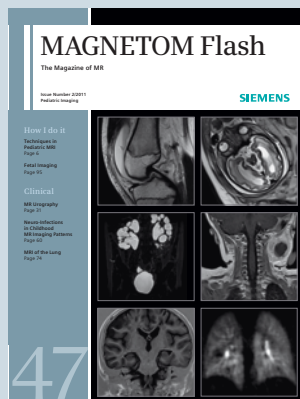
Medical Solutions
Innovations and trends in healthcare. The magazine is designed especially for members of hospital management, administration personnel, and heads of medical departments.



eNews
Register for the global Siemens Healthcare News-letter at www.siemens.com/healthcare-eNews to receive monthly updates on topics that interest you.



AXIOM Innovations
Everything from the worlds of interventional radiology, cardiology, fluoroscopy, and radiography. This semi-annual magazine is primarily designed for physicians, physicists, researchers, and medical technical personnel.



MAGNETOM Flash
Everything from the world of magnetic resonance imaging. The magazine presents case reports, technology, product news, and how-to articles. It is primarily designed for physicians, physicists, and medical technical personnel.

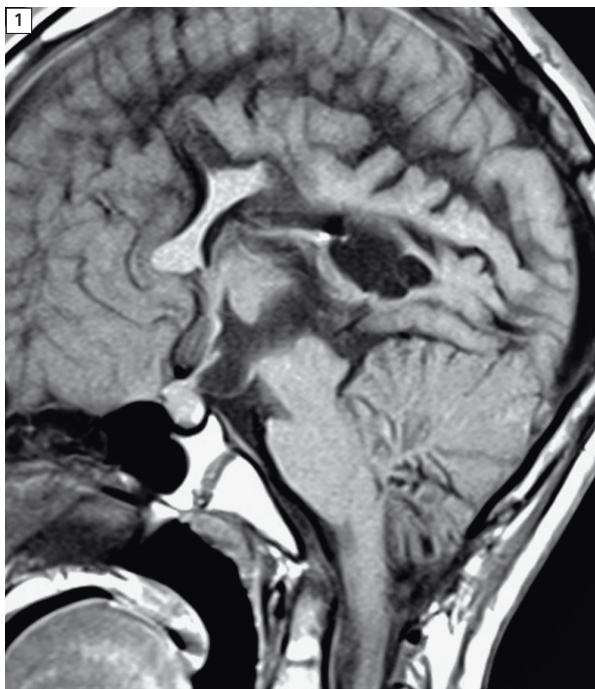


SOMATOM Sessions
Everything from the world of computed tomography. With its innovations, clinical applications, and visions, this semiannual magazine is primarily designed for physicians, physicists, researchers, and medical technical personnel.

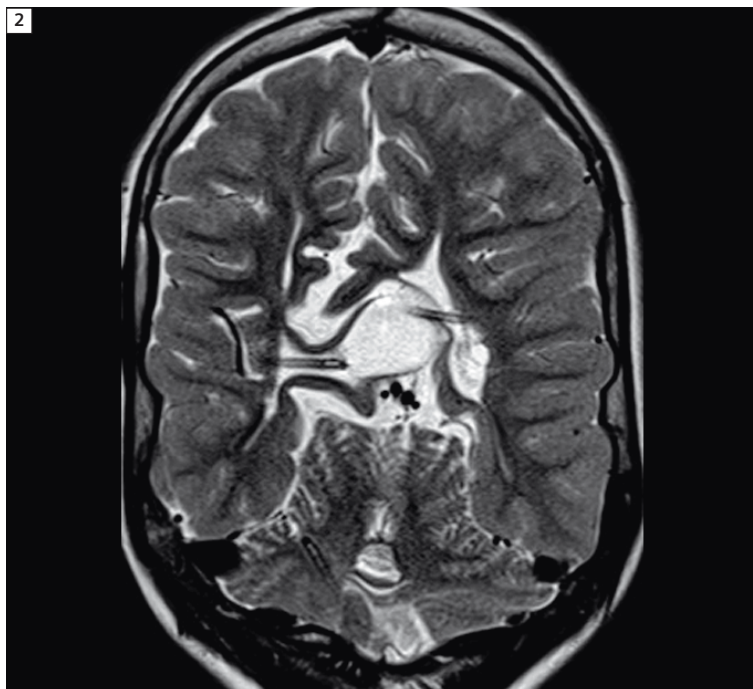


Imaging Life
Everything from the world of molecular imaging innovations. This bi-annual magazine presents clinical case reports, customer experiences, and product news and is primarily designed for physicians, hospital management and researchers.

For current and past issues and to order the magazines, please visit www.siemens.com/healthcare-magazine.



1 Sagittal T1w image depicting callosal dysgenesis and tectal beaking.



2 Coronal T2w image depicting interdigitating gyri.

Case Report: Chiari II Malformation

Raghuram K. Rao, MD, MPH; Harnoor Singh, MD; Claudia C. Cotes, MD

University of Texas-Medical Branch, Galveston, TX, USA

Patient history

This is a 9-year-old girl with a known history of spina bifida and Chiari II malformation. In her past, she has had 2 ventriculoperitoneal shunts placed – one at birth, and another at the age of 3. Since birth, she has been paraplegic. However, until recently, her symptoms have otherwise been controlled. For the past year, she has experienced progressive dysphagia, dysarthria, headaches, and constant darting eye movements.

Sequence details

Images were obtained using a 1.5T Siemens MAGNETOM Espree using a head coil (Figs. 1, 2) and a neck coil (Fig. 3).

Figure 1: Sagittal T1-weighted scan (TR/TE 550/8.8 ms, scan time 2:25 min, slice thickness 5 mm).

Figure 2: Coronal T2-weighted scan (TR/TE 4330/91 ms, scan time 2:16 min, slice thickness 3 mm).

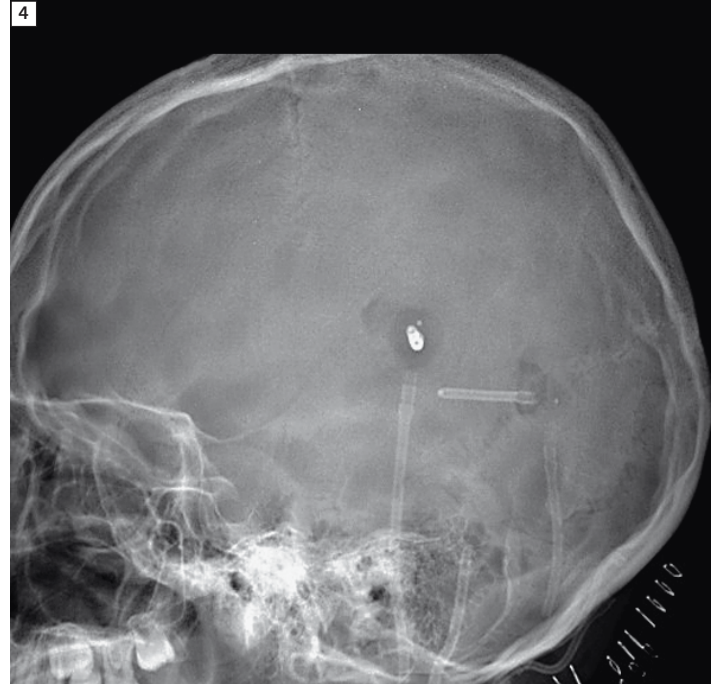
Figure 3: Sagittal T2-weighted scan (TR/TE 4400/90 ms, scan time 2:17 min, slice thickness 3 mm).

Imaging findings

Several findings on the study are seen commonly in cases of Chiari II malformations. In the telencephalon, findings include callosal dysgenesis (Fig. 1) and interdigitating gyri (Fig. 2). With regards to the posterior fossa, the cerebellar tonsils herniate into the posterior cervical canal (Fig. 3). The downward sagging cerebellum also compresses the dorsal brainstem (Fig. 3). Tectal beaking is also seen (Fig. 1).



3 Sagittal T2w image shows that the cerebellar tonsils herniate into the posterior cervical canal and the downward sagging cerebellum compresses the dorsal brainstem.



4 Lateral radiograph of the skull shows the classic finding of a lacunar skull.

No spinal cord anomalies were identified. A lateral radiograph of the skull (on a prior presentation), when ventriculoperitoneal shunt was placed, shows the classic finding of a lacunar skull, or *luckenschadel* (Fig. 4).

Discussion

Chiari II malformations can lead to varying degrees of lower extremity paralysis or neurological manifestations. There are numerous associated findings with Chiari II, which involve the posterior fossa, the supratentorium, and the infratentorium.

Posterior fossa findings:

The findings noted in the posterior fossa involve herniation of the cerebellar tonsils, medulla, vermis, and even the fourth ventricle downward through the foramen magnum; in addition, these structures may push superiorly against the falx ('towering cerebellum') and anteriorly towards the brainstem. The malpositioning can cause obstruction of the fourth ventricle, leading to obstructive hydrocephalus.

Supratentorial findings:

Apart from hydrocephalus, there are numerous other supratentorial findings. As in the sample case, the falx may be fenestrated accompanied by interhemispheric gyral interdigitation. Hypoplasia of the corpus callosum can be seen, in which the corpus may either be partially or completely absent. Other findings include colpocephaly (disproportionately large posterior horns of the lateral ventricles), downward pointing of the lateral ventricles, squaring off of the frontal horns of the lateral ventricles, and a fused and enlarged massa intermedia.

Infratentorial findings:

The anterior shifting of the posterior fossa contents can cause inferior shifting of the pons and medulla and an often kinked appearance of the medulla and tectal beaking. In the spine, syringomyelia, a tethered cord with a lumbosacral myelocele or a myelomeningocele can be seen. Unlike the sample case, Chiari II malformations are nearly always associated with myelomeningoceles.

Osseous findings:

Besides lacunar skull, other osseous findings may be present, including a concave clivus, petrous ridge alterations, gaping foramen magnum, and low-lying transverse sinuses.

Treatment:

Treatment is surgical and includes decompression of the defect by resection of the posterior foramen magnum and C1 ring. In addition intraventricular shunts are able to divert cerebrospinal fluid (CSF) flow appropriately. Fetal surgery is also an option in select patients.

Contact

Raghuram K. Rao, MD, MPH
University of Texas – Medical Branch
Galveston, TX
USA
rkrao@utmb.edu

Optimized Examination Technique Reduces Examination Time for Children with Retinoblastoma by Half

Anton S. Quinsten, RT; Sebastian Blex, RT; Nicola Keiper, RT; Sophia L. Goericke, MD

University Hospital Essen, Diagnostic and Interventional Radiology and Neuroradiology, Essen, Germany

Introduction

Retinoblastoma is the most common (intraocular) eye tumor of childhood with an incidence of approx. one affected child per 18,000 live births. If the tumor is detected and treated at an early stage, more than 95% of patients will survive [1]. Tumors that are present in one eye only are referred to as unilateral retinoblastoma. Approx. 2/3 to 3/4 of affected children experience unilateral retinoblastoma [3]. When the tumors are present in both eyes, they are referred to as bilateral retinoblastoma. Because most patients are children, the examination usually has to be performed under general anesthesia. The most common symptoms include leukocoria, strabismus, glaucoma and loss of vision. In 30% of cases both eyes are affected. The diagnosis is usually made on the basis of a clinical examination, ophthalmoscopy and ultrasound. Magnetic resonance imaging* (MRI) is the procedure of choice for visualizing the local ophthalmic findings, the extent of the tumor and possible associated brain changes,

which is essential for treatment planning. An MRI examination of retinoblastoma poses a major challenge even for the most experienced examiner. Suspected retinoblastoma requires far more than a standard examination of the orbita. Producing high resolution images with optimized sequences and MR hardware is crucial for treatment planning and ultimately for its success. As Technologists we play a significant role in this process.

Examination

Apart from examining the orbits, the brain also needs to be visualized. The MRI examination can provide information on whether there is extraocular tumor growth and/or whether there is a tumor of the bones or brain tissue. Because the patients are children, the examination is performed mostly under general anesthesia, and special care is required before, during and after the examination. Since in a third of cases both orbits are affected, it is advisable to examine both eyes. Previously we used to examine each

eye separately. This used to take about two hours. Now with the new technique the whole examination including both orbits takes approximately 57 minutes. In the following we would like to explain our examination technique, now used routinely, which allows the brain and both eyes to be simultaneously visualized at high resolution in a considerably shorter examination time.

*MR scanning has not been established as safe for imaging fetuses and infants under two years of age. The responsible physician must evaluate the benefit of the MRI examination in comparison to other imaging procedures.

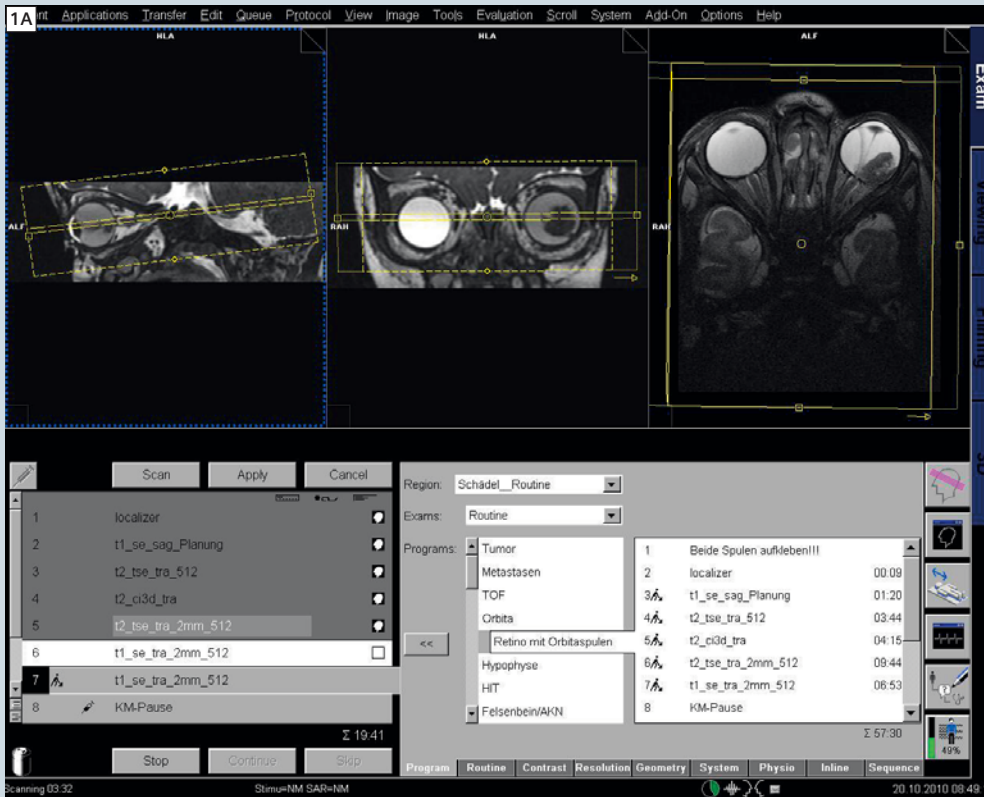
References

- 1 <http://www.uk-essen.de/augenlinik/retinoblastom.html>
- 2 <http://www.onmeda.de/krankheiten/retinoblastom-definition-1779-2.html>
- 3 <http://www.uk-essen.de/augenlinik/retinoblastom.html>
- 4 http://www.kinderkrebsinfo.de/e9031/e10591/e77086/e63970/index_ger.html
- 5 http://www.krebsgesellschaft.de/pat_ka_retinoblastom_definition,108207.html
- 6 <http://www.dr-gumpert.de/html/retinoblastom.html>

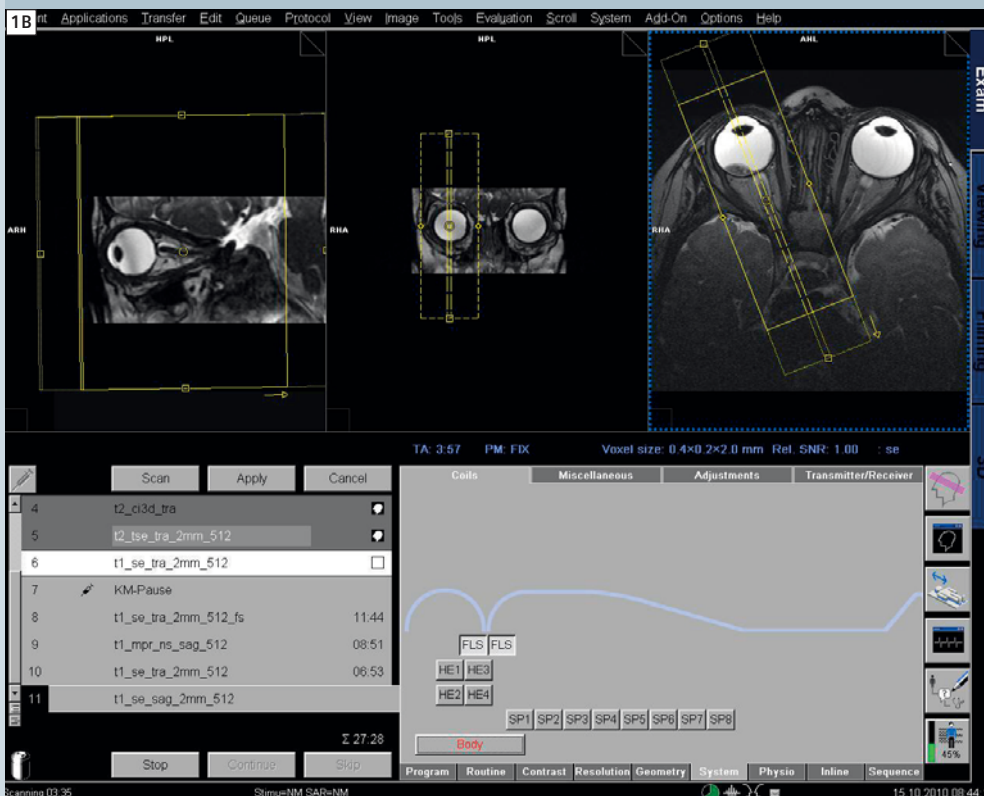
Examination protocol

Sequence	Slice orientation	TR	TE	Slice thickness	FOV	Base resolution	Phase resolution	iPAT	Acquisition time min:sec
Localizer									
T2 TSE complete skull	transverse	5220	106	4 mm	200	512	50	none	03:44
CISS both eyes head coil	transverse	10,54	5,27	0.7 mm	190	256	100	none	04:15
T1 SE both eyes orbit coil	transverse	668	16	2 mm	109	512	50%	none	06:53
T2 TSE both eyes orbit coil	transverse	6020	153	2 mm	109	512	50%	none	09:44
T1 SE FS both eyes orbit coil	transverse	568	16	2 mm	109	512	50	none	11:44
T1 SE both eyes orbit coil	transverse	668	16	2 mm	109	512	50	none	06:53
MPRAGE	sagittal	2070	3,52	1 mm	195	384	75	2	08:51
If nec. with tumors close to papillae T1 SE	sagittal	569	23	2 mm	109	512	50	none	05:08
Total examination time									57:12

Examination planning



1A Axial planning.



1B Sagittal planning.

Technical details

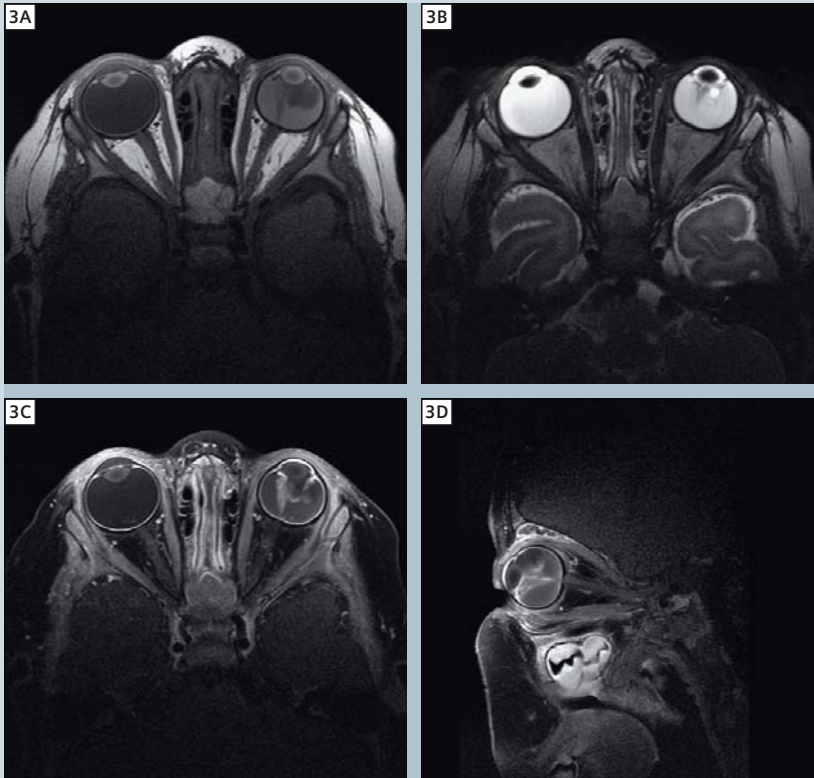
We use two small loop coils from Siemens Healthcare, Erlangen, and place these on the eyes. Both coils are attached securely and connected (Figs. 2B, C).



2 (A) MAGNETOM Aera at University Hospital Essen. (B, C) Patient positioning with 2 small loop coils.

Examination results

Unilateral retinoblastoma



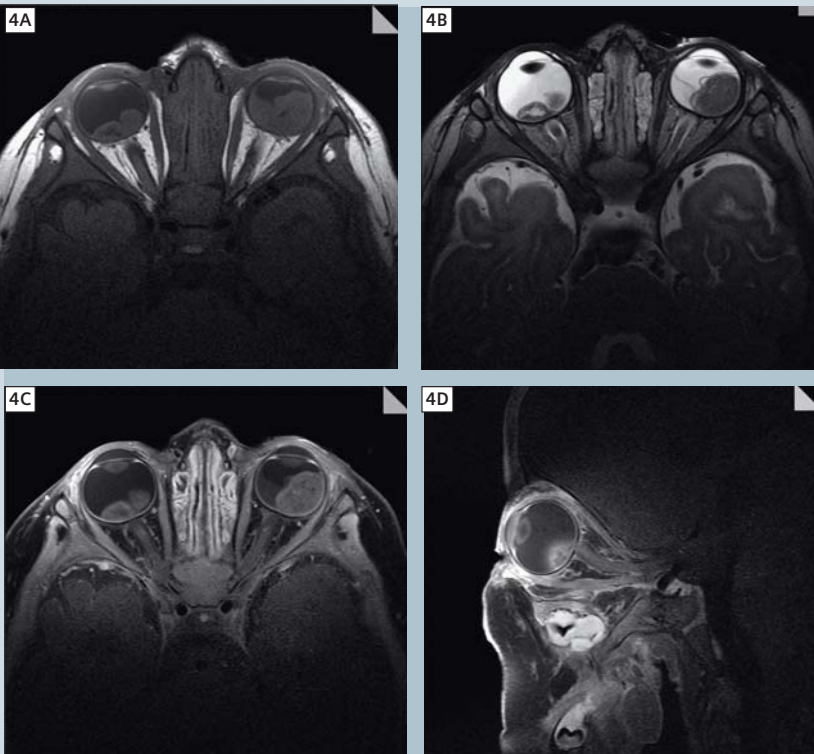
3A Transversal T1-weighted SpinEcho (SE), 2 mm, native.

3B Transversal T2-weighted Turbo SpinEcho (TSE), 2 mm.

3C Transversal T1-weighted SE, 2 mm, post contrast, fatsat.

3D Sagittal T1-weighted SE, 2 mm, post contrast, fatsat.

Bilateral retinoblastoma



4A Transversal T1-weighted SE, 2 mm, native.

4B Transversal T2-weighted TSE, 2 mm.

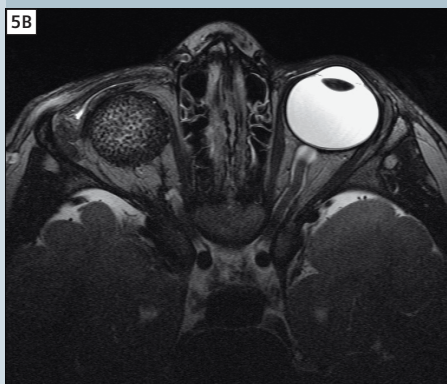
4C Transversal T1-weighted SE, 2 mm, post contrast, fatsat.

4D Sagittal T1-weighted SE, 2 mm, post contrast, fatsat.

Following right-side enucleation.



5A Transversal T1-weighted SE, 2 mm, native.



5B Transversal T2-weighted TSE, 2 mm.



5C Transversal T1-weighted SE, 2 mm, post contrast, fatsat.

Conclusion

In summary, high resolution images can be obtained using two loop coils connected in parallel and a small field-of-view of approximately 100 mm. This is crucial for a confident diagnosis of extraocular tumor growth as well as the assessment of tumor growth, spread of the cancer and whether other anatomical structures have been affected. As both eyes are examined at the same time, examination time can be shortened by half, thus greatly reducing the time the patient is under general anesthesia.

Contact

Anton S. Quinsten
 Essen University Hospital
 Institute for Diagnostic
 and Interventional Radiology
 and Neuroradiology
 Hufelandstrasse 55
 45122 Essen
 Germany
 Phone: +49-201-723-84506
 anton.quinsten@uk-essen.de

Case Report: MRI of the Lung in a Young Child with Abscess Pneumonia Caused by H1N1 Infection

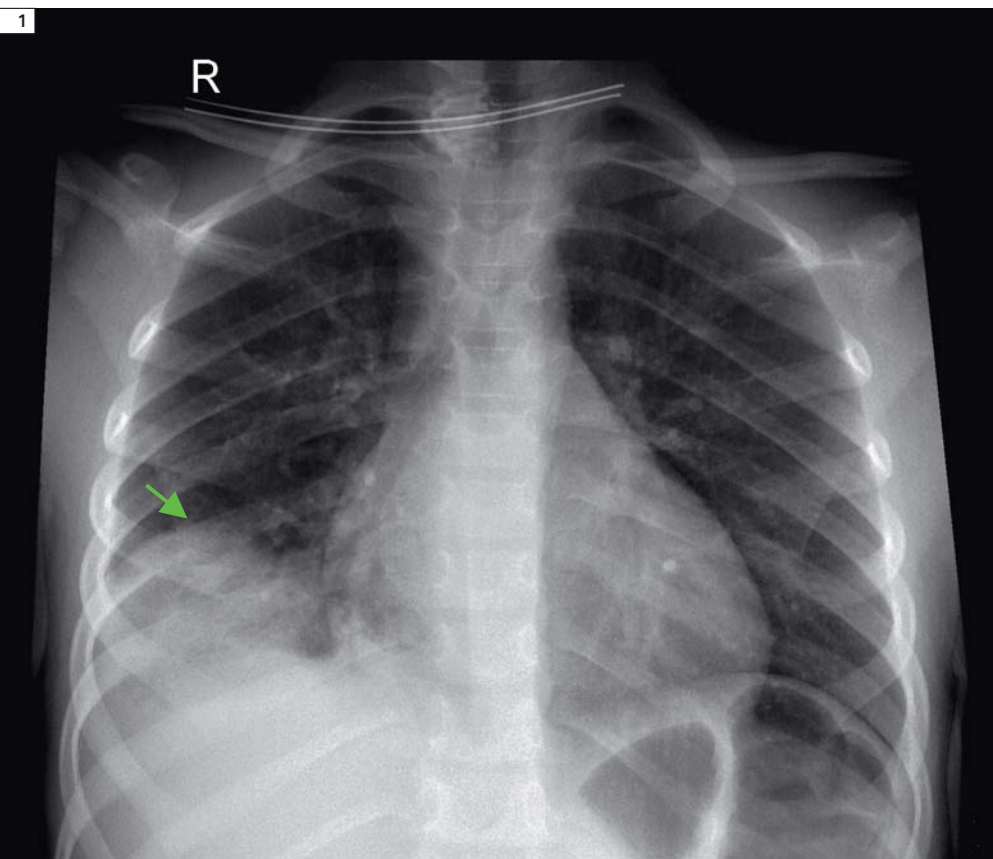
Migle Sumkauskaitė¹; Jens-Peter Schenk, PD²; Olaf Sommerburg, PD³; Michael Puderbach, MD^{1,4}; H.-P.Schlemmer, MD, PD¹; Monika Eichinger, MD¹

¹ German Cancer Research Center (DKFZ), Dept. of Radiology, Heidelberg, Germany

² University Hospital Heidelberg, Div. of Pediatric Radiology, Dept. of Diagnostic and Interventional Radiology, Heidelberg, Germany

³ University Hospital Heidelberg, Div. of Pediatric Pulmonology and Cystic Fibrosis Center, Dept. of Pediatrics III, Heidelberg, Germany

⁴ Chest Clinic Heidelberg, Dept. of Diagnostic and Interventional Radiology, Heidelberg, Germany



1 Chest-X-ray at admission: homogenous opacification of the right lower lung field and obscured costo-diaphragmatic angle (arrow).

Introduction

Influenza is an infectious disease caused by RNA viruses of the family Orthomyxoviridae [1]. The most common symptoms of the infection are: fever, rhinorrhoea, sore throat, cough, muscle pain, frontal/retro-orbital headache, weakness/fatigue [1–3]. Pneumonia is a common complication of influenza in young children. [1]. We present a case of abscess pneumonia caused by H1N1 infection in a young child and discuss the MRI findings of the lungs during the course of the disease.

Patient history

A 5-year-old girl with a history of rhinitis, cough and fever over a period of 2–3 weeks, with proven H1N1 infection but unsuccessfully treated with antibiotics was admitted to our hospital because of progressive dyspnoea and fever of 39.7°C. A chest radiograph showed a consolidation of the right lower lung field (Fig. 1).

Laboratory tests demonstrated nonspecific findings of systemic inflammatory illness:

CRP of 203.9 mg/l (normal < 5 mg/l), erythrocyte count 4.0 /pl (normal 3.9–5.3/pl), haemoglobin 10.8 g/dl (normal 11–14.5 g/dl),

leukocyte 12.34/nl (normal 4.5–13.0/nl). Therapy with Cefuroxim and Oseltamivir was started. Under treatment the girl's clinical situation worsened and lung abscess was suspected following ultrasound examination of the chest. Cross sectional imaging was therefore requested and MRI examination of the thorax was performed.

Imaging findings

MRI evaluation of the thorax demonstrated right lower and middle lobe consolidation with multiple abscesses (Figs. 2A–C), enlarged mediastinal lymph nodes and small bilateral pleural effusion (Figs. 2A, B).

Treatment with Meropenem and Clindamycin was started immediately, the latter being replaced by Vancmycin four days later. A follow-up MRI examination was performed after two weeks. MRI showed progression of the pleural effusion on the right side, unchanged

right lower and middle lobe consolidation as well as left lower lobe bronchial wall thickening (Fig. 3).

During the following few days the pleural effusion was drained and the antibiotic treatment was changed to Tazobactam and Clindamycin.

A second follow-up MRI after further two weeks demonstrated a decrease of pleural effusion and of infiltrates in the right lower lobe with residual dystelectasis. However, a progress of the infiltration in the left lower lobe (Figs. 4A–C) and basal perfusion defects on the right side, as well as dorso-basal defects on the left side (Fig. 4D), were seen.

After clinical restitution a final follow-up MRI was performed 4 months later showing a small dystelectasis in the right lower lobe and pleural thickening as sequelae of the consolidation and abscess pneumonia (Figs. 5A, B) and normal homogenous perfusion of the whole lung (Fig. 5C).

Sequence details

The T2-weighted *syngo* BLADE sequence parameters were:

TR 3994 ms, TE 116 ms, FA 146°, slice thickness 4 mm, with navigation triggering.

The T2-weighted HASTE sequence parameters were:

TR 571 ms, TE 42 ms, FA 160°, slice thickness 6 mm, patient adapted field-of-view, with respiratory gating (approximately 90 s).

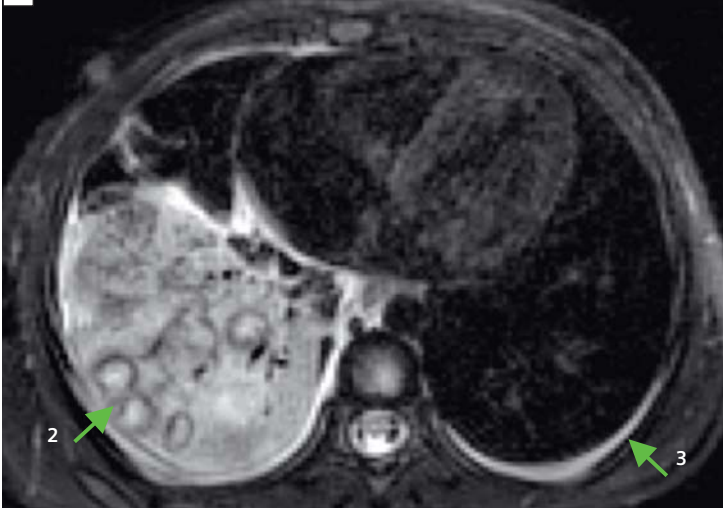
The T1-weighted VIBE sequence parameters were:

TR 5.46 ms, TE 2.38 ms, FA 18°, slice thickness 4 mm, with inspiratory breathhold.

In non-compliant patients or smaller* children, a T1-TSE-sequence can be performed within 3 acquisitions in free breathing with TR 775 ms, TE 17 ms, FA 160°.

Table 1: Sequence parameters

Sequence	Technique	Respiratory phase	TR (ms)	TE (ms)	Flip angle (°)
BLADE	T2-weighted	navigation triggering	3994	116	146
HASTE	T2-weighted single-shot sequence	respiratory gating	571	42	160
VIBE	T1-weighted 3D gradient echo	inspiratory breath hold	5.46	2.38	18



2 First MRI: axial T2-weighted HASTE (**2A**), *syngo* BLADE (**2B**) and T1-weighted VIBE image post contrast (**2C**) showing abscess pneumonia of the right lower lobe. Areas of a homogenous increase in T2w signal (consolidation) in the right lower lobe (1) and multiple inclusions of in T2w hyper and in T1w hypo intense areas with circular peripheral contrast media enhancement (abscesses, 2) are demonstrated. Additionally a small bilateral pleural effusion is visualized (3).

Discussion

In clinical practice, as a widely available imaging modality, chest x-ray is essential for primary diagnoses of lung diseases. Actually CT is considered to be the “gold standard” for the assessment of lung parenchyma and the majority of lung pathology. However, repeated examinations to evaluate the progress of the disease are frequently necessary in severe illness. This leads especially in small children to cumulative radiation doses, which can be avoided if radiation-free imaging modalities are used.

Magnetic resonance imaging (MRI) as a radiation-free technique was already proposed as a potential alternative for lung imaging in the late 80s [4]. At that time, MRI technology was not able to produce results comparable to CT [5]. New technologies and strategies were able to overcome the inherent difficulties of MRI of the lung [6]. With the introduction of parallel imaging in clinical practice, faster image acquisition became possible and thus substantial improvement in temporal and/or spatial resolution [7–9]. MRI has a lower spatial resolution than CT, but its major advantage is the possibility to characterize different aspects of tissue based on different contrasts in T1w and T2w, as well as enhancement after contrast media administration. Additionally, MRI is able to visualize different regional functional aspects of the lung parenchyma (pulmonary hemodynamics, perfusion, ventilation).

Today, lung MRI is considered a sensitive detector of infiltrative and solid lung pathology. It is therefore the ideal follow-up assessment of pneumonia, pleural disease or chronic lung patients with pulmonary exacerbations. In children with cystic fibrosis it is more and more used as a monitoring strategy for lung disease progression [10].

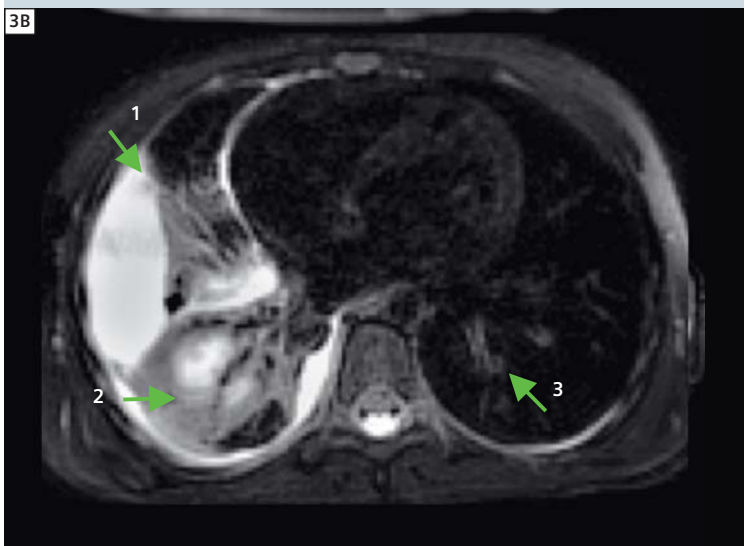
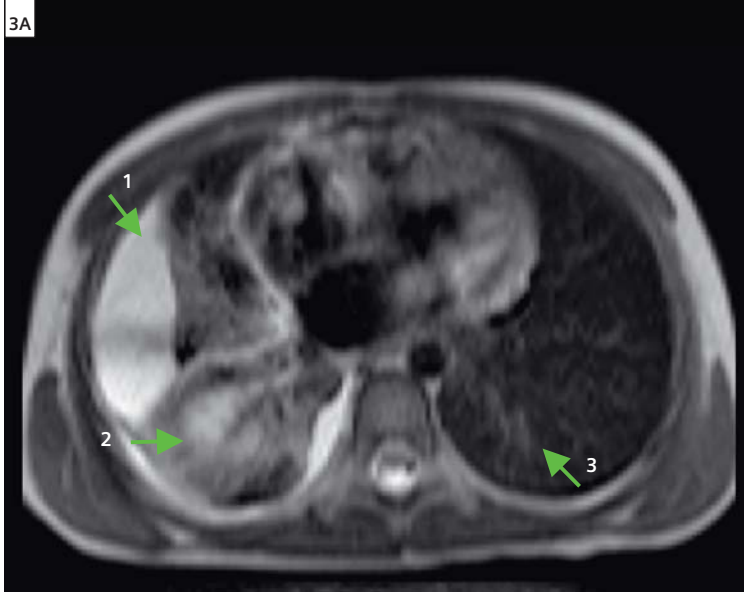
In this report we present a child with a severe abscess pneumonia caused by H1N1 virus infection. In addition to the areas of consolidation, abscesses were found in the right lower lobe accompanied by bilateral pleural effusion. For assessment of lung parenchyma, T2-weighted images as well as

T1-weighted images before and after contrast media injection are performed. T1-weighted sequences pre- and post-contrast are used for the detection of lymph nodes especially in the mediastinum and tumor infiltration into the thorax wall. T2-weighted sequences are nowadays the method of choice for the assessment of lung parenchyma, and additionally enable visualization of the pathology of mediastinum and thoracic wall.

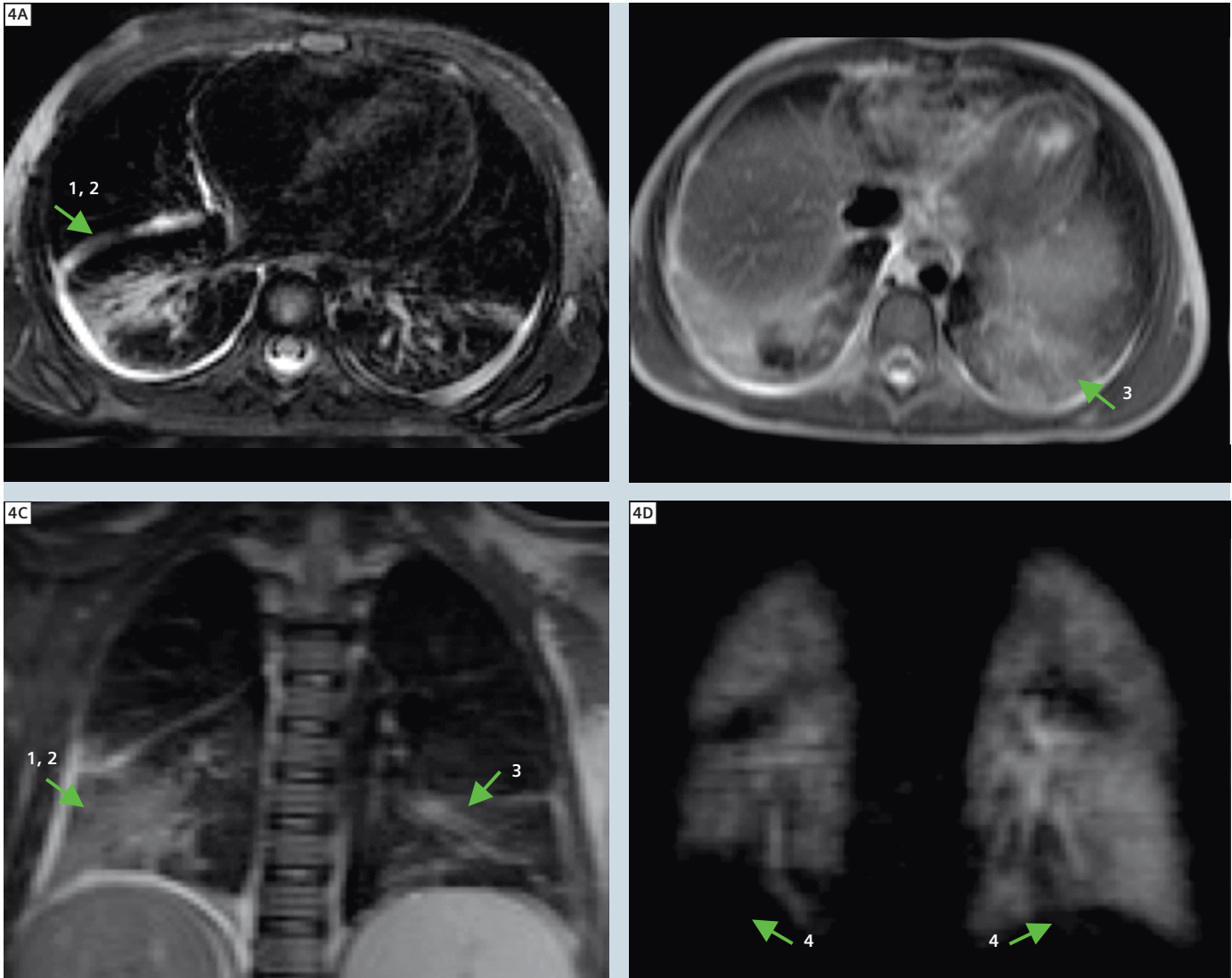
Ex vivo experiments and in vivo experience have shown that solid lung pathology can be successfully detected with fast T1-weighted gradient echo sequences (T1-GRE). For lung nodules larger than 4–5 mm, 3D gradient echo sequences reach the detection rates of conventional helical CT with a single row detector technique [11]. The T2-weighted ‘Half-Fourier single-shot turbo spin-echo’ (HASTE) sequence has a sensitivity of 85%–90% for lung nodules larger than 4 mm and a sensitivity of 100% for lung lesions larger than 8 mm [12, 13]. Post-contrast imaging is necessary for differentiation of pleural processes, such as empyema, abscesses or metastatic spread of malign tumors, as well as for the evaluation of solid intraparenchymal benign/malign tumor masses [12].

In airways disease the reflex of hypoxic vasoconstriction leads to impaired perfusion in less ventilated lung areas. To detect lung perfusion defects, an injection of contrast media at the same time that a repeated 3D GRE sequence with high temporal resolution is acquiring MRI data is necessary.

In the presented case, MRI examinations were performed on a 1.5 Tesla MR scanner (MAGNETOM Avanto, Siemens Erlangen, Germany). Orientated on a previously published standard protocol for lung image examination [11], a navigator triggered T2w BLADE and T2w HASTE sequence as well as a T1w VIBE sequence pre- and post-contrast media in inspiratory breath hold were used. For functional assessment a 3D GRE sequence with high temporal resolution with parallel contrast media injection was performed.



3 First follow-up MRI: axial T2-weighted HASTE (3A), syngo BLADE (3B) and T1-weighted VIBE image post contrast (3C): progressive pleural effusion on the right side (1) and unchanged right lower lobe consolidation with abscesses (2). Bronchial wall thickening is visible in the left lower lobe (3).



4 Second follow-up MRI: axial T2-weighted syngo BLADE (**4A**) as well as axial and coronal HASTE (**4B**, **4C**) show a partial resolution of infiltration and pleural effusion in the right lower lobe (1, 2) but a new infiltrate in the left lower lobe (3). Subtraction image of MR perfusion from a dorsal slice (**4D**) show basal right sided and dorso-basal left-sided perfusion defects (4) corresponding to the areas of consolidation.

Perfusion imaging was performed using a time-resolved 3D GRE pulse sequence with TR 1.8 ms, TE 0.68 ms, FA 18°. With this sequence an image data set of the whole lung was acquired within 1.2 seconds. A total of 25 data sets were acquired continuously from the start of an intravenous injection of 0.1 mmol/kg body weight of Gadopentetat (Magnevist, Bayer Vital, Leverkusen, Germany) at a rate of 3 ml/s. Image data were post-processed for image assessment by subtraction of the baseline images without contrast from those with maximal con-

trast. Parallel imaging modalities with PAT 2 were used for all images. The presented case shows that the detection of lung pathology and its development during the course of a severe illness can be achieved with MRI. A combination of T1w and T2w sequences together with functional imaging provides relevant information and is able to guide therapeutic decisions. In-room time for a patient receiving this protocol takes about 20–30 minutes. Considering the highly-relevant information acquired without ionizing radiation,

this seems acceptable for clinicians. Moreover, repeated examination can be performed without compromising the patient, which is important particularly in children for follow-up examination. In conclusion, MRI of the lung should be considered for the assessment of parenchymal lung changes and especially if radiation safety aspects are of major interest.

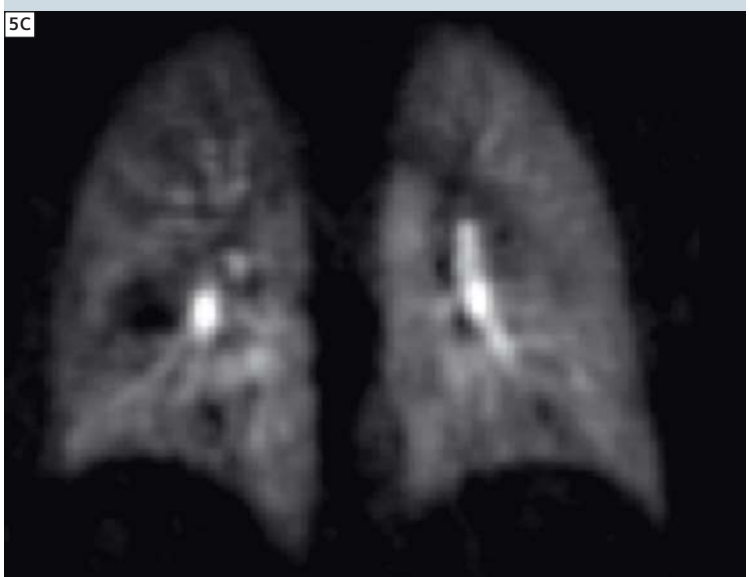
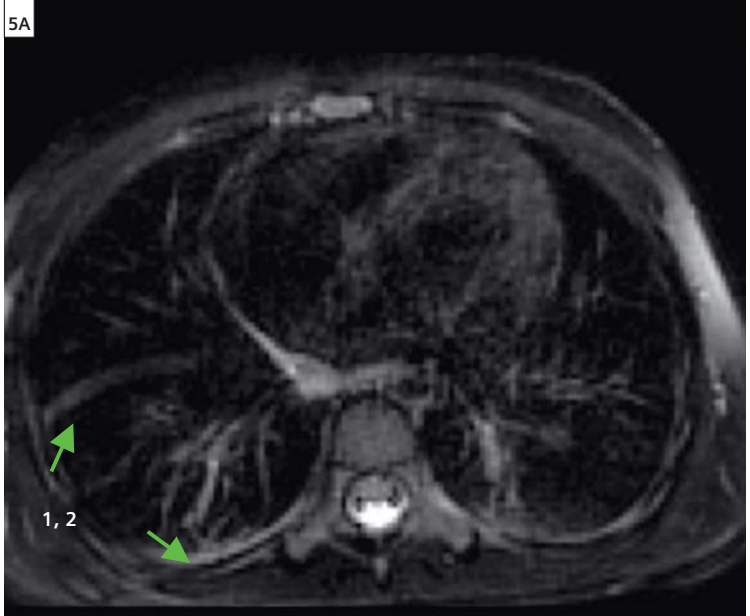
References

- 1 Delaney JW, Fowler RA. 2009 influenza A (H1N1): a clinical review. *Hosp Pract (Minneapolis)*. 2010;38(2):74–81.
- 2 Smith SM, Gums JG. Antivirals for influenza: strategies for use in pediatrics. *Paediatr Drugs*. 2010 Oct 1;12(5):285–99.
- 3 Nelson Textbook of Pediatrics Elsevier 18th edition 2011, editors: Robert M. Kliegman, MD, Richard E. Behrman, MD, Hal B. Jenson, MD and Bonita M.D. Stanton, MD.
- 4 Fiel SB, Friedman AC, Caroline DF et al. Magnetic resonance imaging in young adults with cystic fibrosis. *Chest*. 1987;91:181–184.
- 5 Carr DH, Oades P, Trotman-Dickenson B et al. Magnetic resonance scanning in cystic fibrosis: comparison with computed tomography. *Clin Radiol*. 1995;50:84–89.
- 6 Kauczor HU, Heussel CP, Schreiber WG et al. [New developments in MRI of the thorax]. *Radiologe*. 2001;41:279–287.
- 7 Swift AJ, Woodhouse N, Fischele S et al. Rapid lung volumetry using ultrafast dynamic magnetic resonance imaging during forced vital capacity maneuver: correlation with spirometry. *Invest Radiol*. 2007;42:37–41.
- 8 Heidemann RM, Griswold MA, Kiefer B et al. Resolution enhancement in lung 1H imaging using parallel imaging methods. *Magn Reson Med*. 2003;49:391–394.
- 9 Fink C, Bock M, Puderbach M et al. Partially parallel three-dimensional magnetic resonance imaging for the assessment of lung perfusion-initial results. *Invest Radiol*. 2003;38:482–488.
- 10 M. Puderbach, M. Eichinger, J. Haeselbarth, A. Niemann, M. Mall, H.-U. Kauczor Magnetic Resonance Imaging (MRI) for early diagnosis of lung changes in Children with Cystic Fibrosis *AJRCCM*, 2008;177:773, Abstract issue.
- 11 Puderbach M, Hintze C, Ley S, Eichinger M, Kauczor H-U, Biederer J. MR imaging of the chest: A practical approach at 1,5 T. *Eur J of Radiology*, 2007: 64: 345–355.
- 12 MRI of the lung, Springer-Verlag Berlin Heidelberg, 1st edition 2009, editor: Kauczor H.-U.
- 13 Biederer J, Hintze C, Fabel M MRI of pulmonary nodules: technique and diagnostic value. *Cancer Imaging*, 2008: 8(1): 125–130.

*MR scanning has not been established as safe for imaging fetuses and infants under two years of age. The responsible physician must evaluate the benefit of the MRI examination in comparison to other imaging procedures.

Contact

Monika Eichinger, MD
 Department of Radiology, E010
 German Cancer Research Center
 Im Neuenheimer Feld 280
 69120 Heidelberg
 Germany
 Phone: +49 6221 422498
 m.eichinger@dkfz-heidelberg.de



5 MRI after clinical restitution: T2-weighted axial syngo BLADE image (5A) and T2-weighted axial HASTE image (5B) demonstrate the residual infiltrates in the right lower lobe with dysatelectasis (1) and pleural thickening (2). Subtraction image of MR perfusion from a dorsal slice shows homogenous perfusion (5C).

Case Report: Virtual MR Bronchoscopy in the Fetus*

Heron Werner^{1,4}; Pedro Daltro^{1,4}; Thomas M. Doring^{1,2,4}; Marcio Bernardes^{1,2}; Jorge R. Lopes dos Santos³; Ricardo Fontes³; Simone Belmonte²; Romeu Cortes Domingues^{1,2}

¹*Clínica de Diagnóstico por Imagem (CDPI, DASA), Rio de Janeiro, Brazil*

²*Clínica Multiimagem (MI, DASA), Rio de Janeiro, Brazil*

³*Instituto Nacional de Tecnologia (INT), Rio de Janeiro, Brazil*

⁴*Department of Radiology, Universidade Federal do Rio de Janeiro (UFRJ), Rio de Janeiro, Brazil*

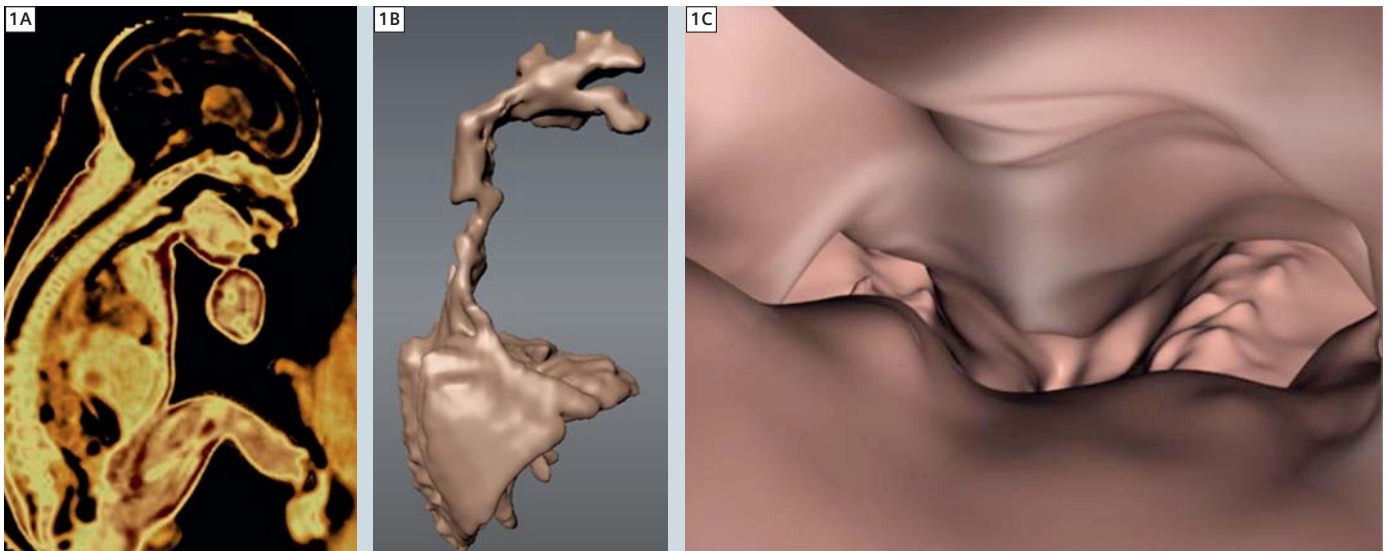
Objective

To show magnetic resonance imaging (MRI) with virtual bronchoscopy (VB) in the evaluation of fetal airway patency.

Introduction

'Virtual bronchoscopy' is a technique that involves the creation and evaluation of representations of the bronchial tree and surrounding structures using spatial information derived from imaging modalities other than the bronchoscope itself [1]. Initially, these two-dimen-

sional and later three-dimensional (3D) bronchial tree representations were generated from computed tomography images. However, VB can now also be performed using data from MRI. There are several software programs available to help generate accurate and realistic



1 Post-processing sequence TrueFISP 3D (1A), a volume rendering (thin VRT) thickness of 1.8 mm. 3D view of the lungs with airway paths (sagittal view, 1B) and virtual bronchoscopic image of normal carina and mainstem bronchi (1C).

*MR scanning has not been established as safe for imaging fetuses and infants under two years of age. The responsible physician must evaluate the benefits of the MRI examination compared to other imaging procedures.

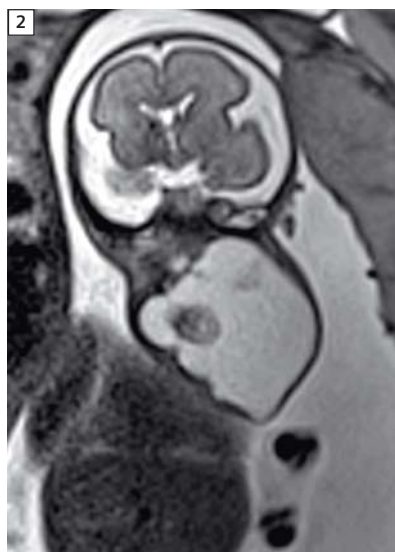
renderings of the bronchial tree [3, 4]. MR images are a prerequisite to obtain good quality images of the airway paths of the fetus. MRI is used to generate a 3D model of the airway; in most cases volume rendering techniques (VRT) are used and do also allow interactive fly through e.g. for intervention planning. In addition, VB based on MRI provides additional information about anatomy beyond the airway wall is important for therapy planning e.g. surgery. The development of imaging technology has led to vast improvements in fetal evaluation. The primary method of fetal assessment is the ultrasound examination because it is effective, patient-friendly, cost-efficient and considered to have no collateral effects [2]. When ultrasound cannot provide sufficiently high-quality images or further (functional) information is required, MRI is

used. Its high-resolution with excellent contrast fetal imaging allows visualization of internal tissues to be realized [5]. In this article we describe how VB was performed in both a normal fetus that underwent MRI at 28 weeks gestation due to placenta previa with suspicion of placenta accreta, and also in a 37 week fetus with cervical teratoma.

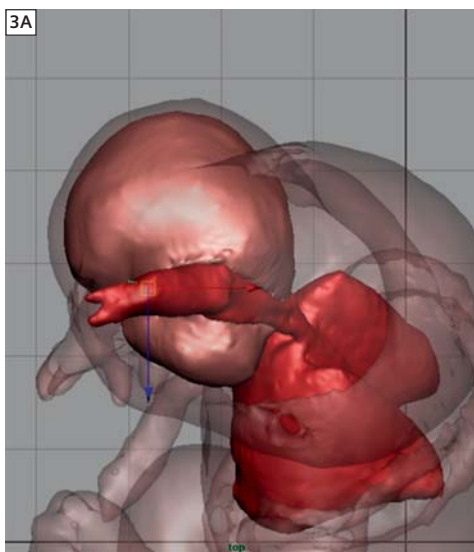
Methods

MRI examination was performed using a 1.5T scanner (MAGNETOM Avanto, Siemens Healthcare, Erlangen, Germany). The protocol involved a T2-weighted single shot Turbo Spin Echo sequence in the three planes of the fetal body (HASTE; shortest repetition time (TR); echo time (TE) 140 ms; field-of-view 300–200 mm; matrix 256×256; slice thickness 4 mm; acquisition time 17 s; 40 slices). In addition, we applied a

3D T2-weighted balanced steady state sequence (TrueFISP) in the sagittal plane (TRUFI; TR 3.02 ms; TE 1.34 ms; voxel size 1.6×1.6×1.6 mm³; flip angle 70°; parallel acquisition PAT factor 2; acquisition time, 0.26 s). The entire examination time was less than 20 minutes. The 3D MRI datasets were reconstructed to produce an interactive surface model of the fetal respiratory tract that could be viewed from any angle. First, a 3D model of the fetal airway was created from the overlapping image layers generated by MRI using the Mimics software (Materialise, Leuven, Belgium), which allowed the surface of the airway to be delineated using contrast detection in the relevant areas of interest. The 3D model thereby generated was exported using the standard triangular language file format and then converted into an OBJ file using the MAYA 3D modeling



2 T2-weighted sequence (coronal view) of the fetus (28 weeks) with teratoma.



3 (3A) 3D reconstruction showing the teratoma and its relationship to the upper airway, trachea and lung as well as virtual fly-through (3B).



4 3D view of the fetus obtained by TrueFISP 3D.

software (Autodesk, San Rafael, CA, USA) [6, 7]. This program allows the virtual positioning of observation cameras while working with multiple on-screen windows. Since the development of the 3D model, the software has allowed the user to determine the best positioned viewpoints for visualization of the 3D model and also facilitated the adjustment of lighting parameters to improve contrast resolution. Using the navigation mode it is also possible to perform virtual bronchoscopy to visualize the upper respiratory tract from the pharynx downwards through the tracheobronchial tree with a quality similar to that obtainable by videotaped bronchoscopy.

Results

There were two main outcomes: the possibility of creating 3D virtual airway paths from fetuses with cervical tumors, and the carrying out of VB based on those images.

After delivery of the child and based on VB, a complete resection of the teratoma was conducted.

Conclusion

It was demonstrated that MRI data can be used to create a 3D model of the respiratory tract in a normal and abnormal fetus. We believe that this technique could become a useful tool for the assessment of fetal airway patency.

References

- 1 Ferguson JS, McLennan G. Virtual bronchoscopy. *Proc Am Thorac Soc.* 2005; 2: 488–491.
- 2 Frates M, Kumar AJ, Benson CB, Ward VL, Tempany CM. Fetal anomalies: comparison of MR imaging and US for diagnosis. *Radiology* 2004; 232: 398–404.
- 3 Lam WW, Tam PKH, Chan FL, Chan K, Cheng W. Esophageal atresia and tracheal stenosis: Use of three-dimensional CT and virtual bronchoscopy in neonates, infants, and children. *AJR* 2000; 174: 1009–1012.
- 4 Merritt SA, Gibbs JD, Yu KC, Patel V, Rai L, Cornish DC, Bascom R, Higgin WE. Image-guided bronchoscopy for peripheral lung lesions. *Chest* 2008; 134: 1017–1026.
- 5 Prayer D, Brugger PC, Prayer L. Fetal MRI: techniques and protocols. *Pediatr Radiol* 2004; 34: 685–693.
- 6 Werner H, Dos Santos JRL; Fontes R, Daltro P, Gasparetto E, Marchiori E, Campbell S. Virtual bronchoscopy in the fetus. *Ultrasound Obstet Gynecol* 2011; 37: 113–115.
- 7 Werner H, Dos Santos JRL; Fontes R, Daltro P, Gasparetto E, Marchiori E, Campbell S. Additive manufacturing models of fetuses built from three-dimensional ultrasound, magnetic resonance imaging and computed tomography scan data. *Ultrasound Obstet Gynecol* 2010; 36: 355–361.

Contact

Heron Werner
Clínica de Diagnóstico
por Imagem (CDPI, DASA)
Rio de Janeiro
Brazil
heron.werner@gmail.com

Expert Talks

Don't miss the talks of experienced and renowned experts covering a broad range of MRI imaging



Dynamic 3D MRA – Clinical Concepts (syngo TWIST)

Jörg Barkhausen, M.D.
University Hospital, Essen



Clinical Applications of Arterial Spine Labeling (syngo ASL)

John A. Detre, M.D.
University of Pennsylvania



Clinical Applications of Diffusion-Tensor Imaging (syngo DTI)

Tammie L. S. Benzinger, M.D., Ph.D.
Washington University School of Medicine



Breast Cancer Management – Cross Modality Approach

John F. Nelson, M.D.
Battlefield Imaging



MRI in Sports Medicine

John A. Carrino, M.D., M.P.H.
Johns Hopkins University, School of Medicine

Visit us at

www.siemens.com/magnetom-world

Go to

Education > e-trainings & Presentations

Pediatric Congenital Heart MR Imaging at 3T and 1.5T Systems

Pamela K. Woodard, MD¹; Agus Priatna, Ph.D.²; Scott Love, BS, RT¹; Gary McNeal, M.S.²; Patrick Broderick, MD³; Joseph Billadello, MD.⁴; Constantine Raptis, MD¹; Gautam Singh, MD³

¹Mallinckrodt Institute of Radiology, Washington University School of Medicine, St Louis, Missouri, USA

²R&D Collaborations, Siemens Healthcare, USA

³Division of Cardiology, St. Louis Children's Hospital, Washington University School of Medicine, St. Louis, Missouri, USA

⁴Cardiovascular Division, Barnes-Jewish Hospital, Washington University School of Medicine, St. Louis, Missouri, USA

Introduction

The performance of pediatric MR imaging comes with a set of requirements over and above MR imaging in the adult patient. A good anesthesia team is necessary for infants* and toddlers, and conscious sedation may be required for the 5–7 year old. Gadolinium based contrast volumes are small and, while power injectors may be used in toddlers and older

children, contrast injection in infants often must be done by hand through small-gauge intravenous catheters. Cardiac MR imaging adds complexity with its respiratory motion suppression and cardiac gating requirements in a patient population often unable to breath-hold and with fast heart rates. While cardiac MR is performed in children for

assessment of a number of entities, including cardiomyopathy and myocarditis assessment, the most common indication is assessment of congenital heart disease. Congenital heart disease imaging adds cardiac anatomy ambiguity to the already complex patient. Cardiac MR imaging in these patients often requires on-the fly alteration in scan plane set

Table 1: Example pediatric imaging protocols for 1.5T and 3T cardiac MR scanning.

1.5T	3.0T
TrueFISP localizers	TrueFISP localizers
HASTE axial and coronal stacks thru chest	HASTE axial and coronal stacks thru chest
TrueFISP axial stack thru chest	TrueFISP axial stack thru chest
TrueFISP cine vertical long axis single image	TurboFLASH cine vertical long axis single image
TrueFISP cine horizontal long axis stack	TurboFLASH cine horizontal long axis stack
TrueFISP cine short axis stack	TurboFLASH cine short axis stack
TrueFISP LVOT image	TurboFLASH LVOT image
TrueFISP radial hi-res cine aortic valve	TurboFLASH aortic valve
TrueFISP sagittal through main PA	TurboFLASH sagittal through main PA
FLASH-cine phase contrast across aortic and pulmonic valves, for flow quantification	FLASH-cine phase contrast across aortic and pulmonic valves, for flow quantification
TWIST dynamic contrast enhanced MRA in selected plane, use half dose (0.05 mmol/kg) high relaxivity agent such as MultiHance	TWIST dynamic contrast enhanced MRA in selected plane, use half dose (0.05 mmol/kg) high relaxivity agent such as MultiHance
PSIR delayed enhanced TrueFISP short axis stack; single LA image	PSIR delayed enhanced TurboFLASH short axis stack; single LA image

up to accommodate anomalous cardiac axes for functional imaging and across great vessels for flow quantification.

Methods

When performing cardiac MR imaging in children regardless of the indication, consideration must be given to respiratory motion suppression and cardiac gating. While older children can breathhold and have heart rates similar to those of adults, imaging of infants and younger children requires sequence modification to adapt to free-breathing and higher heart rates.

Respiratory motion suppression

Static bright and black blood sequences: Respiratory motion suppression can be performed using several methods other than breathhold, depending upon the cardiac sequence. Static steady state free precession (TrueFISP) bright blood sequences as well as black-blood half Fourier single shot turbo-spin echo (HASTE) can be performed as single shot techniques, with all lines of k-space acquired in a single heartbeat. TrueFISP techniques with inversion recovery can also be performed for delayed contrast enhanced imaging using single shot acquisition of k-space. While disadvantages include lower spatial resolution, single shot sequences, because of their fast acquisition, are relatively insensitive to both respiratory motion and arrhythmias or variations in heart rate.

Cine sequences:

Bright blood cine steady state free precession (TrueFISP) or gradient recalled echo (TurboFLASH) sequences can be performed at multiple (usually 3) averages to reduce respiratory motion artifact. Alternatively, non-triggered real-time TrueFISP cines may be performed, with the R-wave providing time-stamp information for ventricular size and function parameter calculation. While real-time techniques are quick and useful for functional parameter calculation, a disadvantage is their low resolution making them a poor option for simultaneous anatomy assessment.

TrueFISP coronary/anatomy assessment: Bright blood TrueFISP volumetric imaging of the coronaries and cardiovascular anatomy can be performed without added intravenous contrast agent using navigators for respiratory motion suppression. These navigators, which are set up to monitor diaphragmatic motion and to acquire data in end expiration, are ideal for children who often have regular respiratory patterns and are sedated.

Cardiac gating

EKG-gating for cardiac MR in children can often be easier than EKG-gating for adults. While it is true that some children with cardiomyopathies and congenital heart disease have arrhythmias, they are less likely to have the irregular heart rate of atrial fibrillation so common in older adults. Their fast heart rates, in general, tend to shorten the MR acquisition and, therefore, the overall examination time. Difficulties arise when the heart rates are too fast to permit adequate T2-weighting, (such as with T2-weighted Turbo Spin Echo sequences) or are too short to permit adequate recovery of the inversion recovery pulse used to null the myocardium in post contrast sequences [1]. In these cases, the acquisition can be set to occur over multiple heartbeats to maintain adequate T2-weighting or to permit adequate recovery of the inversion recovery pulse. Arrhythmias can be addressed with single shot techniques in static data acquisition as described above or through real-time cine data acquisition, again with the caveat that for both, the spatial resolution will be relatively poor.

Suggested pediatric protocols for 3T MAGNETOM Trio, A Tim system, and 1.5T MAGNETOM Avanto

Standard 6-channel body array coils may be used for toddlers and older children. Infants may require placement in a head coil.

The principal difference between the protocols as optimized for the 1.5T and 3T systems is the more frequent use of gradient recalled echo (TurboFLASH) sequences at 3T, particularly, in patients

with MR-compatible metallic implants in whom MR imaging is desired. While TrueFISP sequences can be performed at 3T, ideal conditions for TrueFISP imaging, such as high flip angle and short TR may not be met because of increased specific absorption rate (SAR) and frequency off-resonance effects. For instance, in order to keep the SAR within limits at 3T, the flip angle must be reduced for TrueFISP sequences [2]. This causes a drop in blood pool signal and decreases the contrast between the blood pool and myocardium. Consequently, while blood-pool/myocardial contrast-to-noise (CNR) with gradient recalled echo TurboFLASH sequences may be less than in TrueFISP imaging at 1.5T, TrueFISP CNR on 3T will be lower secondary to lower flip angle requirements secondary to SAR. In addition, increased sensitivity to flow-induced noise, known as the magneto-hydrodynamic effect, can interfere with EKG-gating at 3T. Adjusting frequency offsets on a slice orientation basis may decrease off-resonance effects, but increases overall study time. Thus, because of these limitations for TrueFISP imaging at 3T, TurboFLASH sequences are frequently substituted in pediatric cardiac MR imaging protocols.

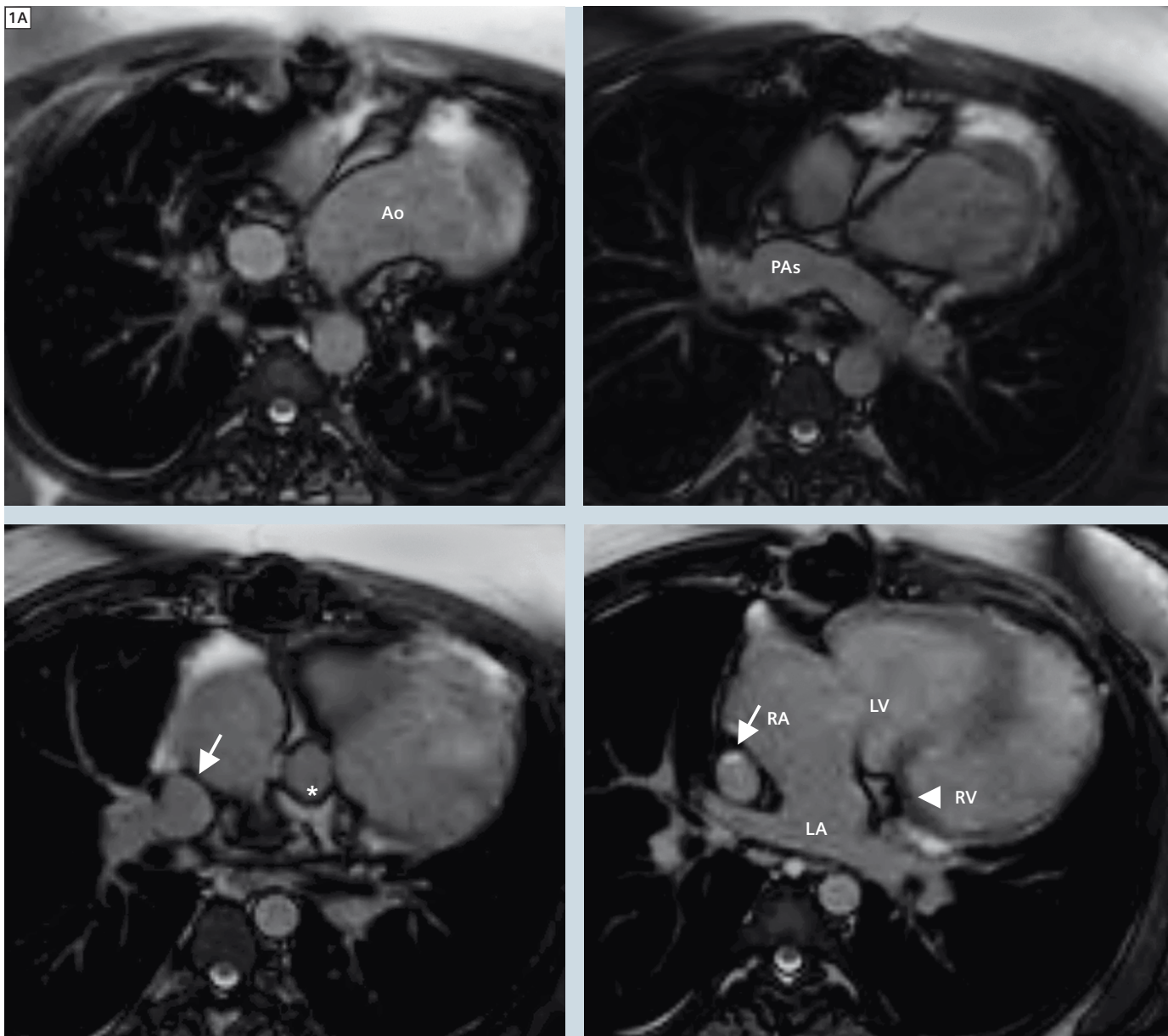
Conversely, contrast-enhanced MR angiography usually performs well at 3T. The time-resolved MR angiography sequence, *syngo* TWIST, can be very useful at both 3T and 1.5T for demonstrating the presence of intracardiac shunts, leaks across baffles, or conduits status post repair, using a relatively low gadolinium-based intravenous contrast dose [3]. Delayed contrast-enhanced MR imaging, in general, is used infrequently in congenital heart imaging, however, it may have utility in assessing patients followed post-operatively. Its presence may have predictive value in some patient populations, such as those patients status post Fontan, where enhancing ventricular fibrosis is associated with increased arrhythmias and downstream ventricular dysfunction [4].

Clinical cases

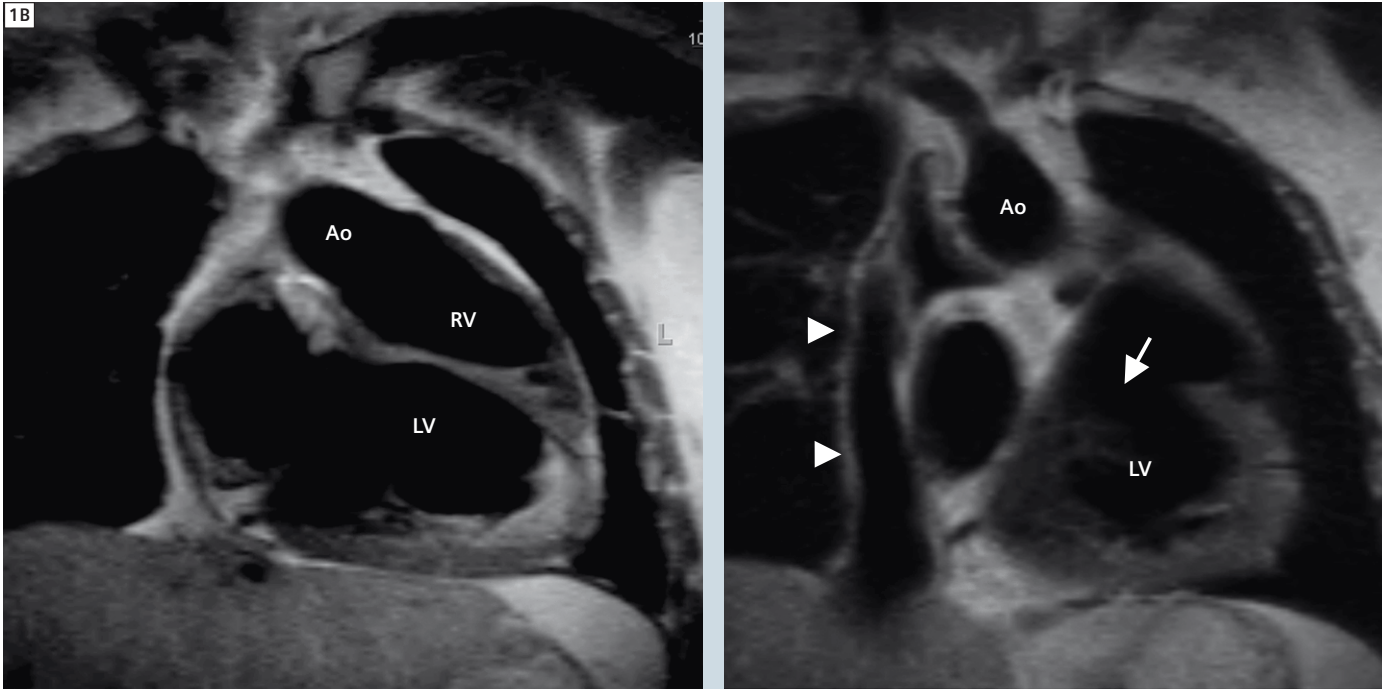
Cases were performed on either a 1.5T MAGNETOM Avanto or 3T MAGNETOM Trio, A Tim System MR system.

Patient 1 (1.5T MAGNETOM Avanto)

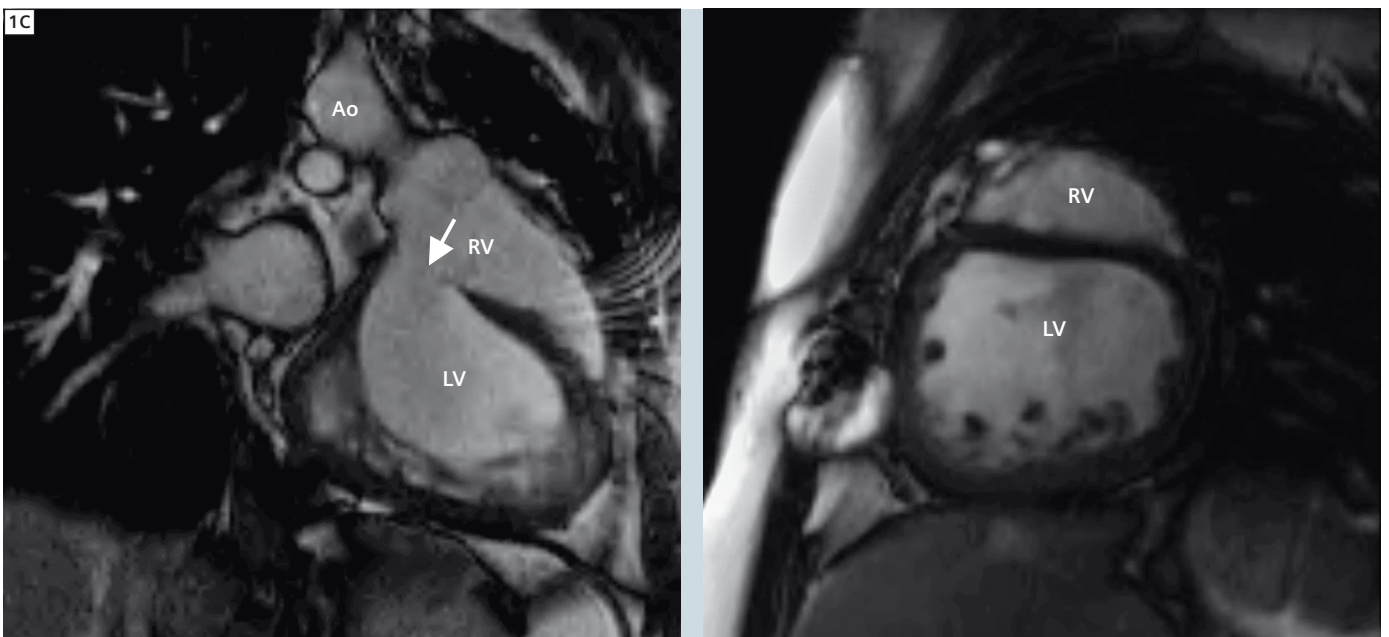
18-year-old patient with L-loop transposition of the great vessels and tricuspid atresia.



1A Static transverse TrueFISP images show aorta (Ao) arising from the right ventricle (RV). Note that the RV is posterior and that the left ventricle (LV) is anterior. Arrowhead points to the atretic tricuspid valve, which has been replaced by a fat bar. While the left atrium (LA) and right atrium (RA) remain in their anatomically correct locations, there is a large atrial septal defect (ASD) between them. The pulmonary arteries (PAs) are fed by a total cavopulmonary shunt/tunneled Fontan (arrow). Asterisk shows the small remnant pulmonic valve (PAs now disconnected). Transverse TrueFISP stack of images through the chest obtained prior to imaging along cardiac axes can be useful in defining orientation and configuration of great vessels.



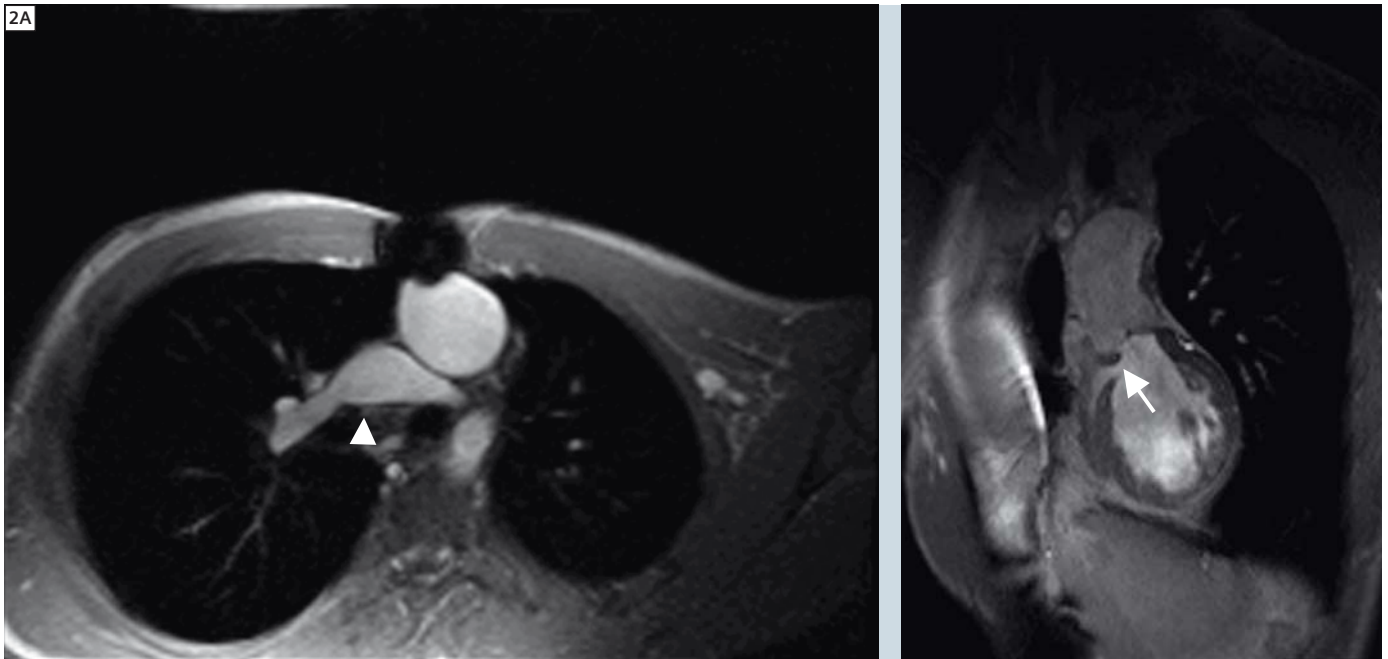
1B Coronal black-blood HASTE images show the typical 'piggyback' configuration of the ventricles with the smaller right ventricle situated superior to the dilated left ventricle. Arrow points to a large ventricular septal defect (VSD). Arrowheads point to the tunneled Fontan.



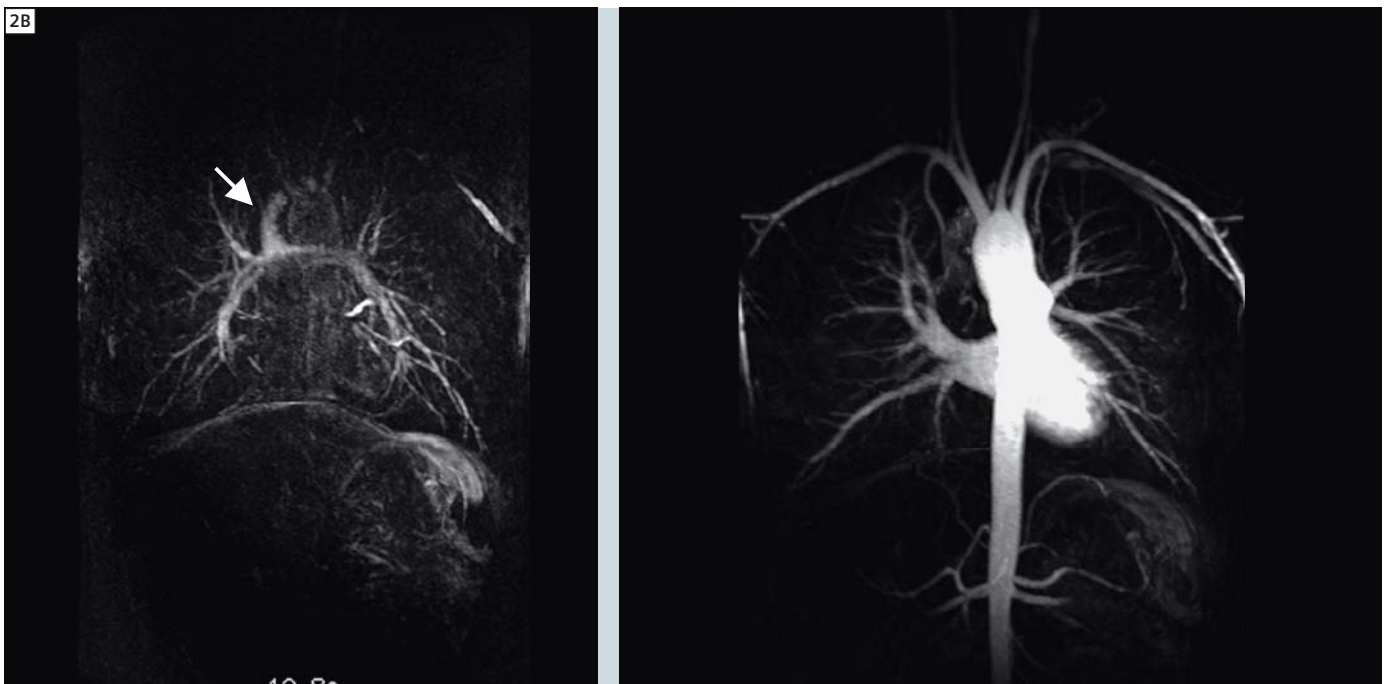
1C Single frames from long axis and short axis cine images again show smaller RV situated superior to the larger LV. Again, note the Ao arising from the RV, and the large VSD (arrow).

Patient 2 (3T MAGNETOM Trio, A Tim System)

18-year-old patient with tricuspid atresia and univentricular heart, status post tunneled Fontan.



2A TurboFLASH sequence shows D-loop transposition of the great vessels with the Ao arising anterior and to the left of the PA. Arrow points to a small VSD between the functionally single ventricle and tiny residual RV.



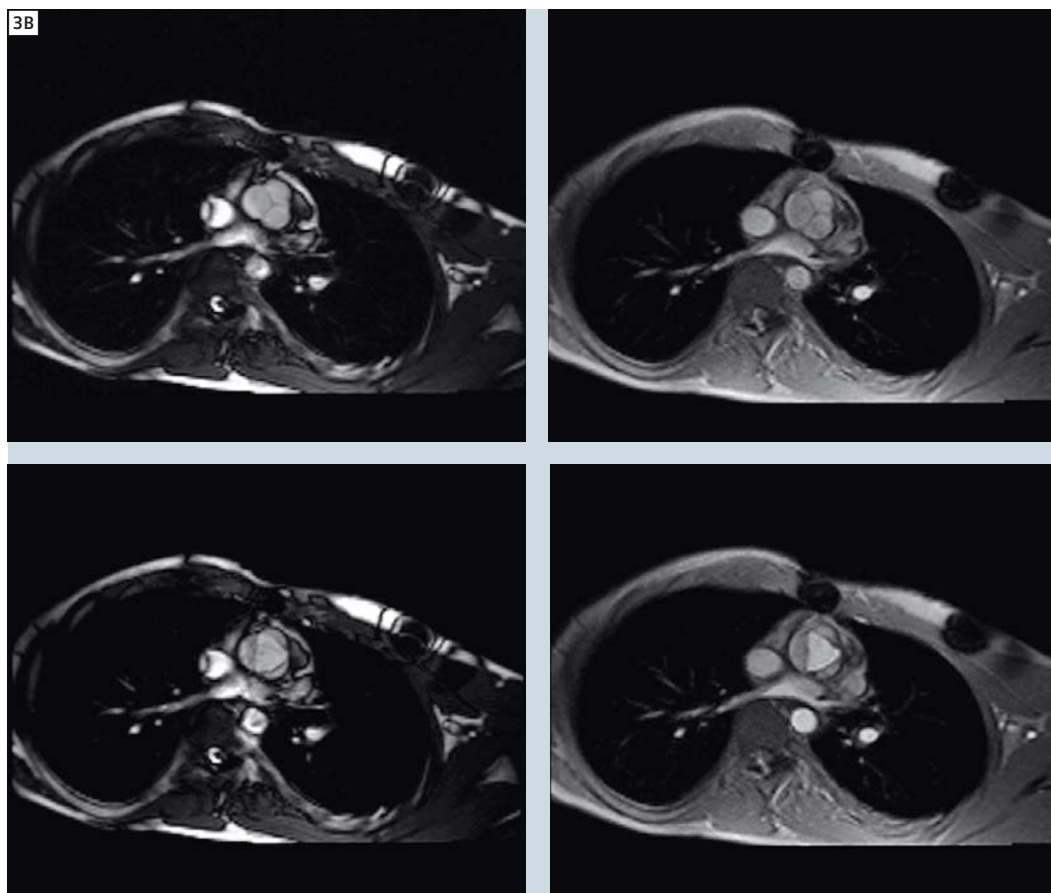
2B *syngo* TWIST time-resolved MR angiogram captures anatomy at various time points of enhancement. These images show the bidirectional Glenn shunt (arrow) feeding the pulmonary arteries (12.8 sec) and Norwood-enhanced Ao later in the contrast bolus (20.3 sec).

Patient 3 (3T MAGNETOM Trio, A Tim System)

19-year-old male patient with tricuspid atresia and normally related vessels, status post total cavo-pulmonary shunt/Fontan.



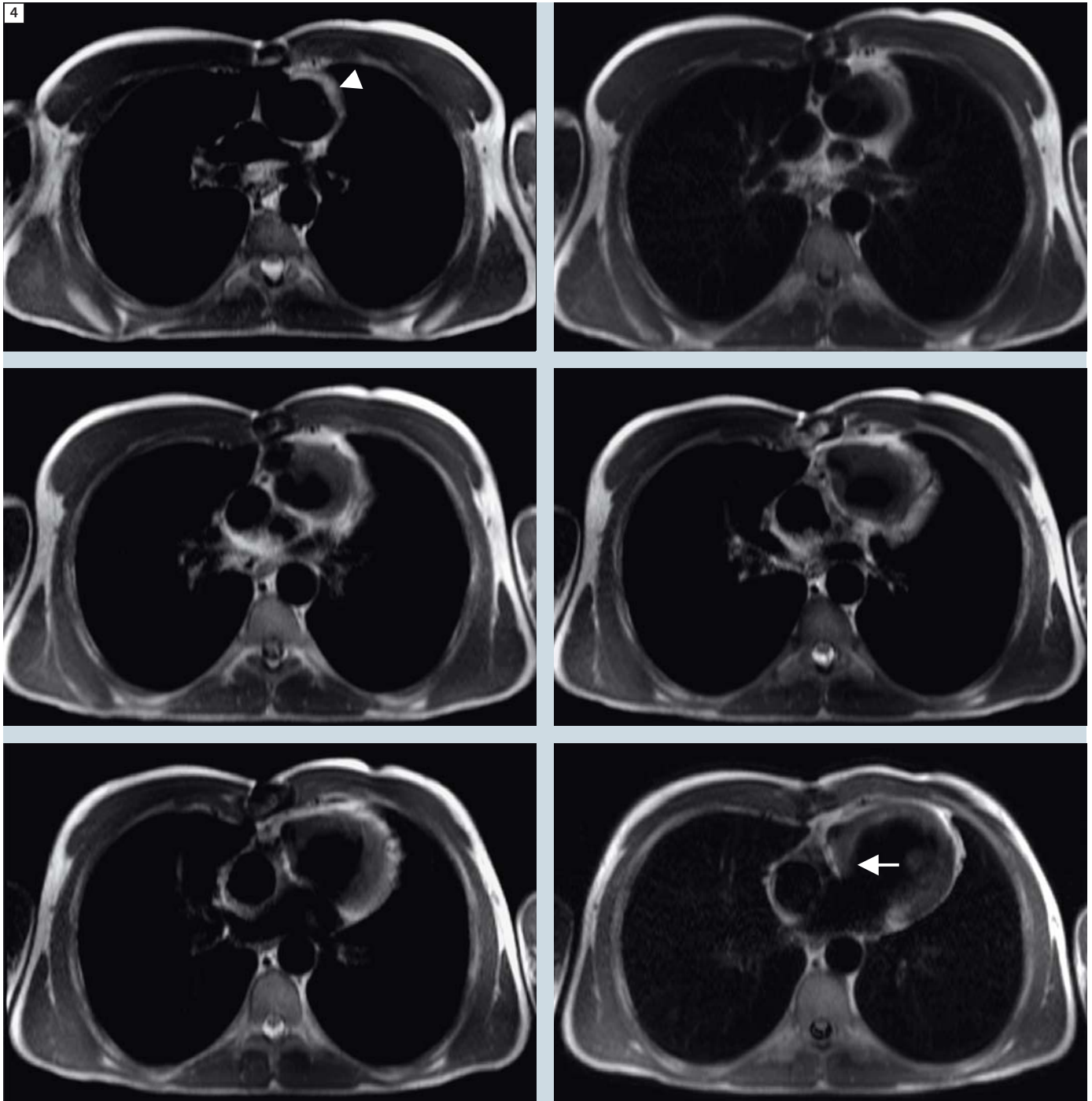
3A Coronal maximum intensity projection of the time resolved syngo TWIST acquisition showing Fontan (arrows).



3B Example of aortic valve acquired with TrueFISP (left) and TurboFLASH (right) sequences. Top row images are acquired at diastole and bottom row images at systole. As shown on these valve images, acquisitions with TurboFLASH sequences at 3T show better blood-tissue contrast and fewer artifacts. With valves this blood-tissue contrast is accentuated because of the time-of-flight (TOF) nature of TurboFLASH sequences not present in TrueFISP.

Patient 4 (3T MAGNETOM Trio, A Tim System)

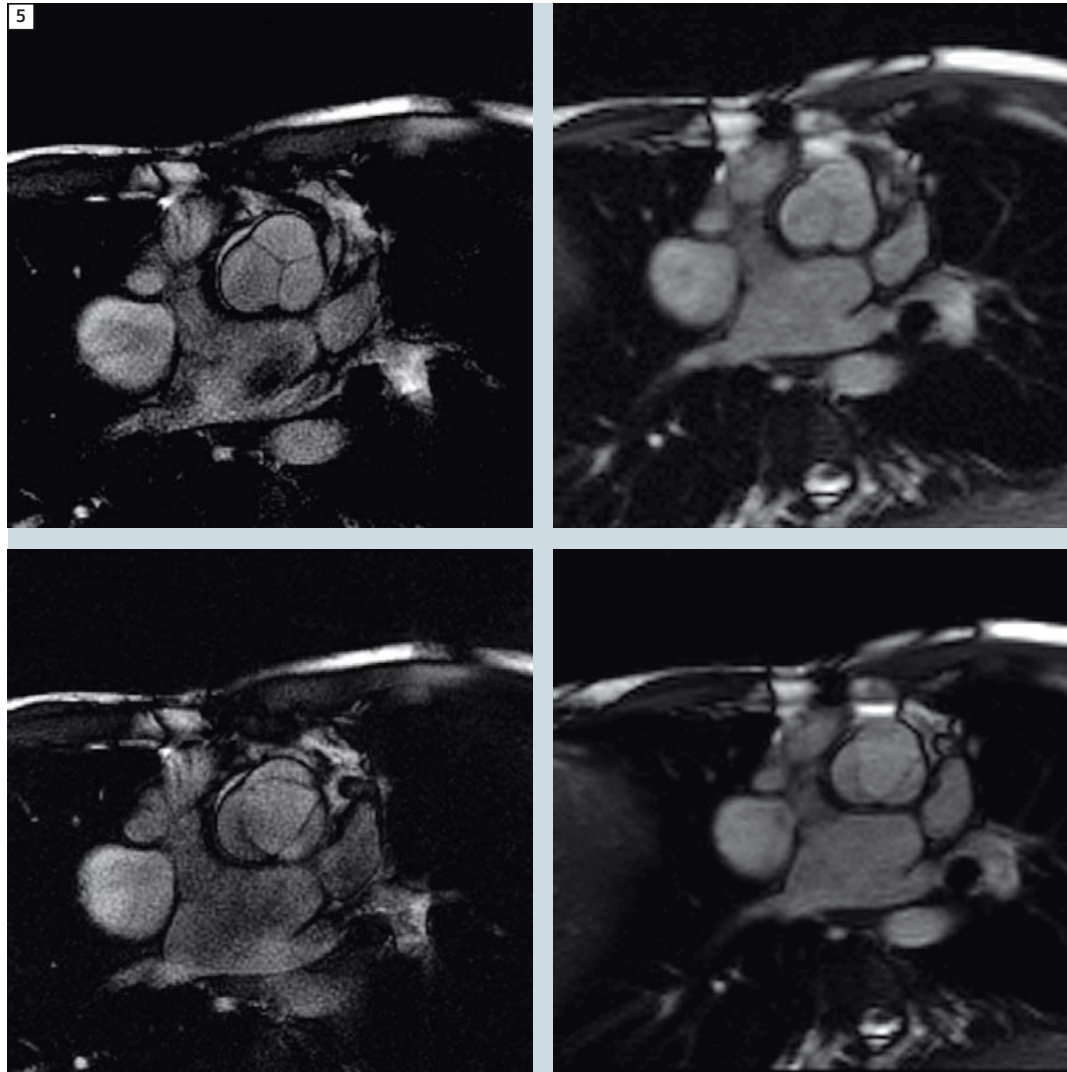
18-year-old male patient with D-loop transposition, tricuspid atresia and interrupted aortic arch, repaired with total cavopulmonary shunt/Fontan and Norwood/Damus-Kaye-Stansel procedure (widening of the Ao by joining it to the main PA).



4 Transverse black-blood HASTE images show functionally single ventricle with atresia of the tricuspid valve (arrow). Arrowhead points to the augmented ascending Ao. Asterisk is in total cavo-pulmonary shunt.

Patient 5 (1.5T MAGNETOM Avanto)

19-year-old male patient with D-transposition, tricuspid atresia and Fontan repair.



5 Aortic valve acquired with the TurboFLASH sequence (right) and radial TrueFISP cine sequence (left), shows how the radial high resolution cine sequence may be useful in obtaining good quality imaging of valves at 1.5T. Top row shows aortic valve in diastole and bottom row shows aortic valve in systole. This radial TrueFISP sequence is less useful at 3T imaging because of the artifact caused by magneto-hydrodynamic effects.

References

- 1 Bailliard F, Hughes ML, Taylor AM. Introduction to cardiac imaging in infants and children: Techniques, potential, and role in the imaging work-up of various cardiac malformations and pediatric heart conditions. *European Journal of Radiology* 68: 191-198, 2008.
- 2 Daga C, Ditchfield M. 3T MRI in paediatrics: Challenges and clinical application. *European Journal of Radiology* 68: 309-319, 2008.
- 3 Krishnam MS, Tomasian A, Lohan DG, Tran L, Finn JP, Ruehm SG. Low-dose, time-resolved, contrast-enhanced 3D MR angiography in cardiac and vascular diseases: correlation to high spatial resolution 3D contrast-enhanced MR. *Clinical Radiology* 63: 744-755, 2008.
- 4 Rathod RH, Prakash A, Powell AJ, Geva T. Myocardial fibrosis identified by cardiac magnetic resonance late gadolinium enhancement is associated with adverse ventricular mechanics and ventricular tachycardia late after Fontan operation. *J Am Coll Cardiol* 55: 1721-1728.

Contact

Professor Pamela K. Woodard, MD
Washington University
Mallinckrodt Institute of Radiology
510 S. Kingshighway Blvd.
St. Louis, MO, 63110-1076
Phone: 314-747-3878
woodardp@mir.wustl.edu

*MR scanning has not been established as safe for imaging fetuses and infants under two years of age. The responsible physician must evaluate the benefit of the MRI examination in comparison to other imaging procedures.

Case Report:

ASD (Ostium Secundum Defect)

Harnoor Singh, MD; Raghuram K. Rao, MD, MPH; Claudia C. Cotes, MD

University of Texas-Medical Branch, Galveston, TX, USA

Patient history

This is a 16-year-old female who presented to her primary care clinician with three episodes of dizziness upon standing. Her laboratory workup was unremarkable and her electrocardiogram showed a normal sinus rhythm with normal axis. Thereafter, she received an echocardiogram, which revealed a normal cardiac situs, normal four chamber intracardiac anatomy, a mildly hypoplastic right ventricular cavity, and tricuspid regurgitation. She then received a cardiac MRI for further workup.

Sequence details

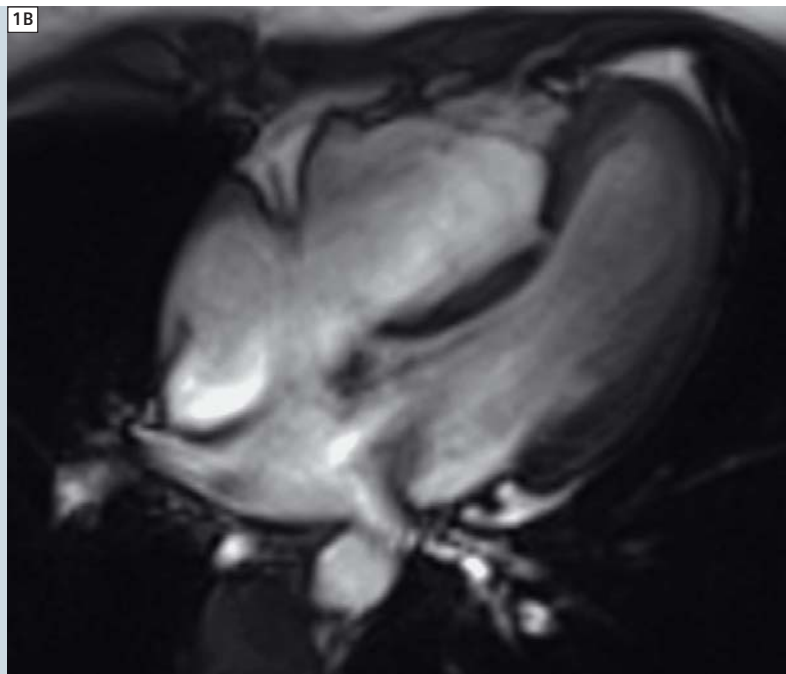
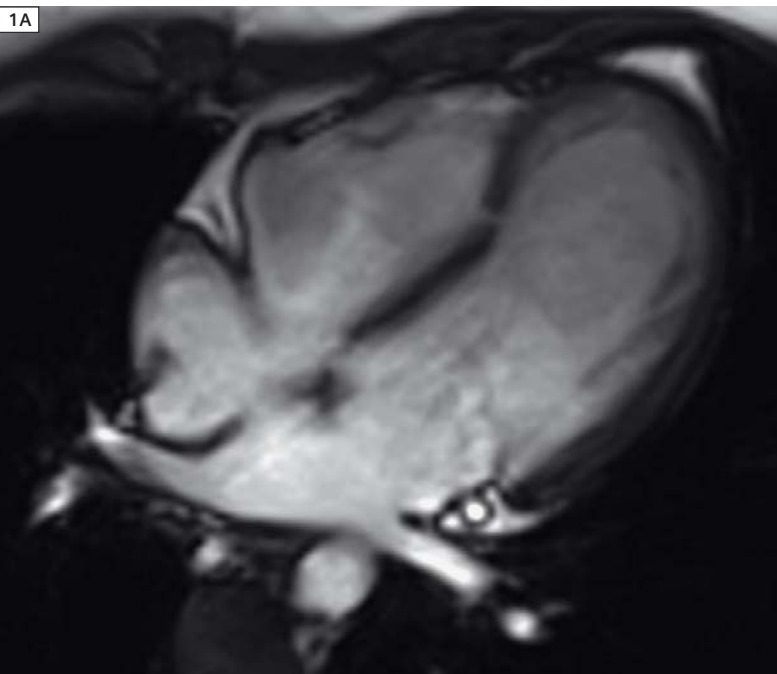
Images were obtained using a 3 Tesla MAGNETOM Verio (Siemens Healthcare, Germany) with a body flex coil anteriorly and the spine coil posteriorly. All four images were obtained under an axial cine TrueFISP Gradient Echo technique. Four chamber stacked short axis (PSIF) and HASTE images using iPAT (integrated parallel acquisition technique) were performed (TR 46 ms, TE 1.3 ms, slice thickness 8 mm, scan time 10 s).

Imaging limitation: A thin fossa ovalis can be confused with an ostium secundum atrial septal defect (ASD) on static

MR images. This can be avoided using cine MRI techniques, which demonstrate a flow void extending into the right atrium due to a left-to-right shunt from the ASD.

Imaging findings

Sequential MR images from the cine (Figs. 1A–D) illustrate a small defect in the mid-portion of the atrial septum, representing an ostium secundum defect. In addition, there is a separate small defect in the mid-portion of the muscular ventricular septum.



1 Cine TrueFISP images showing ostium secundum defect.

Discussion

ASD is the second most common congenital heart defect after ventricular septal defect (VSD), and the most common to become symptomatic in adulthood. Ostium secundum defects account for majority of the ASDs. Females are affected more often than males. ASDs can be associated with syndromes, which include Holt Oram Syndrome (in which an ASD is accompanied by upper extremity anomalies) and Trisomy 21. A majority of the children with Trisomy 21 have an ostium primum and atrioventricular septal defect. Common signs and symptoms include dyspnea, accentuation of right precordial thrust, systolic ejection murmur, and wide splitting of P2. Adults may develop pulmonary hypertension from unknown cases of ASD.

Radiology findings

Primary diagnosis is made by echocardiography in infants and children. Chest radiographs can show cardiomegaly. Often, an electrocardiogram can show right axis deviation. A cine MRI, has a sensitivity and specificity of over 90% in delineating septal defects, and can be particularly useful when other tests are inconclusive [1]. MRI is very useful for depiction of function, flow, and anatomy in older children.

Treatment

Spontaneous closure occurs in many children with secundum ASD. A transcatheter percutaneous closure device is the treatment of choice, if necessary. A primum ASD is not amenable to a closure device and patients are operated on at 3–5 years of age.

Surgical repair is done in the first year of life for symptomatic AV canal defects. Large defects may require a Dacron patch or suture closure.

Reference

- 1 Kafka H, Mohiaddin RH. Cardiac MRI and pulmonary MR angiography of sinus venosus defect and partial anomalous pulmonary venous connection in cause of right undiagnosed ventricular enlargement. *AJR Am J Roentgenol.* Jan 2009; 192(1):259-66.

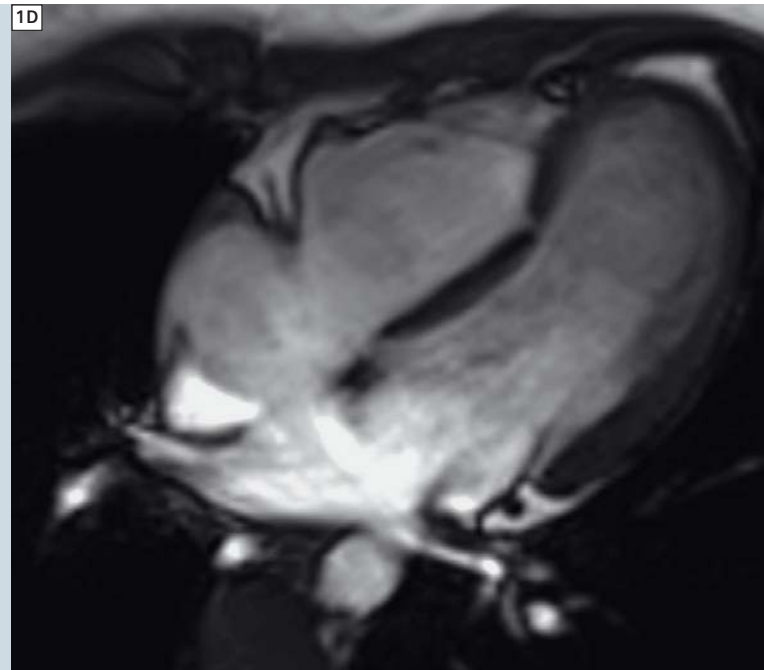
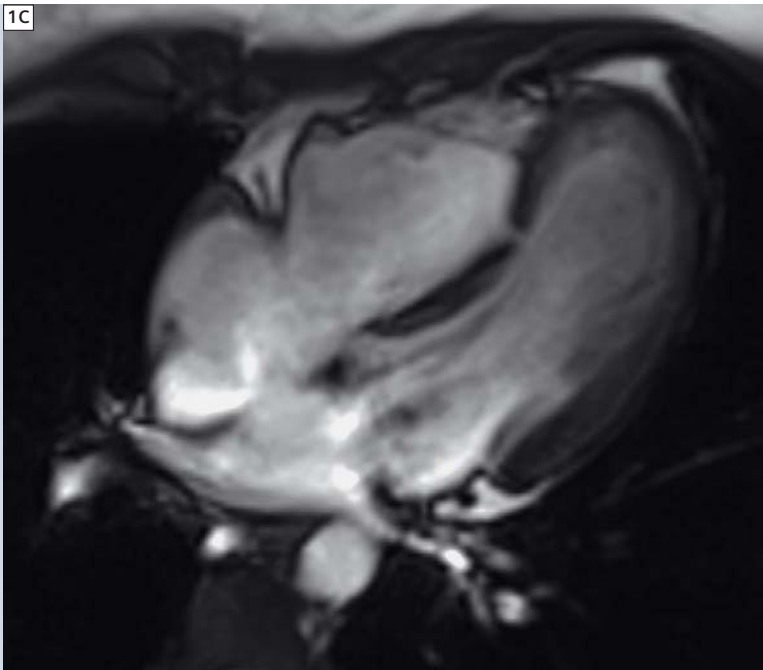
Contact

Harnoor Singh, MD
University of Texas-Medical Branch
Galveston, TX
USA
ha3singh@utmb.edu



MAGNETOM_World

The cine images for this case are available at our **MAGNETOM World internet page.**



Missing information?



To make sure you have all the information you need, register for our free monthly newsletter on clinical MRI information. Check out case reports from MAGNETOM users around the world and stay up-to-date with Siemens software applications.

Register at
www.siemens.com/magnetom-world
Go to
[Publications > Subscriptions](#)

Fetal Imaging: How I do it

Aaron J. Flammang, MBA, BS RT (R) (MR)

Siemens Corporate Research, Center for Applied Medical Imaging, Baltimore, MD, USA

Objective

The goal of this work is to serve as a guide for those interested in performing fetal MR imaging* (MRI). The proceeding is based entirely on current and past clinical experience. Although fetal MRI is not a new topic, many struggle to establish a program that can offer a comprehensive set of tools to diagnose disease of the fetus. It is well documented that in most cases fetal ultrasound can provide the clinical answer. In those cases in which results are less than conclusive, for reasons such as fetal position or beam limitations related to either equipment or maternal condition, fetal MRI has been shown to augment patient care.

Patient preparation

When considering fetal MRI, one must first give attention to the act of patient preparation. In this respect, patient refers to the mother. Providing clear and precise instructions prior to the examination is one of the best known ways to improve exam efficiency and effectiveness. You should give explicit instructions on breathholding (should there be any). Provide a brief introduction to the sounds generated by the machine and explain that the sounds occur because the scanner is acquiring images. Assure the mother that at all points during the study there will be a member of the imaging team (Medical Doctor or Technologist) in close contact via the communications equipment provided. Most importantly, explain the importance of

remaining motionless through the procedure. Bear in mind two things:

1. The mother will be lying supine or possibly in a decubitus position, which may be uncomfortable. Be sensitive to this.
2. There is a high likelihood that she or even others accompanying her will be nervous, as fetal MRI is not a commonly indicated study.

The protocol

To some, the protocol is the most daunting part of performing fetal MRI. Once you understand the needs of the physician and the various pathologies you wish to diagnose, it becomes quite simple to design an imaging protocol. Whether you perform breathholds for any part of the examination is really up to the individual facility. It is often found unnecessary, given today's fast imaging techniques. Most of these sequences lend themselves well to T2 contrast, which is of primary concern. Gross pathologies, particularly those of the neurologic system, are well displayed with such contrast. If your goal is to achieve T1-weighting, techniques like 3D VIBE, 2D FLASH and TurboFLASH can be employed with moderate breathholds (below 25 seconds). Typically, the focus of T1-weighted imaging is the fetal brain and largely to determine the presence of blood byproduct. The 2D techniques have the added benefit of physiologic triggering through the use of 2D PACE. The mainstay of any fetal MRI protocol is TrueFISP (True Free Induction with Steady State Precession) and HASTE (Half Fourier Single Shot Turbo Spin Echo). While TrueFISP contrast is derived from a relationship of T1/T2 due to multiple signal sampling, it can be consid-

ered significantly T2-weighted. HASTE, on the other hand, can be thought of in terms of a more traditional Turbo Spin Echo technique with a very long echo train (roughly half the number of phase encoding steps). The contrast presented by HASTE is more a 'pruist' concept of T2-weighting.

The typical workflow of a fetal MRI protocol is described below:

1. 3 plane free breathing FLASH localizer.
2. Transversal, sagittal, and coronal TrueFISP orthogonal to abdomen and pelvis of the mother (performed free breathing in this case).
3. Transversal, sagittal, and coronal HASTE to the fetus (or fetal head), with concatenations equal to the number of slices. (The selection of "Breath Hold" in PACE tab allows for manual start in the inline display.)
4. HASTE 'Thick Slab' (80–100 mm) with a very late TE (500 ms or greater) acquired in a sagittal orientation to the fetus.
5. HASTE 'Thin Multi-Slab' (10–20 mm) with moderately late TE (150 ms or greater) acquired in a sagittal orientation to the fetus.
6. Any T1w or diffusion-weighted (DWI) measurement you wish to run.

A list of typical scan parameters can be found in Table 1. The three plane localizer can be taken directly from the abdomen/library/localizer section of your Siemens protocol tree. The other protocols can also be adapted from the Siemens tree. Under the abdomen/library there is a category for 'T2', which contains examples of TrueFISP and HASTE. These protocols are a good starting point because they make use of minimal refocusing flip angles for HASTE and non-

*MR scanning has not been established as safe for imaging fetuses and infants under two years of age. The responsible physician must evaluate the benefit of the MRI examination in comparison to other imaging procedures.

Table 1: Fetal imaging parameters

	Localizer	t2_trufi_three planes_4mm	t2_HASTE_three planes_3mm	t2_HASTE_thick slab	t2_HASTE_thin slab
Sequence Type	FLASH	TrueFISP	HASTE	HASTE	HASTE
Slices	13	45	40	1	5
FOV Read	440 mm	380 mm	340 mm	350 mm	340 mm
Slice Thickness	8 mm	4 mm	3 mm	80–110 mm	10 mm
Distance Between Slices	NA	0 mm	0.5 mm	NA	0 mm
TR	7 ms	4.22 ms	2000–3000 ms	4500 ms	3000 ms
TE	2.50 ms	1.75 ms	150 ms	670 ms	260 ms
Averages	2	1	1	1	1
PAT	GRAPPA 2	GRAPPA 2	GRAPPA 2	GRAPPA 2	GRAPPA 2
Flip Angle	18 degree	65 degree	160 degree	170 degree	160 degree
Fat Suppression	None	None	None	None	None
Base Resolution	256	320	256	384	384
Phase Resolution	192	240	230	288	307
Phase/Slice Partial Fourier	None	None	$\frac{5}{8}$	$\frac{5}{8}$	$\frac{5}{8}$
Rectangular FOV	0%	0%	0%	0%	0%
Receiver Bandwidth	280 Hz/Px	460 Hz/Px	320 Hz/Px	310 Hz/Px	310 Hz/Px
Time of acquisition	21 s	32 s	2 min 01 s	4.5 s	15 s

1 Exam Explorer - \\SIEMENS\abdomen\library\T2

Object Edit Tools Insert Help

Protocol Name	Duration
1 t2_tse_tra_p2_mbh	00:36
2 t2_tse_tra_p2_mbh_320	00:36
3 t2_haste_tra_p2_mbh	00:44
4 t2_haste_cor_p2_mbh	00:45
5 t2_haste_cor_p2_mbh_320	00:38
6 t2_hasteirm_tra_p2_mbh	00:42
7 t2_hasteirm_cor_p2_mbh	00:42
8 t2_tirm_tra_p2_mbh	01:06
9 t2_tirm_tra_p2_mbh_320	01:00
10 t2+t2_haste_tra_mbh	00:46
11 ___ fatsat ___	
12 t2_tse_fs_tra_p2_mbh	00:40
13 t2_tse_fs_tra_p2_mbh_320	00:40
14 t2_haste_fs_tra_p2_mbh	00:44
15 t2_haste_fs_tra_p2_mbh_320	00:44
16 t2_haste_fs_cor_p2_mbh	00:45
17 t2+t2_tse_fs_tra_p2_mbh	01:03
18 ___ highres ___	
19 t2_tse_tra_p2_mbh_320_4mm	00:54
20 t2_tse_fs_tra_p2_mbh_320_4mm	00:54
21 ___ cholangiography ___	
22 t2_haste_cor_thin_slab_p2	00:18
23 t2_haste_cor_thin_slab_p2_384	00:21
24 t2_haste_fs_cor_thick_sl_p2_384	00:05
25 ___ trufi ___	
26 t2_trufi_tra_p2_bh	00:14
27 t2_trufi_cor_p2_bh	00:20
28 t2_trufi_tra_p2_bh_4mm	00:18
29 t2_trufi_sag_p2_bh_4mm	00:21
30 t2_trufi_cor_p2_bh_4mm	00:22
31 t2_trufi_sag_p2_bh_320	00:10

Waiting for patient registration. Unsafe removal of PNP device - Drive(G:)

1 Abdomen library of the Siemens protocol tree.

maximum excitation angle for TrueFISP. In addition, it is advised whenever possible to utilize iPAT (integrated Parallel Acquisition Technique) to reduce the number of acquired phase encoding steps. This not only reduces the specific absorption rate (SAR) for the study, but also serves to shorten acquisition and 'shot' time for HASTE, making images sharper. The necessary thick and thin slab protocol steps can also be located here under the heading 'cholangiography'. See Figure 1 for the location of protocols. One may inquire as to the reasoning behind the 'manual start' recommendation for HASTE. We find that

doing so allows us to better ensure sufficient relaxation has occurred from one slice to the next, thereby producing images with better signal-to-noise ratio (SNR). A mental count of two seconds or so should be sufficient. The thick and thin slab HASTE acquisitions provide a profile of the fetus as well as an overall view of the placenta and umbilical cord.

Common pitfalls-associated artifacts

Movements of the fetus are the most common source of image artifacts, especially in HASTE images. The biggest issue associated with movement is amniotic

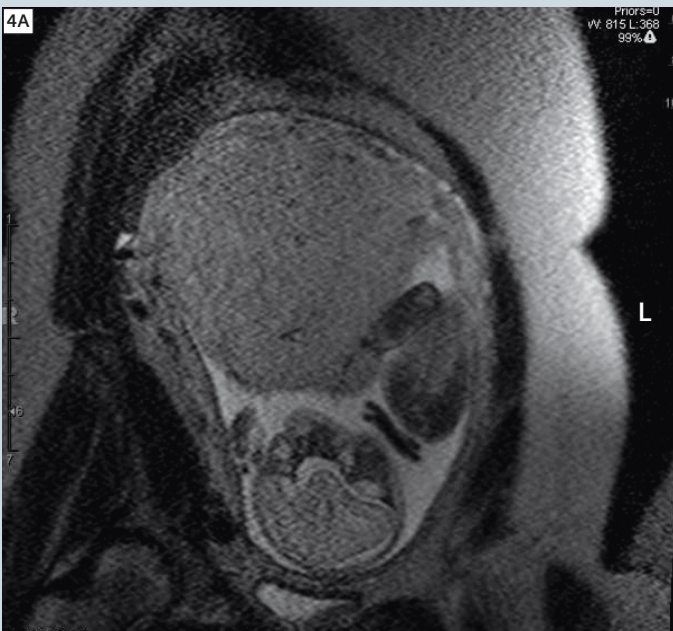
fluid suppression. This results from typical slice excitation in which we assume all tissue is stationary. After excitation and during the process of encoding data for the slice, even small movements on the part of the fetus can cause unexcited spins associated with surrounding fluid to move into the imaging plane. The resulting artifact is shown in Figure 2 as a signal void surrounding the fetus. In essence, this could most easily be described as a flow related artifact. Having control over the slice acquisition through manual starts allows the user to recognize this and provide a brief imaging respite to allow the fetus to return to



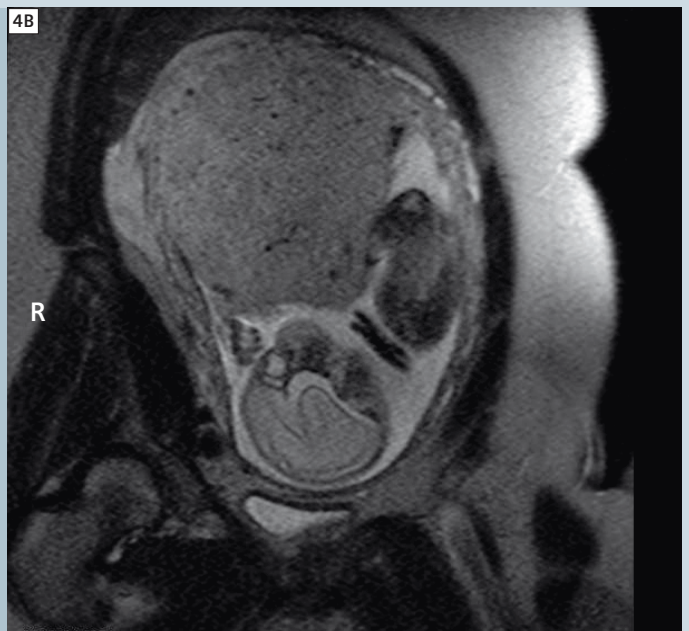
2 Flow related artifact caused by fetus movement.



3 Manual start of slice acquisition allows for motion-free images.



4A Insufficient Tim Matrix Mode setting.



4B 'Triple Mode' – correct Tim Matrix Mode setting.



5 Side-by-side positioning of two Body Matrix coils.

include the entire uterus in a single field-of-view and the signal should be relatively homogeneous. Using workflow features such as 'AutoCoil Select' is recommended. At the very least, this ensures appropriate selection of the posterior elements of the Spine Matrix. One may need to adjust the Body Matrix coil anteriorly to assure proper signal distribution throughout the volume. It is advised, if you have more than one Body Matrix coil, to connect them in a side-by-side fashion. This can be particularly helpful in cases where fetal development is further along, as shown in Figure 5.

Acknowledgements

I would like to thank the doctors and technologists of Johns Hopkins University Hospital for providing valuable feedback as well as protocol and procedure optimization. There are in particular two members of the team that deserve special recognition. Dr. Thierry A G M Huisman MD for his years of experience, knowledge and of course guidance provided the ground work for a successful Fetal MRI program. It is his dedication and drive that continues to advance the practice beyond the clinical routine. Scott Pryde (Chief MRI Technologist) provided the means to examine the special needs of this patient subset and create an ideal workflow. Scott invested himself in the set up and modification of the exam protocols and continues to train a competent staff in a non standard imaging procedure. Scott also provided many of the image examples used to illustrate this work.

a quiet state before continuing. When the scan is completed, you may go back and acquire only the slice or slices that were disturbed to complete the exam Figure 3.

Another common artifact to consider arises from the dependence of the exam on the use parallel acquisition. The user may observe reduced SNR resulting from incorrect application of the technique. The most common example of this is insufficient number of coil elements aligned perpendicular to the phase encoding direction of a given slice group. This could be due to an unsuitable chosen phase encoding direction, complex multi-angle slice prescription or even an insufficient Tim Matrix Mode setting. The effect of the latter and its correction are shown in Figure 4. Matrix Mode CP

is used with a PAT factor of two in the example on the left, while the corrected image on the right shows an image acquired using 'Triple Mode'. It is important to remember that the user has tools such as the PAT monitor to guide this part of the workflow.

Coil usage

Although it is reasonable to see how some patients may benefit from slightly different positioning strategies (e.g. left or right lateral decubitus), it is far more common to image the mother in a supine orientation. Regardless of the patient's position, placement of coils is crucial. This may take some experience. It is recommended to evaluate the 3 plane localizer to determine if sufficient coverage is achieved. Ideally, you will need to



→ Follow this QR code or visit us at www.siemens.com/magnetom-world to download the .edx files for MAGNETOM Avanto and MAGNETOM Espree.

Contact

Aaron J. Flammang, MBA, BS RT (R) (MR)
Clinical Research Scientist
Siemens Corporate Research
Center for Applied Medical Imaging
Baltimore, MD
USA
aaron.flammang@siemens.com

Case series: Fetal* MR Imaging of the Brain at 3T

Jacques F. Schneider

University Children's Hospital, Basel, Switzerland

Background

Fetal MR imaging (MRI) is a recognized complementary method to fetal ultrasound to identify fetal central nervous system (CNS) pathology. It can provide additional and diagnostically-relevant information, add certainty to ultrasound diagnosis and help parental counselling. In most imaging centers MRI is performed at 1 or 1.5 Tesla field strength, with no proven deleterious effect on the fetus to date. According to national and international guidelines, fetal MRI is recommended from the second trimester of gestation, and specific absorption rates (SAR) for each pulse sequences are limited by the manufacturers to ensure that increase in body temperature is less than 0.5°C. Experimental physical evidence suggests that SAR deposition to the fetus in utero is only minimally higher at 3 Tesla, and still within the guidelines recommendation, but care still needs to be taken.

This case series intends to provide an insight into the enhanced visualization of fetal CNS in selected brain pathologies at 3 Tesla.

Materials and methods

All images in this case series were acquired on a 48-channel whole-body 3T scanner (MAGNETOM Skyra) with a combination of the Body Matrix coil anteriorly and integrated spine coil posteriorly. Fetal brain protocol typically consists of T2-weighted (w) HASTE single-shot in all three planes, T1w FLASH in the axial plane, Diffusion-tensor imaging in the axial plane. Selected sequence parameters were as follows and adapted to the patient:

Sequence parameters

Axial / Coronal / Sagittal T2w HASTE (free-breathing)

TR/TE = 1100 / 96 ms, SL = 3 mm, FOV = (280*280) mm², matrix = (256*230) px²

Axial T1w FLASH (breathhold)

TR/TE = 122 / 2.46 ms, SL = 3 mm, FOV = (280*280) mm², matrix = (224*168) px²

Axial epi2D mddw20 (free-breathing)

TR/TE = 4300 / 85 ms, SL 3 mm, FOV = (220*220) mm², matrix = (142*142) px², b-value = 800

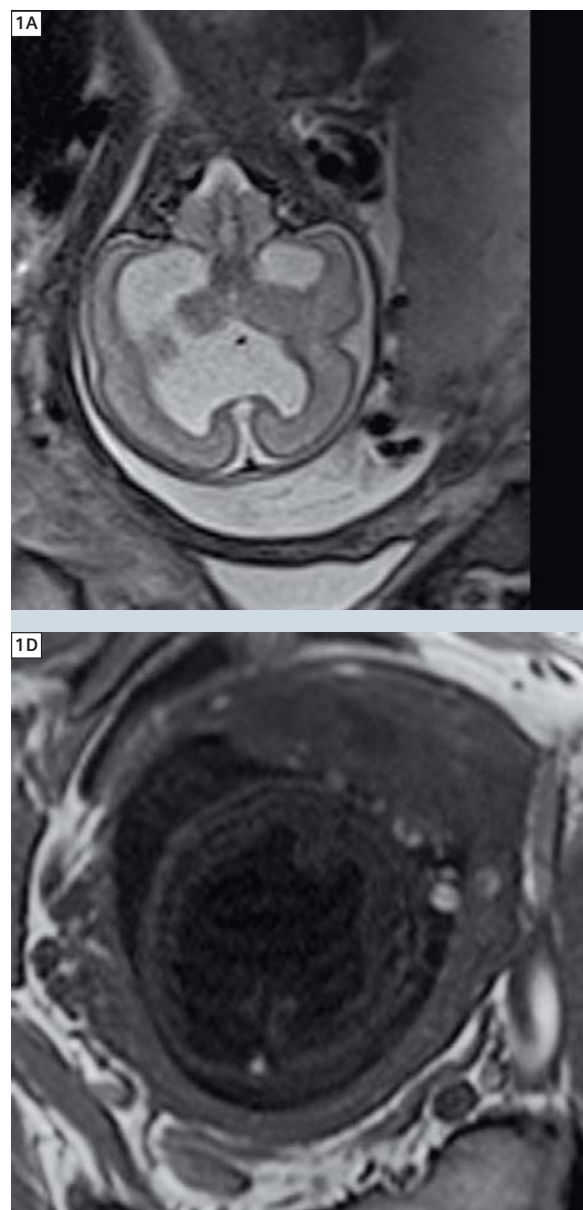
Sagittal T2w trufi2d (breathhold)

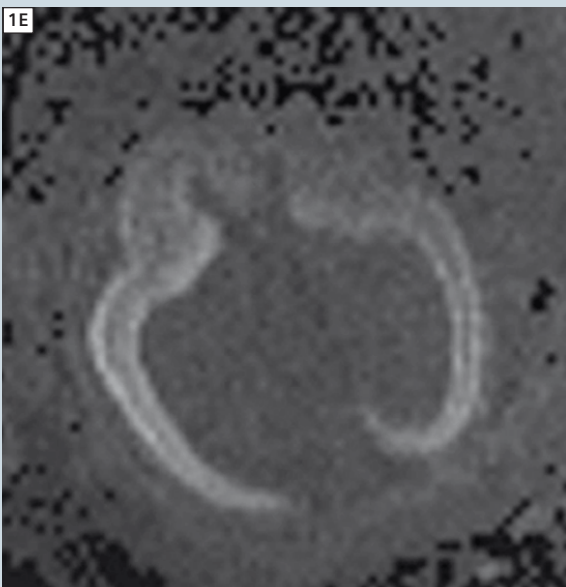
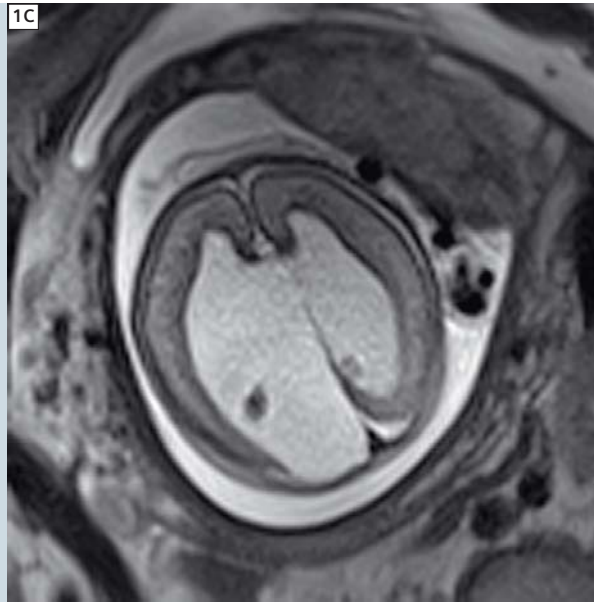
TR/TE = 3.88 / 1.7 ms, FOV = (376*376) mm², matrix = (614*768) px²

Conclusion

This short case series shows that fetal MRI at 3T is feasible and delivers excellent visualization of fetal brain and spine structures. With growing experience, the use of 3T systems for fetal MRI could add much-needed certainty in the diagnostic workup of fetal brain pathologies.

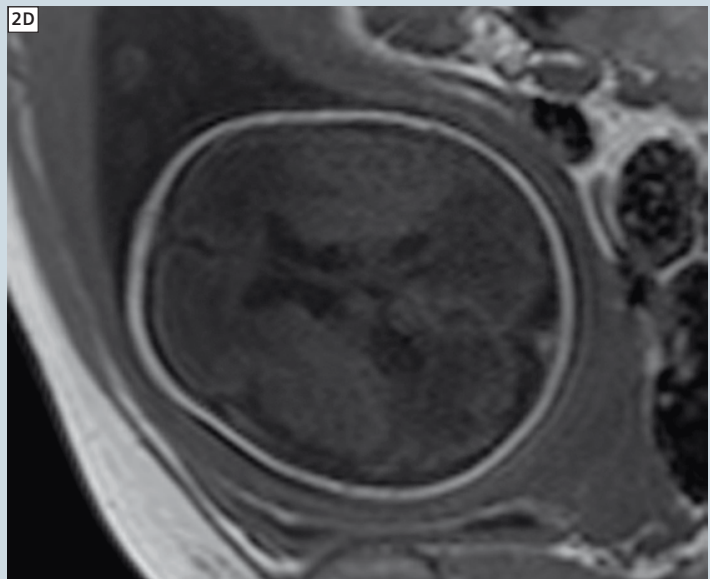
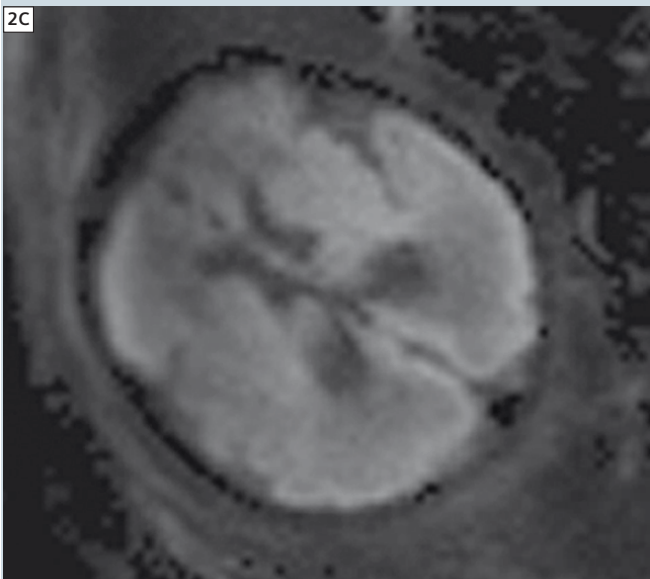
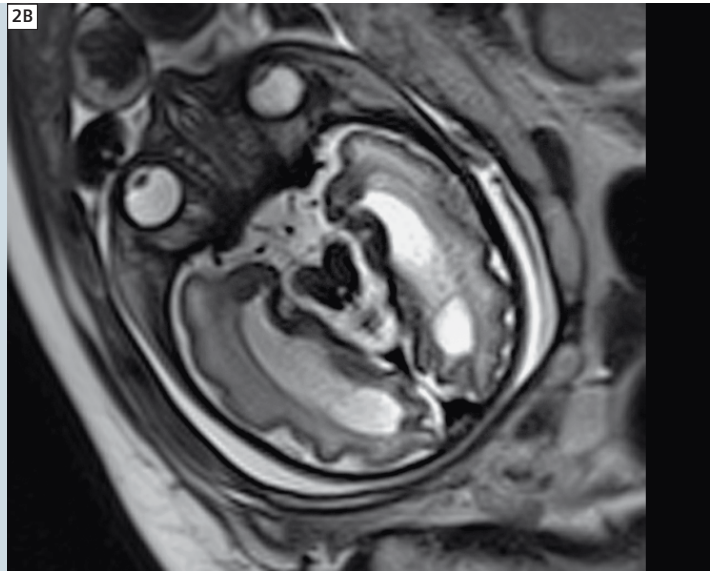
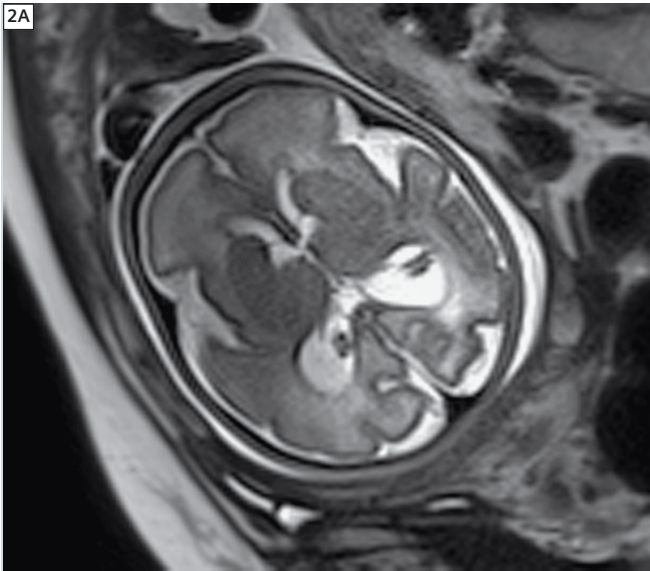
*MR scanning has not been established as safe for imaging fetuses and infants under two years of age. The responsible physician must evaluate the benefits of the MRI examination compared to other imaging procedures.





Case 1

A 30-year-old female in her 23rd week of pregnancy was referred for a fetus presenting with hydrocephalus, thickened neck sign, incomplete falx and suspicion of corpus callosum agenesis. Imaging findings show only a partial absence of the corpus callosum with persistency at the genu (1A) and a massive dilatation of the ventricular system (1B, 1C). There is also a parafalcine cyst on the right side (1C). No calcification or bleeding (1D) and no parenchymal diffusion anomaly were detected (1E).



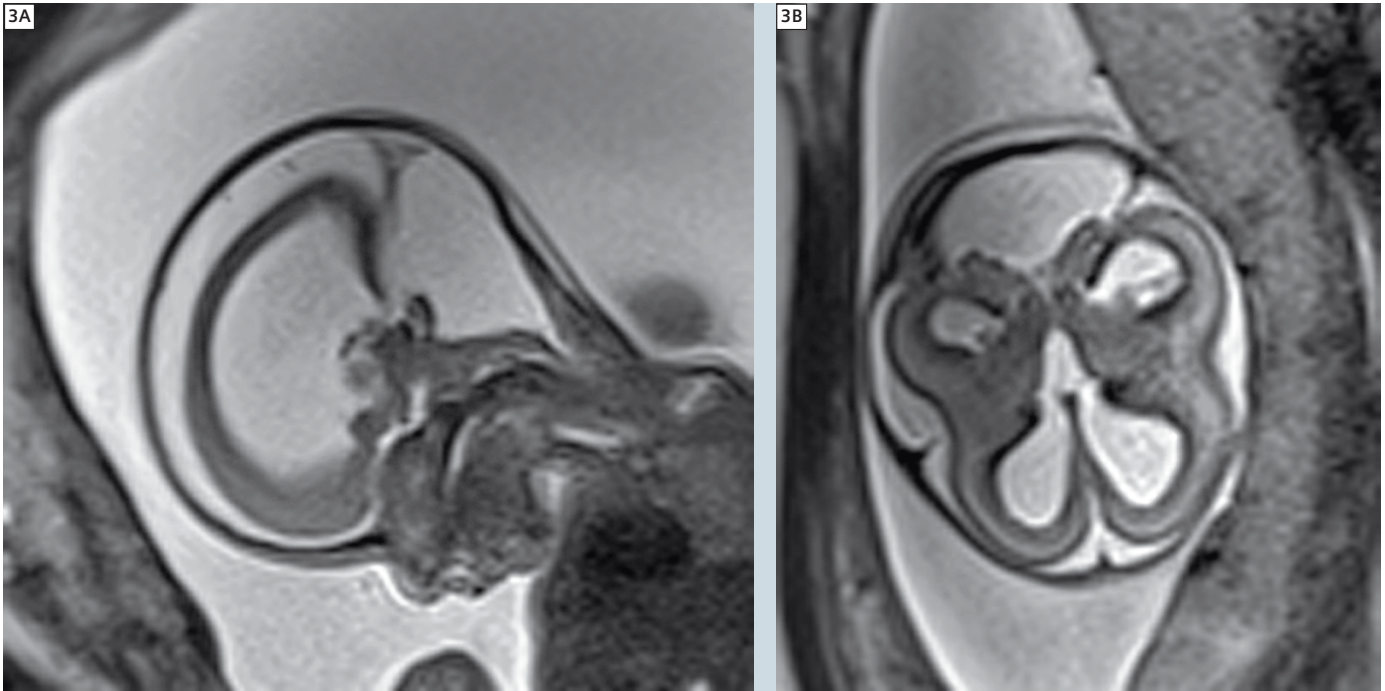
Case 2

A 29-year-old female in her 26th week of pregnancy was referred for a fetus with progressive hydrocephalus and inconsistent visualization of the midline structures. MRI shows intact corpus callosum and midline structures, a moderate dilatation of both side ventricles but clear depiction of cysts at the caudothalamic groove (2A), as well as intraventricular septations in both occipital horns (2B), raising the suspicion of an intrauterine infection. Diffusion trace images did not show parenchymal ischemia or infarctions (2C) nor were calcifications detected on T1w imaging (2D). Recent cytomegalovirus infection was subsequently confirmed in the mother, and in the fetus after delivery.

Contact

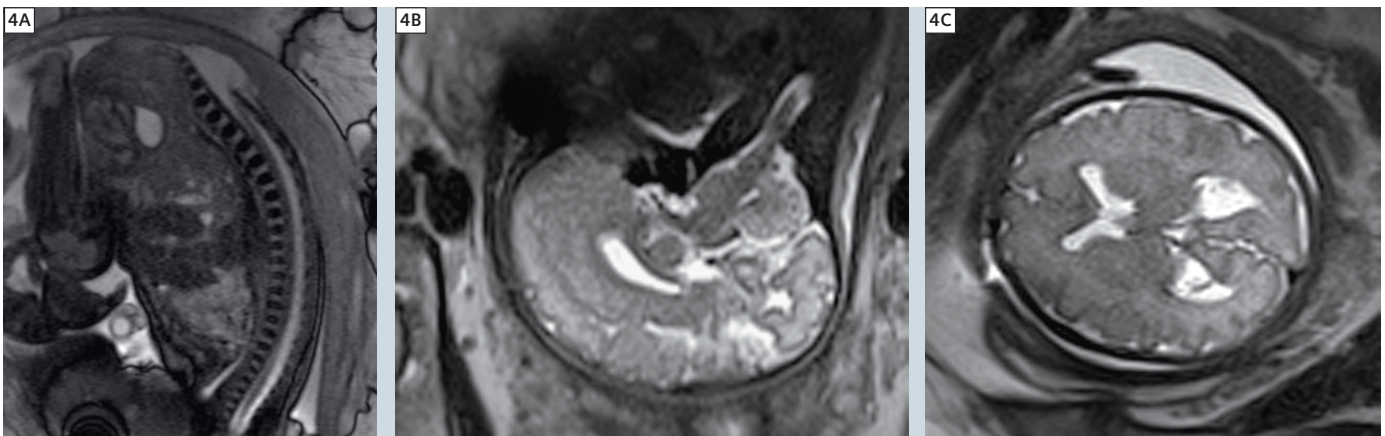
Jacques Schneider, MD
 Head of Pediatric Radiology
 University Children's Hospital UKBB

CH-4005 Basel
 Switzerland
 Phone +41 61 704 2632
 jacques.schneider@ukbb.ch



Case 3

A 30-year-old female in her 26th week of pregnancy was referred for a fetus presenting with massive hydrocephalus and a large posterior fossa. MRI findings demonstrate massive dilatation of both side ventricles, a cystic dilatation of the posterior fossa (3A), a large communication between the retrocerebellar space and the fourth ventricle (3B) and a partial absence of the vermis (3A–B). These findings are characteristic for a malformation of the Dandy-Walker variant type.



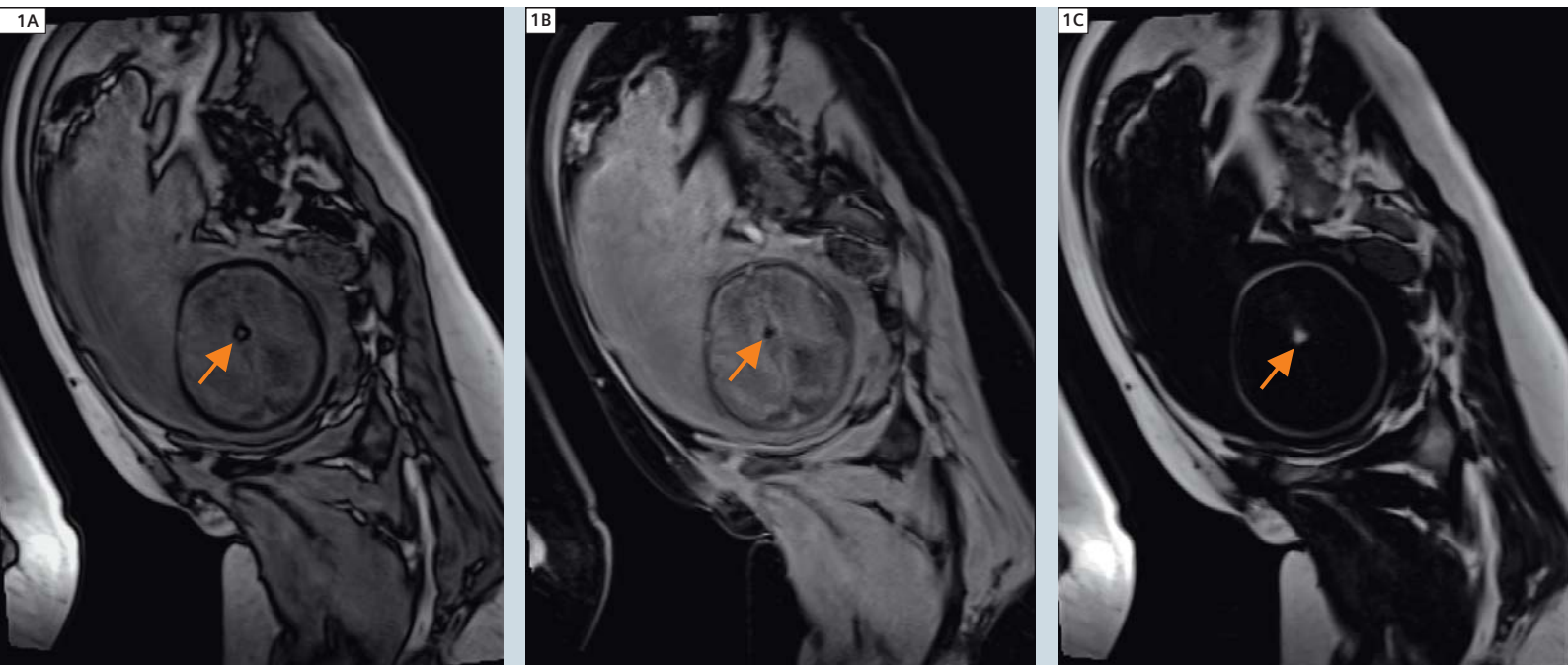
Case 4

A 35-year-old woman in her 36th week of pregnancy was referred for a suspicion of myelomeningocele and Arnold Chiari II malformation. MRI clearly depicts the defect of the posterior spine at the level of the promontorium at L5 with tethered cord and myelomeningocele (4A). Nevertheless, at the craniocervical junction the usual signs of an Arnold-Chiari II malformation are missing (4B), and no hydrocephalus was present (4C).

Case Report: Intracranial Lipoma Confidently Diagnosed Antenatally using the Dixon Technique

Sally Agnew; A. Michelle Fink

Children's MRI Centre, Royal Children's Hospital, Melbourne, Victoria, Australia



1 T1w opposed-phase image derived from a 3D T1w FLASH Dixon acquisition shown in (1A). Corresponding qualitative water (1B) and fat image (1C) allow to characterize the lesion as fatty (arrows).

Patient history

34-year-old female carrying a fetus* of 33 weeks gestational age, presented after an obstetric ultrasound demonstrated severe bilateral ventriculomegaly, dysplastic corpus callosum and a solid midline brain mass of inconclusive characteristics. Suspicion of lipoma or teratoma.

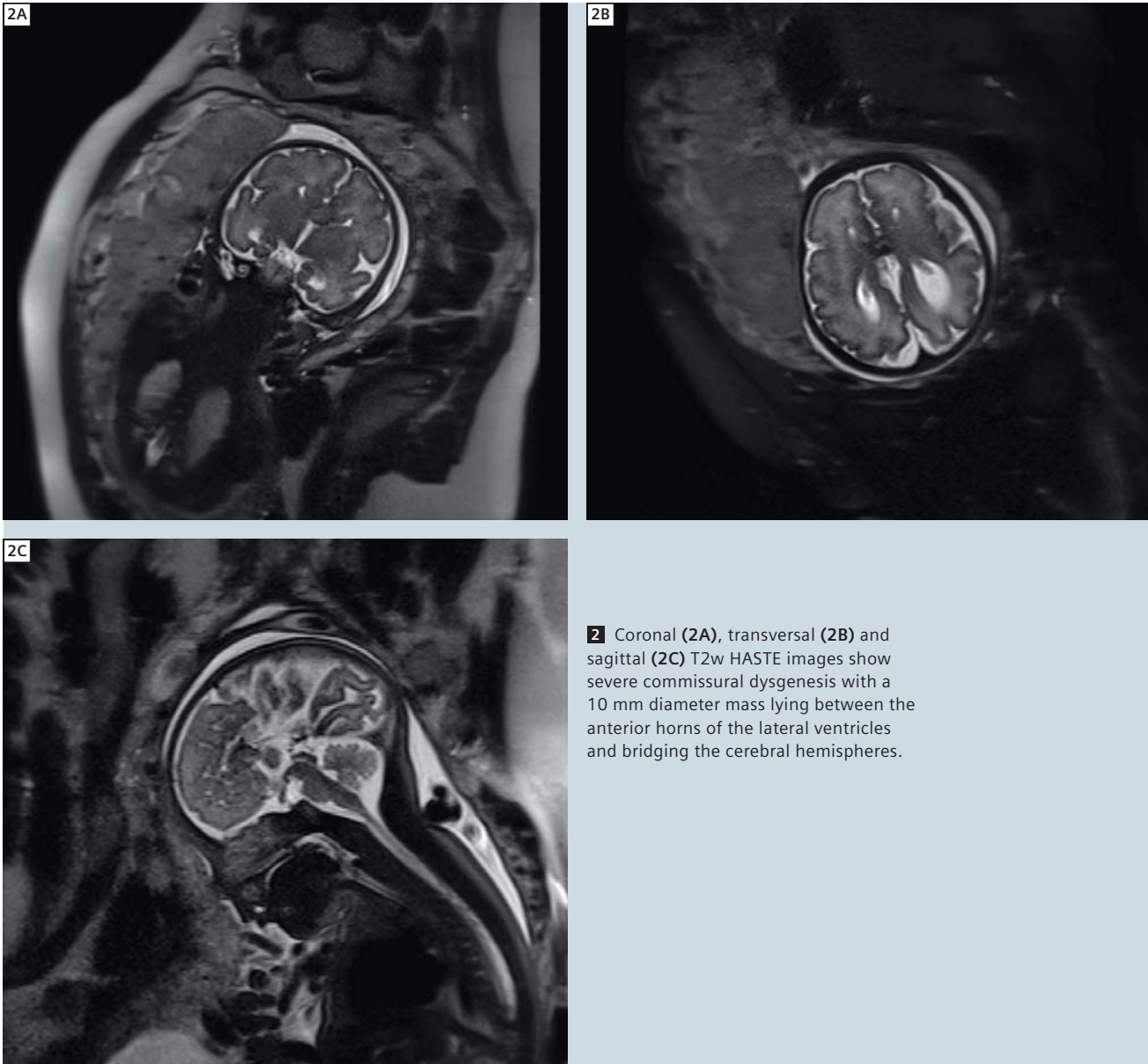
Sequence details

Images were acquired on a 1.5T MAGNETOM Avanto using a 32-channel cardiac coil and software version syngo MR B17.

T1-weighted VIBE, with Dixon in-phase, out-of-phase, water suppressed and fat saturated images. TR 7.5 ms, TE 2.4 ms, BW 300 Hz/px, slice thickness 3 mm, FOV 380 mm, matrix (158 x 320) mm². T2-weighted HASTE with fat saturation. TR 1260 ms, TE 122 ms, BW 121 Hz/px, 3 mm, FOV 240 mm, matrix (192 x 256) mm².

Imaging findings

Severe commissural dysgenesis with a 10 mm diameter mass lying between the anterior horns of the lateral ventricles and bridging the cerebral hemispheres. The signal of the mass is nearly all fatty, in keeping with a lipoma. Due to the location of the mass it can be more accurately described as a pericallosal lipoma. Associated atrial ventriculomegaly was again demonstrated.



2 Coronal (2A), transversal (2B) and sagittal (2C) T2w HASTE images show severe commissural dysgenesis with a 10 mm diameter mass lying between the anterior horns of the lateral ventricles and bridging the cerebral hemispheres.

Comments

The T1-weighted Dixon technique enabled a conclusive diagnosis of the fetal intracranial brain mass. The chemical shift artifact; a signal drop-out at the fat-fluid interface, was present due to the fatty mass and the high water content of the fetal brain. The mass produced high signal on the water suppressed image and a signal void on the fat saturated image, clearly characterizing the mass as fatty and hence in keeping with a lipoma.

Acknowledgments

Michael Kean for his assistance in sequence adaptation.
Vanessa Orchard and Glenn Cahoon for prior developments in RCH fetal scanning.

Contact

Sally Agnew
Children's MR Centre
Royal Children's Hospital
Melbourne
Australia
Phone: (03) 9345 4309
sally.agnew@rch.org.au

*MR scanning has not been established as safe for imaging fetuses and infants under two years of age. The responsible physician must evaluate the benefit of the MRI examination in comparison to other imaging procedures.

Case Report: Fetal* MRI of Triplets for Evaluation of the Urinary Tract

A. Zahiri, MD¹; R. Beigi¹; A.M. Kajbaf Zade, MD²

¹Ghaem Hospital of Karaj, Department of Radiology, Tehran, Iran

²Ghaem Hospital of Karaj, Department of Urology, Tehran, Iran

With increasing numbers of women undergoing hormone therapy and in vitro fertilization, the total numbers of born multiples have been demonstrably increasing. Excluding these two groups of women, the theoretical relativity in a normal population for twins is approximately 1:85, and for triplets 1:7,000. Multiples very often show a reduced growth as compared to singles, which can already be seen for triplets during the 28th week of gestation. Furthermore, a multiples pregnancy should be

regarded as a high-risk pregnancy for the mother as well as for the children. The diagnosis of multiples pregnancy as well as the follow-up of the multiples is very often supported by ultrasound. As MRI plays an increasing role in the further diagnostic work-up of unclear findings of ultrasound, the imaging of twins with fetal MRI is not an uncommon situation nowadays, although the imaging of triplets remains a very unusual procedure. In addition, the imaging of multiples with MRI requires additional efforts

in the examination itself as well as in reading.

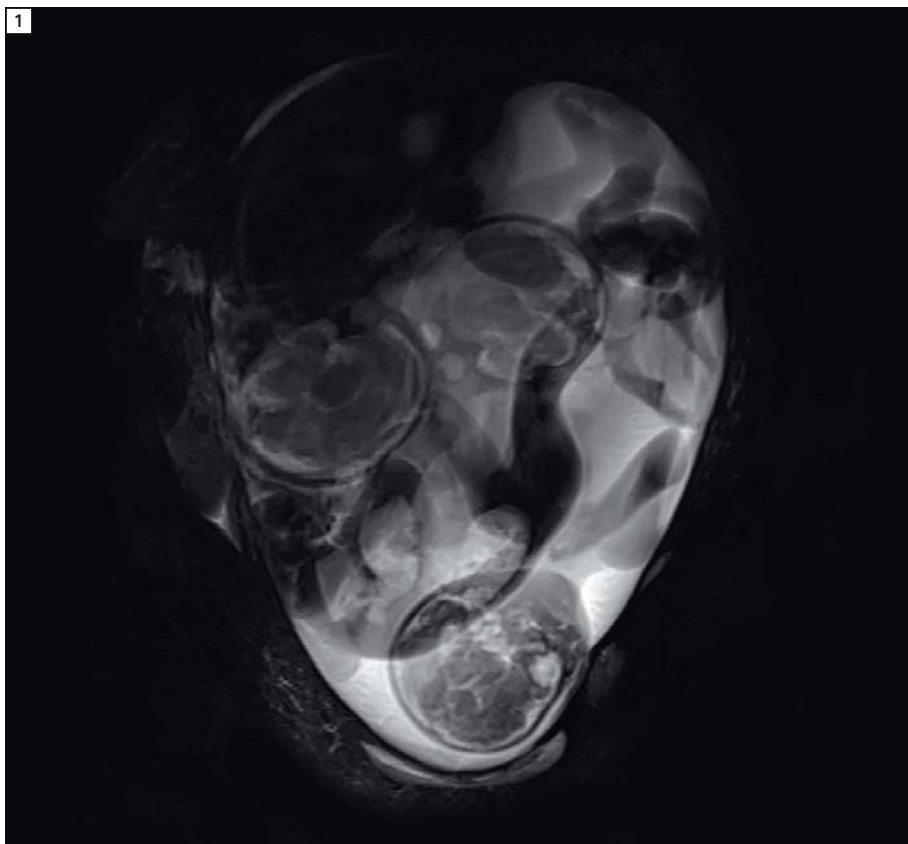
At our institution, we had the chance to image triplets after unclear ultrasound findings.

The referring physicians demanded an evaluation of the urinary tracts of the triplets of a 25-year-old mother by fetal MRI. MRI was conducted using a 1.5 Tesla Tim system MAGNETOM Avanto, using the Body Matrix and the integrated Spine Matrix coil. For fast and reliable assessment of the urinary tracts of the triplets we used a thick-slice heavily T2-weighted HASTE sequence.

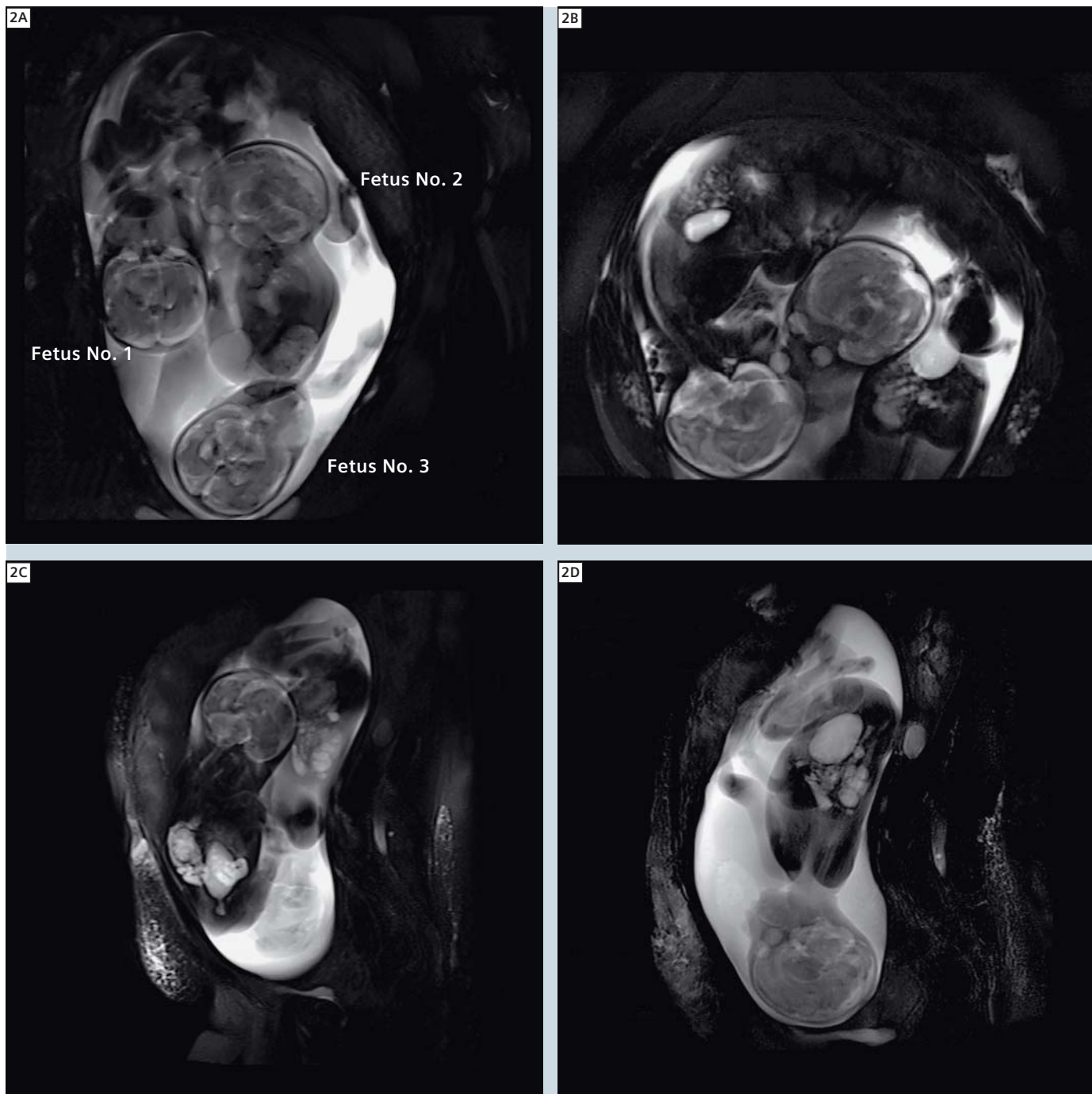
MRI demonstrated a typical triple pregnancy with one female fetus in cephalic presentation and normal developed genitor-urinary (GU) tract system. The other two fetuses were male and showed changes to the GU system. One male fetus was also imaged in a cephalic position at the left side of the amniotic cavity and MRI revealed a unilateral stenosis at the junction of ureter and bladder (UVJ) with dilatation of the upper urinary tract including the renal calyx. The other male fetus was shown to be in breech position and a dilatation of both sides of the whole upper urinary tract including the renal calix as well as distension of the bladder as typically seen in PUV was shown.

After termination of pregnancy by cesarean section, the third male fetus expired shortly after birth and surgery on the other fetuses confirmed our MRI diagnosis.

The two other fetuses had safe termination. The fetus with unilateral UVJ stenosis is under medical observation and a single injection of botax at UVJ for release of stenosis.



1 Fetal MRI of triplets.



2 Thick-slice HASTE to evaluate the urinary tract of the triplets.

*MR scanning has not been established as safe for imaging fetuses and infants under two years of age. The responsible physician must evaluate the benefit of the MRI examination in comparison to other imaging procedures.

Contact
 Dr. Alireza Zahiri, MD
 Ghaem Hospital of Karaj
 MRI Department
 Department of Radiology

4rah dolatabad-7tir SQ
 Karaj, Tehran 31397
 Iran
 alirezazahiri2002@yahoo.com

Case series: MR Imaging of the Fetus*

Nguyen Thi Thu Trang, MD¹; Ha To Nguyen, MD¹; Gregor Kasprian, MD²; Lisa Chuah, PhD³

¹Department of Diagnostic Radiology, Maternal and Obstetrics Tu Du Hospital, Ho Chi Minh City, Vietnam

²Department of Radiology, Division of Neuroradiology, Medical University of Vienna, Vienna, Austria

³Siemens Healthcare, Regional Headquarters, Singapore

Background

Fetal MRI is increasingly being used as an adjunct to prenatal ultrasound (US) in the clinical setting. This case series features a number of fetal imaging cases at Tu Du Hospital, a specialized obstetrics and gynecology hospital in Ho Chi Minh City, Vietnam. Since the installation of a MAGNETOM Espree in April 2011 (the first MR system in the hospital), approximately 20 fetal MR imaging cases were performed to date. As noted in Aaron Flammang's How-I-do-it article in this issue of MAGNETOM Flash, ultrasound can resolve most clinical diagnostic questions. Nevertheless, beyond situations related to

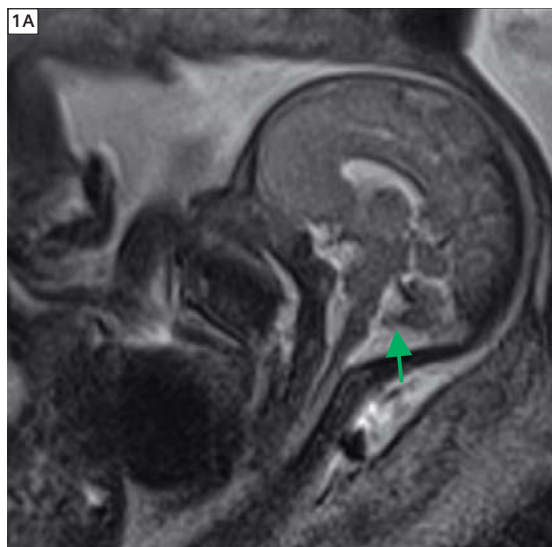
ultrasound-associated limitations (e.g., obese mother, fetal position/condition, smaller, sector-shaped field-of-view), MRI can, in some cases, provide additional, complementary findings, improve diagnosis and modify the treatment approach across a number of conditions (e.g., cerebral malformations and acquired pathologies, pulmonary malformations, renal abnormalities, detection of cleft lip and palate) [1, 2, 3]. These cases were selected to highlight situations where MR imaging had provided additional information in fetuses with sonographically diagnosed or suspected pathologies.

Materials and methods

All patients reported in the case series were scanned on a 1.5T MAGNETOM Espree (software version *syngo* MR B17) using a combination of two 6-element Body Matrix coils and the 24-element Spine Matrix coil. In all cases, the mother was scanned in a left lateral decubitus position, which can be achieved comfortably within the 70 cm bore of the MAGNETOM Espree. For all the cases reported below, ultrasound was first performed, with MR imaging requested to provide additional information for diagnostic confirmation and/or prediction of postnatal outcome.

Case 1 34-week-old fetus with hemorrhage in the left cerebellum and heart defects

The ultrasound on the 28-year-old mother had suggested the presence of vermian hypoplasia and MRI was requested for confirmation. The size and shape of the vermian looked normal on MR images (Fig. 1A). MR imaging additionally revealed a left cerebellar hemispheric lesion as the result of hemorrhage (Figs. 1B, 1C, 1D).

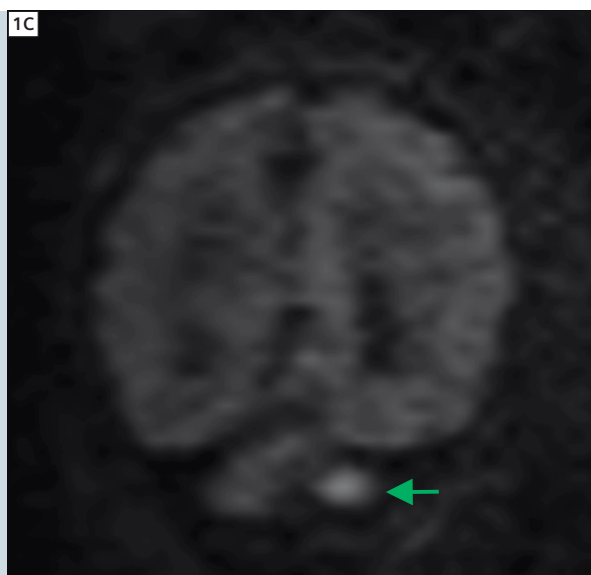
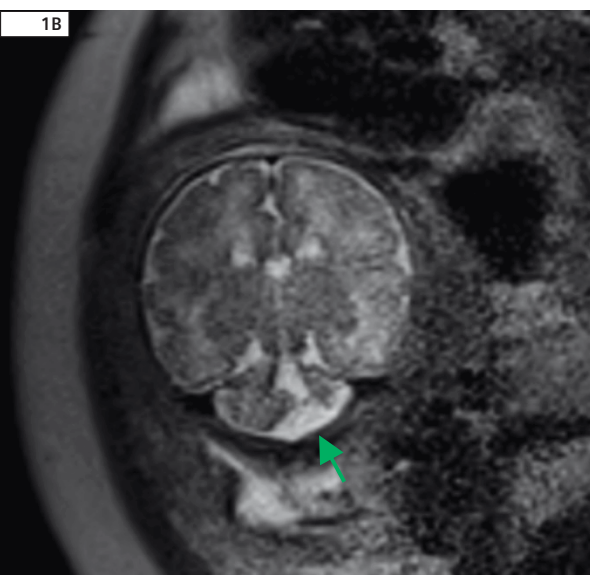


1A The vermian appears to be normal in shape and size as seen on sagittal T2w HASTE images of the fetal brain. HASTE: 18 slices, SL 4 mm (no gap), TR/TE 2600/102 ms; FOV (280*280) mm²; matrix (230*256) px², BW 476 Hz/px, acquisitions 1.

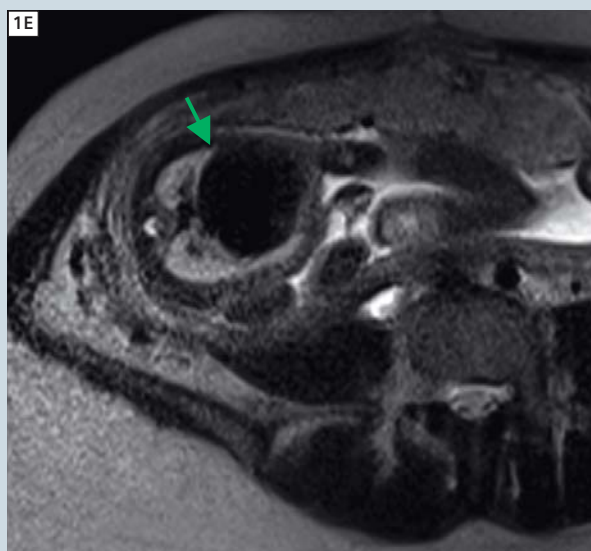
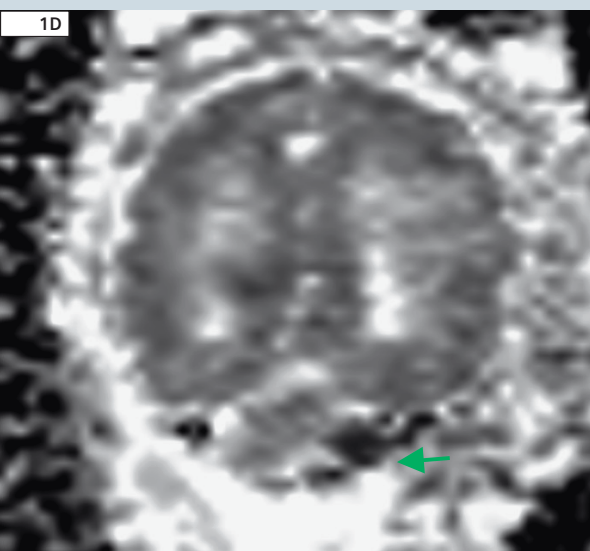
MR imaging also indicated congenital heart disease (oversized heart) which was not noted in the ultrasound report (Fig. 1E). However, MR is not the typical modality of choice for cardiac imaging in

the fetus as the fetal heart is small with a high beat rate and cardiac triggering is not possible in the fetal setting [4] (but see [5]). The mother underwent another ultrasound examination which allowed

the diagnosis of heart defects. The fetus was brought to term but died approximately two week postpartum with death attributed to cardiac failure.



1B-D A lesion present in the left cerebellum as seen in the coronal T2w HASTE image was revealed by EPI diffusion-weighted imaging (1C, b700) and ADC maps (1D) to be the result of a recent hemorrhage. HASTE: 18 slices, SL 4 mm (no gap), TR/TE 2600/102 ms; FOV (280*280) mm²; matrix (230*256) px², BW 476 Hz/px, acquisitions 1; EPI diffusion: 20 slices, SL 4 mm (no gap), TR/TE 6400/87 ms, FOV (280*280), Matrix (112*160) px²; BW 1157 Hz/px, PAT factor 2; b values: 0, 700; flip angle 90°, acquisitions 1.



1E The presence of an abnormally large heart was noted on the axial T2w HASTE images. HASTE: 20 slices, SL 4 mm (no gap), TR/TE 2600/102 ms, FOV (260*260) mm², matrix (205*256) px², BW 476 Hz/px, PAT factor 2, acquisitions 1.

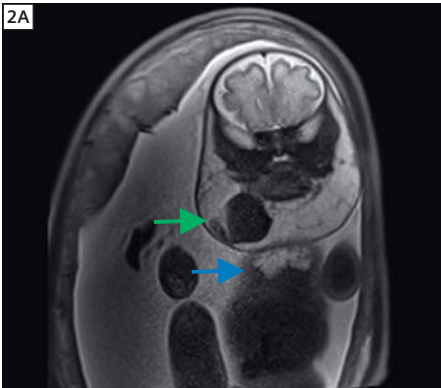
Case 2 28-week-old fetus with large lymphangioma

The ultrasound examination had shown the presence of a large lymphangioma at the neck region of the 28-week-old fetus. MR imaging was requested to establish the extent of the abnormal

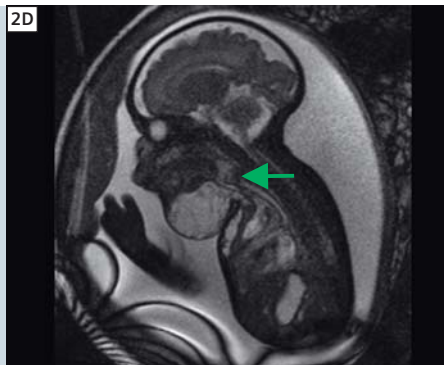
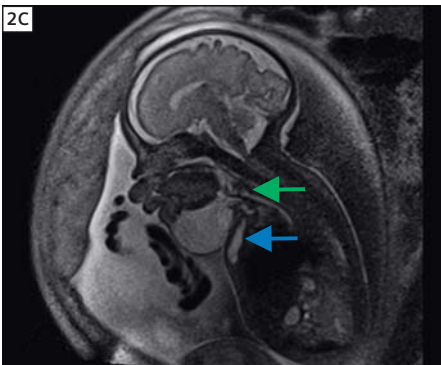
tissue and to inform on the prognosis of the fetus.

A large cystic lesion in the neck, consistent with a lymphangioma, was clearly visualized in the MR images (Fig 2A, 2B). In addition, MR imaging established the lymphangioma to extend to the front of the sternum (Fig. 2A, 2C). Crucially, MR

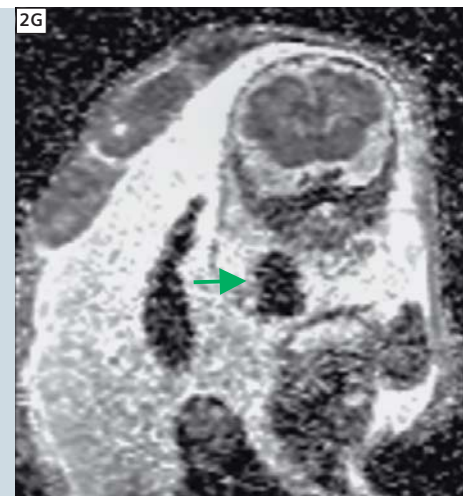
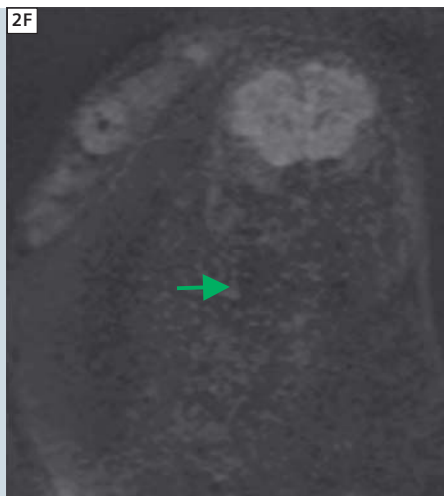
imaging indicated no narrowing or displacement of the trachea (Figs. 2C, 2D). The dark mass within the lymphangioma was determined to be a chronic intracystic hemorrhage, also seen as dark on EPI diffusion images and ADC maps (Figs. 2E, 2F, 2G) and T1 FLASH images. The fetus is presently under follow-up.



2A-B The lymphangioma of the neck as seen in coronal T2w HASTE images. An old intracystic hemorrhage can also be seen (green arrow). HASTE: 22 slices, SL 4 mm (no gap), TR/TE 2600/102 ms, FOV (280*280) mm², matrix (230*256) px², BW 476 Hz/px, acquisitions 1.



2C-D Sagittal T2w HASTE (2C) and T2w TrueFISP (2D) images indicate no narrowing or displacement of the trachea (green arrow). A cystic lymphangioma is also seen on the front of the sternum (blue arrow). HASTE: 26 slices, SL 4 mm (no gap), TR/TE 2600/102 ms, FOV (280*280) mm², matrix (230*256) px², BW 476 Hz/px, Acquisitions 1. TrueFISP: 22 slices, SL 4 mm (no gap), TR/TE 4.6/2.3 ms, FOV (300*300) mm², matrix (240*320) px², flip angle 69°, acquisitions 2.



2E-G The intracystic hemorrhage was seen as hypointense on coronal EPI diffusion (2E b0; 2F b700) and diffusion ADC (2G) images. EPI diffusion: 20 slices, SL 4 mm (no gap), TR/TE 6400/87 ms, FOV (280*280) mm², matrix (112*160) px²; BW 1157 Hz/px, PAT factor 2; b values: 0, 700; flip angle 90°, acquisitions 1.

Case 3 34-week-old fetus with diaphragmatic hernia

Early ultrasounds (22 GW and 24 GW) of this fetus had not noted any abnormalities. However, at 34 weeks, congenital diaphragmatic hernia was diagnosed with ultrasound and MR was requested

to provide prediction of postnatal outcome. MR imaging indicated herniation of the bowel and spleen, with hypoplasia of the left lung and heart (Figs. 3A–C). However, as MRI-based lung volumetry of the right lung indicated a normal volume of 40 ml (see [6] for a summary of

normal fetal lung volumes), postnatal viability was considered to be positive. The fetus was brought to term and immediately transferred to the pediatric unit for treatment.

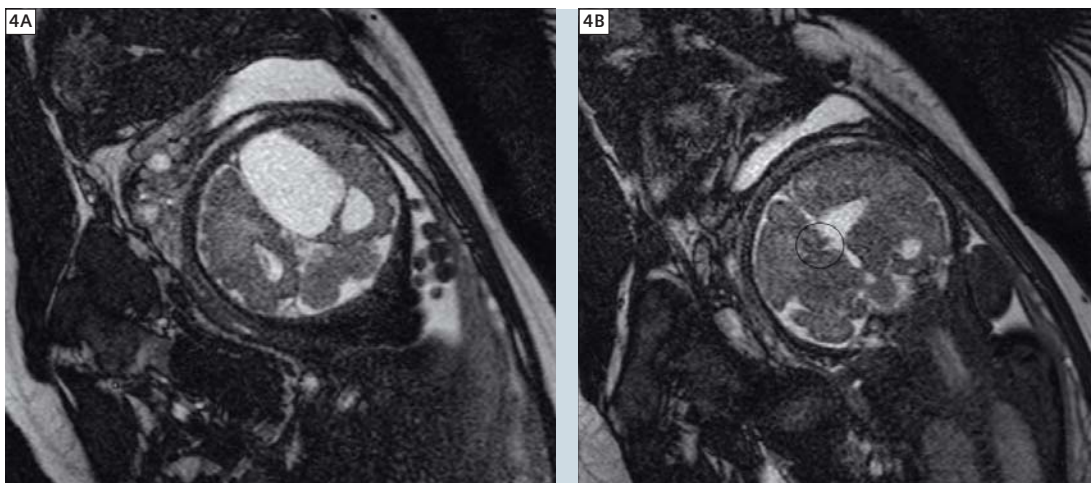


3A–C Axial HASTE (3A), sagittal TrueFISP (3B), and coronal TrueFISP (3C) images show an intact right lung (a) with compression of the heart (b) and the left lung (c) by the bowels (d) and spleen. HASTE: 25 slices, SL 4 mm (no gap), TR/TE 2800/102 ms, FOV (280*280) mm², matrix (205*256) px², BW 476 Hz/px, PAT factor 2, acquisitions 1. Sagittal TrueFISP: 20 slices, SL 4 mm (no gap), TR/TE 4.1/2.1 ms, FOV (340*340) mm², matrix (384*512) px², BW 488 Hz/px, flip angle 70°, acquisitions 1. Coronal TrueFISP: 20 slices, SL 4 mm (no gap), TR/TE 4.1/2.1 ms, FOV (300*300) mm², matrix (384*512) px², BW 488 Hz/px, flip angle 70°, acquisitions 1.

Case 4 32-week-old fetus with a midline arachnoid cyst and corpus callosum agenesis

The presence of an interhemispheric cyst was noted on ultrasound and MR imaging indicated that it may be an arachnoid cyst (Figs. 4A, 4B). In addition, MR indi-

cated an associated partial agenesis of the corpus callosum (Fig 4B). The fetus is presently under follow-up.



4A–B Coronal TrueFISP images which show a large arachnoid cyst in the left hemisphere and partial agenesis of the corpus callosum (4B). Coronal TrueFISP: 25 slices, SL 4 mm (no gap), TR/TE 4.7/2.4 ms, FOV (288*288) mm², matrix (240*320) px², BW 488 Hz/px, flip angle 70°, acquisitions 1.

Case 5 20-week-old fetus with cyst in spleen

Ultrasound in this 19-week-old fetus had suggested the presence of a cyst in the left diaphragm. However, MR imaging indicated the presence of a large splenic cyst, seen on the T2w HASTE and T2w TrueFISP images as a hyperintense mass dorsolateral to the stomach (Figs. 5A, B). The patient is presently under follow-up.

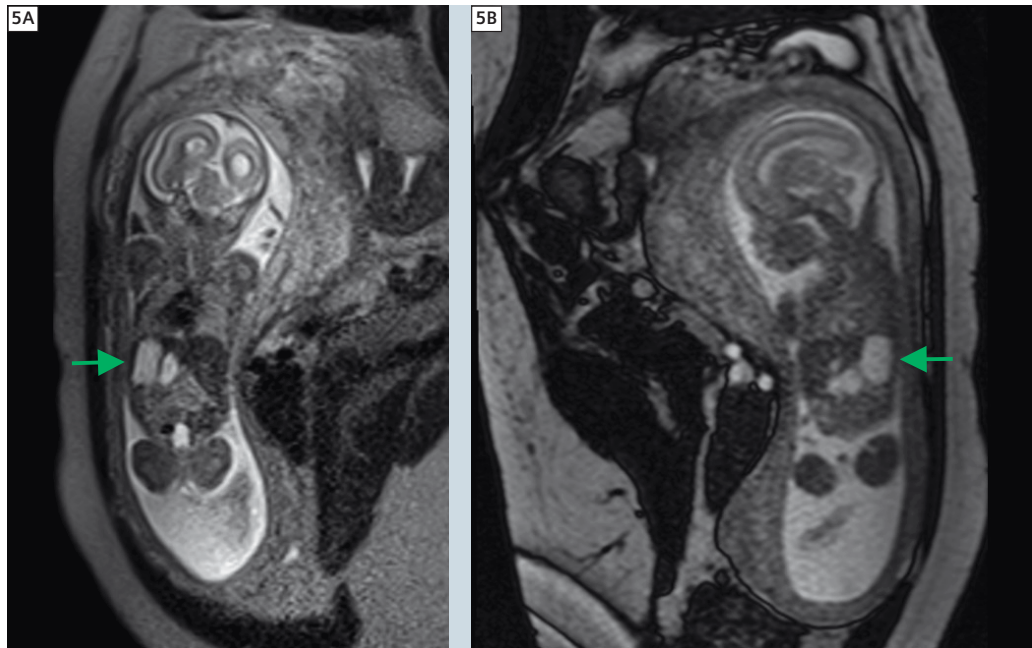
Conclusion

Fetal MR imaging was recently implemented in Vietnam. While this is a new service, with only a small number of patients at this point, this case series demonstrates that MR can offer complementary information to ultrasound, to improve prenatal diagnosis and management.

With growing experience and expertise and increased acceptance of this procedure amongst the gynecologists and pediatricians, it is expected that this service will grow and will play an increasingly important role in prenatal diagnosis and management. The information from ultrasound and MRI are typically complementary. However, in the future, MR imaging may make its most significant contributions to fetal imaging through the provision of metabolic and functional information such as spectroscopy, functional MRI (fMRI), diffusion-weighted imaging (*syngo* REVEAL) and tractography [7, 8, 9, 10] and enabling the examination of fetal anatomy at the microstructural level.

Acknowledgements

Invaluable technical support and expertise was provided by Mr Ha-Thuc Nhan, Application Specialist, Chi Anh Med-Tech Co Ltd, in sequence optimization, data collection and selection of images for this article.



5A–B Coronal HASTE (5A) and sagittal TrueFISP (5B) images show a large cyst in the spleen, dorsolateral to the stomach. HASTE: 12 slices, SL 4 mm (0.4 mm gap), TR/TE 2600/102 ms, FOV (260*260) mm², matrix (205*256) px², BW 476 Hz/px, PAT factor 2, acquisitions 1. TrueFISP: 13 slices, SL 4mm (no gap), TR/TE 4.3/2.1 ms, FOV (300*300) mm², matrix (384*512) px², BW 488 Hz/px, flip angle 70°, acquisitions 1.

References

- Jelin AC, Norton ME, Bartha AI, Fick AL et al. (2008). Intracranial magnetic resonance imaging finds in the surviving fetus after spontaneous monochorionic cotwin demise. *Am J Obstet Gynecol*; 199: 398.e1–395.e5.
- Nemec SF, Kasprian G, Brugger PC, Bettelheim D et al. (2011). Abnormalities of the upper extremities on fetal MRI. *Ultrasound Obstet Gynecol*, Manuscript in press.
- Mailáth-Pokorny M, Worda C, Krampl-Bettelheim E, Watzinger F. (2010). What does magnetic resonance imaging add to the prenatal ultrasound diagnosis of facial clefts? *Ultrasound Obstet Gynecol*, 36: 445–451.
- Brugger PC (2011) MRI of the fetal heart. In: D Prayer (ed) *Fetal MRI* (pp 247–258). Springer: Heidelberg.
- Manganaro L, Savelli S, Di Maurizio M, Perrone et al. (2009). Assessment of congenital heart disease (CHD): Is there a role for fetal magnetic resonance imaging (MRI)? *Eur J Radiol*, 27: 172–180.
- Kasprian G (2011) MRI of the normal fetal lung. In: D Prayer (ed) *Fetal MRI* (pp 215–234). Springer: Heidelberg.
- Garel C. (2008). Fetal MRI: What is the future. *Ultrasound Obstet Gynecol*, 31: 123–128.
- Kasprian G, Brugger PC, Weber M, Krssak M et al. (2008). In utero tractography of fetal white matter development. *Neuroimage*, 43: 213–224.
- Mitter C, Kasprian G, Brugger PC, Prayer D. (2011). Three-dimensional visualization of fetal white-matter pathways in utero. *Ultrasound Obstet Gynecol*, 37: 252–253.
- Story L, Damodaram MS, Allsop JM, McGuinness A et al. (2010). Proton magnetic resonance spectroscopy in the fetus. *Eur J Obstet Gynecol Reprod Biol*, manuscript in press.

*MR scanning has not been established as safe for imaging fetuses and infants under two years of age. The responsible physician must evaluate the benefit of the MRI examination in comparison to other imaging procedures.

Contact

Nguyen Thi Thu Trang, MD
Department of Diagnostic Radiology
Maternal and Obstetrics Tu Du Hospital
284 Cong Quyns, District 1
Ho Chi Minh City
Vietnam
nhenconbs@gmail.com

Erratum

We have to point out an error that slipped through quality control in the previous issue of MAGNETOM Flash (1/2011):

The Greek letters are missing in Joachim Graessner's "Frequently Asked Questions: Diffusion-Weighted Imaging (DWI)"

Please visit www.siemens.com/magnetom-world to download the corrected PDF.

determines the strength and duration of the diffusion gradients. It combines the following physical factors into one b-value and is measured in s/mm² [1].

$$b = \gamma^2 G^2 \delta^2 (\Delta - \delta/3)$$

The signal ratio diffusion-weighted to non diffusion-weighted signal is:

$$\frac{S}{S_0} = e^{-\gamma^2 G^2 \delta^2 (\Delta - \delta/3) D} = e^{-bD}$$

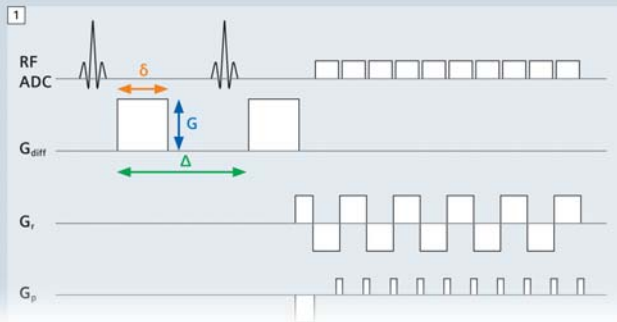
- S₀ – signal intensity without the diffusion weighting
- S – diffusion-weighted signal
- γ – gyromagnetic ratio
- G – amplitude of the two diffusion gradient pulses
- δ – duration of the pulses
- Δ – time between the two pulses
- D – diffusion coefficient is a measure of the strength (velocity) of diffusion

the greater the diffusion coefficient, i.e. the ADC in our in vivo case. If you choose the b-value the reciprocal magnitude of the expected ADC (D) in the focus tissue you make the exponent of the exponential function being '-1'. This means your signal S is reduced to about 37% of its initial value S₀.

What is the optimum b-value?

A b-value of zero delivers a T2-weighted EPI image for anatomical reference. The b-values should attenuate the healthy background tissue more than the lesion at a level so that the intensity differences are about a factor of two at a comfortable signal-to-noise ratio (SNR) level i.e. there is signal left in the highest b-value image.

In the range of clinically-relevant b-values (up to approximately 1,000), then the greater the b-value, the stronger the diffusion weighting and the higher



MAGNETOM Flash – Imprint
© 2011 by Siemens AG, Berlin and Munich,
All Rights Reserved

Publisher:
Siemens AG
Medical Solutions
Business Unit Magnetic Resonance,
Karl-Schall-Straße 6, D-91052 Erlangen,
Germany

Editor-in-Chief: Dr. Matthias Lichy, M.D.
(matthias.lichy@siemens.com)

Associate Editor: Antje Hellwich
(antje.hellwich@siemens.com)

Editorial Board: Christiane Bernhardt;
Peter Kreisler, Ph.D.; Wellesley Were;
Milind Dhamankar, M.D.; Michelle Kessler;
Gary McNeal; Sunil Kumar, M.D.

Production: Norbert Moser, Siemens AG,
Medical Solutions

Layout: independent Medien-Design
Widenmayerstrasse 16, D-80538 Munich

Printer: Mediahaus Biering GmbH,
Freisinger Landstr. 21, 80939 Munich, Germany

**MAGNETOM Flash is also available
on the internet:**
www.siemens.com/magnetom-world

Note in accordance with § 33 Para.1 of the German Federal Data Protection Law: Despatch is made using an address file which is maintained with the aid of an automated data processing system.

MAGNETOM Flash with a total circulation of 35,000 copies is sent free of charge to Siemens MR customers, qualified physicians, technologists, physicists and radiology departments throughout the world. It includes reports in the English language on magnetic resonance: diagnostic and therapeutic methods and their application as well as results and experience gained with corresponding systems and solutions. It introduces from case to case new principles and procedures and discusses their clinical potential.

The statements and views of the authors in the individual contributions do not necessarily reflect the opinion of the publisher.

The information presented in these articles and case reports is for illustration only and is not intended to be relied upon by the reader for instruction as to the practice of medicine. Any health care practitioner reading this information is reminded that they must use their own learning, training and expertise in dealing with their individual patients. This material does not substitute for that duty and is not intended by Siemens Medical Solutions to be used for any purpose in that regard. The drugs and doses mentioned

herein are consistent with the approval labeling for uses and/or indications of the drug. The treating physician bears the sole responsibility for the diagnosis and treatment of patients, including drugs and doses prescribed in connection with such use. The Operating Instructions must always be strictly followed when operating the MR system. The sources for the technical data are the corresponding data sheets. Results may vary. Partial reproduction in printed form of individual contributions is permitted, provided the customary bibliographical data such as author's name and title of the contribution as well as year, issue number and pages of MAGNETOM Flash are named, but the editors request that two copies be sent to them. The written consent of the authors and publisher is required for the complete reprinting of an article.

We welcome your questions and comments about the editorial content of MAGNETOM Flash. Please contact us at magnetomworld.med@siemens.com. Manuscripts as well as suggestions, proposals and information are always welcome; they are carefully examined and submitted to the editorial board for attention. MAGNETOM Flash is not responsible for loss, damage, or any other injury to unsolicited manuscripts or other materials. We reserve the right to edit for clarity, accuracy, and space. Include your name, address, and phone number and send to the editors, address above.

MAGNETOM Flash

The Magazine of MR

Issue Number 2/2011
Pediatric Imaging

SIEMENS

How I do it

Techniques in
Pediatric MRI
Page 6

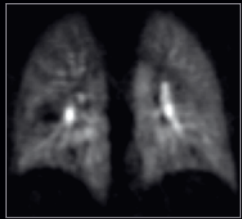
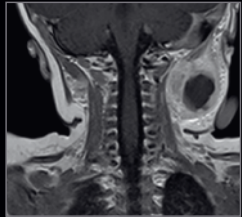
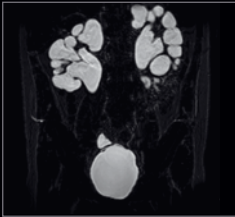
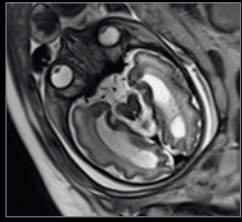
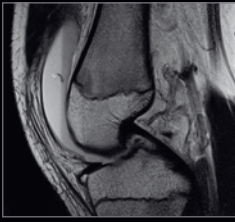
Fetal Imaging
Page 95

Clinical

MR Urography
Page 31

Neuro-Infections
in Childhood –
MR Imaging Patterns
Page 60

MRI of the Lung
Page 74



Please enter your business address

Institution

Department

Function

Title

Name

Street

Postal Code

City

State

Country

MR system used

Please include me in your mailing list for the following Siemens Healthcare customer magazine(s):

Medical Solutions

MAGNETOM Flash

SOMATOM Sessions

AXIOM Innovations

Stay up to date with the latest information
Register for:

E-mail

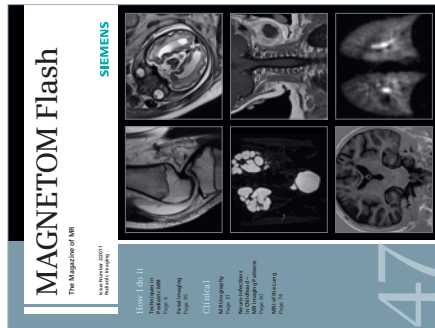
Please print clearly!

Yes, I consent to the above information being used for future contact regarding product updates and other important news from Siemens.

unsubscribe from info service

47

MAGNETOM Flash



Siemens AG
Medical Solutions
Magnetic Resonance
Antje Hellwich - Marketing
P.O. Box 32 60
D-91050 Erlangen
Germany



→ Visit www.siemens.com/magnetom-world
for case reports,
clinical methods,
application tips,
talks and much more
clinical information.

SUBSCRIBE NOW!

– and get your free copy of future
MAGNETOM Flash! Interesting information from
the world of magnetic resonance – gratis to your
desk. Send us this postcard, or subscribe online at
www.siemens.com/MAGNETOM-World

Global Siemens Headquarters

Siemens AG
Wittelsbacherplatz 2
80333 Muenchen
Germany

www.siemens.com/healthcare-magazine

Global Siemens Healthcare Headquarters

Siemens AG
Healthcare Sector
Henkestrasse 127
91052 Erlangen
Germany
Phone: +49 9131 84-0
www.siemens.com/healthcare

Order No. A91MR-1000-83C-7600 | Printed in Germany | CC MR 01000 ZS 091135. | © 09.11, Siemens AG

On account of certain regional limitations of sales rights and service availability, we cannot guarantee that all products included in this brochure are available through the Siemens sales organization worldwide. Availability and packaging may vary by country and is subject to change without prior notice. Some/All of the features and products described herein may not be available in the United States.

The information in this document contains general technical descriptions of specifications and options as well as standard and optional features which do not always have to be present in individual cases.

Siemens reserves the right to modify the design, packaging, specifications and options described herein without prior notice. Please contact your local Siemens sales representative for the most current information.

Note: Any technical data contained in this document may vary within defined tolerances. Original images always lose a certain amount of detail when reproduced.

Global Business Unit

Siemens AG
Medical Solutions
Magnetic Resonance
Henkestr. 127
DE-91052 Erlangen
Germany
Phone: +49 9131 84-0
www.siemens.com/healthcare

Local Contact Information

Asia

Siemens Pte Ltd
The Siemens Center
60 MacPherson Road
Singapore 348615
Phone: +65 6490-8096

Canada

Siemens Canada Limited
Medical Solutions
2185 Derry Road West
Mississauga ON L5N 7A6
Canada
Phone: +1 905 819-5800

Europe/Africa/Middle East

Siemens AG
Medical Solutions
Henkestr. 127
91052 Erlangen
Germany
Phone: +49 9131 84-0

Latin America

Siemens S.A.
Medical Solutions
Avenida de Pte. Julio A. Roca No 516,
Piso 7
C1067ABN Buenos Aires
Argentina
Phone: +54 11 4340-8400

USA

Siemens Medical Solutions U.S.A., Inc.
51 Valley Stream Parkway
Malvern, PA 19355-1406
USA
Phone: +1-888-826-9702